


# IMPACT DAMAGE IN CURVED GRAPHITE/EPOXY PANELS WITH CLAMPED EDGES

THESIS

Ronald B. Perry, Captain, USAF

AFIT/GAE/ENY/90D-19

DEPARTMENT OF THE AIR FORCE
AIR UNIVERSITY
AIR FORCE INSTITUTE OF TECHNOLOGY

Wright-Patterson Air Force Base, Ohio

AFIT/GAE/ENY/90D-19

# IMPACT DAMAGE IN CURVED GRAPHITE/EPOXY PANELS WITH CLAMPED EDGES

THESIS

Ronald B. Perry, Captain, USAF

AFIT/GAE/ENY/90D-19



Approved for public release; distribution unlimited

AFIT/GAE/ENY/90D-19

# IMPACT DAMAGE IN CURVED GRAPHITE/EPOXY PANELS WITH CLAMPED EDGES

THESIS

Presented to the Faculty of the School of Engineering

of the Air Force Institute of Technology

Air University

In Partial Fulfillment of the

Requirements for the Degree of

Master of Science in Aeronautical Engineering

Ronald B. Perry, B.S.

Captain, USAF

December 1990

## Preface

IN MEMORIUM

Captain Wayne P. Wilsdon, GAE90-D

There are several people who deserve special recognition for their assistance in completing this effort. First, thanks to my advisor, Dr Anthony Palazotto, for the many constructive recommendations he has made, which have helped in meeting the research goals developed for this program. Second, thanks are well deserved by Captain John Daniels and other members of the Composites Facility of the Wright Research and Development Center (WRDC) for fabricating the materials, providing the test facility and data acquisition equipment and especially for their immense help in conducting the experiments. Third, thanks go to the AFIT Machine Shop for manufacture of the special equipment needed for these tests and to John Weier of the WRDC Instrumentation Group for applying the strain gauges on all panels. Finally, I owe a great deal to my wife, Carol, for her understanding and patience throughout the course of this effort.

This work was sponsored in part by a research contract from the Air Force Office of Scientific Research.

Ronald B. Perry

## Table of Contents

## List of Figures

## List of Tables

## Abstract

Graphite/epoxy curved cylindrical panels were impacted in the center by an impact machine capable of measuring load during the test. Load, deflection and strain as functions of time were measured for six symmetric layup configurations for impact energies of 0.5 to 4.5 ft-lb. Damage was produced in all panels for certain impact energies. The extent and location of damage was determined from C-scans and optical microscopy of panel cross-sections. The cross-sections indicated that both delamination and transverse cracking contribute to internal damage.

An in-house nonlinear finite element code was used to predict the panel deflections and stresses. The analysis produces good results in predicting the $[0/90]_{3s}$ panel deflection and indicated transverse failure stresses were present in the panel center region. The deflections indicated that the panel was in between simply supported and clamped boundary conditions, with good agreement obtained for hinged support at each edge.

# IMPACT DAMAGE IN CURVED GRAPHITE/EPOXY PANELS WITH CLAMPED EDGES

## I. Introduction

### 1.1 Background

Composite materials, particularly those employing high strength-to-weight fibers are seeing increased use in a number of aerospace applications. Composites offer the advantages of tailoring material properties to provide the greatest strength in the direction of highest load. Graphite/epoxy has several distinct advantages for aerospace applications. It has both high strength-to-weight and high stiffness-to-weight ratios, allowing aircraft designers significant weight savings opportunities. It has good fatigue properties and is resistant to many environmental factors.

Initially, composites in aerospace vehicles were used for secondary structures such as the aircraft control surfaces. However, efforts continue for application of composites as primary structure components including the fuselage, tail, wings and engine mounts.

Similarly, analysis of composite materials has progressed through several stages of development, from simple orthotropic models based on plane stress toward more complex analytical and numerical methods taking into account the out of plane stresses, interlaminar shear stresses and interlaminar failure criteria.

Interest in the response of composite plates and shells to transverse impact loading and their damage resistance has increased in

recent years also. Composites are susceptible to damage from impact by objects dropped from a small height, such as tools dropped during manufacture or repair. Several types of damage can result from impact, including delaminations, transverse cracks in the layers, surface damage or indentation and layer tensile failure.

A great deal of experimental work has been performed on the impact of flat composite plates, primarily under simply supported boundary conditions. These experiments have relied heavily on post-test characterization as a means of quantifying the damage present in the panels. For example, O'Kane and Benham (16) showed that a damage threshold exists, below which no damage occurs, based primarily on the results of C-scans of the specimens. Cantwell and Morton (1) used optical microscopy results to formulate a semi-empirical methodology for predicting low velocity impact damage in composite beams. Wu and Springer (24) did similar research on plates, comparing the micrograph results to a 3-D finite element model analysis. Foos (8) used C-scans and stereo x-rays to investigate the location and shape of delaminations in flat plates. Senn (20) obtained stereo x-rays and optical microscopy on cylindrical panels.

Another measure of damage is the reduction in panel strength under various loading conditions. Compressive load is of primary interest, since delaminations separate the plies and thus can significantly

influence the buckling response. Post-impact strength has been used as a measure of damage in both flat and curved composite structures (10,16, 20).

Instrumentation to measure the applied force-time history and impact velocity have been used on recent tests of flat plates by Foos (8) and cylindrical panels by Senn (20). Use of additional instrumentation such as strain gauges has been extremely sparse. Lin and Lee (13) tested glass fiber composite cylindrical panels with strain gauges on the surface away from the impact point. The response time of the strain gauges is completely adequate to measure dynamic events of duration of a few microseconds (15), so there should be no difficulty in measuring the vibrational response of the panel as a whole to impact.

Analytical approaches to the solution of the dynamic response of orthotropic cylindrical panels have been relatively few (13,18). However, several approaches have been pursued for orthotropic flat panels which can be used for comparison (3,6,17,21,24). There are two ways to implement the loading function in the analysis. One method is to use the Hertz law to predict the contact force function and solve simultaneously for the deflections (3,17,21,24). A simplification of this would be to assume inelastic impact and apply conservation of momentum to determine the impact loading (13). The other approach is to treat the load function as an input to the solution (6,18). If the ratio of impactor mass to target mass is very large, the details of the contact force are of lesser importance (3) and the methods produce similar results.

## 1.2 Purpose

The purpose of this research is to compare damage resulting from impact in cylindrical graphite/epoxy panels to a dynamic analysis of the impact. Six different ply layups were used. The threshold energy at which damage occurs was determined for these cases experimentally. Using the load measured during the experiment as the applied force, the experiments were analyzed with a finite element model based on shell elements incorporating transverse shear deformation. The panel deflection and stress under conditions producing damage were then compared to the experimental results.

## 1.3 Scope

The experiments performed as part of this thesis incorporated both post-test inspection of the samples and in-situ instrumentation to characterize the response of cylindrical composite panels to impact loading. In addition to the use of C-scans, optical microscopy and strain gauges, the panel deflection was measured using a noncontacting optical sensor. The impact energy necessary to produce damage in six different ply layups was determined.

Comparison to the experimental data was made with a finite element model incorporating transverse shear deformation theory. The load function was treated as a known input function in this analysis. The deflection of the panel and the stresses in the panel were calculated using the impact load measured in the experiment. The analytical results for a panel with hinged edges compare well with the results obtained experimentally.

# II. Experimental Procedures

The experiments are a major portion of the work accomplished for this thesis. In chapter 2, the materials and equipment used to complete the experiments are identified and described. Equipment performance parameters and data collection techniques are explained.

## 2.1 Materials

The specimens used in this series of tests were curved cylindrical panels made of AS4/3501-6 graphite/epoxy. The panels were 12 and 24 plies thick (0.06 and 0.12 inches). The panels were fabricated as 21.2 inch by 38.2 inch sheets from pre-impregnated tape on a curved mandrel. These large panels were vacuum bagged on the mandrel and cured in a large autoclave using the standard cure cycle contained in Appendix A. Eight individual panels were cut from these large panels using a high pressure water jet saw. The size of each cut panel was 8 by 8 inches measured along the surface, with a radius of curvature of 12 inches on the external surface.

Fiber volume fraction and void content were measured from the material left from the cutting process at selected locations from the panel center and edges. The results of these measurements indicate a slightly higher void content (1.51 percent average) than that obtained in flat panels (typically less than 1 percent). The curvature of the panel causes some difficulty in control of the resin flow, making the void content slightly higher.

Each panel was scanned using an Aerotech 25 MHz, 0.25 inch, alpha transducer attached to a one-inch lucite delay line. The signals were

visually monitored for loss of back-surface signal or echo signals between the front and back surface signals. The panels showed thinning around the edges, but no defects were found in any of the panels. It is thought that the thinning was caused by the water jet eroding horizontally during the cutting process. However, the thinned region is a small area compared to the area of the panel which is clamped in place during testing, so it should have a negligible effect on the test results.

## 2.2 Impact Facility and Equipment

The experiments were performed at the Low Velocity Impact Facility in the Wright Research and Development Center (WRDC) Structural Test Facility (building 65), Wright-Patterson Air Force Base, Ohio. The impact machine is a General Research Corporation GRC 8250 Dynatup drop weight impact test machine, shown in Figure 2.1. The impactor drop weight is 6.84 lb, so the impact assembly mass is 0.213 slugs or about 3.1 kg. This is the mass of the entire lower portion of the impactor assembly which is dropped, including both the impact tup and the brackets which hold it centered on the impact site. The impactor assembly is adjusted to the correct drop height using a cable to raise and lower the impactor. The upper piece of the assembly has a clevice which is released to drop the lower part of the assembly onto the panel. The drop weight assembly slides down along a set of lubricated tubes to keep the impactor aligned on the center of the impact zone. A set of pneumatic brakes are initiated so as to catch the impactor as it rebounds off the panel, preventing multiple bounces on the panel.

Figure 2.1. Dynatup Impact Test Machine

Single impact events are needed in order to characterize the damage accurately, since multiple bounces could influence the damage results.

The panel is placed on an aluminum support block manufactured for previous tests by Senn (20) and secured in place by a curved plate. The complete assembly, shown in Figure 2.2, is then positioned beneath the impactor. The support block and hold-down plate each have a cutout area in the center of 5 by 5 inches. Since the panel is 8 by 8 inches, 1.5 inches of panel edge are clamped on all four sides. In order to attempt to better approximate clamped boundary conditions, the support block and hold-down plate were redrilled, placing three bolts near each of the panel edges.

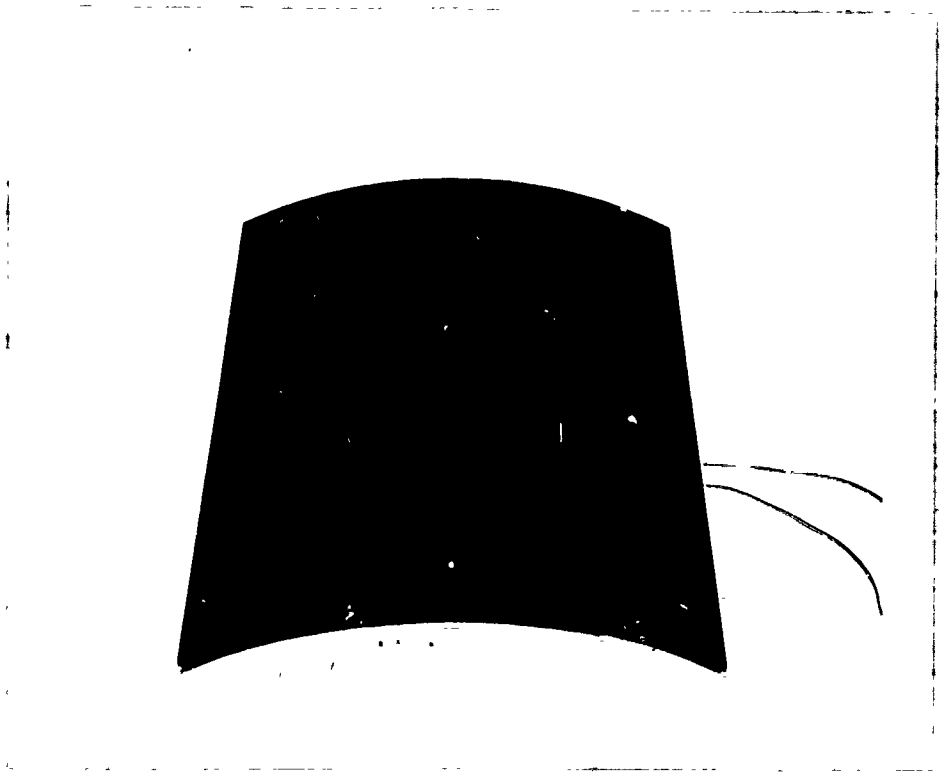

Figure 2.2. Support Block and Hold-down Plate Assembly

## 2.3 Instrumentation

Two instruments are used as part of the standard test equipment included with the impact test machine, a load cell and a velocity detector.

The load cell is attached to the drop weight so that it measures the load applied by the impactor during the time it is in contact with the panel. The velocity is determined based on the time required for a strip of metal (a velocity flag) to pass a photodetector beam placed just above the panel being impacted. A thin metal strip is attached to

the drop weight assembly. When the beam is first occluded by the metal strip, the photodetector senses the drop in light intensity and toggles a voltage signal off. When the metal strip passes the beam of light, the photodetector senses the increase in light intensity and toggles the voltage signal on again.

As described by the manufacturer (9:91-94), if the time $t_2 - t_1$ is the time from the first occlusion of the beam of light to the first reappearance of the beam, and the width of the velocity flag is $x_2 - x_1$, then

$$V_1 = (x_2 - x_1)/(t_2 - t_1) - 1/2\ g\ (t_2 - t_1) \tag{2.1}$$

and

$$V_2 = (x_2 - x_1)/(t_2 - t_1) + 1/2\ g\ (t_2 - t_1) \tag{2.2}$$

where $V_1$ is the velocity when the top of the flag crosses the detector, $V_2$ is the velocity when the bottom of the flag crosses the detector and g is the local gravitational constant ($g = 32.174\ ft/s^2$). Furthermore, the impact velocity can then be found to be

$$V_{impact} = V_2 + g\ (t_3 - t_2) \tag{2.3}$$

where $t_3 - t_2$ is the time from when the bottom of the flag crosses the beam to the time when the impactor hits the panel. $V_{impact}$ is the impact velocity used to determine the impact energy and other parameters.

Besides the data available from the impact machine, two other diagnostics were included in this series of tests. The first additional instrument is an MTI-1000 Fotonic Sensor, shown in Figure 2.3. This is an optical probe used to measure displacement of the panel center. The instrument contains a fiber optic probe which contains both emitting and collecting optical fibers. The emitting fibers send out a beam of light which is focused on a small area of the target. The light must be reflected back into the collecting fibers. Based on the position of the collecting fibers, the amount of light collected is related to the distance from the probe to the reflective surface. The details of the

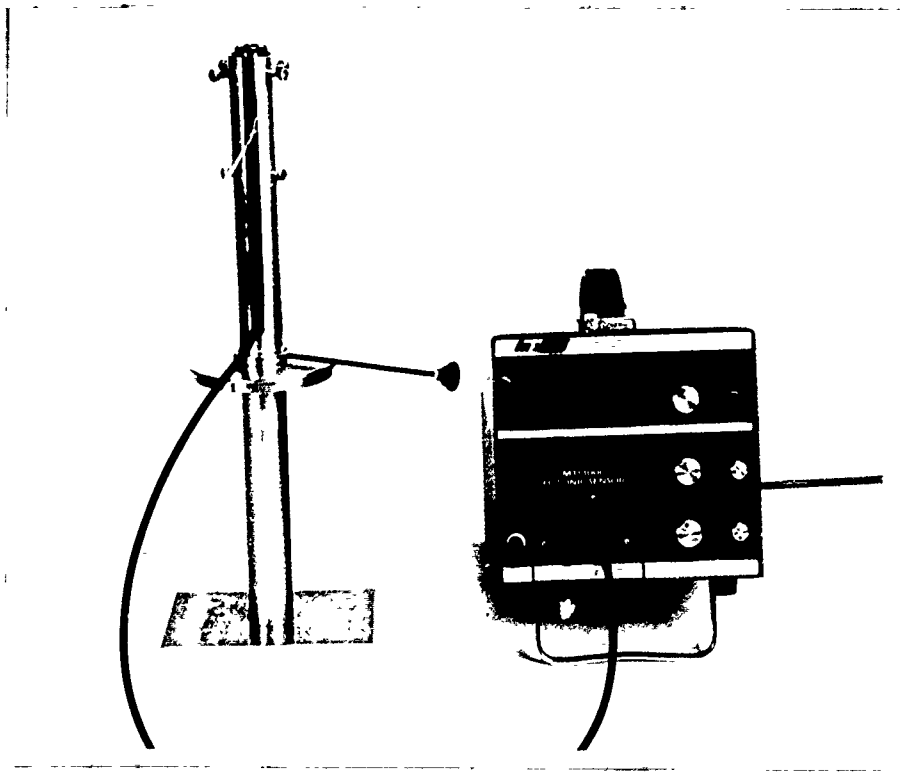

Figure 2.3. MTI-1000 Fotonic Sensor

operating principle of this device are described in References 12 and 14. As the probe is moved away from the surface, the reflected light increases rapidly to a maximum value (at the optical peak), after which it tapers off. An optical extension to the probe (the KD-LS-1A Extender) was used on this test series to increase the standoff distance of the probe.

When the optical extension is used, however, a null point exists when the probe is 0.35 inches from the surface. This is explained in Reference 12 as follows:

> When the distance from the KD-LS-1A to the reflecting target is approximately the same as the focal length, an image of the probe face will appear on the surface of the reflective target. This image is then transmitted back through the KD-LS-1A and is reimaged onto the probe face. Therefore, the returning light enters the fibers it originated from, and the signal fibers receive little light. ... When the target distance is displaced slightly in either direction from the focal point, the image is blurred and the returning light begins to enter the signal fibers. This action generates a peak in output signal at either side of the null. (12)

The experiments were performed with the instrument positioned far enough away from the target so that the signal was never in the null region. The second optical peak occurs at approximately 0.375 inches from the target surface, so a starting position of approximately 0.6 inches from the target was chosen. Using these conditions, the allowable panel deflection could be up to approximately 0.225 inches.

The optical probe is placed vertically beneath the panel in the impact machine. To provide the necessary reflectivity of the surface, a piece of aluminum tape is attached to the panel at the center. The MTI-1000 machine converts the light level seen by the collecting fibers

into a DC voltage which can be read from a panel on the front or from a cable connection on the back. The output voltage was calibrated to correspond to a given position from the surface, as shown in Figure 2.4. Based on changes in the output voltage during the test, the changes in position of the panel can then be calculated.

In addition, a stacked rosette of strain gages was used to measure the surface strain on the lower surface of the panel at a point 0.5 inch along the circumferential direction from the panel center. The strain gages used were Micro Measurements type WK-06-060WR-350. The three legs of the rosette were aligned in the 0, +45 and 90 degree directions, where the 0 degree direction is along the longitudinal axis of the panel, the 90 degree is along the circumferential direction and the coordinate system is right-handed, as seen from the bottom of the panel.

## 2.4 Data Collection and Processing

The signals from the velocity detector and the load cell are both collected by a General Research Corporation GRC 730-I Instrumented Impact Test Data System. This is an IBM PC-XT computer with a high speed data acquisition card. The signals from both the load cell and velocity detector are collected, converted to engineering units and stored on disk.

From the collected data, several important parameters are derived. The impact velocity $V_{impact}$ is found from Equations 2.1-2.3, using the time of first rise in the load cell as $t_3$. The impact energy, $E_{impact}$, can then be found from

$$E_{impact} = 1/2\ m\ (V_{impact})^2 \qquad (2.4)$$

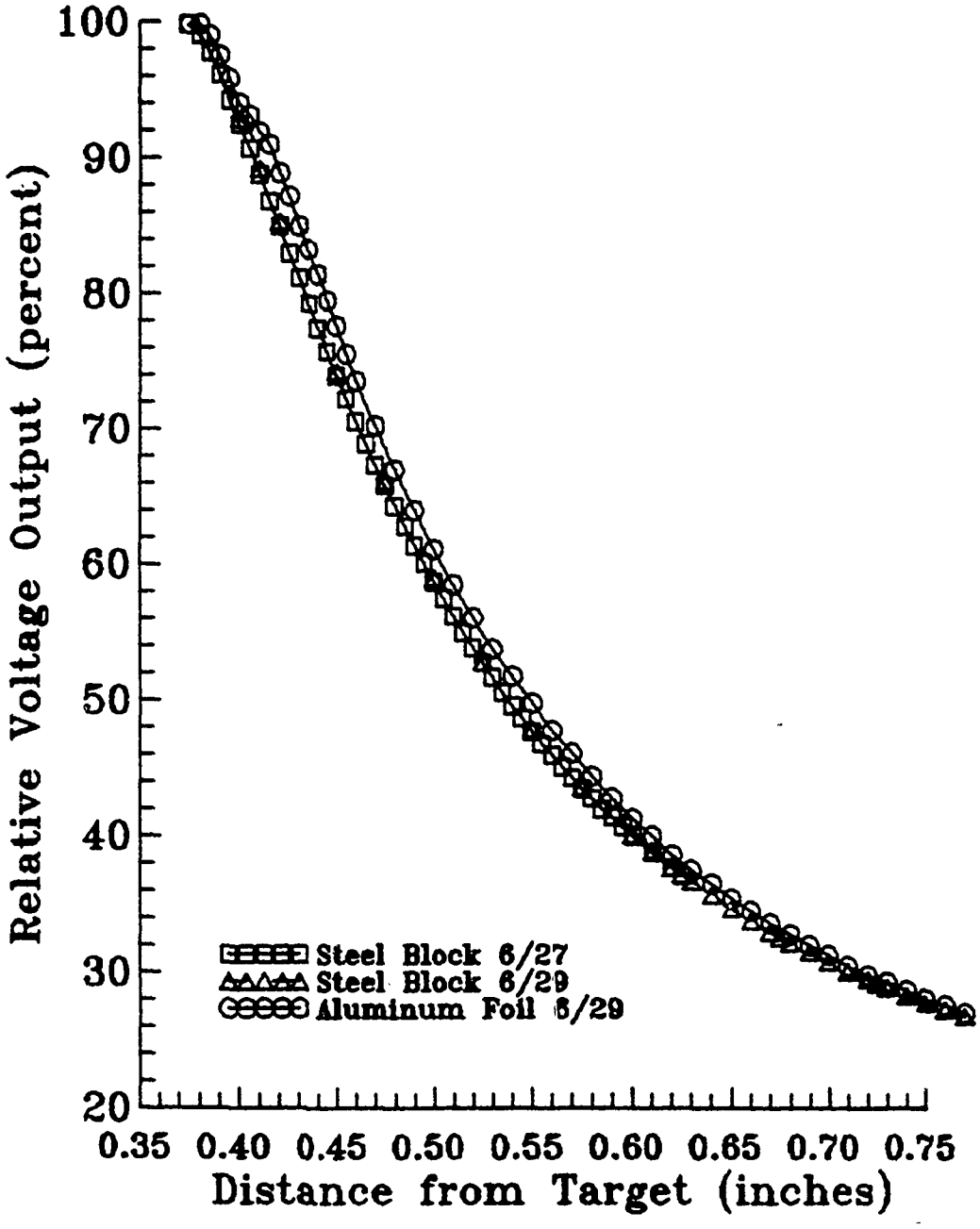


Figure 2.4. Calibration Curve for MTI-1000

The impact energy can also be calculated based on the drop height as $E = mgh$, where h is the drop height, so that the impact velocity can be found from the drop height by

$$V_{impact} = (2\ g\ h)^{1/2} \qquad (2.5)$$

The impact velocity calculated from Equation 2.5 and that obtained from the velocity flag differ by less than 0.1 ft/s under almost all conditions. The difference is caused by imprecision in the measurement of the drop height, which predictably becomes worse for very small drop heights. The impact velocities reported for each test are obtained from the velocity flag (not from Equation 2.5) and the reported impact energy is based on Equation 2.4.

The data obtained by the Dynatup can be used to also determine other parameters such as the velocity as a function of time, v(t); the deflection of the panel as a function of time, x(t); and the energy which is lost or absorbed during the experiment, $E_a$. The procedures are described in Reference 9, and are expanded on here for clarity. These calculations, however, assume that energy is conserved during the impact event, an assumption which would not be correct for panels suscaining any appreciable damage.

If the load function measured by the load cell is denoted as P(t) and the impactor assembly weight is mg, then the total force acting on the load cell is

$$F(t) = mg - P(t) \qquad (2.6)$$

The impactor acceleration after release but prior to impact is g, so the acceleration during the impact process is

$$a(t) = g - P(t)/m \tag{2.7}$$

and from this, the velocity function, v(t), is found from

$$v(t) = \int_t a(\hat{t})d\hat{t} = gt - \frac{1}{m}\int_t P(\hat{t})d\hat{t} \tag{2.8}$$

Signals from the load cell are sampled every 0.025 ms. If impact occurs at sample zero with impact velocity $v_0 = V_{impact}$ and each time increment is $\Delta t$ = 0.025 ms, then the velocity at the nth step is given by

$$v_n = v_0 + n g\Delta t - \frac{1}{m}\sum_{i=1}^{n}\left[\left(\frac{P_{i-1} + P_i}{2}\right)\Delta t\right] \tag{2.9}$$

using the trapezoid rule to approximate the integrated impulse. This is the method in which the software numerically reduces the data.

The position is given by

$$x(t) = \int_t \left[\int_{\hat{t}} a(\tilde{t})d\tilde{t}\right]d\hat{t} = \int_t v(\hat{t})d\hat{t} \tag{2.10}$$

$$= \int_t g\hat{t}\,d\hat{t} - \frac{1}{m}\int_t \left[\int_{\hat{t}} P(\tilde{t})\,d\tilde{t}\right]d\hat{t} \tag{2.11}$$

In numerical form,

$$x_n = x_0 + \sum_{i=1}^{n} \left[ \left( \frac{v_{i-1} + v_i}{2} \right) \Delta t \right] \tag{2.12}$$

Letting $x_0 = 0$ be the initial displacement,

$$x_n = \sum_{i=1}^{n} \left[ \left( \frac{v_{i-1} + v_i}{2} \right) \Delta t \right] \tag{2.13}$$

The absorbed energy, $E_a(t)$, is calculated as the difference between the impact energy and the kinetic and potential energies at time t. Setting time t equal to the time at which the impactor force drops to zero (i.e., it is no longer in contact with the panel) gives the energy absorbed during the test. The absorbed energy is given by (9:94)

$$E_a(t) = T(0) - T(t) - V(t) \tag{2.14}$$

where T(0) is the kinetic energy at the time of impact (the impact energy) and T(t) and V(t) are the kinetic and potential energies of the impactor at the time that the load drops to zero again. The kinetic and potential energies of the panel have been neglected in this calculation.

Each of the three strain gauges were connected to Gould Electronics Model 56-1301-00 programmable signal conditioners containing a bridge circuit. The output voltage from the strain gauge circuits and the MTI-1000 Fotonic Sensor were collected by a Gould high speed data

acquisition system and stored on disk. A Compaq 286 computer served as the controller. Each channel was sampled at 100,000 samples per second (0.010 ms intervals). The signals were then converted to strain and displacement. The data acquisition equipment is shown in Figure 2.5, with the GRC 730-1 at left and the Gould equipment on the right.

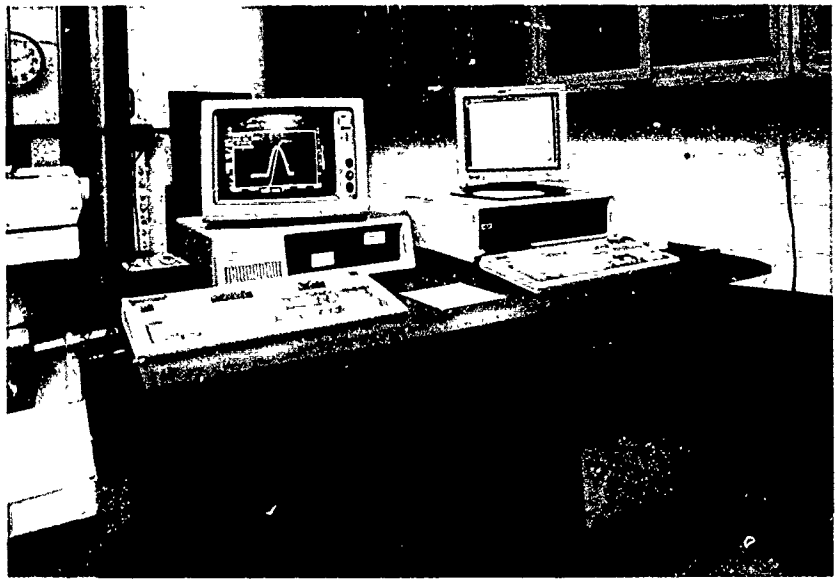

Figure 2.5. Data Collection Equipment

## III. Experimental Results

The experiments produced measurements of a number of parameters during the test. The load, energy, and deflection as functions of time were obtained from the Dynatup. Strain and deflection as function of time were obtained from the strain gauges and MTI sensor. The effect of increasing impact energy (by increasing the drop height) on these are important in determining the panel response. In addition, C-scans and optical microscopy of the panel cross-section beneath the impact point were obtained to characterize the damage. Table 3.2 summarizes the key measurements obtained during the experiments. The results in each category will be discussed in detail.

### 3.1 Impact Energy

The impact energies needed to cause damage in the six different ply configurations are shown in Table 3.1. The $[90/0]_{3s}$ was the most damage sensitive of the 12-ply layups, whereas the $[\pm 45]_{3s}$ was the least damage sensitive. The 24-ply panels were all damaged with the 4.5 ft-lb impact energy, but none of them were damaged at the 3.3 ft-lb energy level.

Table 3.1. Impact Energies Producing Damage in Graphite/Epoxy Panels

| Ply Layup | Impact Energy | Ply Layup | Impact Energy |
|---|---|---|---|
| $[0/90]_{3s}$ | 1.9 ft-lb | $[0/90]_{6s}$ | 4.5 ft-lb |
| $[90/0]_{3s}$ | 1.6 ft-lb | $[90/0]_{6s}$ | 4.5 ft-lb |
| $[\pm 45]_{3s}$ | 2.2 ft-lb | $[\pm 45]_{6s}$ | 4.5 ft-lb |

Table 3.2. Summary of Data Collected from Test Instrumentation

| Test Number | Panel Number | Laminate Configuration | Drop Ht (inches) | Max Load (lbs) | Velocity (ft/sec) | 1/2 mv$^2$ (ft-lb) | Displacement (Dynatup, in) | Displacement (MTI, in) | Strain (0°) | Strain (+45°) | Strain (90°) |
|---|---|---|---|---|---|---|---|---|---|---|---|
| APIT9_401 | 3.2.A(2) #1 | [0/90]3s 12-ply | 2.00 | 215.5 | 3.268 | 1.135 | 0.131 | 0.093 | 2398 | 2013 | 1149 |
| APIT9_402 | 3.2.C #1 | [± 45]3s 12-ply | 2.00 | 192.4 | 3.274 | 1.139 | 0.142 | 0.110 | 4110 | 2583 | 1126 |
| APIT9_403 | 3.2.A(2) #2 | [0/90]3s 12-ply | 2.50 | 235.9 | 3.609 | 1.384 | 0.142 | 0.126 | 2588 | 2083 | 1274 |
| APIT9_404 | 3.2.C #2 | [± 45]3s 12-ply | 2.50 | 219.3 | 3.630 | 1.401 | 0.155 | 0.107 | 4219 | 2814 | 1324 |
| APIT9_405 | 3.2.A(2) #3 | [0/90]3s 12-ply | 3.00 | 255.3 | 3.962 | 1.669 | 0.163 | 0.111 | 2745 | 2150 | 1721 |
| APIT9_406 | 3.2.C #3 | [± 45]3s 12-ply | 3.00 | 242.1 | 3.928 | 1.640 | 0.168 | 0.120 | 4245 | 2744 | 1047 |
| APIT9_407 | 3.2.A(2) #4 | [0/90]3s 12-ply | 3.50 | 281.2 | 4.307 | 1.972 | 0.176 | 0.131 | N/A | 2746 | 2200 |
| APIT9_408 | 3.2.C #4 | [± 45]3s 12-ply | 3.50 | 264.8 | 4.243 | 1.914 | 0.180 | 0.134 | 4673 | 2756 | 1262 |
| APIT9_409 | 3.2.D(1) #1 | [0/90]6s 24-ply | 6.00 | 758.1 | 5.611 | 3.347 | 0.099 | 0.057 | 3267 | 2149 | 723 |
| APIT9_501 | 3.2.D(1) #2 | [0/90]6s 24-ply | 4.00 | 624.1 | 4.584 | 2.234 | 0.081 | 0.052 | 2380 | 1465 | 180 |
| APIT9_502 | 3.2.D(1) #3 | [0/90]6s 24-ply | 8.00 | 689.1* | 6.507 | 4.501 | 0.133 | 0.077 | 2728 | 1479 | 621 |
| APIT9_503 | 3.2.D(1) #4 | [0/90]6s 24-ply | 3.00 | 518.4 | 3.911 | 1.626 | 0.070 | 0.042 | 2209 | 1353 | 259 |
| A9_11r00 | 3.2.E #1 | [90/0]6s 24-ply | 6.00 | 738.0 | 5.605 | 3.339 | 0.100 | 0.064 | 3325 | 2201 | 536 |
| A9_11r01 | 3.2.E #2 | [90/0]6s 24-ply | 8.00 | 758.2* | 6.511 | 4.506 | 0.126 | 0.097 | 3367 | 2194 | 1098 |
| A9_11r02 | 3.2.E #3 | [90/0]6s 24-ply | 4.00 | 636.3 | 4.581 | 2.231 | 0.080 | 0.059 | 2631 | 1782 | 204 |
| A9_11r03 | 3.2.E #4 | [90/0]6s 24-ply | 3.00 | 539.9 | 3.916 | 1.630 | 0.067 | 0.046 | 2418 | 1555 | 224 |
| A9_11r04 | 3.2.B #1 | [90/0]3s 12-ply | 3.00 | 262.7* | 3.932 | 1.643 | 0.145 | 0.093 | 3673 | 2541 | 1474 |
| A91300 | 3.2.B #2 | [90/0]3s 12-ply | 2.50 | 242.6 | 3.624 | 1.396 | 0.136 | 0.101 | 3288 | 2462 | 987 |
| A91301 | 3.2.B #3 | [90/0]3s 12-ply | 2.00 | 214.0 | 3.246 | 1.120 | 0.120 | 0.084 | 3029 | 2045 | 639 |
| A91302 | 3.2.B #4 | [90/0]3s 12-ply | 3.50 | 250.2* | 4.260 | 1.929 | 0.163 | 0.108 | 3352 | 2223 | 1632 |
| A91303 | 3.2.F #1 | [± 45]6s 24-ply | 4.00 | 639.2 | 4.585 | 2.235 | 0.079 | 0.051 | 3928 | 1979 | -597 |
| A91304 | 3.2.F #2 | [± 45]6s 24-ply | 6.00 | 762.4 | 5.599 | 3.333 | 0.099 | 0.076 | 4913 | 2443 | -427 |
| A91305 | 3.2.F #3 | [± 45]6s 24-ply | 8.00 | 855.8* | 6.507 | 4.501 | 0.114 | 0.071 | 5378 | 2442 | -1994 |
| A91306 | 3.2.F #4 | [± 45]6s 24-ply | 2.00 | 486.8 | 3.258 | 1.129 | 0.055 | 0.035 | 2825 | 1316 | -467 |
| A91307 | 3.2.A(2) #5 | [0/90]3s 12-ply | 3.50 | 262.1* | 4.220 | 1.893 | 0.170 | 0.131 | 2993 | 2228 | 2119 |
| A91308 | 3.2.A(2) #6 | [0/90]3s 12-ply | 3.00 | 251.8 | 3.981 | 1.685 | 0.162 | 0.126 | 3012 | 2406 | 1663 |
| A91309 | 3.2.A(2) #7 | [0/90]3s 12-ply | 1.00 | 152.4 | 2.270 | 0.547 | 0.090 | 0.064 | 1694 | 1233 | 629 |
| A92700 | 3.2.A(2) #8 | [0/90]3s 12-ply | 4.25 | 289.8* | 4.707 | 2.355 | 0.188 | 0.141 | 3462 | 2831 | 2409 |
| A92701 | 3.2.C #5 | [± 45]3s 12-ply | 4.25 | 254.2* | 4.746 | 2.394 | 0.208 | 0.146 | 5077 | 3231 | 1501 |
| A92703 | 3.2.C #6 | [± 45]3s 12-ply | 4.00 | 259.6* | 4.580 | 2.230 | 0.200 | 0.138 | 4642 | 2987 | 1377 |
| A92704 | 3.2.B #5 | [90/0]3s 12-ply | 1.25 | 173.6 | 2.551 | 0.692 | 0.095 | 0.085 | 2525 | 1607 | 584 |
| A92705 | 3.2.B #6 | [90/0]3s 12-ply | 4.50 | 242.0* | 4.820 | 2.469 | 0.188 | 0.104 | 3781 | 3102 | 2434 |

* Load at failure

## 3.2 Load

Figure 3.1 shows an example plot of load and energy as functions of time obtained from the Dynatup instrument. Additional plots are included in Appendix B. The load shows a large oscillation beginning as the load reaches a level of about 290 lbs; however the fluctuations subside as the load is removed.

It is expected that these large variations in the force between the plate and the impactor are the result of damage in the material, since they do not occur on tests at lower impact energies. Previous experimenters in impact testing have observed a similar phenomena, attributed to excitation of harmonic oscillations in the impactor or the panel (2). These oscillations were observed to be particularly prevalent in brittle material specimens.

It has been found that as the impact drop height is increased, the maximum load increases, but the time over which the load is applied stays constant. The load-time function can be accurately described as one-half cycle of a sine wave, with the period of the wave being a function only of the ply layup and panel thickness. The integrated impulse, I, can then be expressed as

$$I = \int_0^{\tau} \bar{P} \sin \frac{\pi t}{\tau} dt \qquad (3.1)$$

where $\bar{P}$ is the peak load and $\tau$ is the time over which the load is applied (which is half the period of the loading frequency).

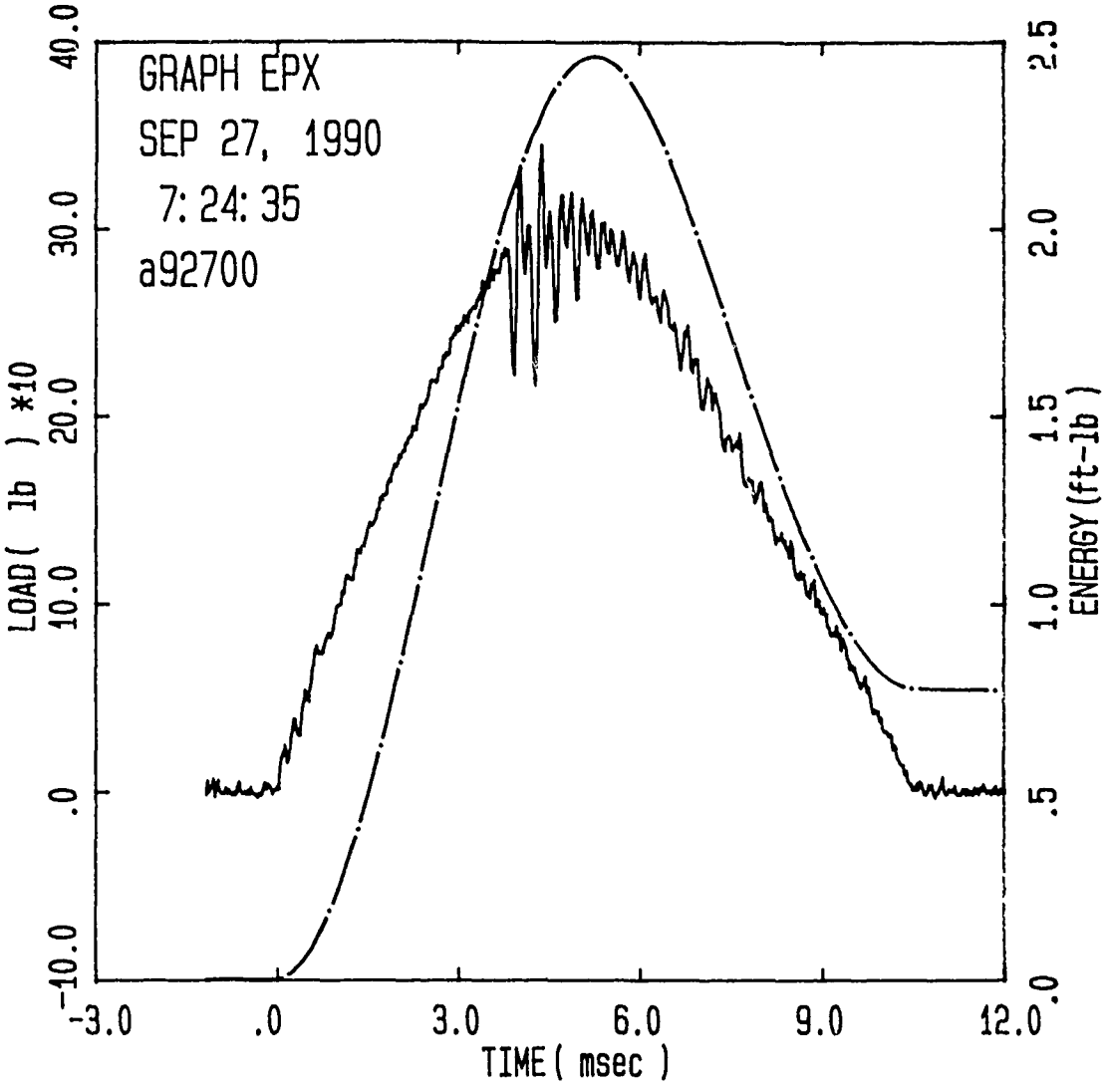


| Specimen Id | Temp ( f) | Impact Veloc. (ft/sec) | Energy (ft-lb ) | Time ( msec ) Max Ld | Time ( msec ) Total | Load ( lb ) Max | Energy (ft-lb ) Maxld | Energy (ft-lb ) Total |
|---|---|---|---|---|---|---|---|---|
| a92700 | 70. | 4.71 | 2.35 | 4.38 | 10.70 | 345.3 | 2.306 | .777 |

Figure 3.1. Example of Load and Energy Plot from Dynatup

This integrates to

$$I = 2\bar{P}\frac{\tau}{\pi} \tag{3.2}$$

For low velocity impact where no damage occurs, if we apply conservation of linear momentum

$$mv_{impact} - mv_{final} = I = 2\bar{P}\frac{\tau}{\pi} \tag{3.3}$$

But $v_{final} = -v_{impact}$, so

$$\bar{P} = \frac{\pi m v_{impact}}{\tau} \tag{3.4}$$

This indicates a load relationship which is directly proportional with impact velocity. Figure 3.2 shows the effect of increasing impact velocity on peak load. The predictions from Equation 3.4 for average $\tau$ are shown for comparison.

For panels in which damage occurred, the load reported is the highest load sustained before failure occurred, not the peak load. This is because, once damage occurs, the large fluctuations in the measured load make it difficult to discern the true load. As can be seen in the figure, the ply layups do follow a nearly proportional relationship with velocity over the range of impact velocities below the damage threshold.

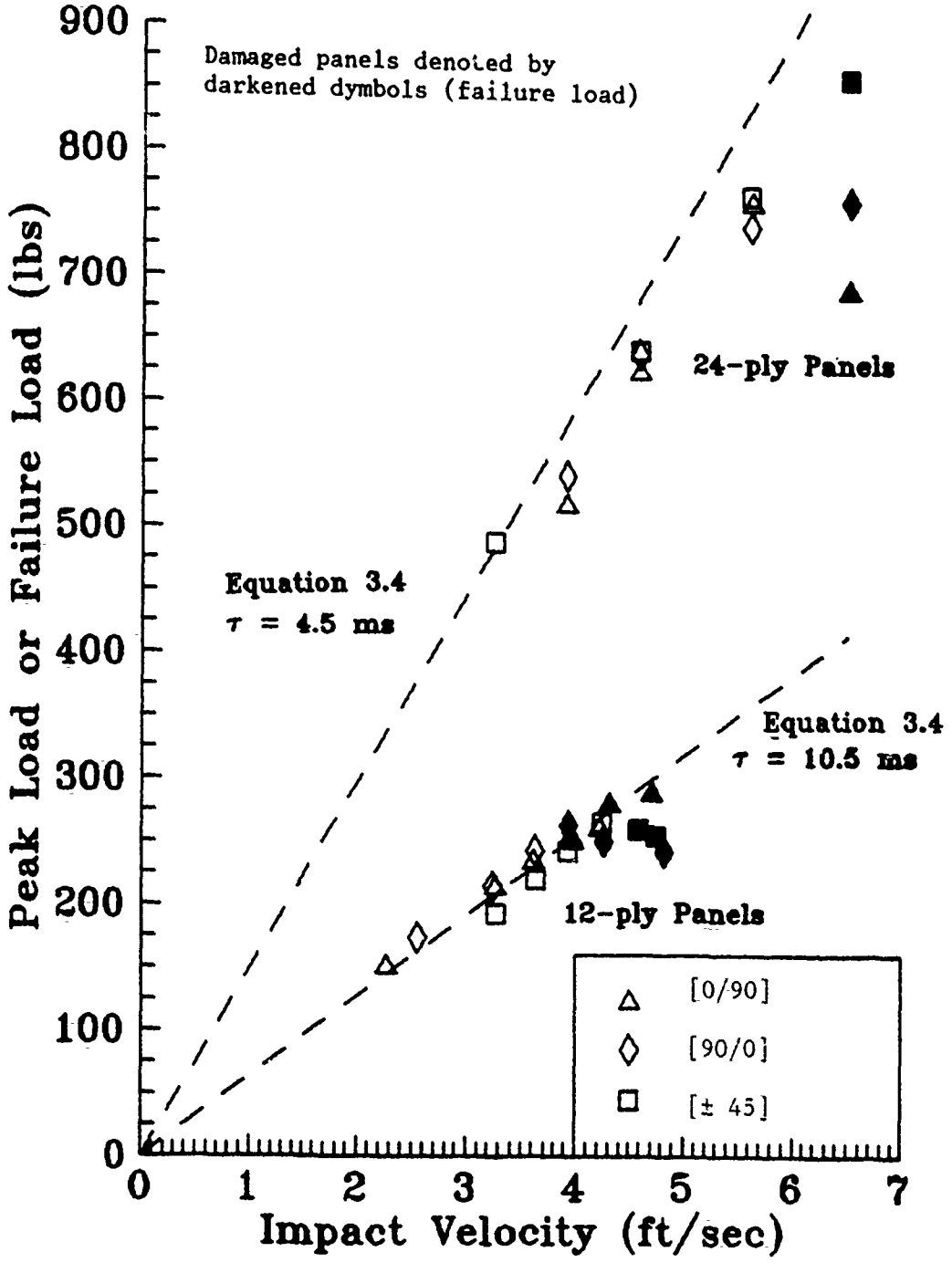


Figure 3.2. Load vs Impact Velocity, Comparison of Experiment to Linear Model

Energy is not conserved, however, during a real impact process. Energy is lost in the nonconservative processes such as the friction between the panel and the plates holding it in place, the material damping process and the actual processes producing damage in the panel. These influences will reduce the impulse measured on the panel, and hence also reduce the maximum force.

3.3 Displacement Measurement from Dynatup

The peak deflections obtained by numerical integration from the Dynatup are summarized in Table 3.2. Deflection plots are shown in Appendix B for all tests performed as part of this test series. As stated in Chapter 2, the absorbed energy assumes conservation of total energy. The absorbed energy measured at the time the load drops to zero is the energy absorbed by the panel due to the sum of processes not accounted for in the integration. Since the Dynatup data acquisition system accounts only for kinetic and potential energies, losses are not taken into account during the load cycle. This creates a problem in that the velocity does not approach zero at the same time that the load reaches its maximum, causing an overprediction of deflection. The time of peak deflection is also shifted forward relative to the load. This illustrates one advantage of a direct measurement of displacement over numerical derivation from the load-time curve.

3.4 Displacement Measurement from MTI-1000

The peak displacements measured by the MTI-1000 are shown in Table 3.2 and Figures 3.3 and 3.4. The displacements at which damage occurs are approximately 0.10 inches for the $[90/0]_{3s}$ panel and 0.13 inches for the $[0/90]_{3s}$ and $[\pm 45]_{3s}$ panels. These displacements are about

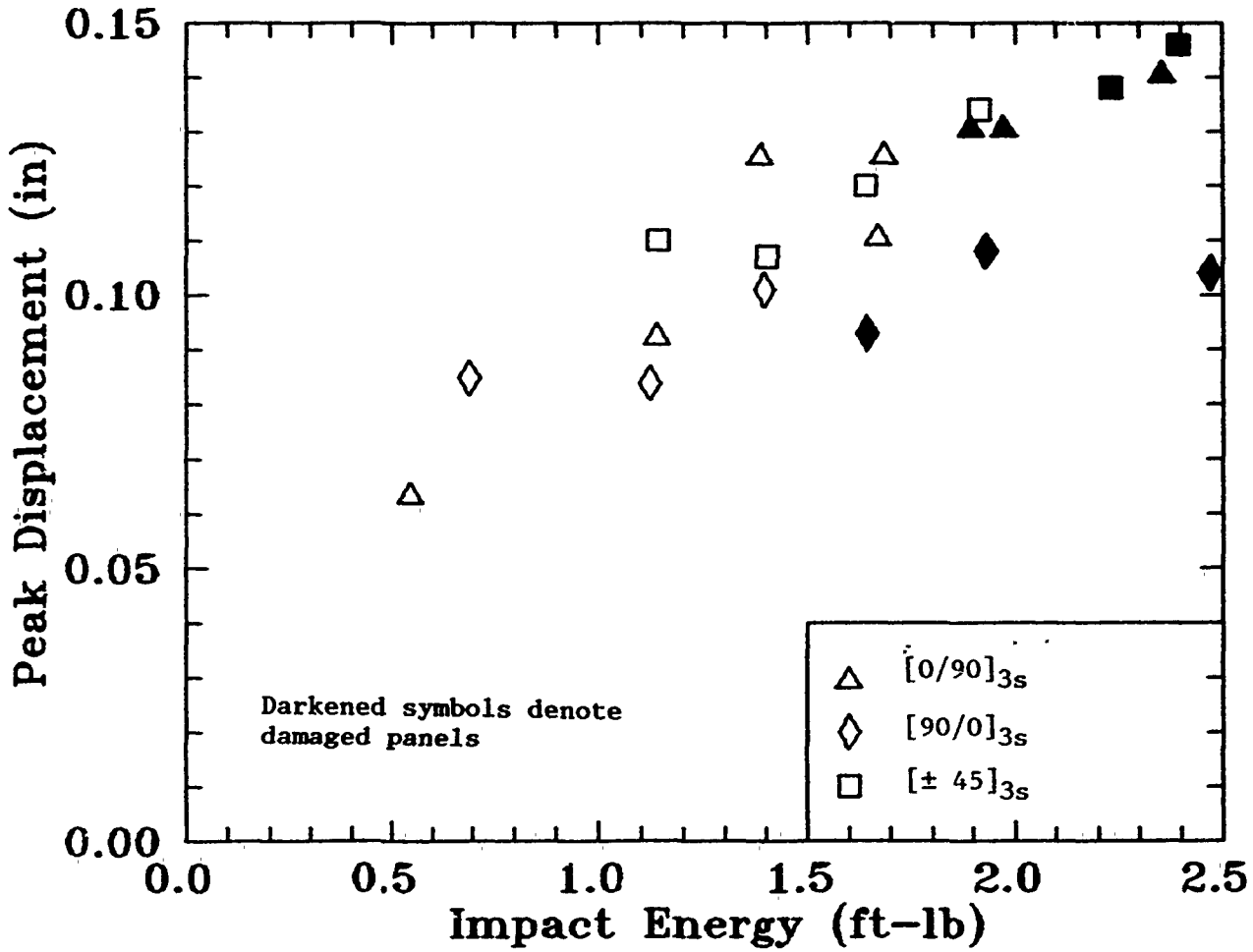


Figure 3.3. Peak Displacements Measured by MTI-1000 Optical Sensor, 12 -ply Panels

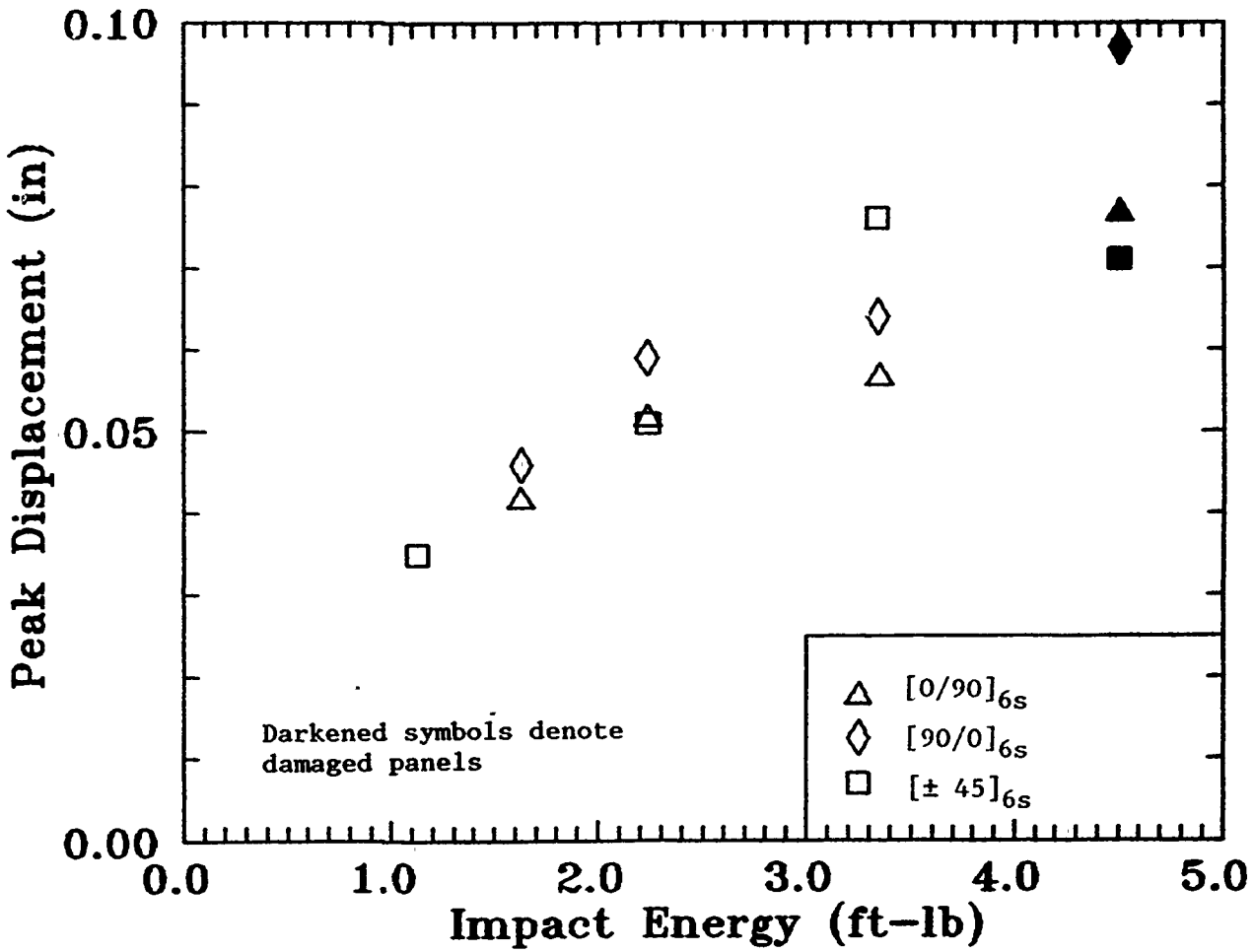


Figure 3.4. Peak Displacements Measured by MTI-1000 Optical Sensor, 24-ply Panels

two times the panel thickness. Generally, if displacements are over half the panel thickness, a nonlinear analysis is necessary. The displacements at which damage occurs in the 24-ply laminates are 0.07 to 0.10 inches, which is less than the thickness of the laminate. It is expected, however, that shear deformation contributes significantly to overall displacement in the thicker panels.

One limitation on the MTI measurement method is that it cannot measure displacements beyond the time at which damage initiates in the panel. At the time that the material fails, the MTI signal rapidly drops. When the load is released, the signal does not return to its original state. The cause of this change in signal is distortion of the reflective tape applied to the panel, resulting in a lower reflectivity. However, the means by which panel damage causes this problem is still unknown.

Examples of this response are shown in Appendix B in tests at the higher impact energies (Figure B.24, for example). Thus, for undamaged panels, the load from the Dynatup and displacement from the MTI are the maximum values recorded during the tests. For tests in which damage occurred, both the load and displacement are the values at the time damage started. One might expect that the load and displacement at which damage occurs are constants. If this were true, the load and displacement values reported would level off at the highest impact energies. However, because the impact event is dynamic, such a straightforward relationship is not observed for most cases.

## 3.5 Strain Gauge Response

The strain gauges measured strain at a point 0.5 inches from the panel center along the circumferential axis of the panel. The strain as a function of time for the three channels (0, +45 and 90 degree directions) are shown in Appendix B. Some interesting differences are observed among the different ply layups.

The $[0/90]_{3s}$ and $[90/0]_{3s}$ laminates show very similar responses, as do the $[0/90]_{6s}$ and $[90/0]_{6s}$ laminates. The shape of the strain-time traces are similar for the three directions and show no changes as the impact energy is increased, until damage in the panels occurs. For the 12-ply laminates, at the time damage occurs in the panel, the 90 degree (circumferential) strain shows a marked increase, whereas the other two strain measurements show only a small change. Examples of this can be seen in Figures B.18, B.21 and B.24 for the $[0/90]_{3s}$ panels and Figures B.36, B.39 and B.42 for the $[90/0]_{3s}$ panels. For the 24-ply panels, the strains show a sudden drop in all measurements, as seen in Figures B.72 and B.84, which is consistent with the large drop in load after failure occurs, shown in Figures B.70 and B.82.

The $[\pm 45]_{3s}$ layup, on the other hand, shows a different response in the 90 degree (circumferential) strain, as shown in Figures B.45, B.48, B.51, B.54, B.57 and B.60. The initial strain response is negative, but then changes to positive as the load is increased. During unloading, the strain response is identical, crossing over from positive to negative before ultimately returning to zero from a negative state.

The $[\pm 45]_{6s}$ panel shows a negative strain in the 90 degree direction throughout the entire loading cycle, as shown in Figures B.87, B.90 and B.93.

The maximum strains recorded during each test are summarized in Table 3.2 and shown in Figures 3.5 through 3.10. More experimental data would be desirable to obtain a more statistically significant result, but the general trend is that the strains increase in a monotonic manner with increasing impact energy. At the highest energies, the 0 and 45 degree strains do not increase as rapidly due to the reduction in load-carrying capability following damage. The 0 and 45 degree strains increase in a near linear relation with impact energy. However, extrapolation to zero impact energy suggests that a nonlinear response must occur at the smallest impact energies.

3.6 C-scans

C-scans of the panels were performed both before and after the experiments. None of the panels showed damage before testing. After being impacted, C-scans of some panels showed no damage at all. Only the panels at the highest impact energies showed damage. These results correlate with the observations of large load oscillations and an audible snap in the panels impacted at higher energies.

C-scans of the panels which sustained damage are shown in Figures 3.11 through 3.16. The $[0/90]_{3s}$ and $[0/90]_{6s}$ damage shape is approximately circular, whereas the damage shape for the $[90/0]_{3s}$ and $[90/0]_{6s}$ panels is elliptic, with the length of the damaged area being greater over the circumferential direction. The $[\pm 45]_{3s}$ and $[\pm 45]_{6s}$ panels show a damage pattern which is rectangular in shape.

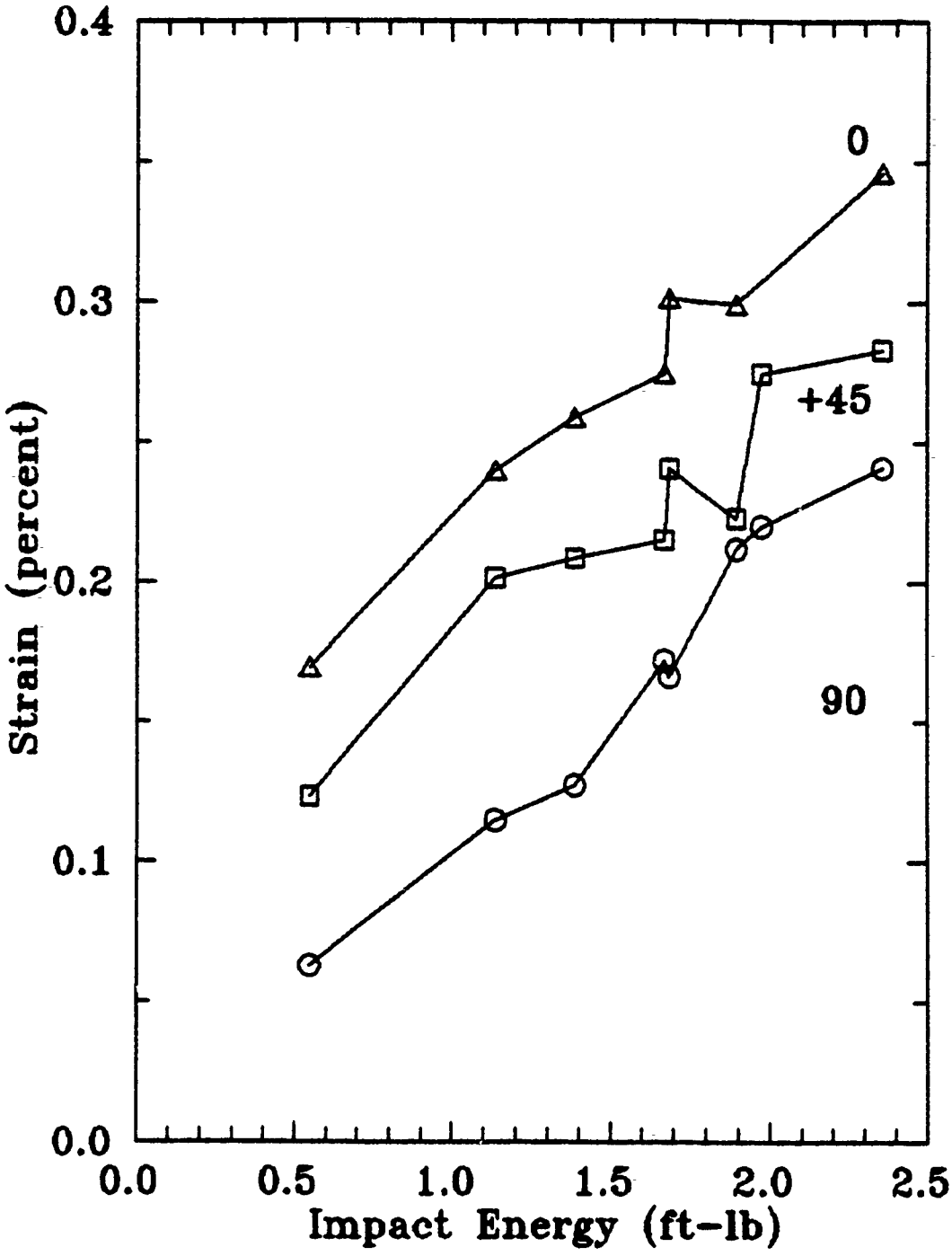


Figure 3.5. Maximum Strains as a Function of Impact Energy, $[0/90]_{3s}$ Panels

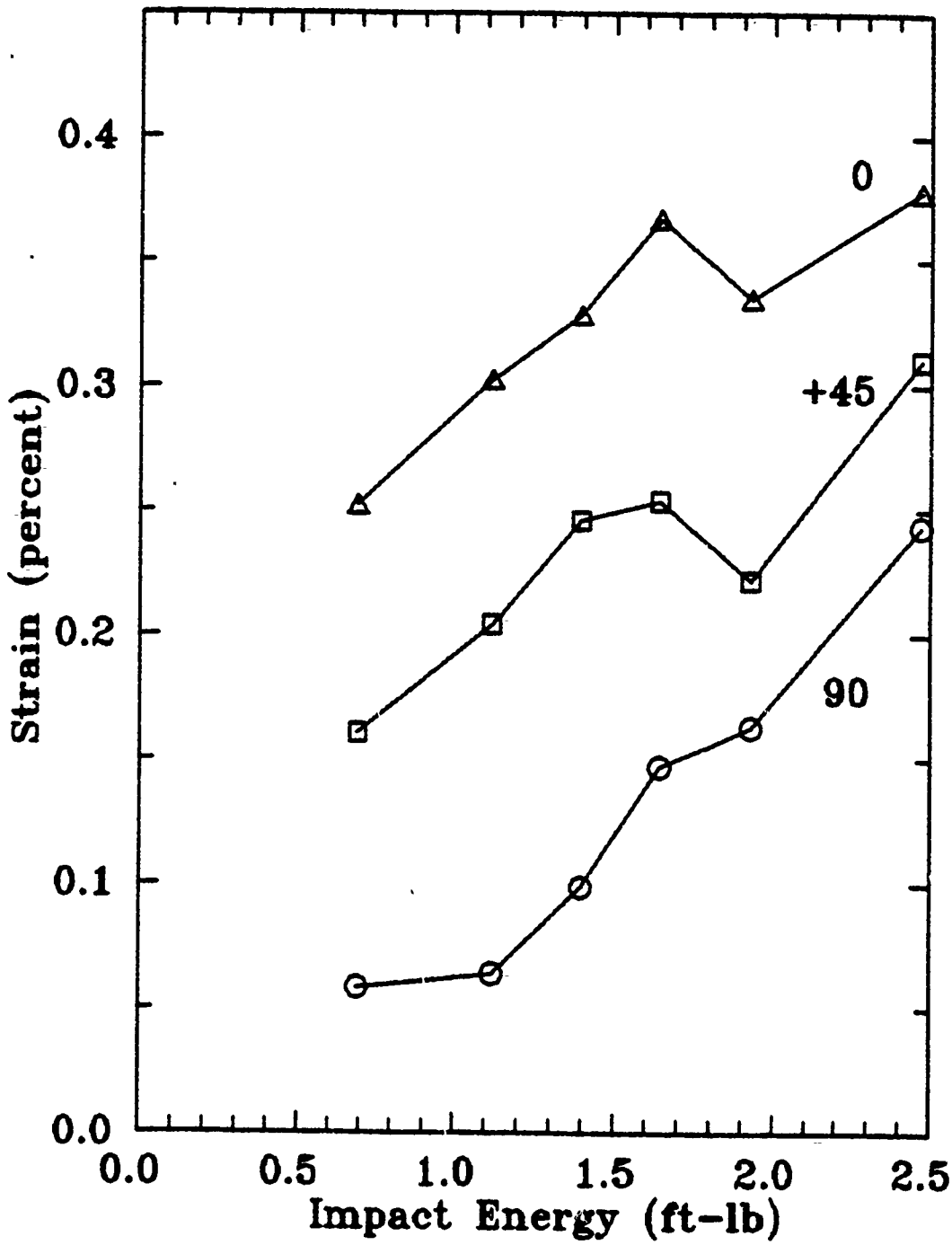


Figure 3.6. Maximum Strains as a Function of Impact Energy, $[90/0]_{3s}$ Panels

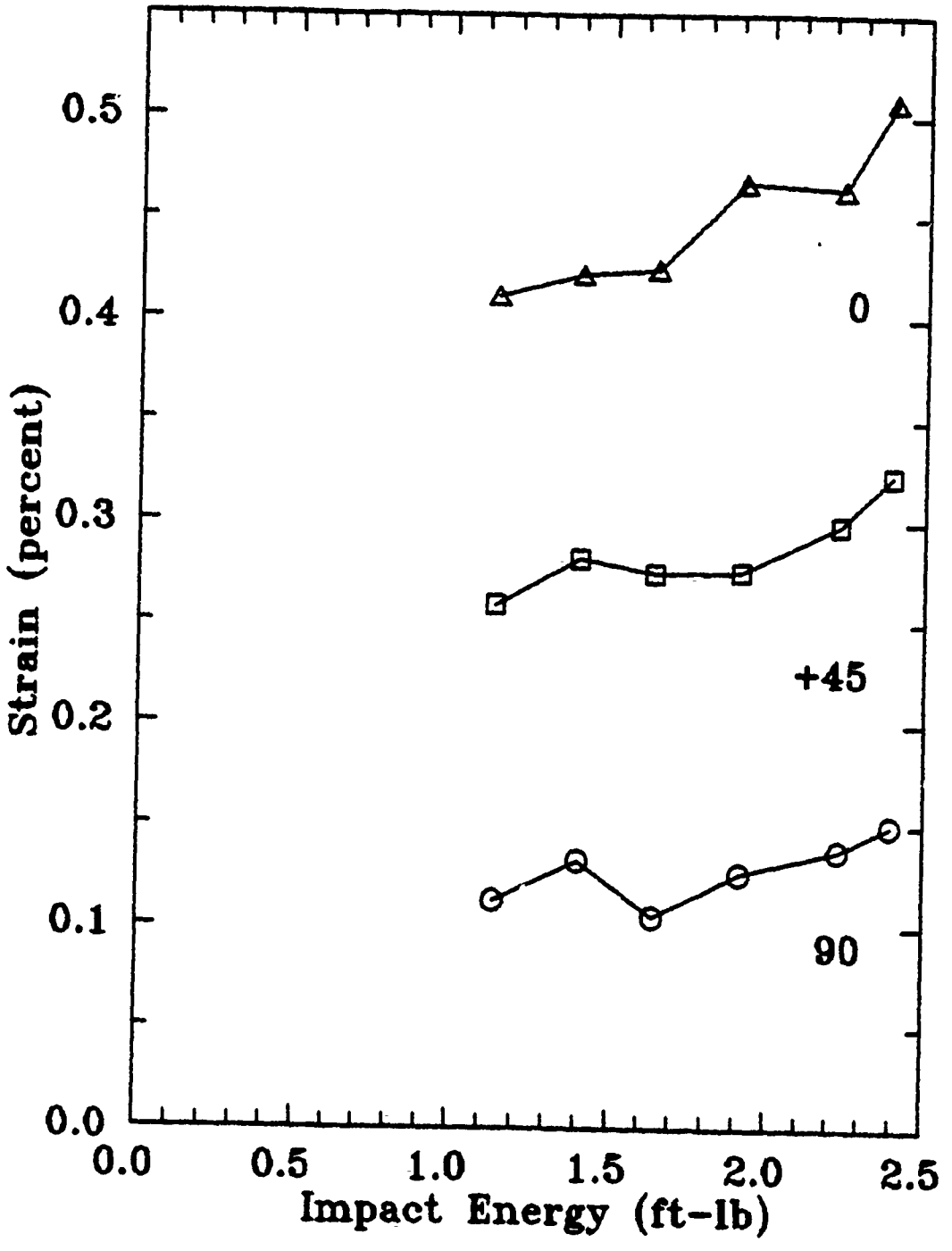


Figure 3.7. Maximum Strains as a Function of Impact Energy, $[\pm 45]_{3s}$ Panels

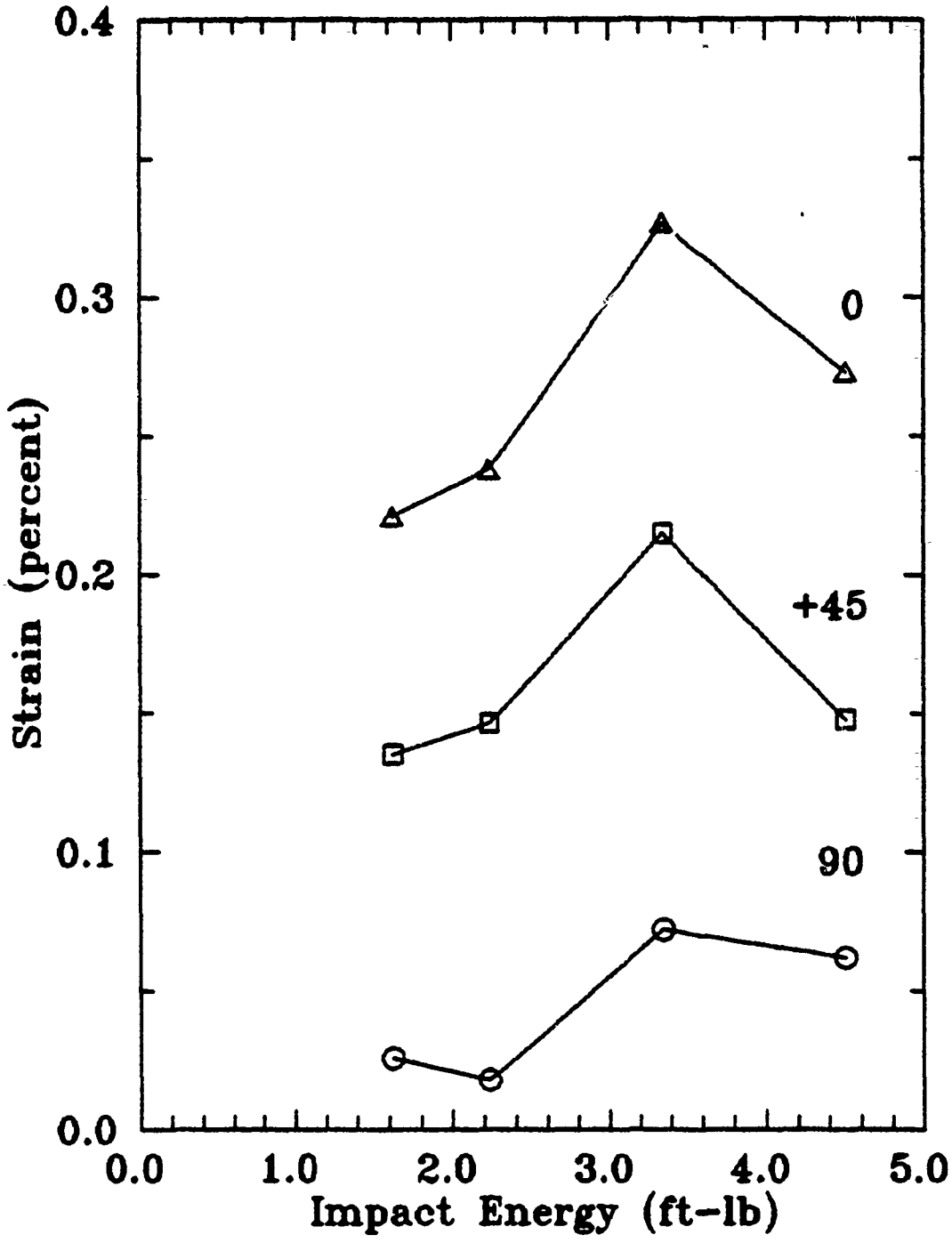


Figure 3.8. Maximum Strains as a Function of Impact Energy, $[0/90]_{6s}$ Panels

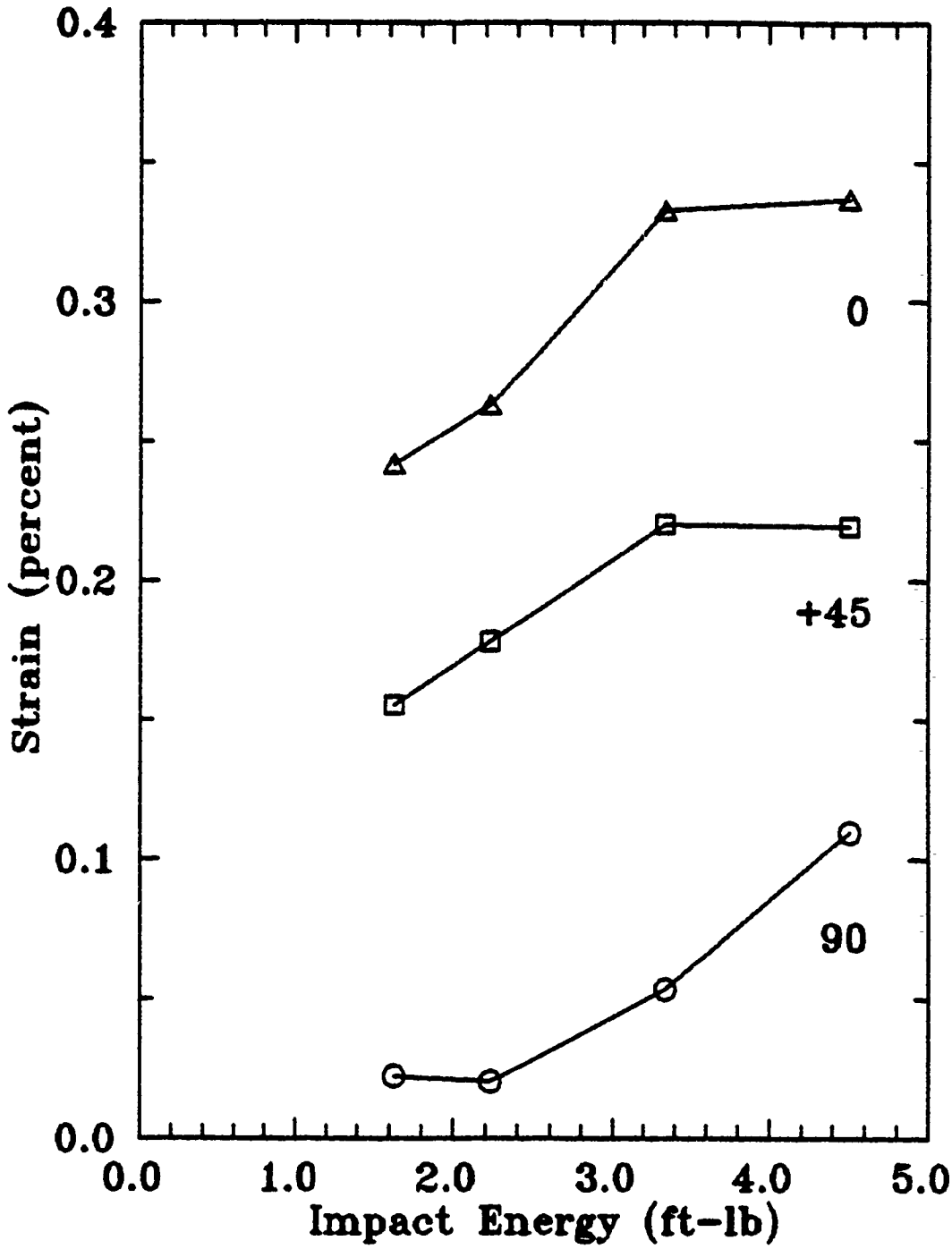


Figure 3.9. Maximum Strains as a Function of Impact Energy, $[90/0]_{6s}$ Panels

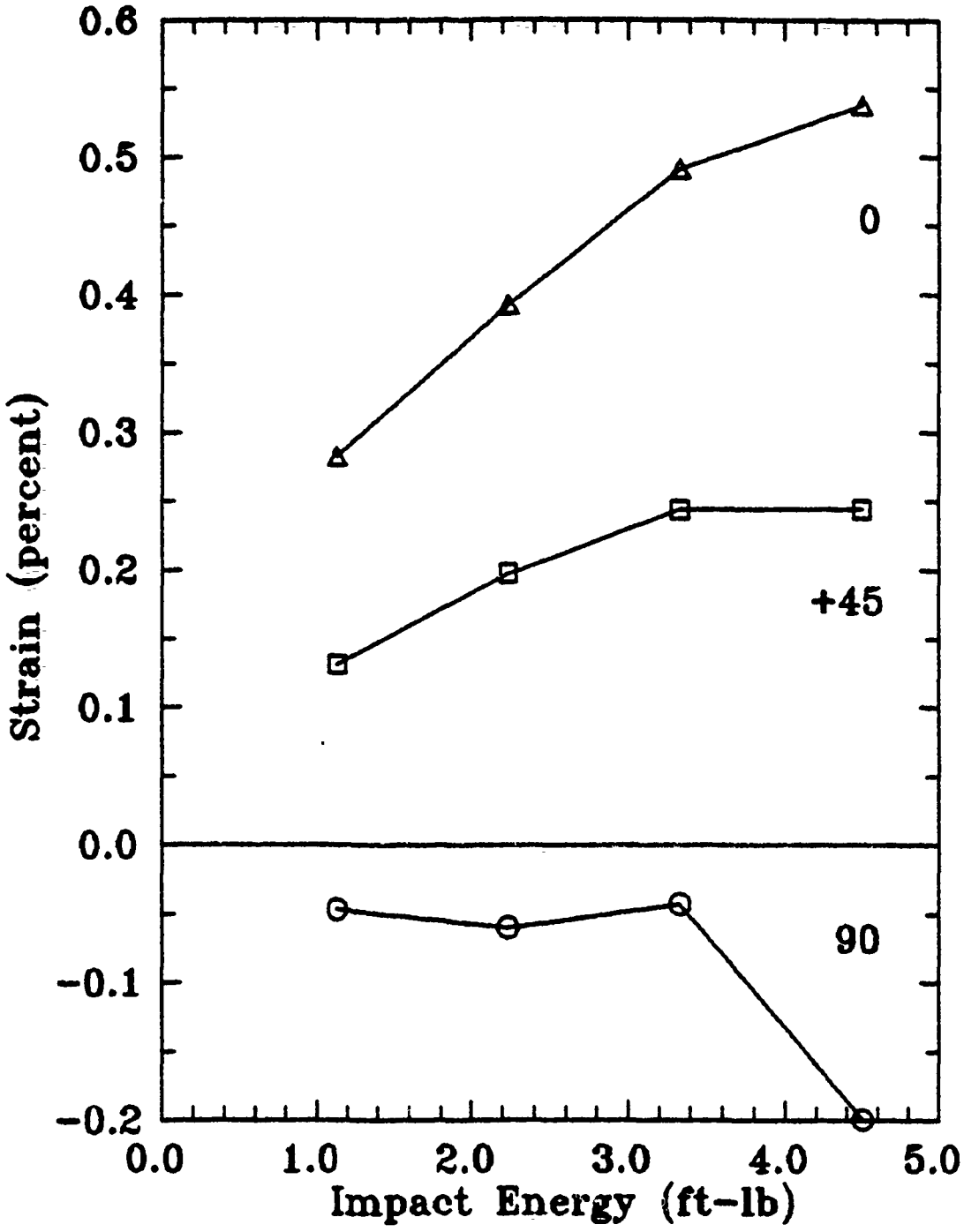


Figure 3.10. Maximum Strains as a Function of Impact Energy, $[\pm 45]_{6s}$ Panels

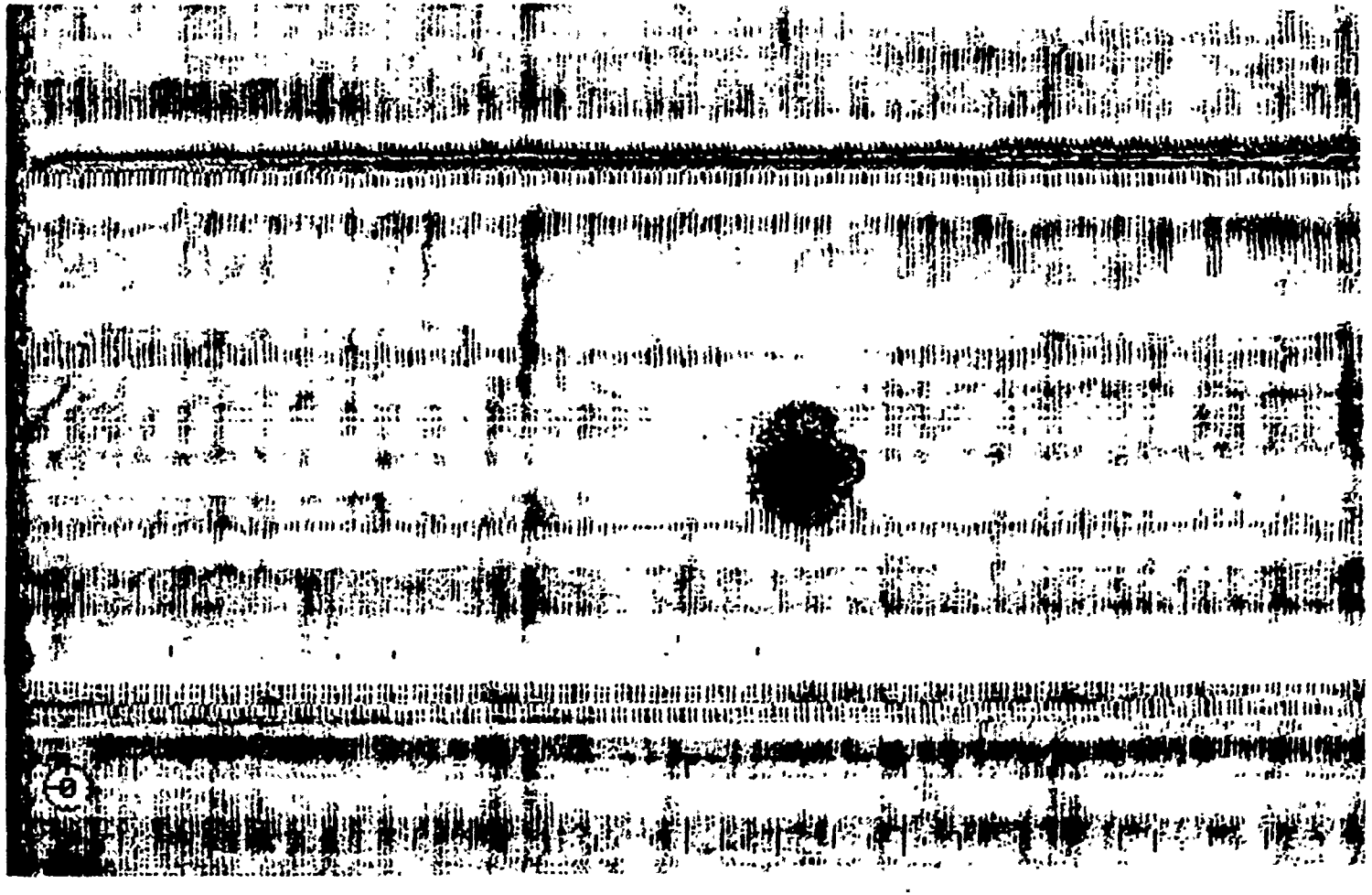

Figure 3.11. C-scan of $[0/90]_{3s}$ Panel, Impact Energy = 1.89 ft-lb

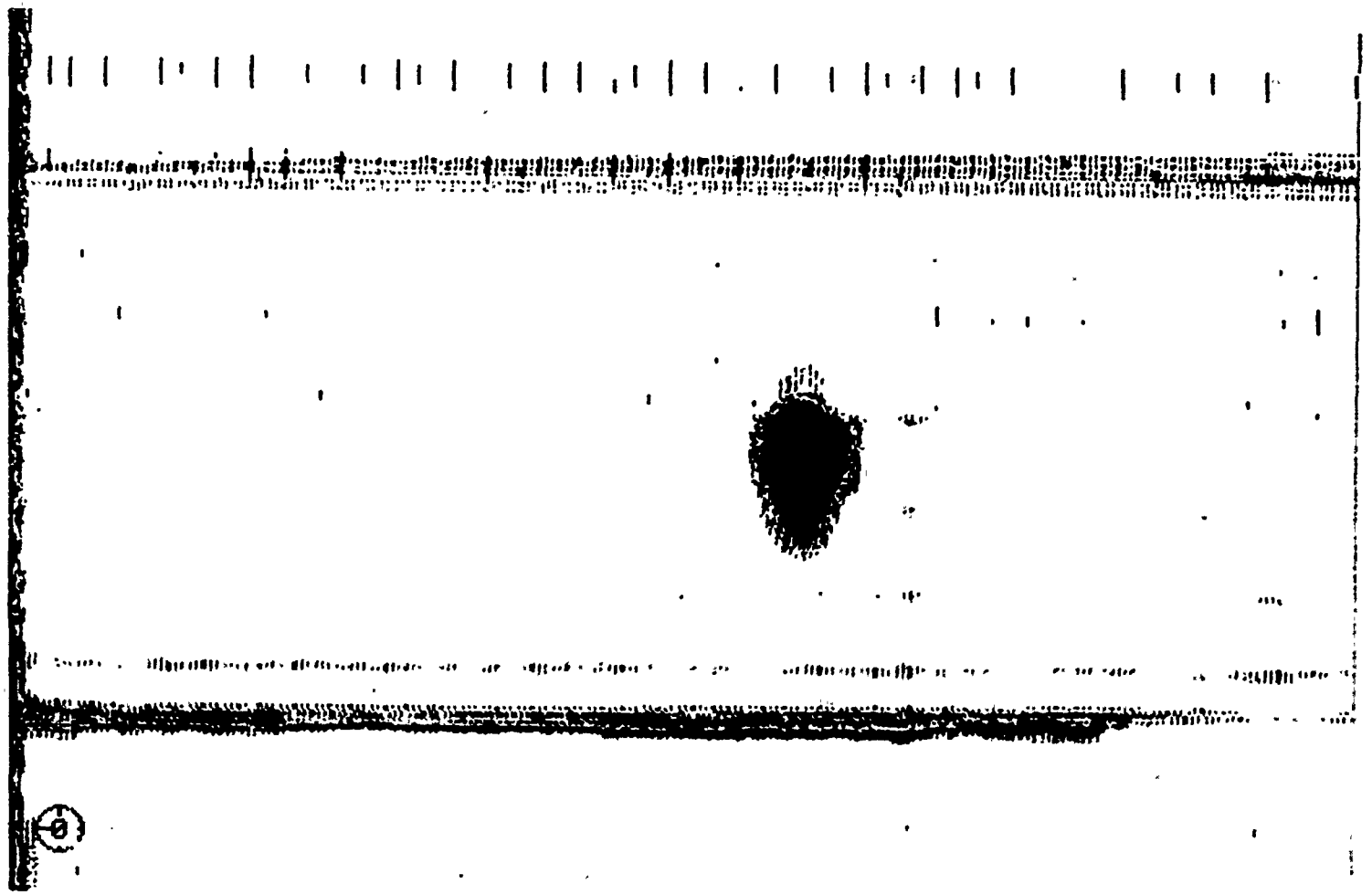

Figure 3.12. C-scan of $[90/0]_{3s}$ Panel, Impact Energy = 1.93 ft-lb

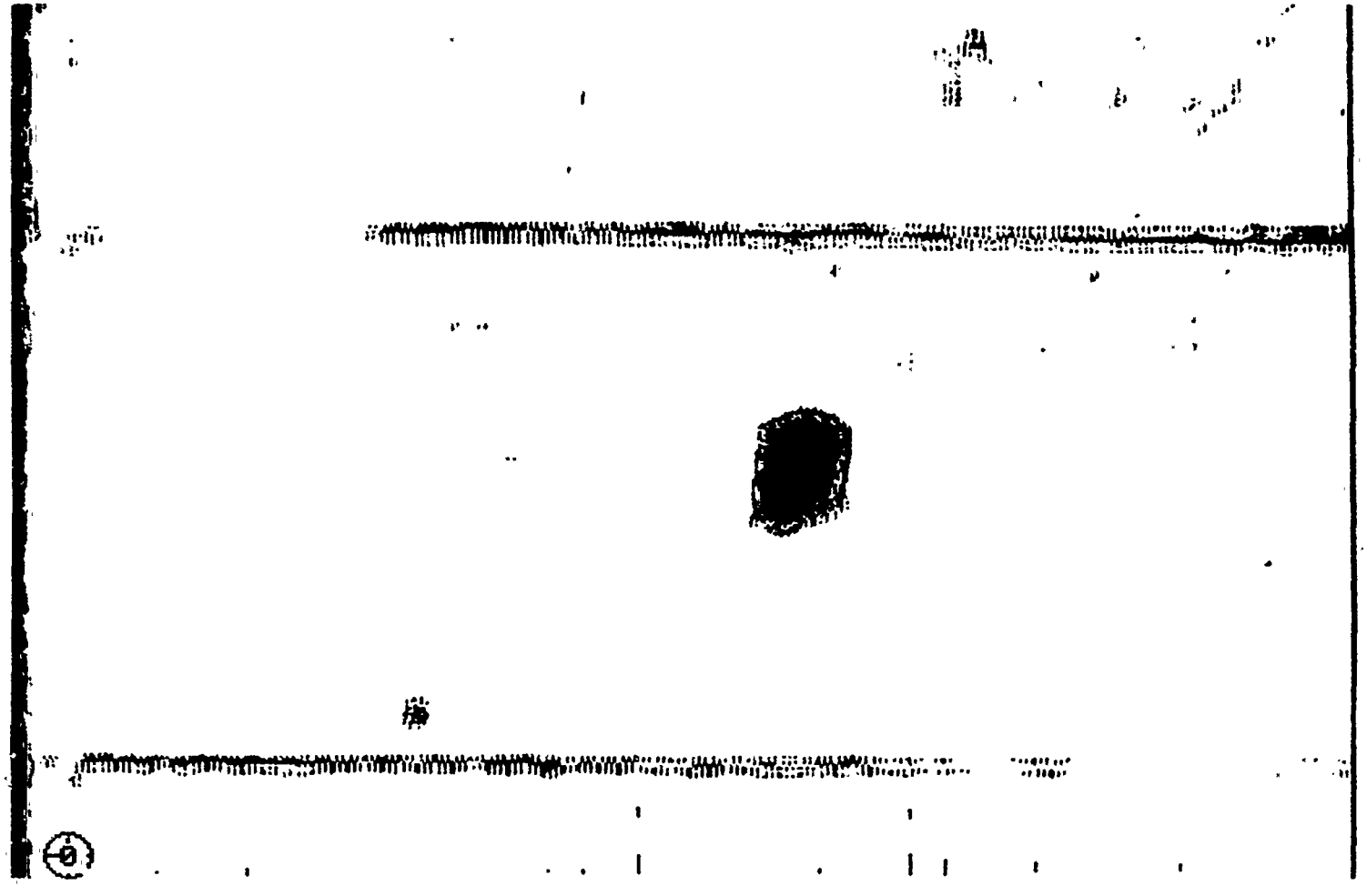

Figure 3.13. C-scan of $[\pm 45]_{3s}$ Panel, Impact Energy = 2.39 ft-lb

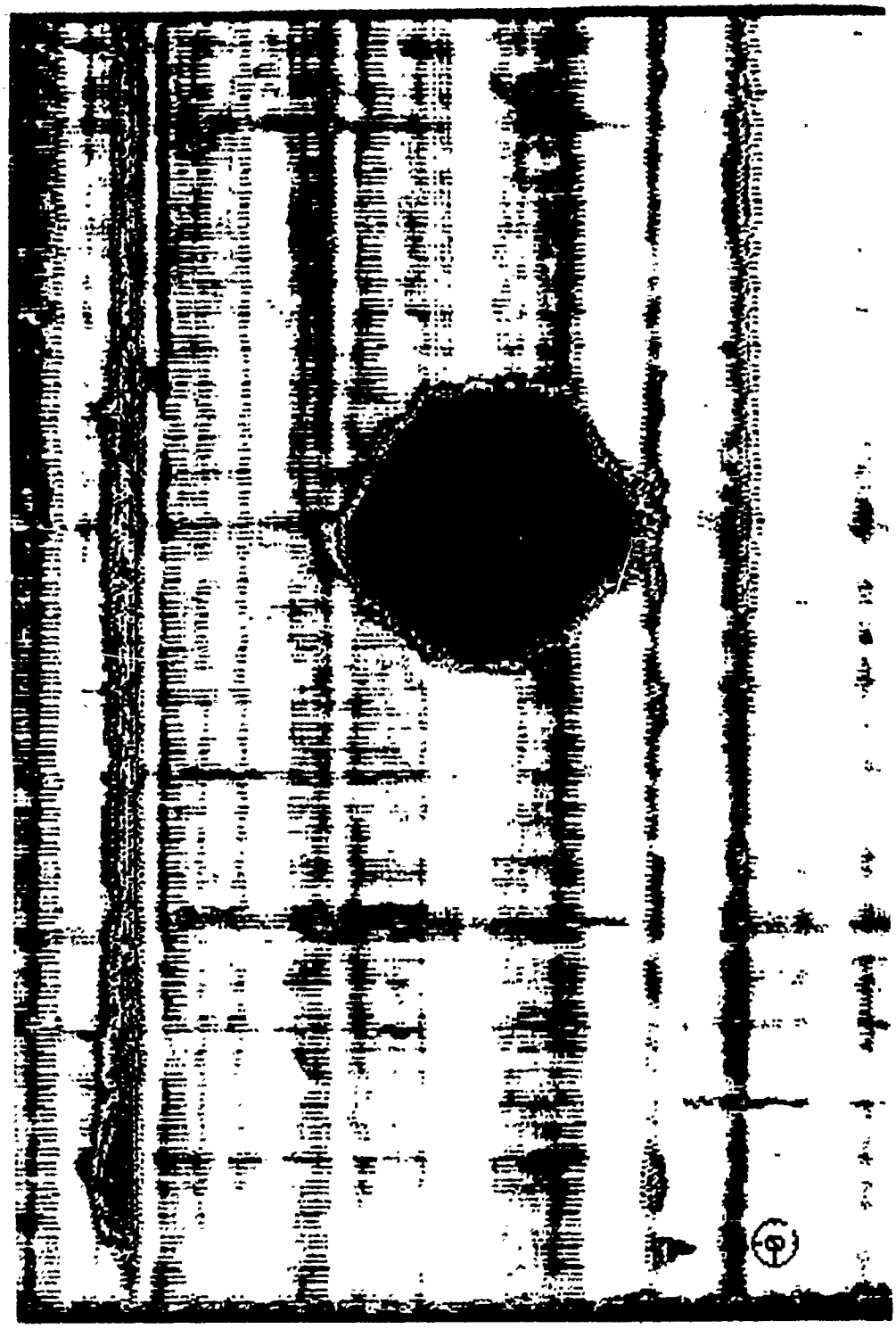

Figure 3.14. C-scan of $[0/90]_{6s}$ Panel, Impact Energy = 4.50 ft-lb

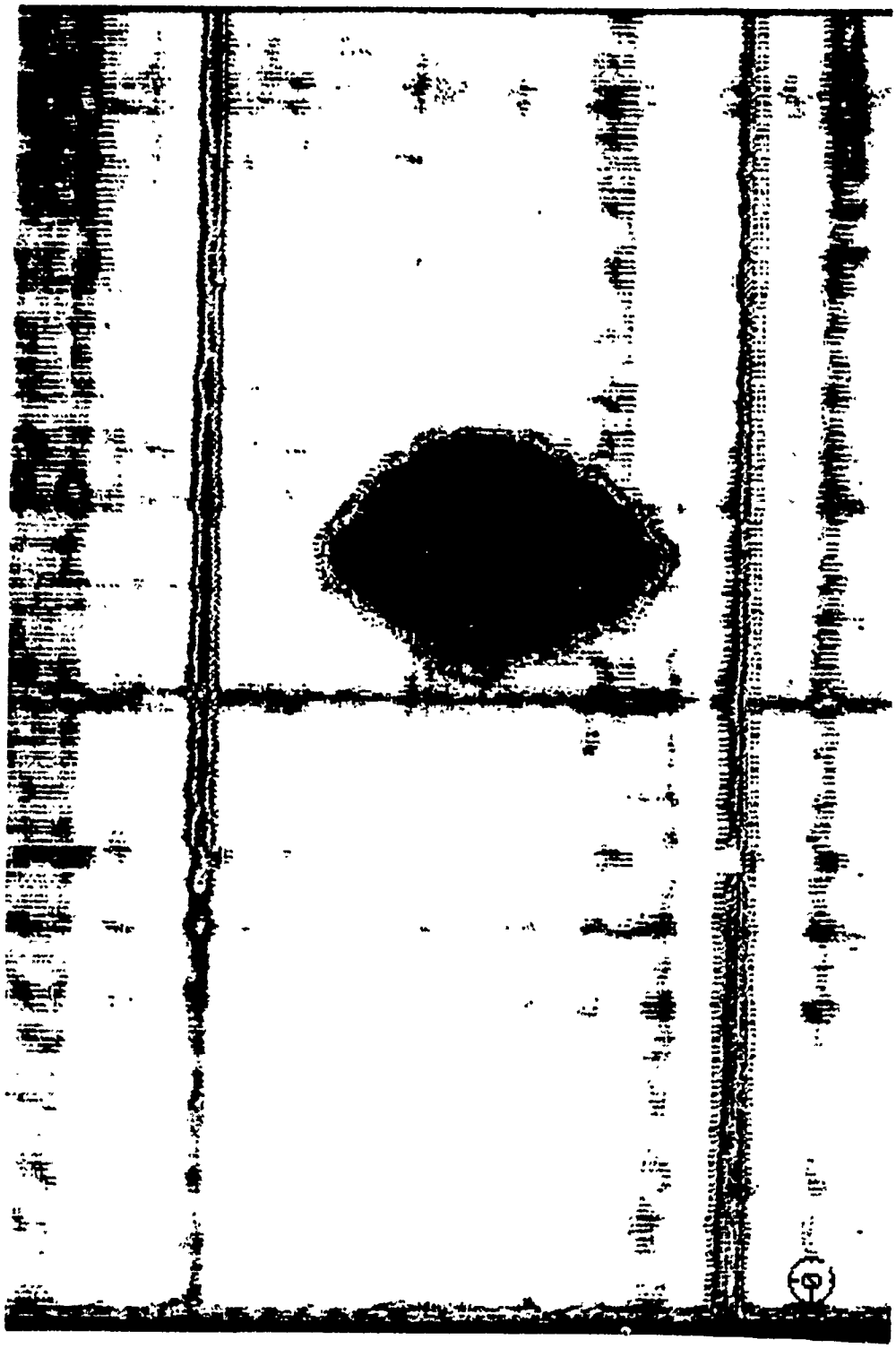

Figure 3.15. C-scan of $[90/0]_{6s}$ Panel, Impact Energy = 4.51 ft-lb

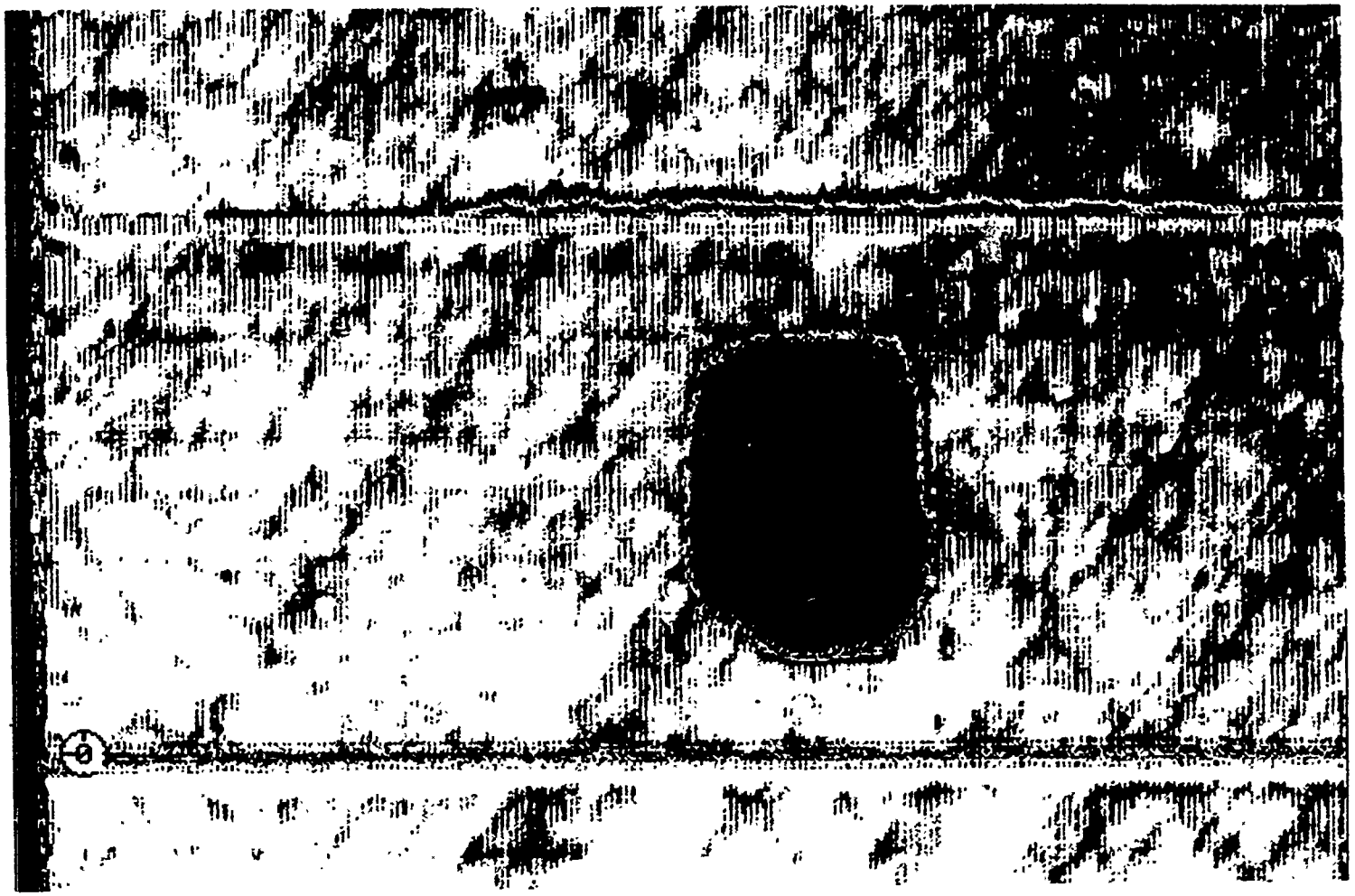

Figure 3.16. C-scan of $[\pm 45]_{6s}$ Panel, Impact Energy = 4.50 ft-lb

The size of the damaged region is greater in the 24-ply panels than in the 12-ply panels. The C-scans, however, show patterns which are the superposition of the vertical projection of all damage in the panel. They give no indication of the depth in the laminate at which damage occurs. The information regarding the depth location where damage is present is obtained from a cross-sectional view of the panel edge.

3.7 Optical Microscopy

The panels which sustained damage were cross-sectioned along the longitudinal axis using a water-cooled diamond saw. The central 3/4 inch area of the panel was removed and potted in epoxy. After curing, the specimens were polished, first with sandpaper and then with diamond paste of increasing fineness down to 1 μm diameter. The samples were photographed with an optical microscope under 50x and higher magnifications.

Photographs of the specimen cross-sections are shown in Figures 3.17 through 3.22. The panels show two modes of damage: delaminations between the individual layers and transverse cracking within the layers. The $[0/90]_{3s}$ panel shows a primary delamination between the fourth and fifth layers from the top surface and a smaller one between the seventh and eighth layers. The panel also shows transverse cracking in the 90 degree plies. The $[90/0]_{3s}$ panel shows a major delamination directly under the first ply from the top of the panel and smaller delaminations between the third and fourth layers, the fifth and sixth layers, the eighth and ninth layers and the tenth and eleventh layers (i.e., on every interface where a 90 degree layer was on top of a 0 degree layer).

The $[\pm 45]_{3s}$ panel shows a complicated pattern of crack branching in which the delaminations cut through layers and continue along a different ply interface.

The 24-ply panels show similar results for the three layups. The $[0/90]_{6s}$ panel shows a pattern of delaminations which form in the center of the panel, become transverse cracks to cut through the 90 degree layers and then continue to the edge of the specimen along the new interface. The main delaminations are between the eleventh and twelfth layers and the eighteenth and nineteenth layers from the top of the panel, but further from the impact point shift to positions between the thirteenth and fourteenth layers and the nineteenth and twentieth layers. The transverse cracks in the layers are oriented at an angle away from the impact point and are more prevalent at the sides of the impact location than directly under the center. The $[90/0]_{6s}$ panel shows a similar pattern, with the primary delamination between the eighteenth and nineteenth layers from the top and smaller delaminations between the seventh and eighth layers, the eleventh and twelfth layers and the thirteenth and fourteenth layers. A large number of angled cracks can also be seen in the 90 degree layers. The $[\pm 45]_{6s}$ panel shows two main delaminations, between the eleventh and twelfth layers and the twentieth and twenty-first layers from the top of the panel. Additional smaller delaminations are observed in the photographs, but they appear larger than they are due to dark residue on the sample surface. A cube of material at the center appears to have failed in a classic shear deformation pattern.

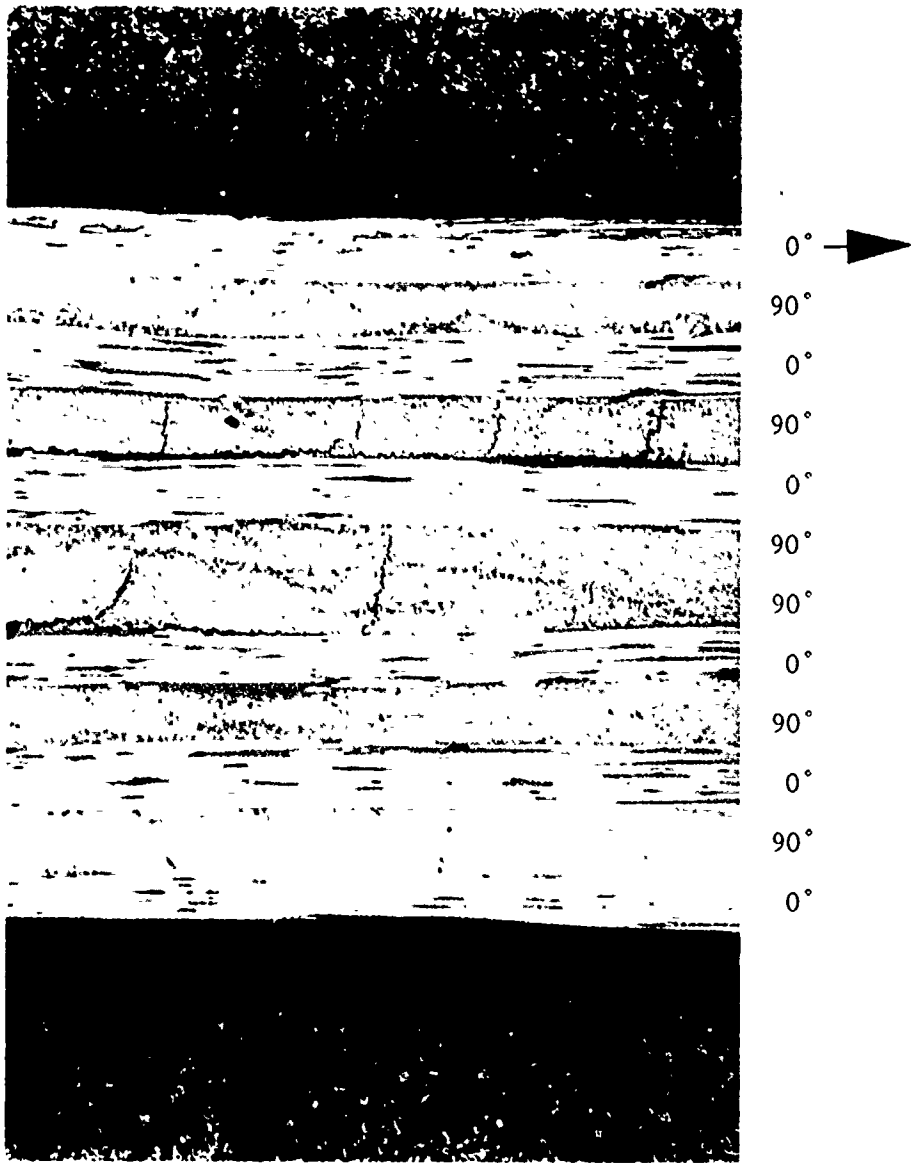


Figure 3.17. View of $[0/90]_{3s}$ Cross-section Beneath Impact Point, 50x Magnification

Figure 3.18. View of $[90/0]_{3s}$ Cross-section Beneath Impact Point, 50x Magnification

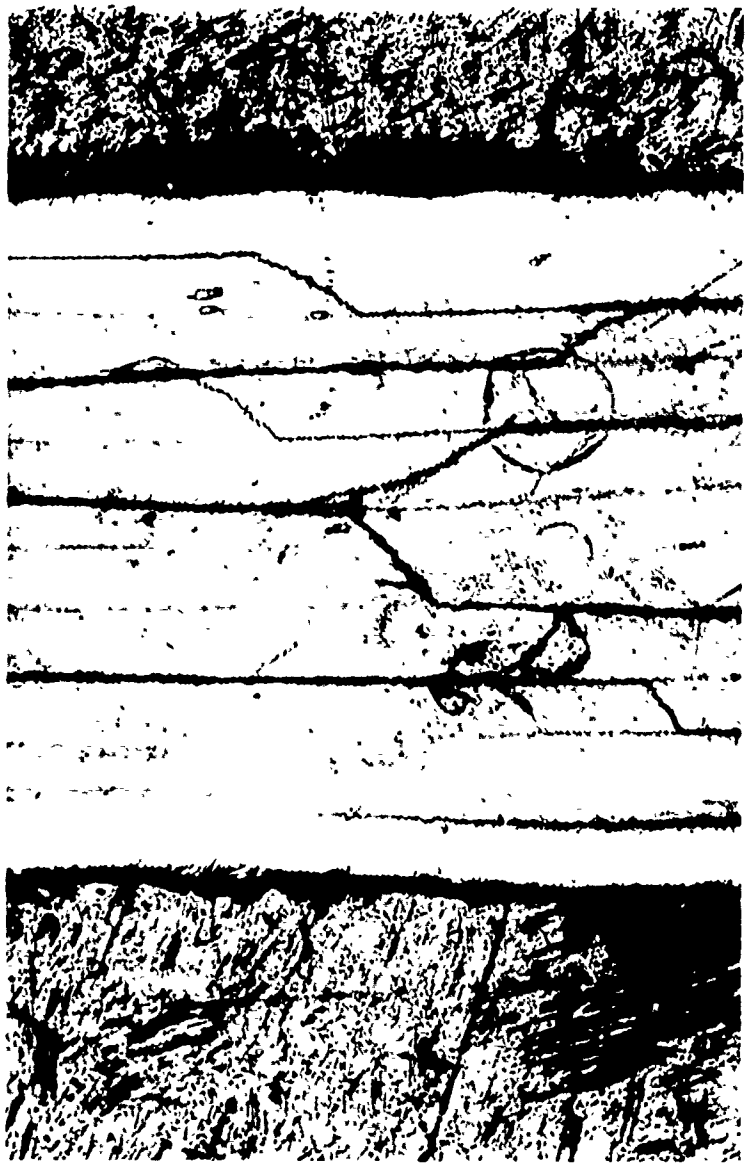

Figure 3.19. View of $[\pm 45]_{3s}$ Cross-section Beneath Impact Point, 50x Magnification

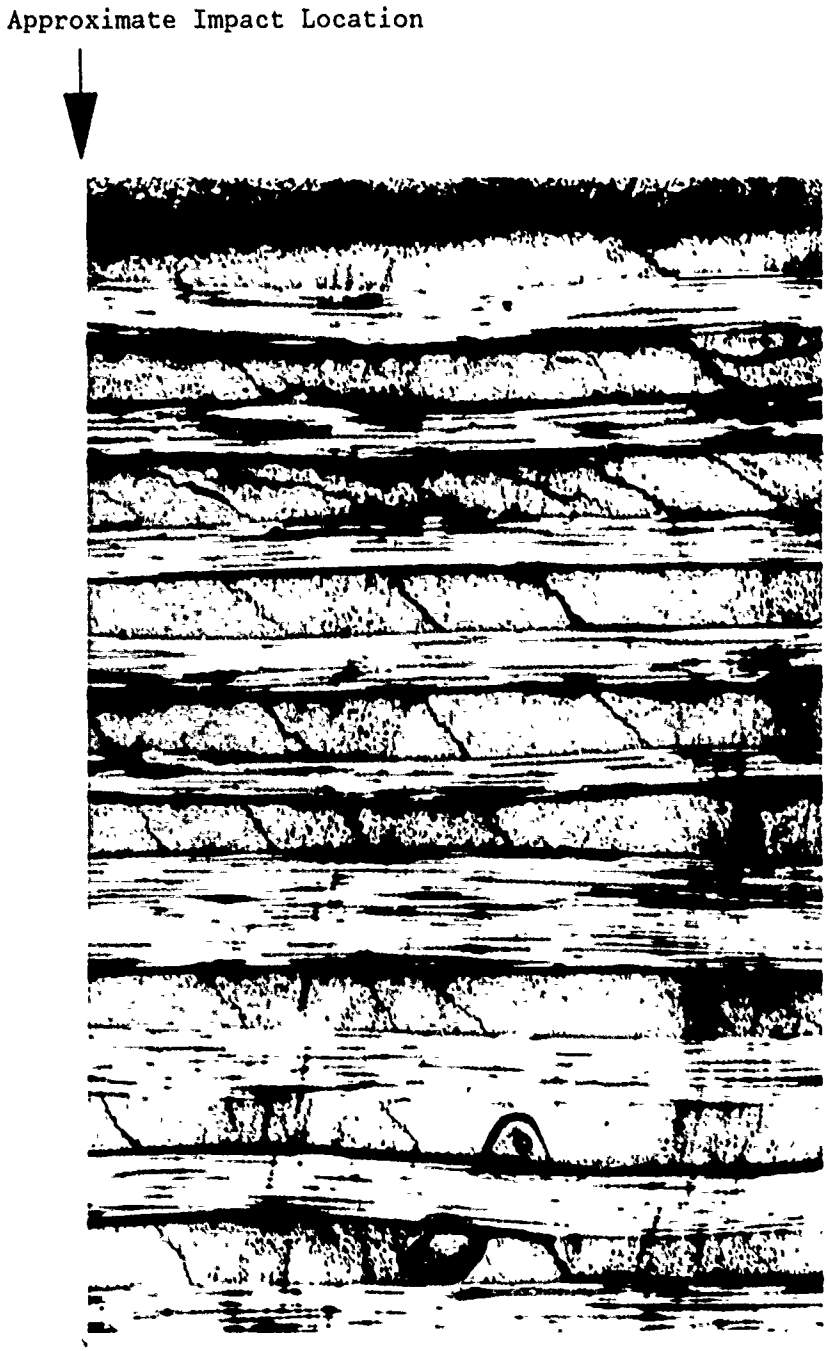


Figure 3.20. View of $[0/90]_{6s}$ Cross-section at Side of Impact Point, 50x Magnification

Figure 3.21. View of $[90/0]_{6s}$ Cross-section Beneath Impact Point, 50x Magnification

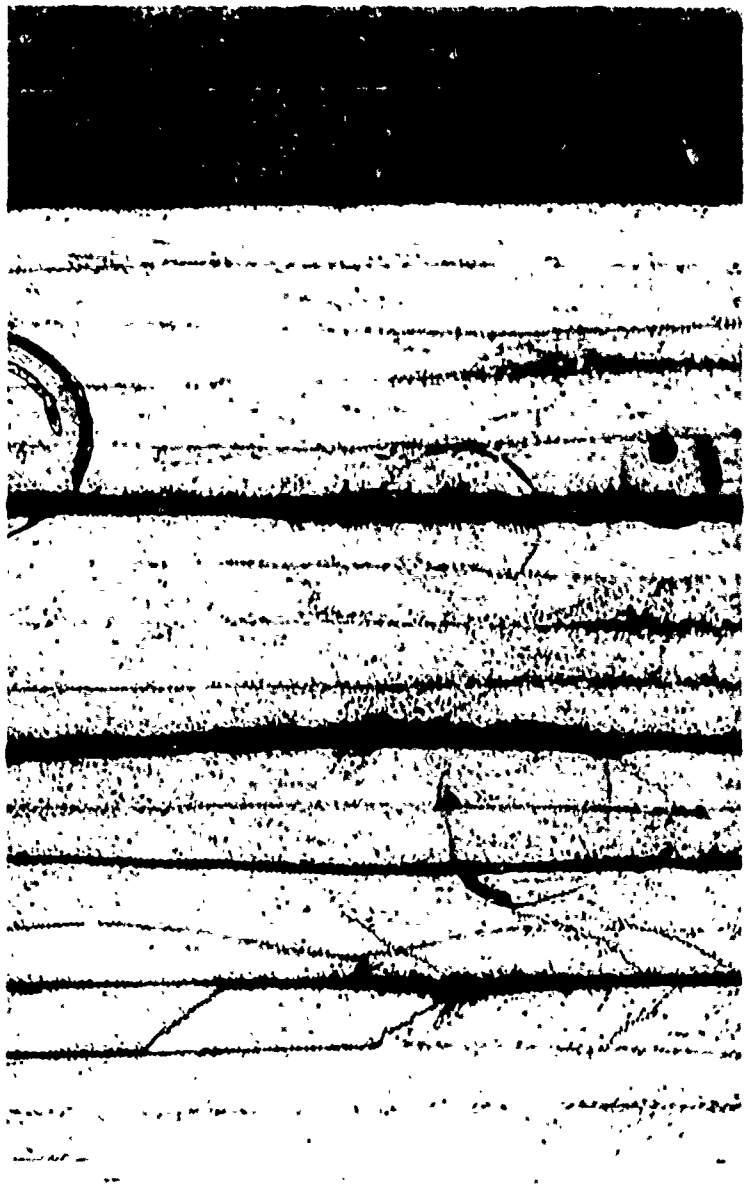

Figure 3.22. View of $[\pm 45]_{6s}$ Cross-section Beneath Impact Point, 50x Magnification

In summary, the panel damage appears to be a combination of delaminations and transverse cracks. For the panels with 0 and 90 degree plies, the delaminations occur along the interface between a 90 degree and 0 degree ply and are larger in area in layers near the back of the panel. The transverse cracks occur only in the 90 degree layers, which is reasonable given their relatively low transverse stiffness and strength. Similar cracks might by expected in the 0 degree layers if a cross-section were taken along the circumferential direction. For the panels containing layers at ±45 degrees, there is a larger number of transverse cracks and delaminations, which appear to interact in crack propagation. In the $[\pm 45]_{ns}$ panels, an overall pattern is not discernable. However, this could be influenced by the fact that the cross-section was not taken along one of the material principal axes.

## 3.8 Summary

Measurements of the load, displacement and strain were obtained for tests from impact energies of 0.5 to 4.5 ft-lb. The impact energies needed to cause damage to six different ply layups were determined. The deflections at failure indicate the need for analysis using a nonlinear model incorporating transverse shear. C-scans and optical microscopy indicate that delaminations occur at interfaces where the fibers are in different directions above and below the delamination. Transverse cracking is observed in the 90 degree layers as well.

# IV. Analysis

In analyzing experiments under impact loading, a dynamic model is needed to solve for the deflections and strains as functions of time. For composites, where shear deformation can be very important, incorporation of the transverse shear terms $\tau_{xz}$ and $\tau_{yz}$ in the solution is necessary for accurate stress solutions.

## 4.1 Background

Previous analyses incorporating transverse shear have been applied primarily to flat plates. Whitney and Pagano (23) applied the bending equations derived by Yang, Norris and Stavsky (25), including transverse shear deformation, for anisotropic laminated plates for simply supported and hinged/free boundry conditions. Dobyns (6) derived solutions based on Whitney and Pagano's work for the simply supported orthotropic flat plate for both static and dynamic loads, assuming that the loading function was given from instrumentation. Rankumar and Thakar (18) used Donnell approximations and a Fourier series expansion in their dynamic analysis to find the radial displacement for a simply supported cylindrical panel under a distributed force. These analyses all assumed that the loading function was a given quantity.

Other analyses have incorporated calculation of the force on the panel as a function of time to form a coupled set of nonlinear equations. Sun and Chattopadhyay (21) calculated the contact force from the Hertz law for a specially orthotropic hinged flat rectangular laminated plate. Christoforou and Swanson (3) produced a closed form solution by linearizing the contact force equations applied to a simply

supported graphite/epoxy flat plate. Qian and Swanson (17) used both the Rayleigh Ritz method and an analytical approach based on Laplace transformations to analyze a simply supported, square composite plate. Newmark integration was used to solve the dynamic equations.

Christoforou and Swanson originally were concerned with a very small impact mass (8.4g). However, they found that by increasing the impactor mass substantially, the response is approximated as "quasi-static", or the behavior exhibited by a spring-mass system (i.e., sinusoidal) with the plate stiffness and impactor mass predominately influencing the equations (3). All of the previous analyses incorporate shear correction factors in the equations based on the Reissner-Mindlin plate equations to satisfy equilibrium.

4.2 Analysis Methodology

Approaches to the solution of nonlinear geometric problems incorporating transverse shear deformation without the use of shear correction factors have been investigated by Reddy (19) and Dennis (5). The static solution derived by Dennis has been incorporated into a dynamic analysis by Tsai and Palazotto (22). This method has been used in the analysis of the experimental data.

Dennis' approach assumes a parabolic transverse shear strain distribution through the thickness, satisfying the requirement that the transverse shear strains be zero at the upper and lower surfaces. The analysis neglects the normal stress $\sigma_{zz}$ based on order of magnitude arguments in comparison with $\tau_{xz}$ and $\tau_{yz}$ for thin shells.

The derivation of the stress-strain relationship for the lamina follows the discussion in Jones (11:34-37). The lamina is assumed to be

transversely isotropic relative to the 2-3 plane. By also assuming $\sigma_{zz} = 0$, but retaining the $\tau_{xz}$ and $\tau_{yz}$ terms, the stress-strain relation reduces to

$$\begin{Bmatrix} \sigma_1 \\ \sigma_2 \\ \tau_{23} \\ \tau_{13} \\ \tau_{12} \end{Bmatrix} = \begin{bmatrix} Q_{11} & Q_{12} & 0 & 0 & 0 \\ Q_{12} & Q_{22} & 0 & 0 & 0 \\ 0 & 0 & Q_{44} & 0 & 0 \\ 0 & 0 & 0 & Q_{55} & 0 \\ 0 & 0 & 0 & 0 & Q_{66} \end{bmatrix} \begin{Bmatrix} \epsilon_1 \\ \epsilon_2 \\ \epsilon_4 \\ \epsilon_5 \\ \epsilon_6 \end{Bmatrix} \qquad (4.1)$$

where $\sigma_1$, $\sigma_2$ and $\sigma_6$ are the in-plane longitudinal, tangential and shear stresses, $\sigma_4 = \tau_{23}$ and $\sigma_5 = \tau_{13}$ are the transverse shear stresses, $\epsilon_1$ and $\epsilon_2$ are the in-plane strains in the fiber direction and tangential to the fiber direction, $\epsilon_4 = \gamma_{23}$ and $\epsilon_5 = \gamma_{13}$ are the engineering transverse shear strains ($\gamma_{23} = 2\,\epsilon_{23}$), and $\epsilon_6 = \gamma_{12}$ is the in-plane engineering shear strain. The coefficients of the matrix [Q] are as follows:

$$Q_{11} = E_1 / (1 - \nu_{12}\nu_{21})$$
$$Q_{12} = \nu_{21}E_2 / (1 - \nu_{12}\nu_{21})$$
$$Q_{22} = E_2 / (1 - \nu_{12}\nu_{21})$$
$$Q_{44} = G_{23};\quad Q_{55} = G_{13};\quad Q_{66} = G_{12}$$

where the terms $E_1$, $E_2$ and $\nu_{12}$ are the longitudinal and tangential moduli and the in-plane Poisson's ratio, $\nu_{21} = \nu_{12}E_2 / E_1$ and $G_{12}$, $G_{13}$ and $G_{23}$ are the shear moduli in the 1-2, 1-3 and 2-3 planes, respectively.

The strain-displacement relationships used in the analysis are the Donnell cylindrical shell relations at the midplane. The expressions derived by Dennis (5: 331-332) based on the Donnell approximations are as follows:

$$\varepsilon_x = \frac{\partial u}{\partial x} + \zeta \frac{\partial \psi_x}{\partial x} + \zeta^3 k \left( \frac{\partial^2 w}{\partial x^2} + \frac{\partial \psi_x}{\partial x} \right) + \frac{1}{2} \frac{\partial^2 w}{\partial x^2} \tag{4.2}$$

$$\varepsilon_s = \frac{\partial v}{\partial s} - \frac{w}{R} + \zeta \left( \frac{\partial \psi_s}{\partial s} - \frac{\frac{\partial v}{\partial s}}{R} \right) + \zeta^3 k \left( \frac{\partial \psi_s}{\partial s} + \frac{\partial^2 w}{\partial s^2} \right) + \frac{1}{2} \frac{\partial^2 w}{\partial s^2} \tag{4.3}$$

$$\varepsilon_{xs} = \frac{\partial u}{\partial s} + \frac{\partial v}{\partial x} + \zeta \left( \frac{\partial \psi_x}{\partial s} + \frac{\partial \psi_s}{\partial x} - \frac{\frac{\partial v}{\partial x}}{R} \right) + \zeta^3 k \left( 2 \frac{\partial^2 w}{\partial x \, \partial s} + \frac{\partial \psi_x}{\partial s} + \frac{\partial \psi_s}{\partial x} \right) + \frac{\partial w}{\partial x} \frac{\partial w}{\partial s} \tag{4.4}$$

and the transverse shear strains are given by

$$\varepsilon_4 = \left( \frac{\partial w}{\partial s} + \psi_s \right) + 3 \zeta^2 k \left( \frac{\partial w}{\partial s} + \psi_s \right) \tag{4.5}$$

$$\varepsilon_5 = \left( \frac{\partial w}{\partial x} + \psi_x \right) + 3 \zeta^2 k \left( \frac{\partial w}{\partial x} + \psi_x \right) \tag{4.6}$$

where u, v and w are the displacements in the x, s and $\zeta$ cylindrical coordinate system, $\psi_x$ and $\psi_s$ are the components of rotation not due to

transverse shear deformation, $\zeta$ is the distance from the midplane measured positive toward the center of the radius of curvature, R is the radius of curvature and $k = -4/3h^2$ is a thickness parameter.

The finite element formulation is based on the 36-DOF shell element shown in Figure 4.1, allowing both rigid body and shear components of rotation at the corner nodes. The solution algorithm developed by Dennis is applied by Tsai and Palazotto to dynamic problems by use of Hamilton's principle to satisfy equilibrium on the potential energy $\Pi_p$, such that

$$\delta \int_{t_1}^{t_2} (E - T - W_e)dt = 0 \tag{4.7}$$

where E contains the strain energy, energy loss due to damping, and the body force energy term, T is the kinetic energy and $W_e$ is the work from external forces. For a shell composed of L layers, the three terms in the variation become (22)

$$\delta E = \int_{\Omega} \sum_{k=1}^{L} \int_{\zeta_{k-1}}^{\zeta_k} \left( \sigma_{ij}^{(k)} \delta \varepsilon_{ij}^{(k)} + c^{(k)} v_j^{(k)} \delta v_j^{(k)} + P_j^{(k)} \delta u_j^{(k)} \right) d\zeta \, d\Omega \tag{4.8}$$

$$\delta T = \int_{\Omega} \sum_{k=1}^{L} \int_{\zeta_{k-1}}^{\zeta_k} \rho^{(k)} v_j^{(k)} \delta u_j^{(k)} \, d\zeta \, d\Omega \tag{4.9}$$

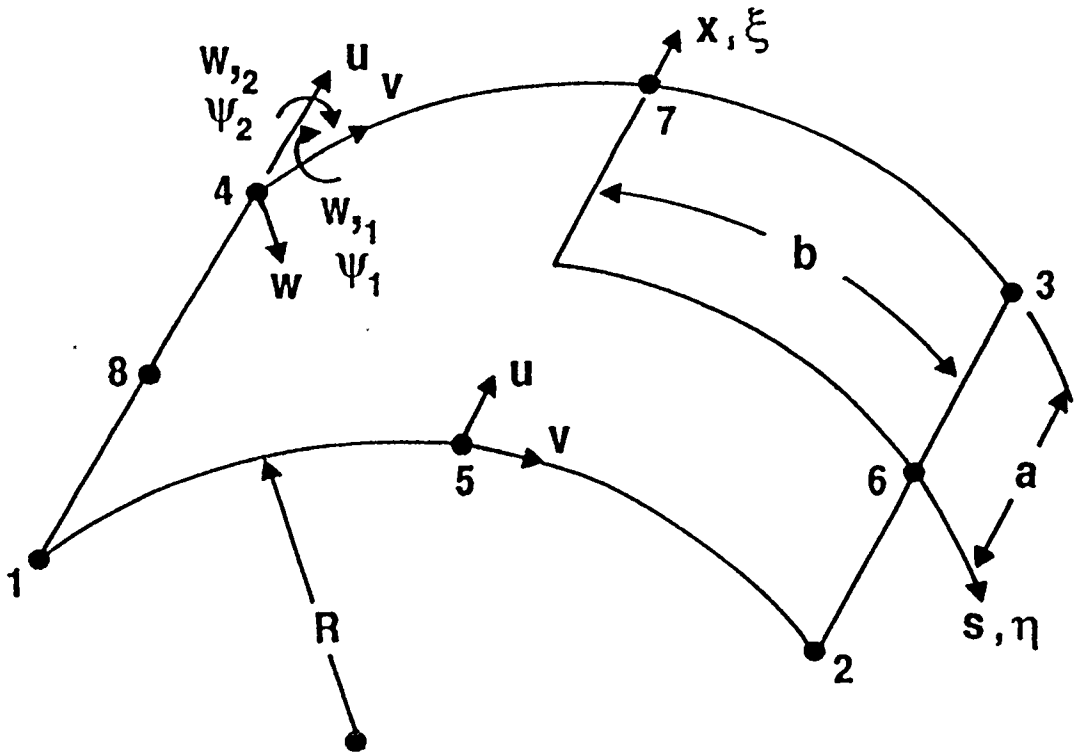


Figure 4.1. Thirty-six DOF Shell Element

and

$$\delta W_e = \int_{\Omega} F_j \delta u_j \, d\Omega = 0 \tag{4.10}$$

where i and j are indices which vary from 1 to 3, $\zeta_{k-1}$ and $\zeta_k$ are the positions of the bottom and top surfaces for the kth layer, $\sigma_{ij}^{(k)}$, $\delta\epsilon_{ij}^{(k)}$, $P_j^{(k)}$, $\delta u_j^{(k)}$, $v_j^{(k)}$, $\rho^{(k)}$, $c^{(k)}$ are (for the kth layer) the stress tensor, variation of the strain tensor, body force vector, variation of the displacement vector, the velocity vector, mass density and damping coefficient. $F_j$ is the vector of applied forces. The summation is over L layers of the laminate and $\Omega$ is the surface area integral of the neutral surface. In our analysis, damping and body forces have been neglected, considerably simplifying the strain energy term (Equation 4.8).

The finite element formulation obtained from Equations 4.7 - 4.10 follows the form

$$[M]\{\ddot{u}\} + [C]\{\dot{u}\} + [K]\{u\} = \{P(t)\} \tag{4.11}$$

However, the global stiffness matrices incorporate terms up to quadratic in displacement. The stiffness matrix [K] is given by (5)

$$[K] = [K_0 + N_1/2 + N_2/3] \tag{4.12}$$

where $K_0$ is an array of constant coefficients, $N_1$ is an array of coefficients that are linear in displacement, $N_2$ is an array of coefficients that are quadratic in displacement, P(t) is a column of loads at the nodes, and {u} is a column of nodal displacements (and rotations).

Force-displacement equilibrium is iteratively solved by the Newton-Raphson method. Newmark integration was used as the time-marching method of integration in all analyses.

4.3 Numerical Results

Analysis of several tests were performed to compare the strains and displacements to experimental results. Because of the limitations on computer speed and memory, only two of the laminates were investigated, the $[0/90]_{3s}$ and $[\pm 45]_{3s}$.

For the $[0/90]_{3s}$ panels (12-ply), only one quadrant of the test area needed to be modeled, since the twisting coefficients $A_{16}$, $A_{26}$, $D_{16}$ and $D_{26}$ are zero for laminates containing only plies with fibers aligned in the 0 and 90 degree directions. An example case was run with 4 by 4, 6 by 6 and 8 by 8 grids of square elements. The difference between the 4 by 4 and 6 by 6 grids was less than 10 percent, whereas the difference between the 6 by 6 and 8 by 8 grids was less than 2 percent. Based on these comparisons, the 8 by 8 grid (0.3125 inch element size) was deemed adequate for analysis of these tests.

For the $[\pm 45]_{3s}$ test, it was necessary to model the full panel. This is because the bending-twisting coefficients $D_{16}$ and $D_{26}$ are not

zero, so the deflection pattern in the panel will not be symmetric in the four quadrants. The element size was kept constant and the total number of elements was quadrupled to 256.

The time step size used was 0.05 ms. It was found that use of a time step of 0.1 ms occasionally produced inaccuracies leading to unstable results causing nonconvergence and program termination. The 0.05 ms time step produced identical results to the 0.02 ms time step, indicating that it was small enough to maintain accuracy in the results.

Other parameters included in the analysis include the following:

Mass density: 1.5088 E-04 slugs / $in^3$

Ply thickness: 0.005 in

$E_1$ = 20.46 E+06 $lbf/in^2$

$E_2$ = 1.34 E+06 $lbf/in^2$

$G_{12}$= 0.8638 E+06 $lbf/in^2$

$G_{13}$= 0.8638 E+06 $lbf/in^2$

$G_{23}$= 0.4319 E+06 $lbf/in^2$

$\nu_{12}$= 0.3131

The load was applied as a point force at the panel center. Material outside the 5 by 5 inch opening was neglected for both clamped and hinged boundary conditions. The boundary conditions are defined as follows:

Clamped:

along x = 0, symmetry B.C.: $u = w_{,x} = \psi_x = 0$

along s = 0, symmetry B.C.: $v = w_{,s} = \psi_s = 0$

along x = +2.5, geometric B.C.: $u = v = w = w_{,s} = \psi_s = \psi_x = 0$

along s = +2.5, geometric B.C.: $u = v = w = \psi_s = w_{,x} = \psi_x = 0$

Hinged:

along x = 0, symmetry B.C.: $u = w_{,x} = \psi_x = 0$

along s = 0, symmetry B.C.: $v = w_{,s} = \psi_s = 0$

along x = +2.5, geometric B.C.: $u = v = w = w_{,s} = \psi_s = 0$

along x = +2.5, geometric B.C.: $u = v = w = w_{,x} = \psi_x = 0$

where ,x and ,s denote derivatives with respect to x and s. Note that shear rotation was permitted at the geometric boundaries for both clamped and hinged cases.

From preliminary results of the model, it has been found that the Donnell shell approximations (7) are adequate to describe the deflection of a composite shell under impact loads far greater than those required to produce material failure. Comparisons with the full nonlinear solution allowing large rotations and displacements were almost identical. For an impact load of 800 lb, the rotations predicted by the analysis did not exceed 11 degrees. Maximum rotations occurred along the longitudinal axis. This is near the upper limit for validity of the Donnell equations. However, as noted by Dennis (5:175,250), when the Donnell equations are applied to a finite element formulation, the resulting analysis can be accurate beyond the applicable range of the

Donnell equations for the entire structure. Since the loads never exceed 300 lb in the actual tests, the rotations will be very small, so Donnell approximations should be accurate for the test conditions.

Three of the $[0/90]_{3s}$ tests were selected for analysis. The tests were those in which the impactor was dropped 1, 2 and 3.5 inches. The corresponding impact energies are 0.55, 1.14 and 1.89 ft-lb. Damage was produced on the 1.89 ft-lb test, so this is a good case for comparison. The maximum displacements at the panel center are shown in Table 4.1, for both clamped and hinged analytical solutions and the experimental measurement from the MTI-1000 Fotonic Sensor.

Table 4.1. Center Deflections of $[0/90]_{3s}$ Panel Under Impact Loading

| Impact Energy (ft-lb) | Maximum Load (lb) | Peak Deflections (in) |
|---|---|---|
| 0.55 | 152 | 0.064 (Experimental)<br>0.0645 (Analysis - Hinged)<br>0.0552 (Analysis - Clamped) |
| 1.14 | 216 | 0.093 (Experimental)<br>0.0954 (Analysis - Hinged)<br>0.0836 (Analysis - Clamped) |
| 1.89 | 262* | 0.131 (Experimental)<br>0.1217 (Analytical - Hinged)<br>0.1090 (Analytical - Clamped) |

* Peak load would have been 280 lb if the panel had not been damaged. Deflections reported at time of damage.

The results are graphically shown in Figure 4.2. At the time that the third panel was damaged, the center deflection was almost exactly half the height from the panel top to its edge. The hinged boundary

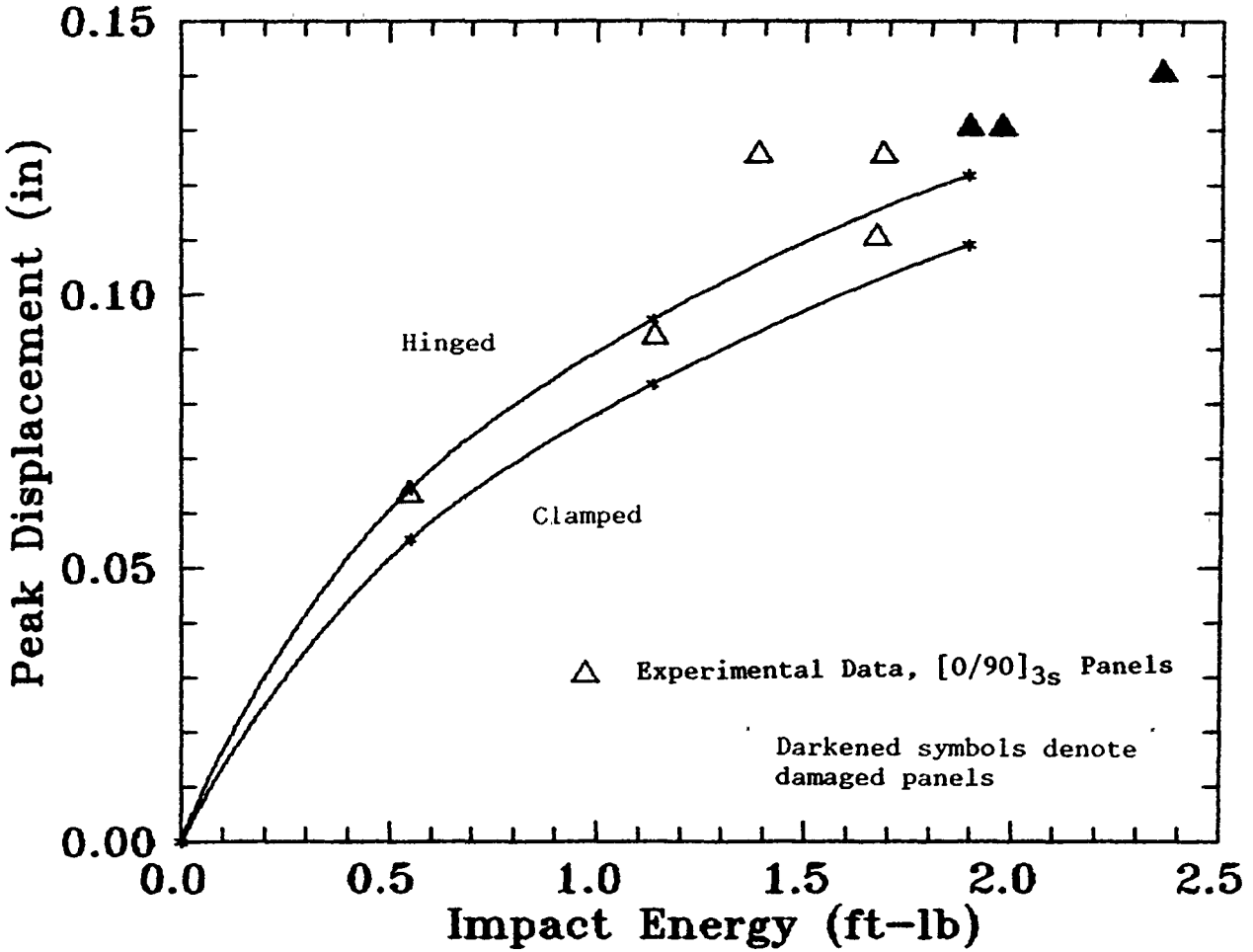


Figure 4.2. Experimental and Analytical Displacements

conditions provide a good comparison with the experimental data. Thus, the hold-down plate may be keeping the panel from pulling out from under it, but in a dynamic sense, the clamping action fails to restrict rotation. Considering the relative stiffness of the materials, this appears reasonable.

In Figure 4.3, the radial displacement contours are shown for the $[0/90]_{3s}$ panel test section at the time of failure, obtained from the analysis. Lines of zero radial displacement are seen to occur at approximately 1/4 the test section width. Within this area, the deflection is inward (positive w), whereas outside the region the displacement is negative in the radial direction. This is more easily visualized in Figure 4.4, where the deformed geometry at the time of damage is shown after conversion to Cartesian coordinates.

The peak tensile stress in the panel occurs on the bottom layer directly beneath the impact point. The maximum tensile stress calculated in the test producing damage is 189 ksi. This is still less than the material ultimate strength, so no fiber breakage is expected. The experiments showed no surface damage at all on either the bottom or top surface. However, the circumferential (or hoop) stress in the 0 degree layer is approximately 19 ksi at the panel center, as shown in Figure 4.5. This is over twice the material transverse strength, so transverse failure of the layer is expected. This would be similar to the damage observed in the 90 degree layers from the cross-sectioned specimens. The hoop stress drops off rapidly, however, so that the region over which this occurs is less than 1/2 inch in diameter.

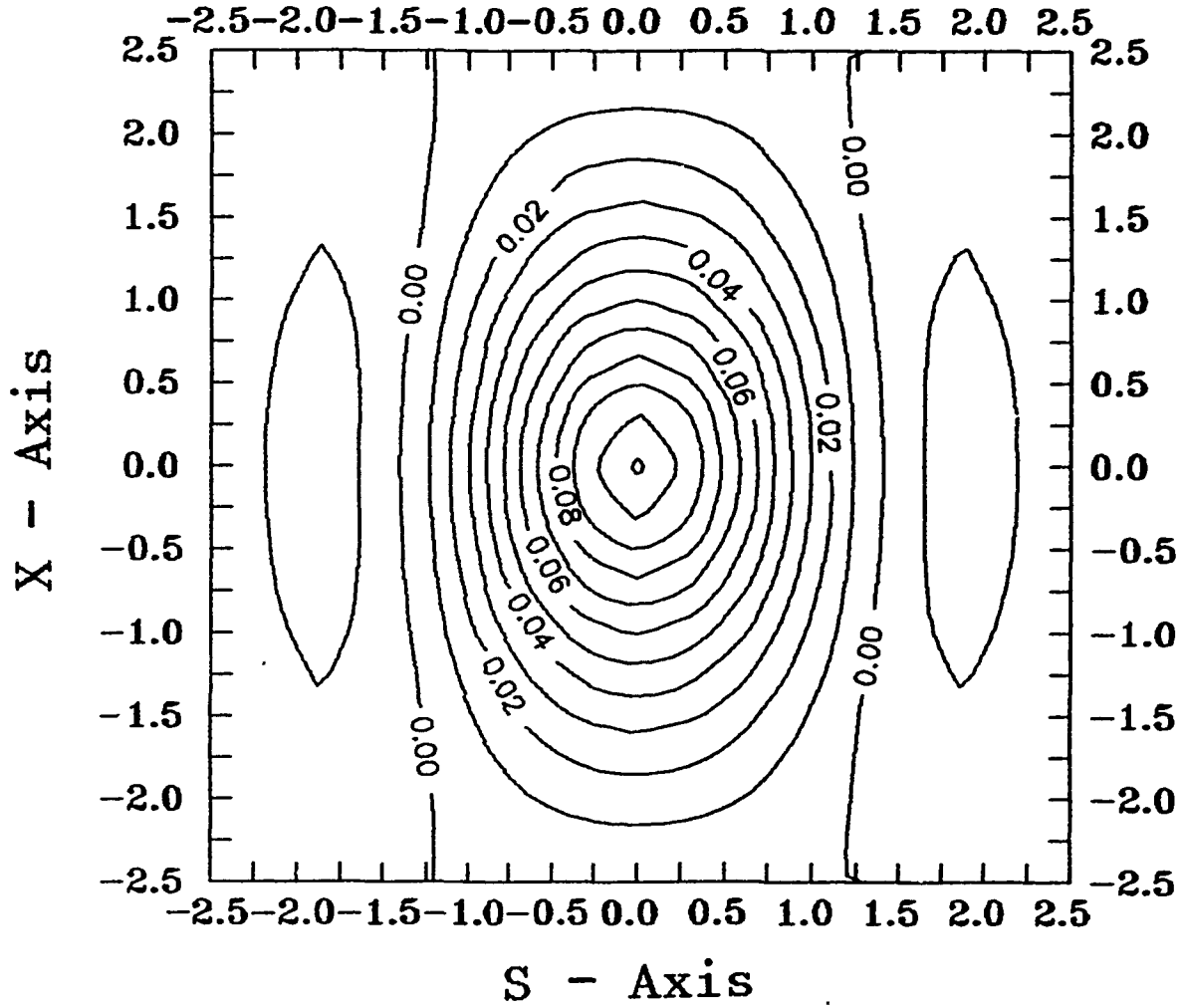


Figure 4.3. Radial Displacement Contours for $[0/90]_{3s}$ Panel at Failure Load of 262 lb

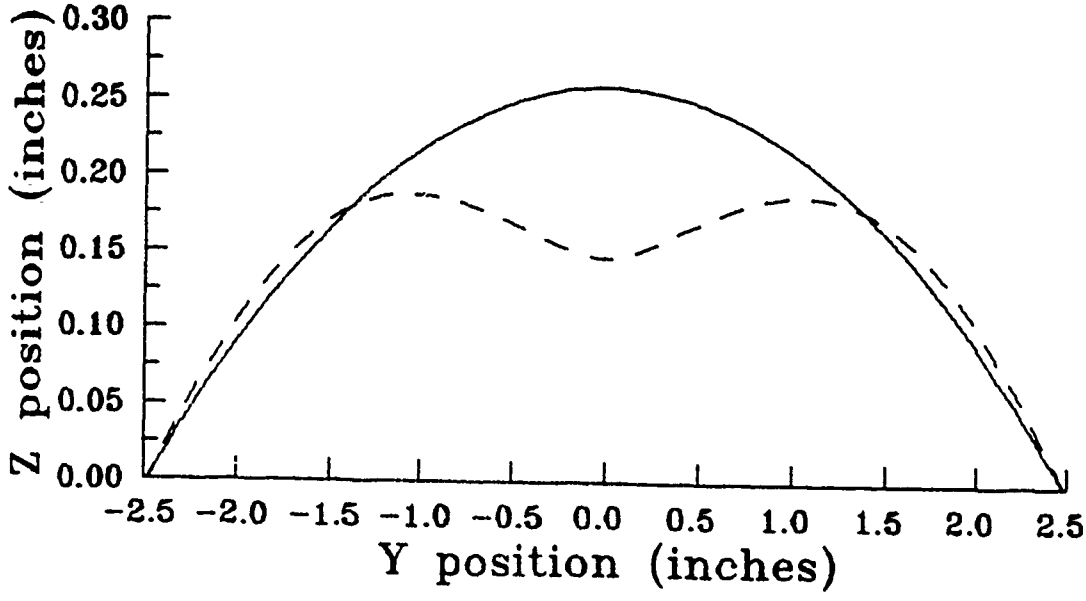


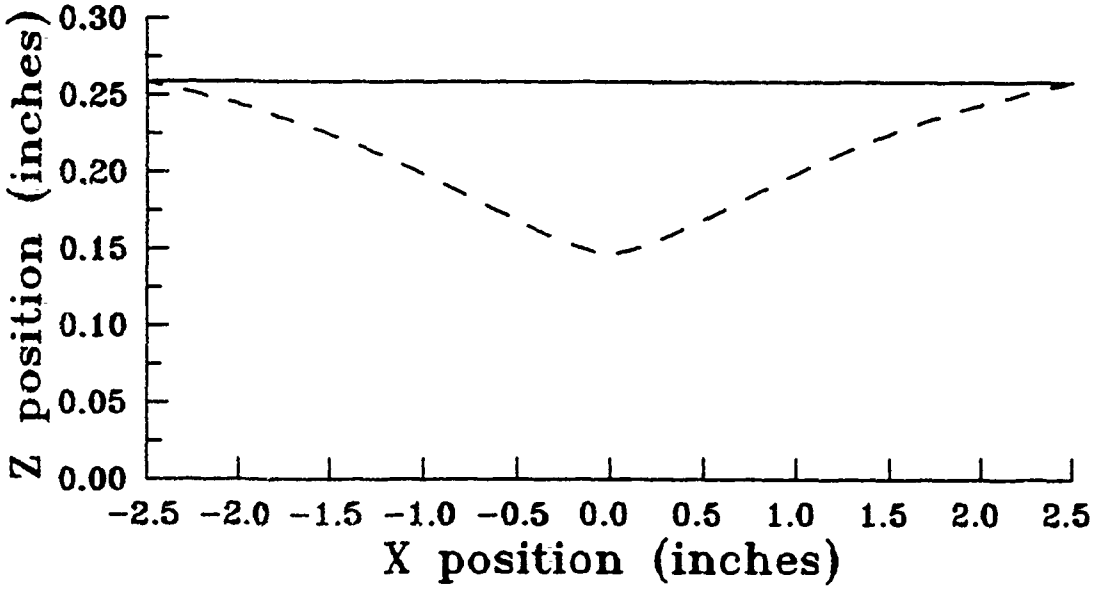


Figure 4.4. Deformed Geometry of $[0/90]_{3s}$ Panel at Time of Failure

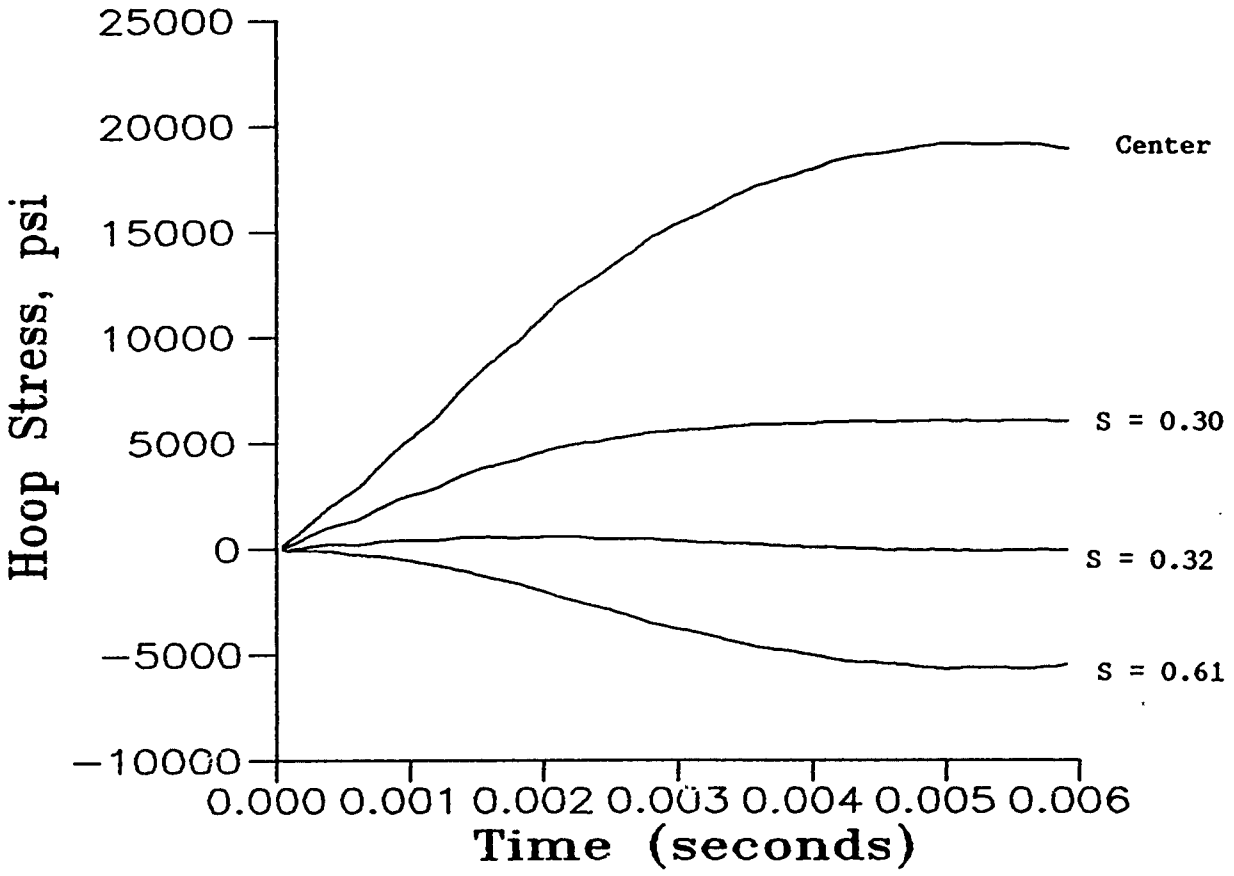


Figure 4.5. Hoop Stress on Bottom Surface of $[0/90]_{3s}$ Panel

One $[\pm 45]_{3s}$ panel was analyzed as well. For the ±45 ply layup, it is necessary to model the entire panel, since the deflection is not symmetric in the four quadrants. A 16 by 16 element model was used, with clamped boundary conditions applied on all four edges and the load applied as a point force at the panel center. Results of the analysis are shown in Table 4.2 for the peak deflection.

Table 4.2. Center Deflection for the $[\pm 45]_{3s}$ Panel

| Impact Energy (ft-lb) | Maximum Load (lb) | Peak Deflection (in) |
|---|---|---|
| 1.91 | 265 | 0.134 (Experimental) |
| | | 0.109 (Analysis - Clamped) |

A contour map of radial contours is shown in Figure 4.6 for this test for the load at the time of damage. It is expected that the hinged boundary conditions would prove more accurate in predicting the peak deflection. Additional analyses should be performed to determine the accuracy of the analysis for other conditions.

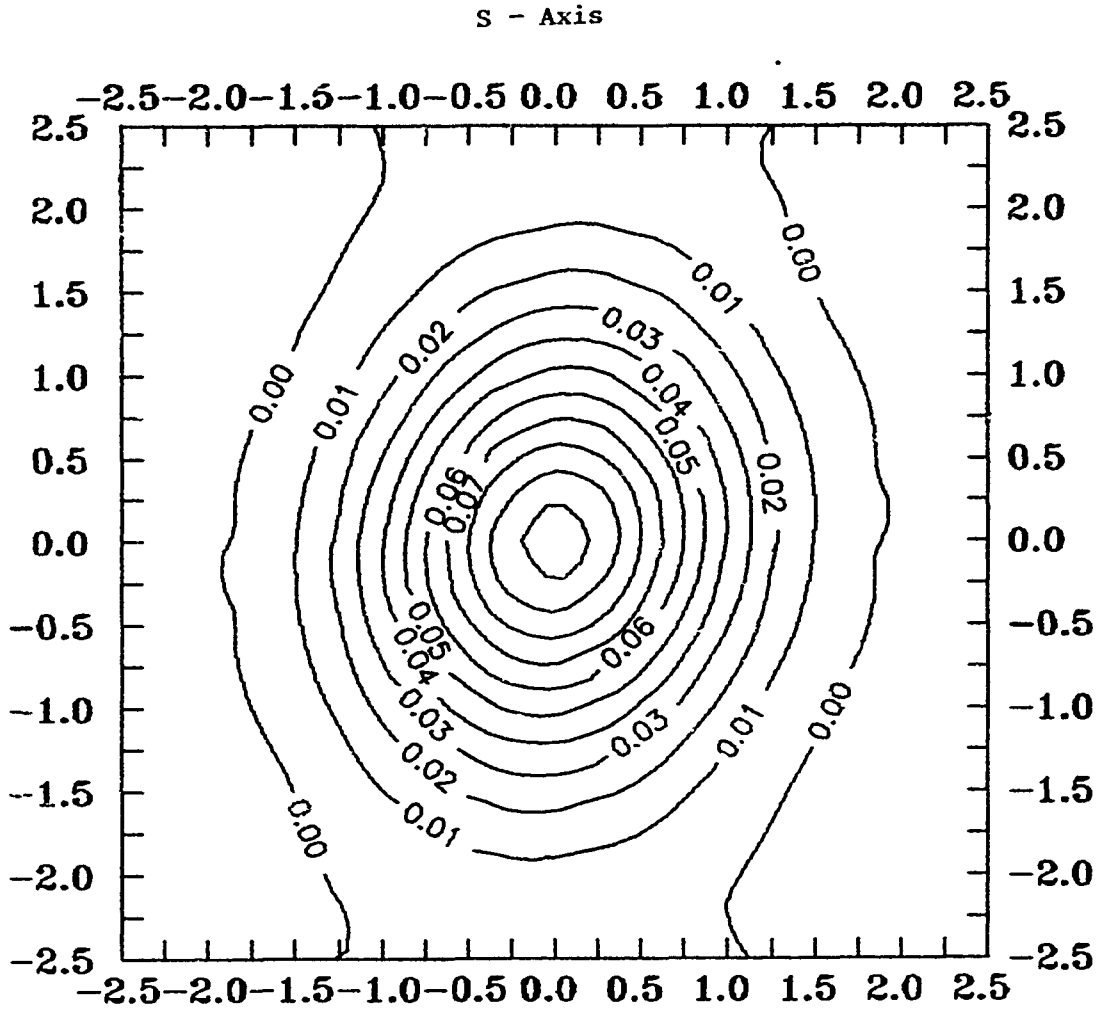


Figure 4.6. Radial Displacement Contours for $[\pm 45]_{3s}$ Panel at Maximum Load

## V. Conclusions

Impact damage in graphite/epoxy panels occurs initially from transverse cracking and delaminations. Only at much higher impact energies is it necessary to consider surface damage and fiber failure. The impact energies necessary to produce damage in 12-ply panels can be less than 2 ft-lb. For 24-ply panels, damage occurs in the range of 4-5 ft-lb.

Damage can be characterized by C-scan and optical microscopy of panel cross-sections. The C-scans indicate the general shape of the damage, whereas the cross-sections identify the layers (or interfaces) in which the damage is present. Damage in the form of transverse cracks is prevalent in all ply layups studied. Delaminations occur at interfaces where the directional stiffness changes (by a change in ply angle).

The deflections of the panel which correlate with the impact energies necessary to cause damage are approximately 1.5 to 2 times the thickness of the panel for the 12-ply and 0.8 times the thickness for 24-ply panels.

The deflections have been measured using a noncontacting optical sensor with overall success. The deflections could be measured accurately up to the time of failure.

A dynamic finite element model incorporating nonlinear geometry and transverse shear deformation predicted the peak deflections of the panel accurately by treating the boundary conditions as hinged. Although clamped boundary conditions were not obtained, the panel edges were restrained from in-plane motion.

## Appendix A: Autoclave Cycle for AS4/3501-6 Graphite/Epoxy

1. Apply full vacuum, 25" Hg minimum, and 85 psi internal pressure to the autoclave.

2. Heat air to 240 ± 5°F, in 30 minutes.

3. Hold the part at 240 ± 5°F, 85 psi and full vacuum for 60 minutes.

4. Increase the pressure to 100 psi and vent the vacuum.

5. Heat air to 350 ± 5°F in 30 ± 5 minutes.

6. Hold the part at 350 ± 5°F and 100 psi for 120 minutes.

7. Cool the part below 150°F in 120 minutes while maintaining 100 psi.

8. Vent the pressure and open the autoclave.

## Appendix B: Experimental Data

Included in the Appendix are plots of all data collected during the experimental test series. For each test, three figures are shown. The first figure gives the load-time relationship (solid line) and the energy-time relationship (dashed line) derived by numerical integration from the initial velocity and the integrated impulse measured and recorded from the Dynatup impact test fixture. The energy value at the end of the load is the residual or absorbed energy. The second plot shows the displacement-time function similarly derived by numerical integration of the velocity. Positive time begins for these plots at the initiation of the load function.

The third figure for each test is a composition of plots showing the strain gage response and the deflection based on the MTI Fotonic Sensor optical probe. Positive time for these plots begins at the time the photoelectric eye on the velocity flag is first occluded by the falling impactor. The methods by which these data were collected and analyzed are discussed in the main body of the thesis.

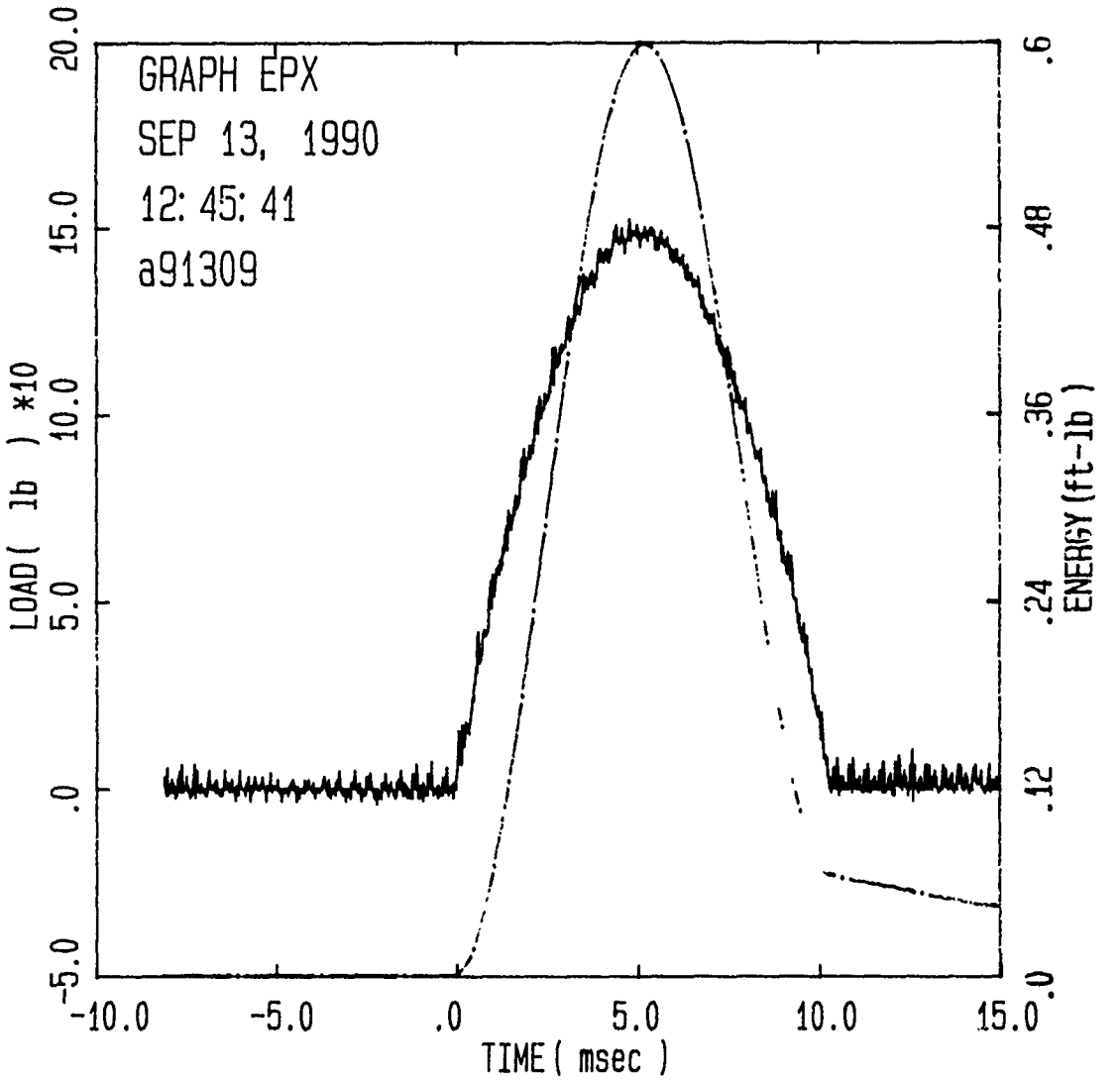


| Specimen Id | Temp ( f) | Impact Veloc. (ft/sec) | Energy (ft-lb ) | Time ( msec ) Max Ld | Time ( msec ) Total | Load ( lb ) Max | Energy (ft-lb ) Maxld | Energy (ft-lb ) Total |
|---|---|---|---|---|---|---|---|---|
| a91309 | 70. | 2.27 | .55 | 4.77 | 10.30 | 152.4 | .589 | .065 |

**Figure B.1. Load and Energy from Dynatup for $[0/90]_{3S}$ Panel, Impact Energy = 0.55 ft-lb**

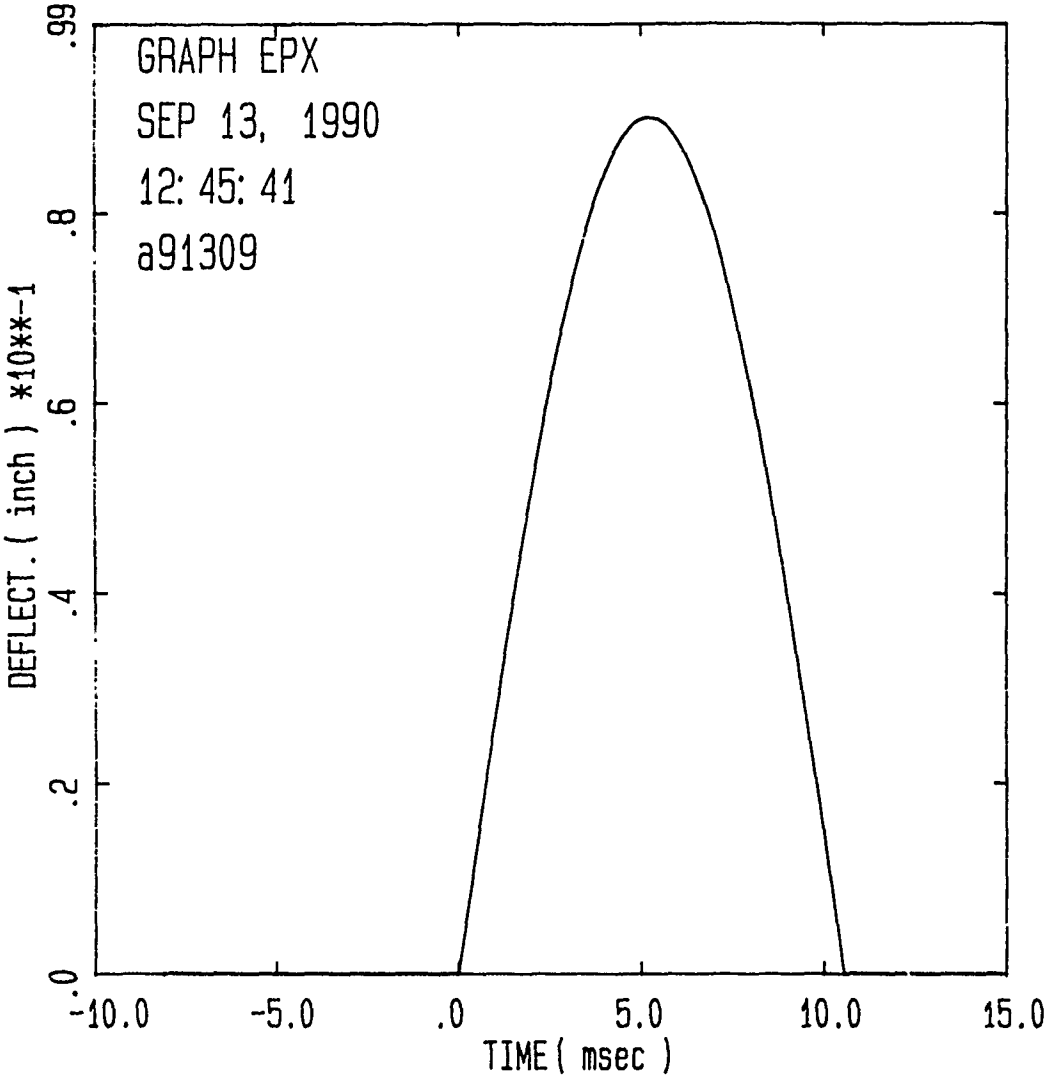


| Specimen Id | Temp ( f) | Impact Veloc. (ft/sec) | Energy (ft-lb ) | Time ( msec ) Max Ld | Time ( msec ) Total | Load ( lb ) Max | Energy (ft-lb ) Maxld | Energy (ft-lb ) Total |
|---|---|---|---|---|---|---|---|---|
| a91309 | 70. | 2.27 | .55 | 4.77 | 10.30 | 152.4 | .589 | .065 |

**Figure B.2. Deflection from Dynatup for $[0/90]_{3S}$ Panel, Impact Energy = 0.55 ft-lb**

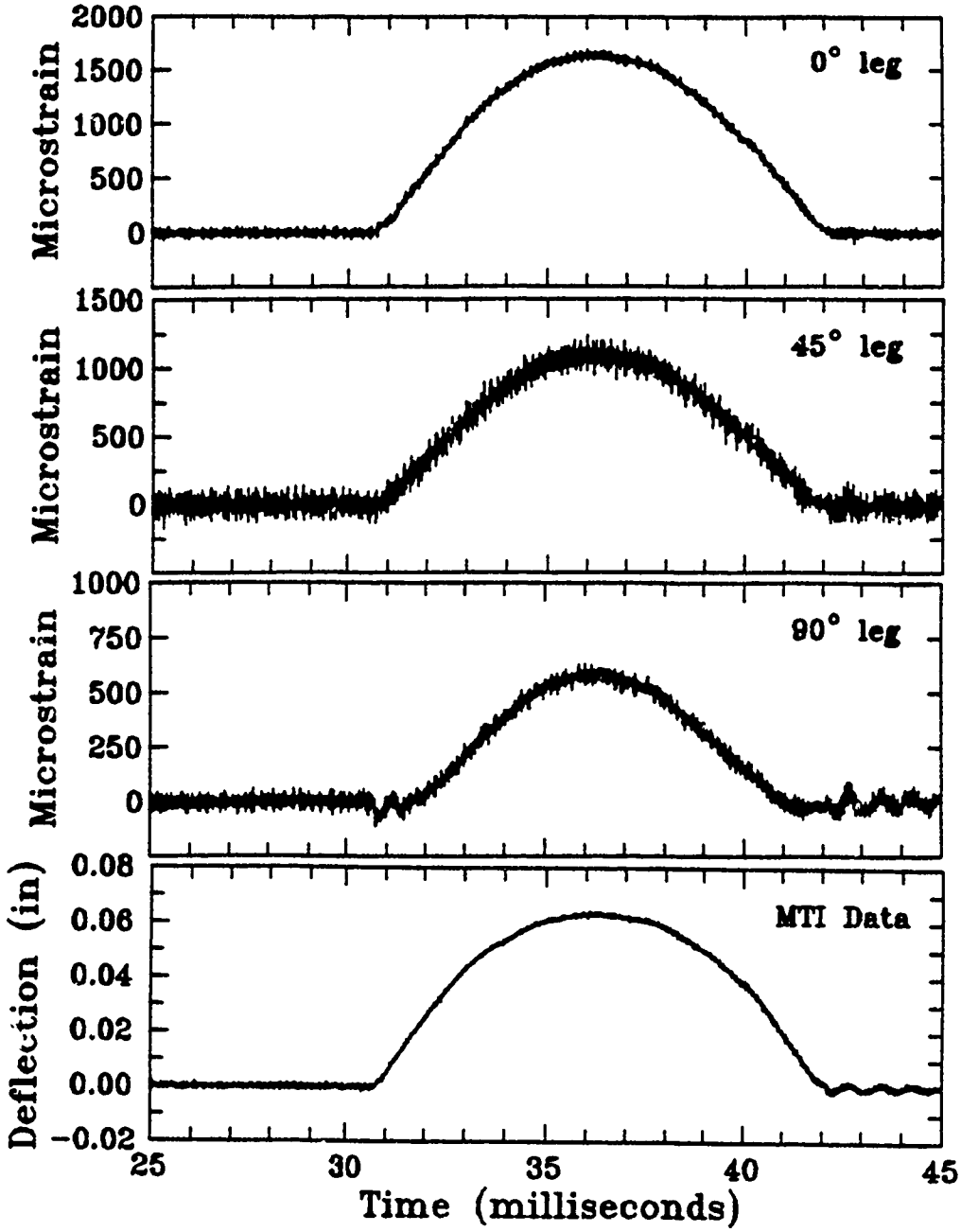


Figure B.3. Strain and Deflection for $[0/90]_{3S}$ Panel, Impact Energy = 0.55 ft-lb

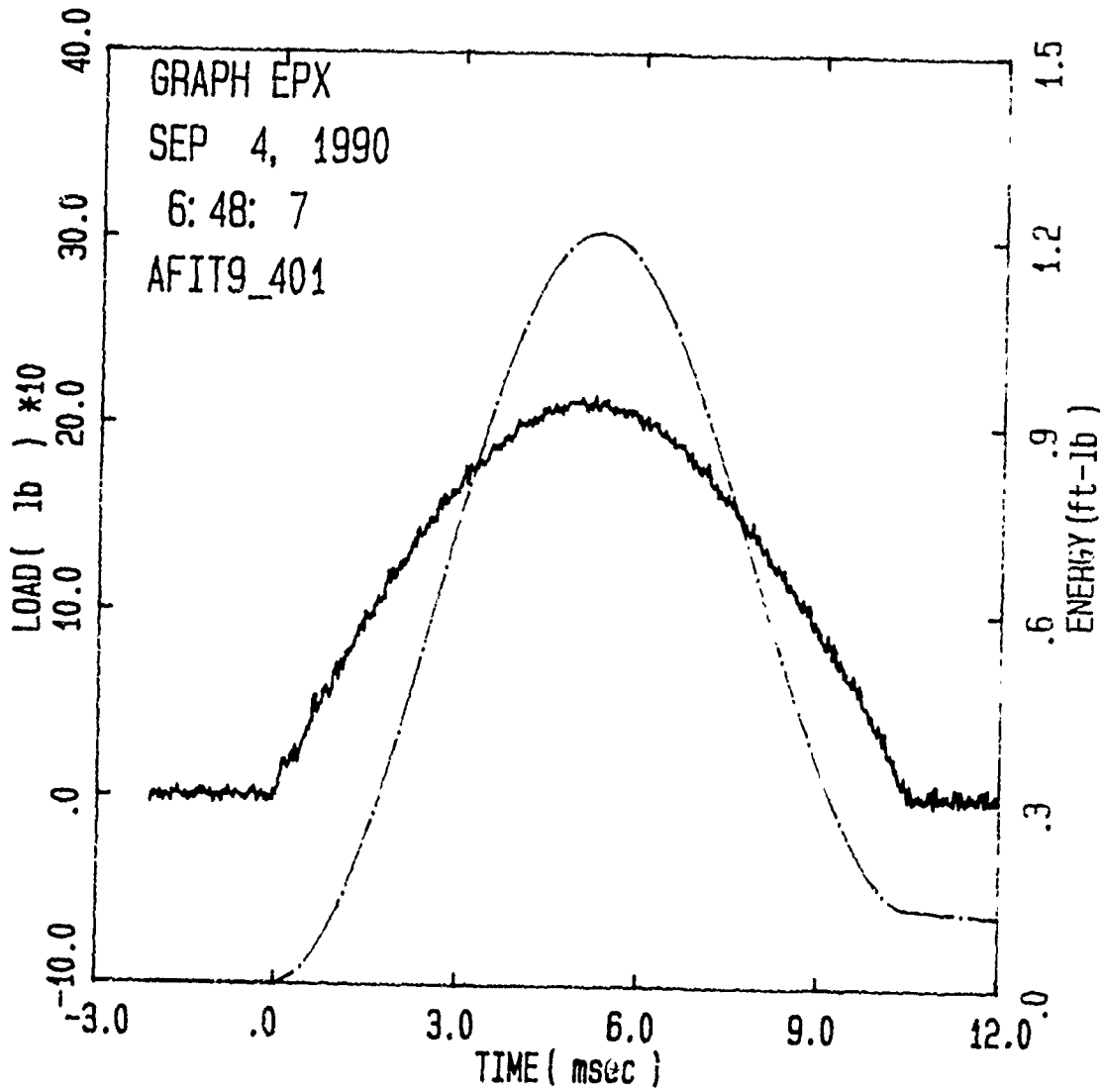


| Specimen Id | Temp (f) | Impact Veloc. (ft/sec) | Impact Energy (ft-lb) | Time (msec) Max Ld | Time (msec) Total | Load (lb) Max | Energy (ft-lb) MaxId | Energy (ft-lb) Total |
|---|---|---|---|---|---|---|---|---|
| AFIT9_401 | 70. | 3.37 | 1.13 | 5.22 | 10.57 | 215.5 | 1.210 | .128 |

Figure B.4. Load and Energy from Dynatup for $[0/90]_{3S}$ Panel, Impact Energy = 1.14 ft-lb

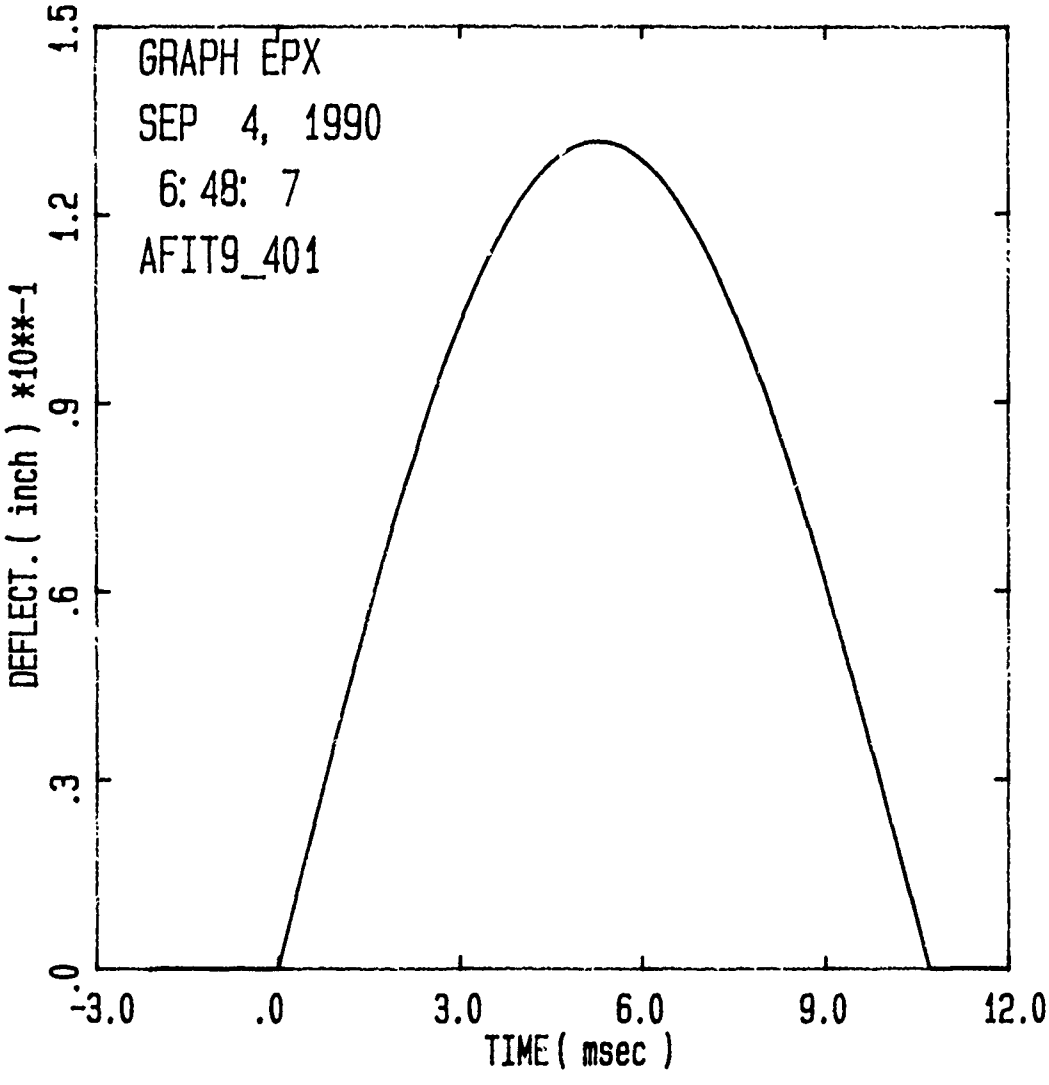


| Specimen Id | Temp | Impact Veloc. | Energy | Time | | Load | Energy | |
|---|---|---|---|---|---|---|---|---|
| | ( f) | (ft/sec) | (ft-lb ) | ( msec ) | | ( lb ) | (ft-lb ) | |
| | | | | Max Ld | Total | Max | Maxld | Total |
| AFIT9_401 | 70. | 3.27 | 1.13 | 5.22 | 10.57 | 215.5 | 1.210 | .128 |

Figure B.5. Deflection from Dynatup for $[0/90]_{3S}$ Panel, Impact Energy = 1.14 ft-lb

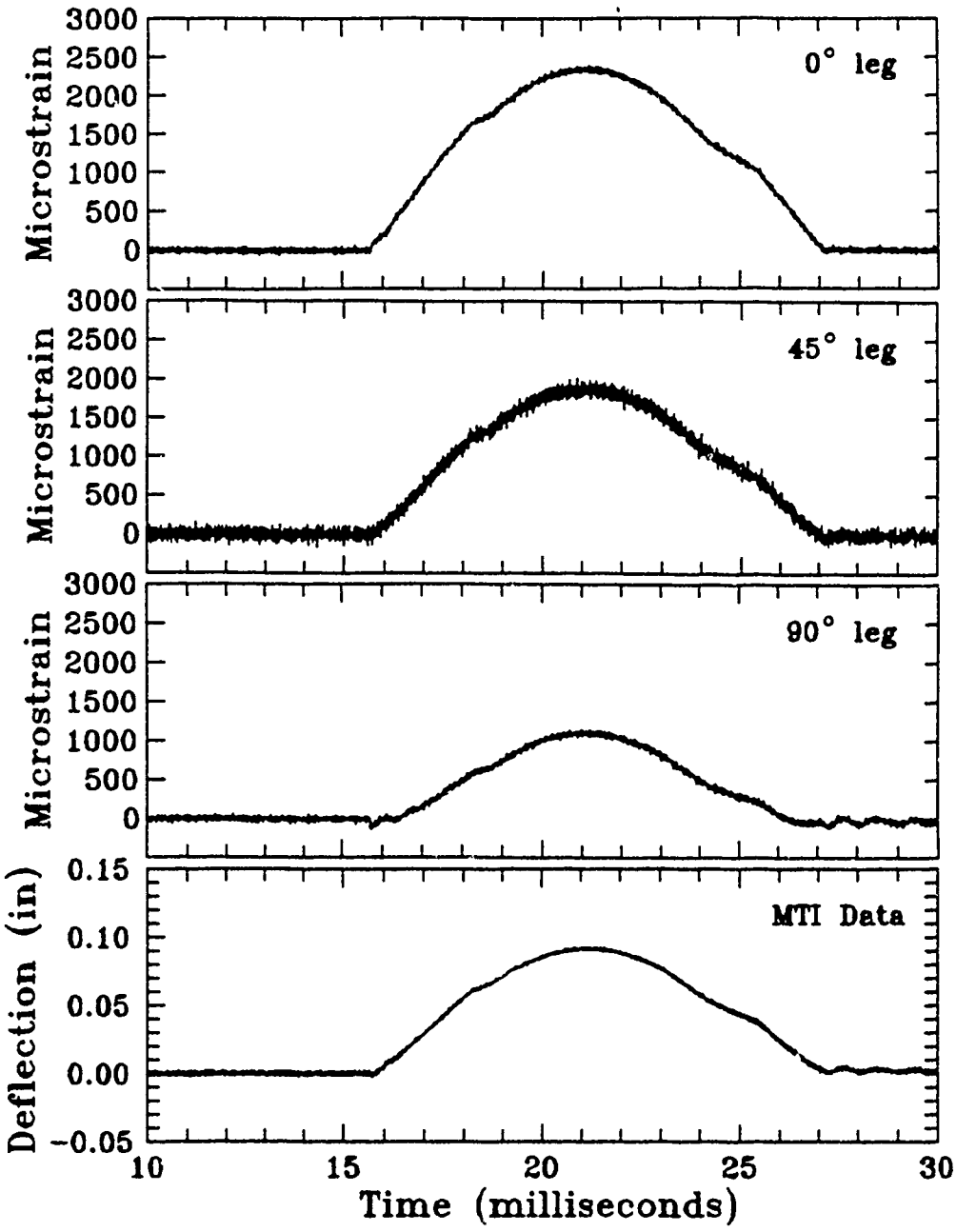


Figure B.6. Strain and Deflection for $[0/90]_{3S}$ Panel, Impact Energy = 1.14 ft-lb

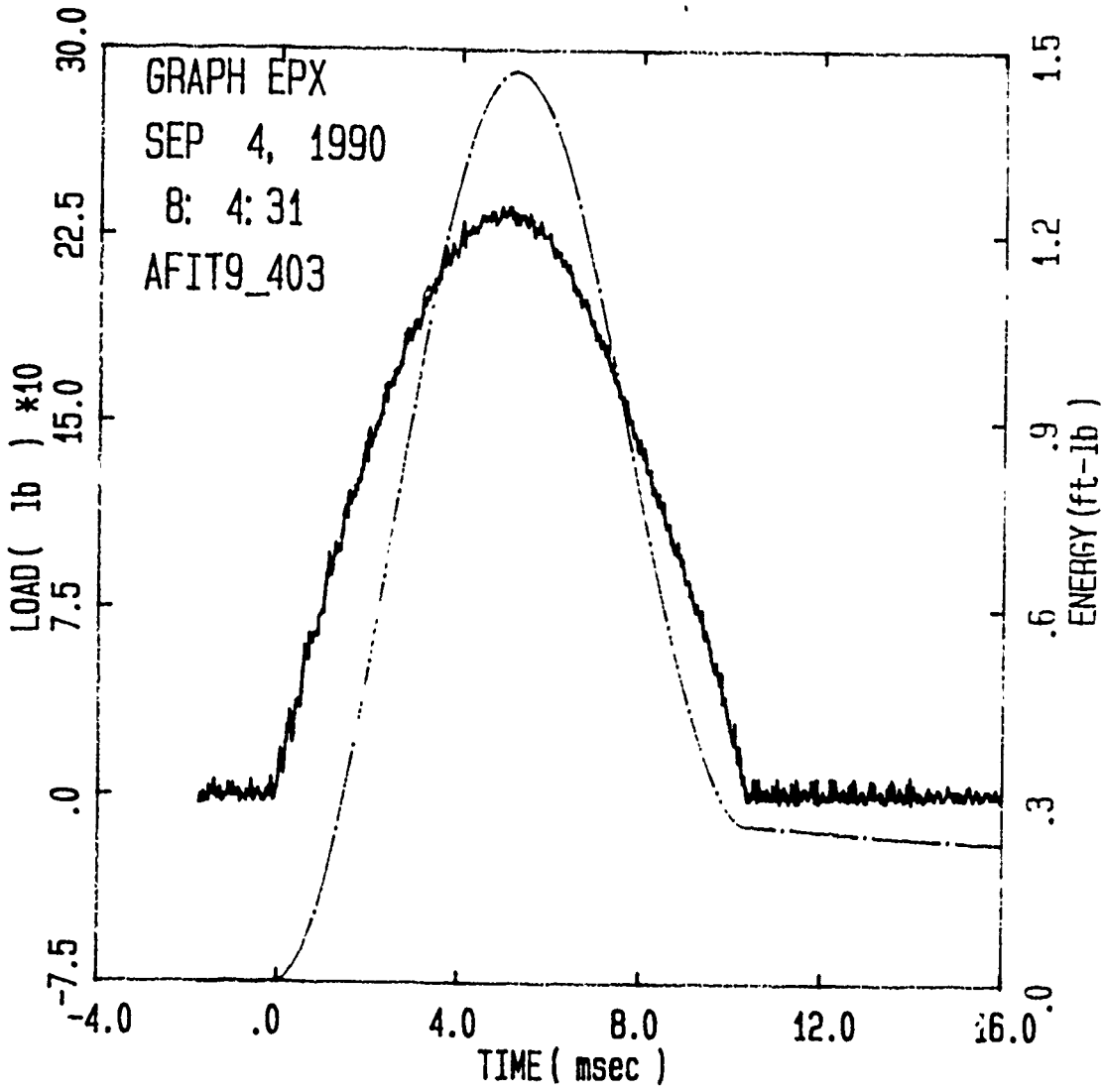


| Specimen Id | Temp (f) | Impact Velcc. (ft/sec) | Energy (ft-lb) | Time ( msec ) Max Ld | Time ( msec ) Total | Load ( lb ) Max | Energy (ft-lb ) Maxld | Energy (ft-lb ) Total |
|---|---|---|---|---|---|---|---|---|
| AFIT9_403 | 70. | 3.61 | 1.38 | 4.90 | 10.38 | 235.9 | 1.455 | .253 |

Figure B.7. Load and Energy from Dynatup for $[0/90]_{3S}$ Panel, Impact Energy = 1.38 ft-lb

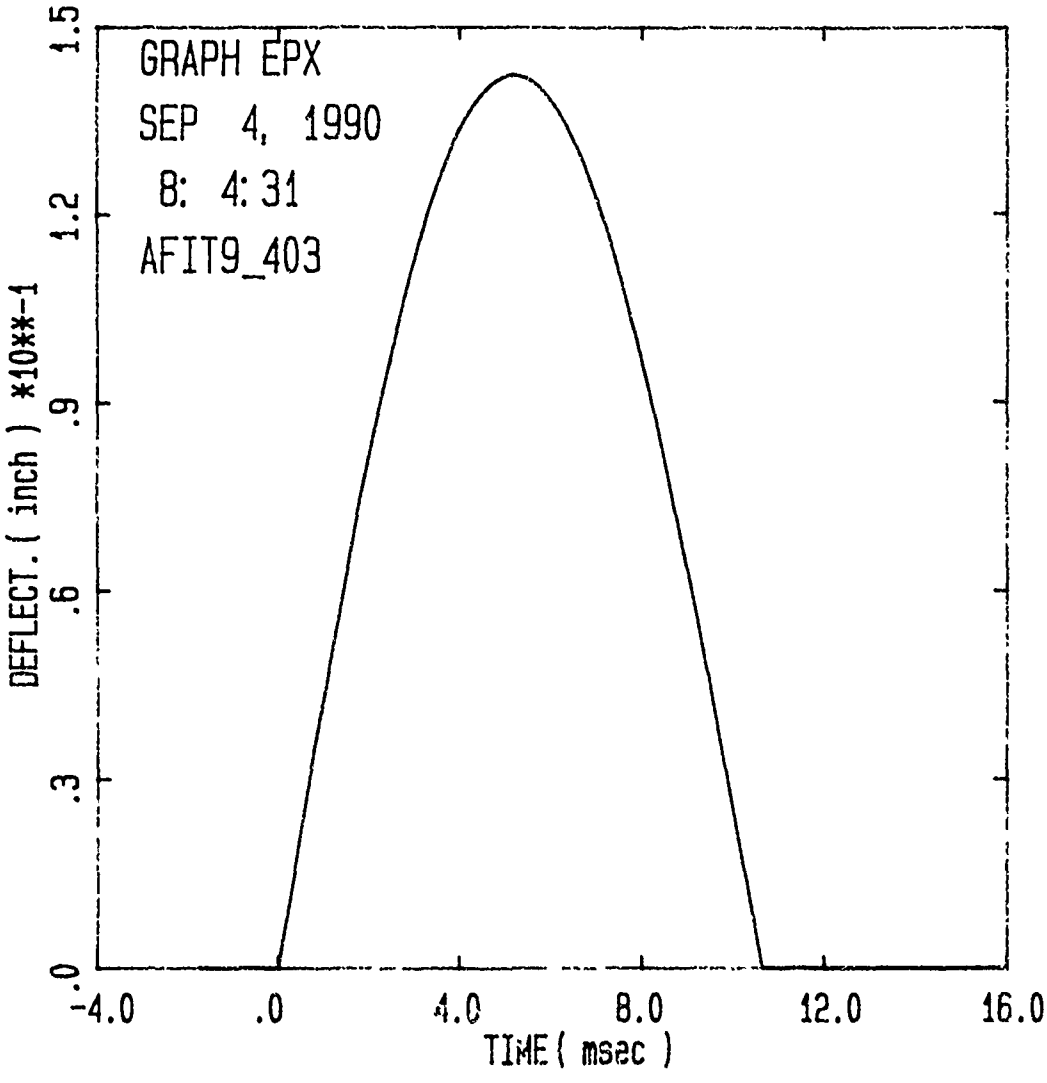


| Specimen Id | Temp (f) | Impact Velocity (ft/sec) | Impact Energy (ft-lb) | Time (msec) Max Ld | Time (msec) Total | Load (lb) Max | Energy (ft-lb) MaxId | Energy (ft-lb) Total |
|---|---|---|---|---|---|---|---|---|
| AFIT9_403 | 70. | 3.61 | 1.38 | 4.90 | 19.38 | 235.9 | 1.455 | .253 |

Figure E.8. Deflection from Dynatup for $[0/90]_{3S}$ Panel, Impact Energy = 1.38 ft-lb

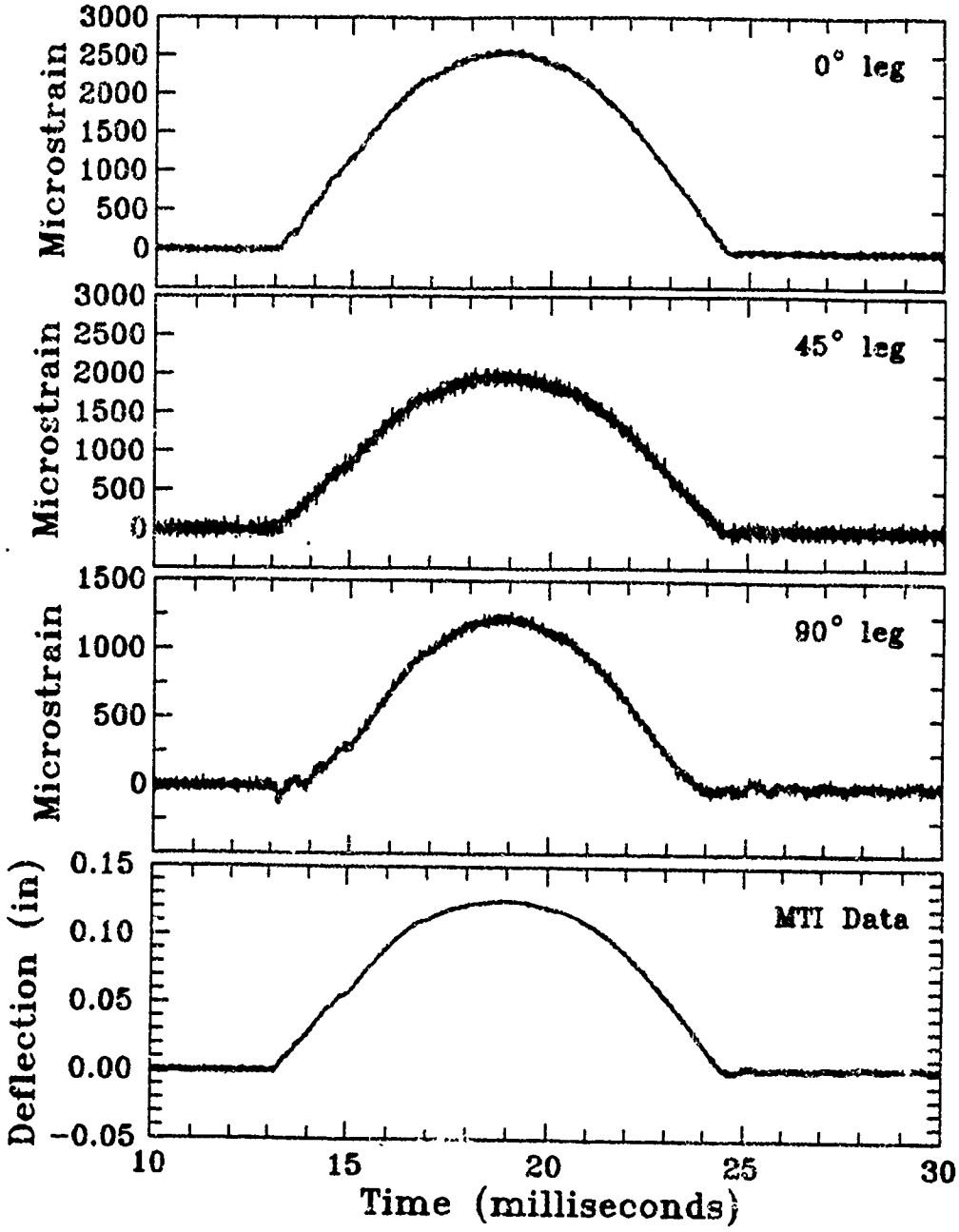


Figure B.9. Strain and Deflection for $[0/90]_{3S}$ Panel, Impact Energy = 1.38 ft-lb

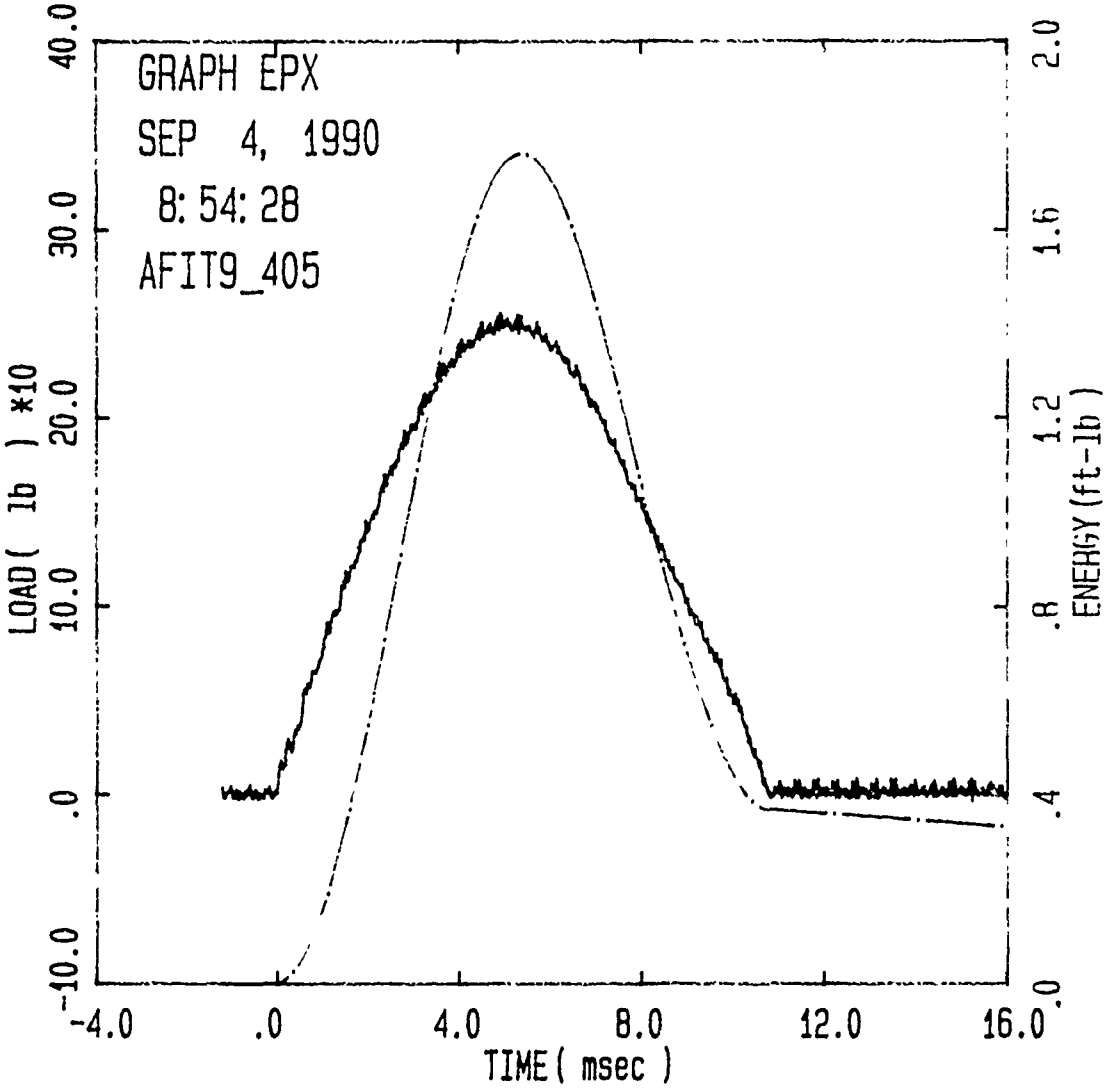


| Specimen Id | Temp | Impact Veloc. | Energy | Time | | Load | Energy | |
|---|---|---|---|---|---|---|---|---|
| | ( f) | (ft/sec) | (ft-lb ) | ( msec ) | | ( lb ) | (ft-lb ) | |
| | | | | Max Ld | Total | Max | Maxld | Total |
| AFIT9_405 | 70. | 3.96 | 1.67 | 4.93 | 10.82 | 255.3 | 1.731 | .369 |

Figure B.10. Load and Energy from Dynatup for $[0/90]_{3S}$ Panel, Impact Energy = 1.67 ft-lb

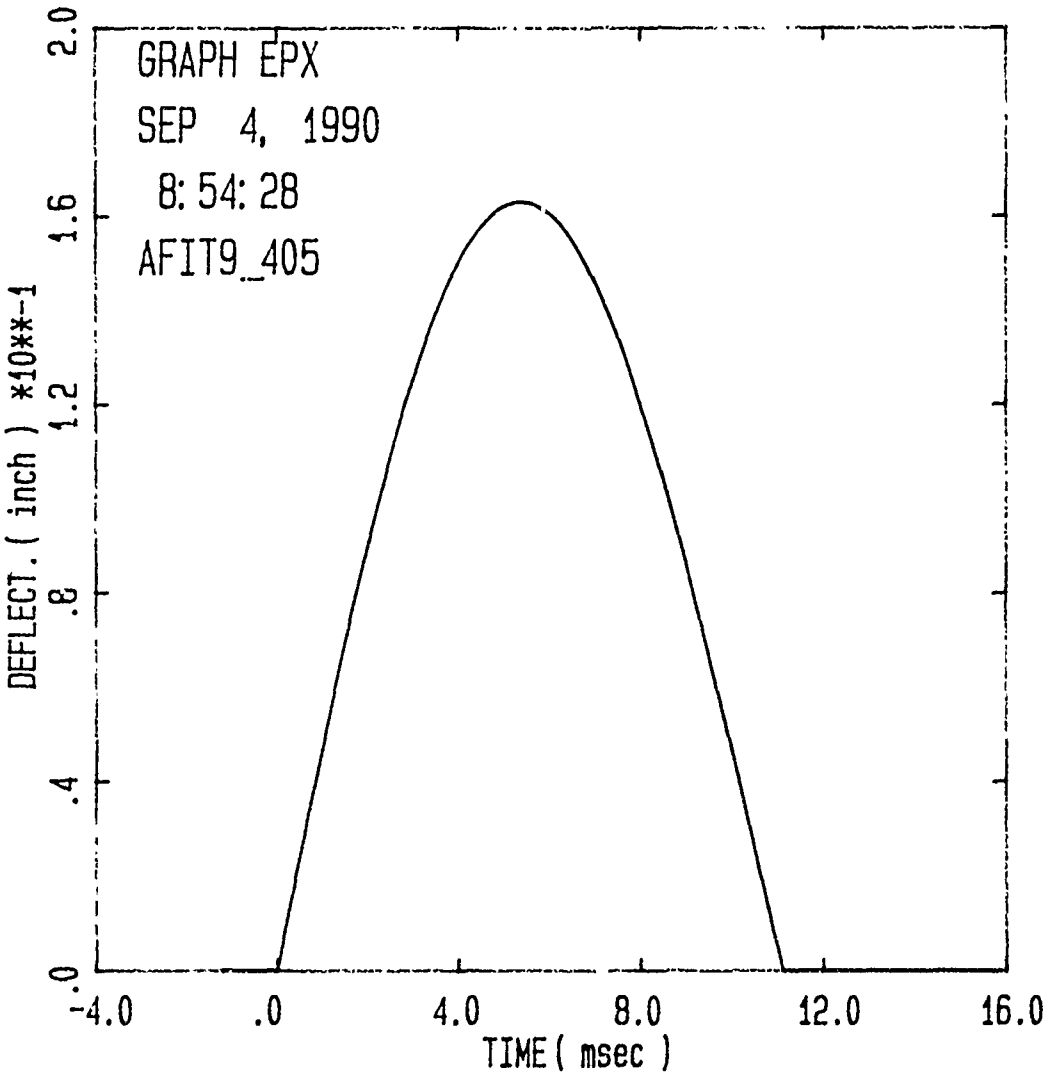


| Specimen Id | Temp ( f) | Impact Veloc. (ft/sec) | Energy (ft-lb ) | Time ( msec ) Max Ld | Time ( msec ) Total | Load ( lb ) Max | Energy (ft-lb ) Maxld | Energy (ft-lb ) Total |
|---|---|---|---|---|---|---|---|---|
| AFIT9_405 | 70. | 3.96 | 1.67 | 4.93 | 10.82 | 255.3 | 1.731 | .369 |

Figure B.11. Deflection from Dynatup for $[0/90]_{3S}$ Panel, Impact Energy = 1.67 ft-lb

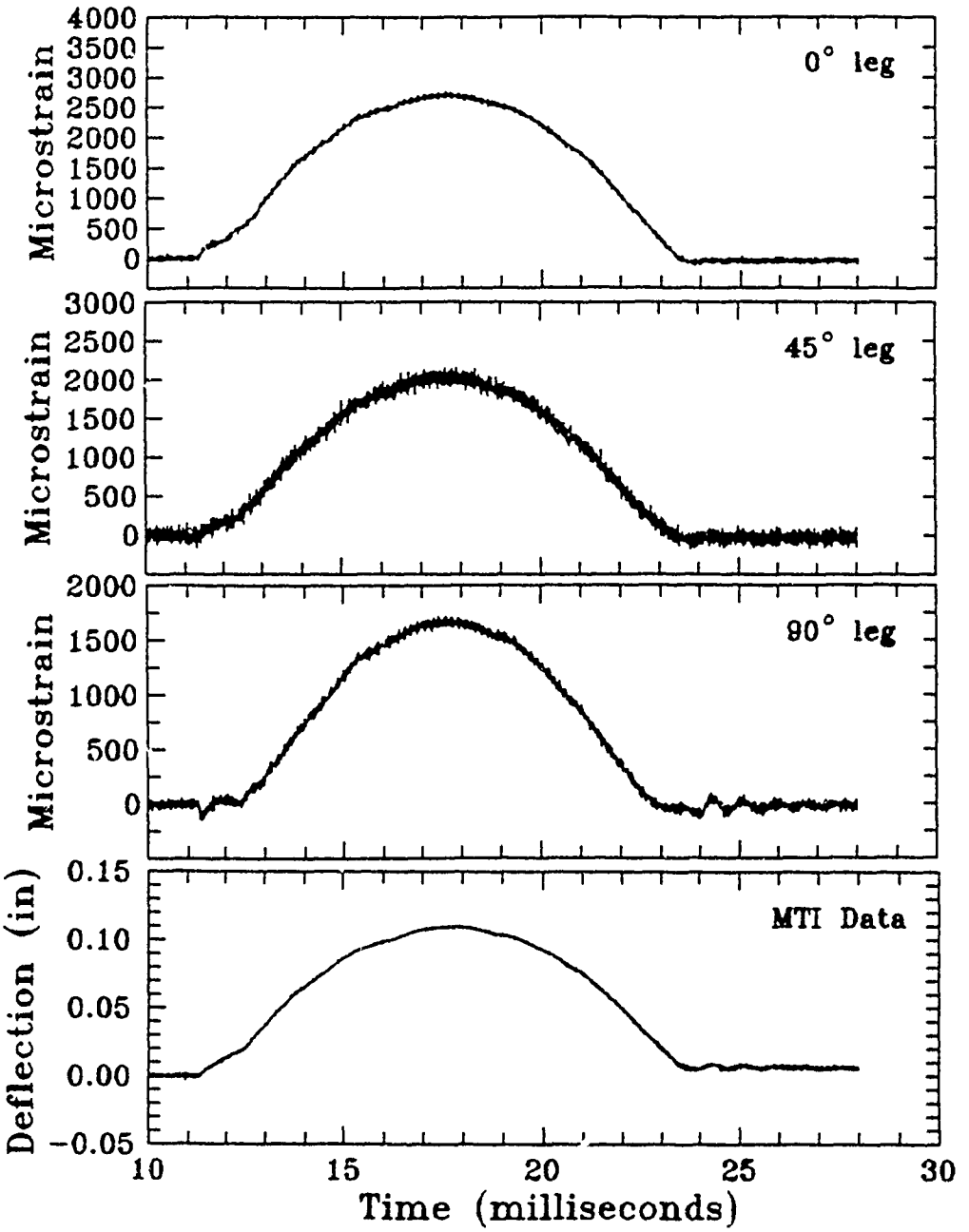


Figure B.12. Strain and Deflection for $[0/90]_{3S}$ Panel, Impact Energy = 1.67 ft-lb

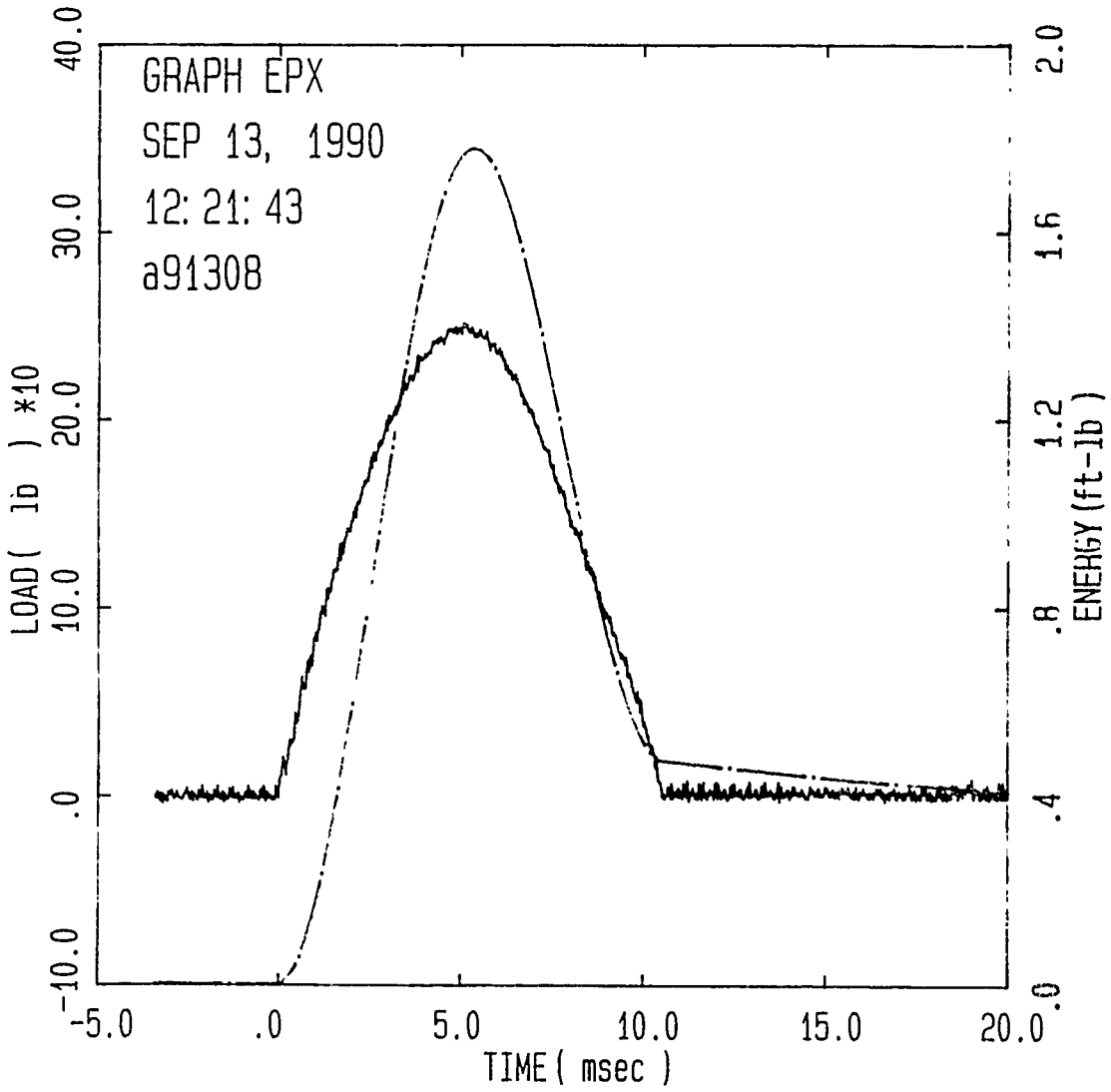


| Specimen Id | Temp ( f) | Impact Veloc. (ft/sec) | Impact Energy (ft-lb ) | Time ( msec ) Max Ld | Time ( msec ) Total | Load ( lb ) Max | Energy (ft-lb ) Maxld | Energy (ft-lb ) Total |
|---|---|---|---|---|---|---|---|---|
| a91308 | 70. | 3.98 | 1.68 | 5.07 | 10.55 | 251.8 | 1.766 | .475 |

Figure B.13. Load and Energy from Dynatup for $[0/90]_{3S}$ Panel, Impact Energy = 1.68 ft-lb

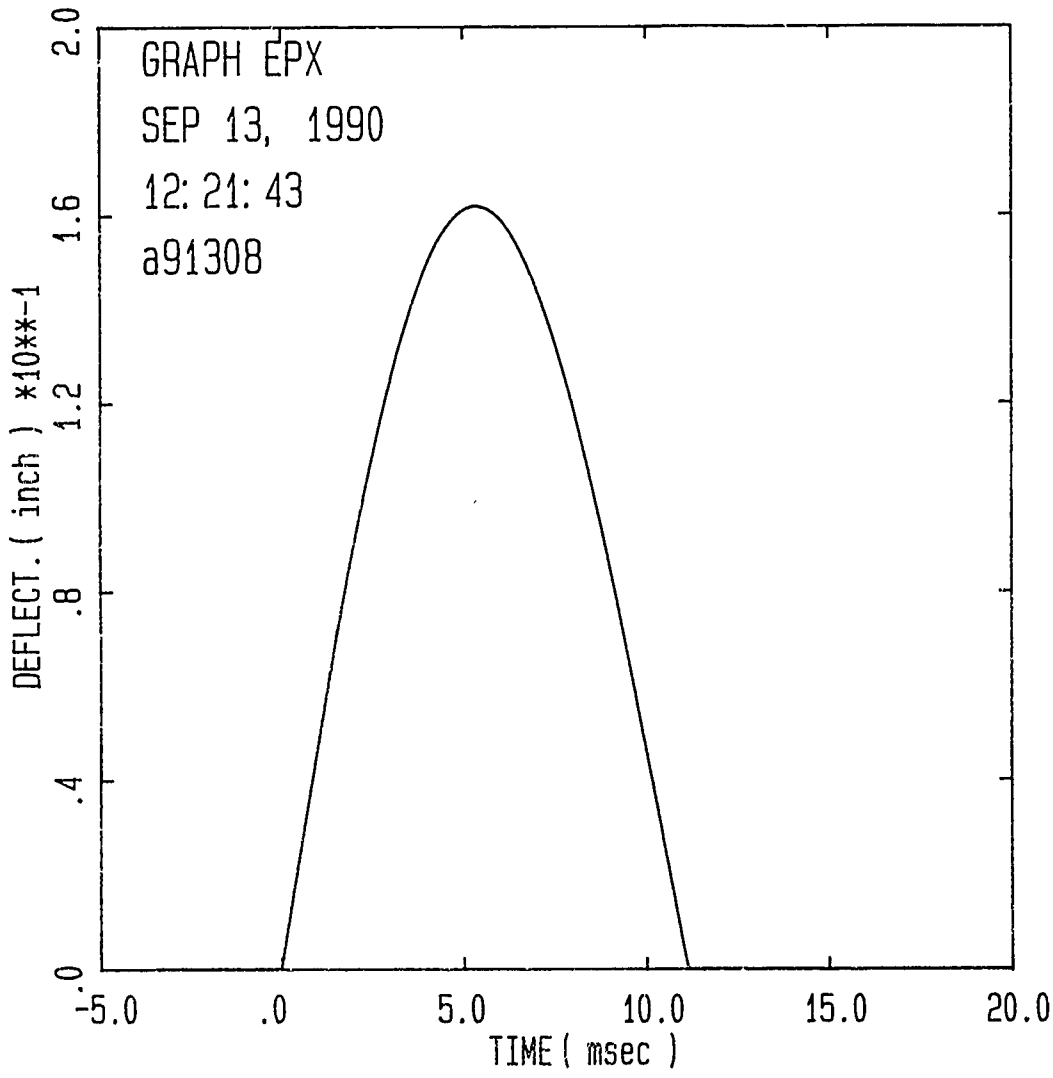


| Specimen Id | Temp | Impact Veloc. | Energy | Time | | Load | Energy | |
|---|---|---|---|---|---|---|---|---|
| | ( f) | (ft/sec) | (ft-lb ) | ( msec ) | | ( lb ) | (ft-lb ) | |
| | | | | Max Ld | Total | Max | Maxld | Total |
| a91308 | 70. | 3.98 | 1.68 | 5.07 | 10.55 | 251.8 | 1.766 | .475 |

Figure B.14. Deflection from Dynatup for $[0/90]_{3S}$ Panel, Impact Energy = 1.68 ft-lb

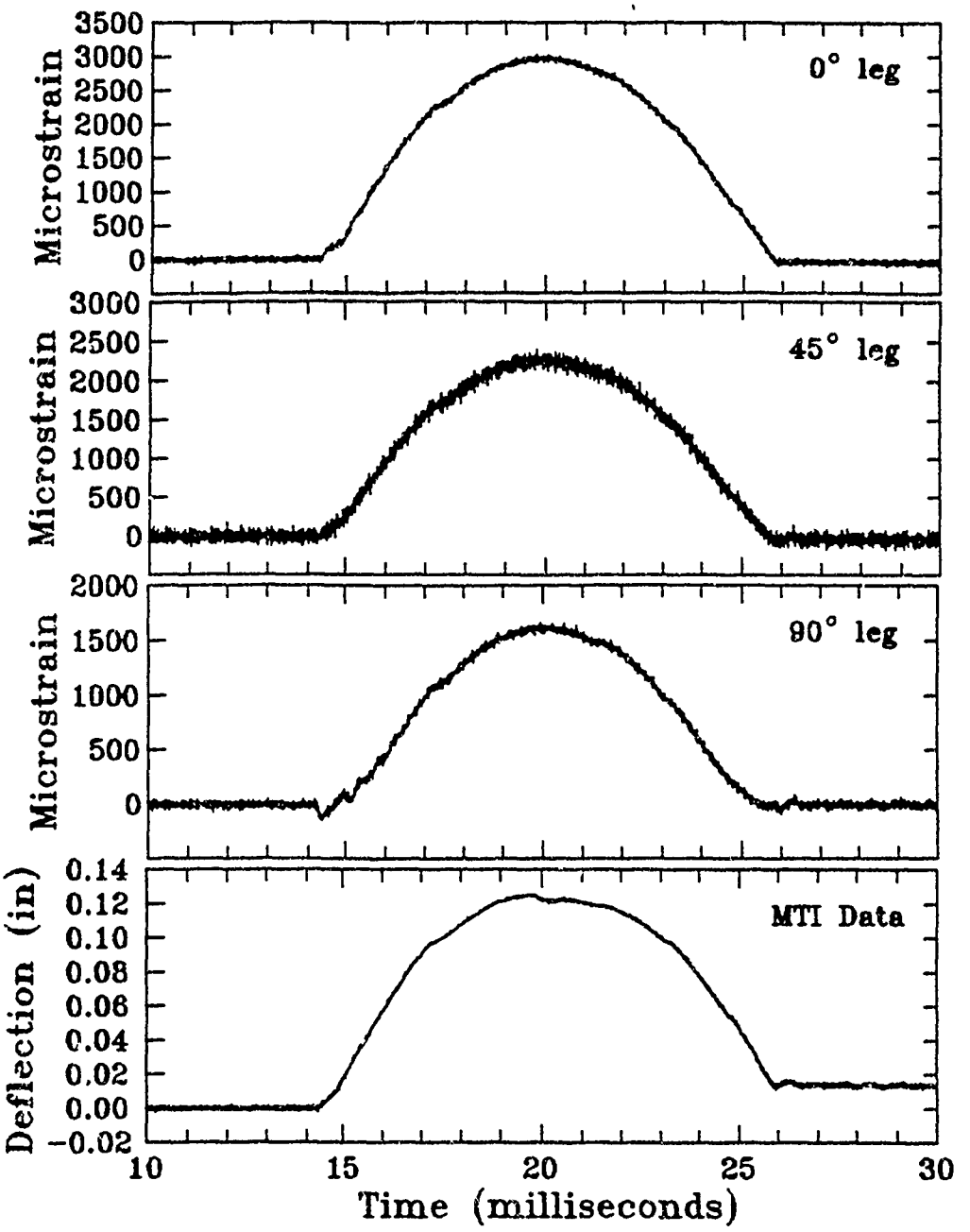


Figure B.15. Strain and Deflection for $[0/90]_{3S}$ Panel, Impact Energy = 1.68 ft-lb

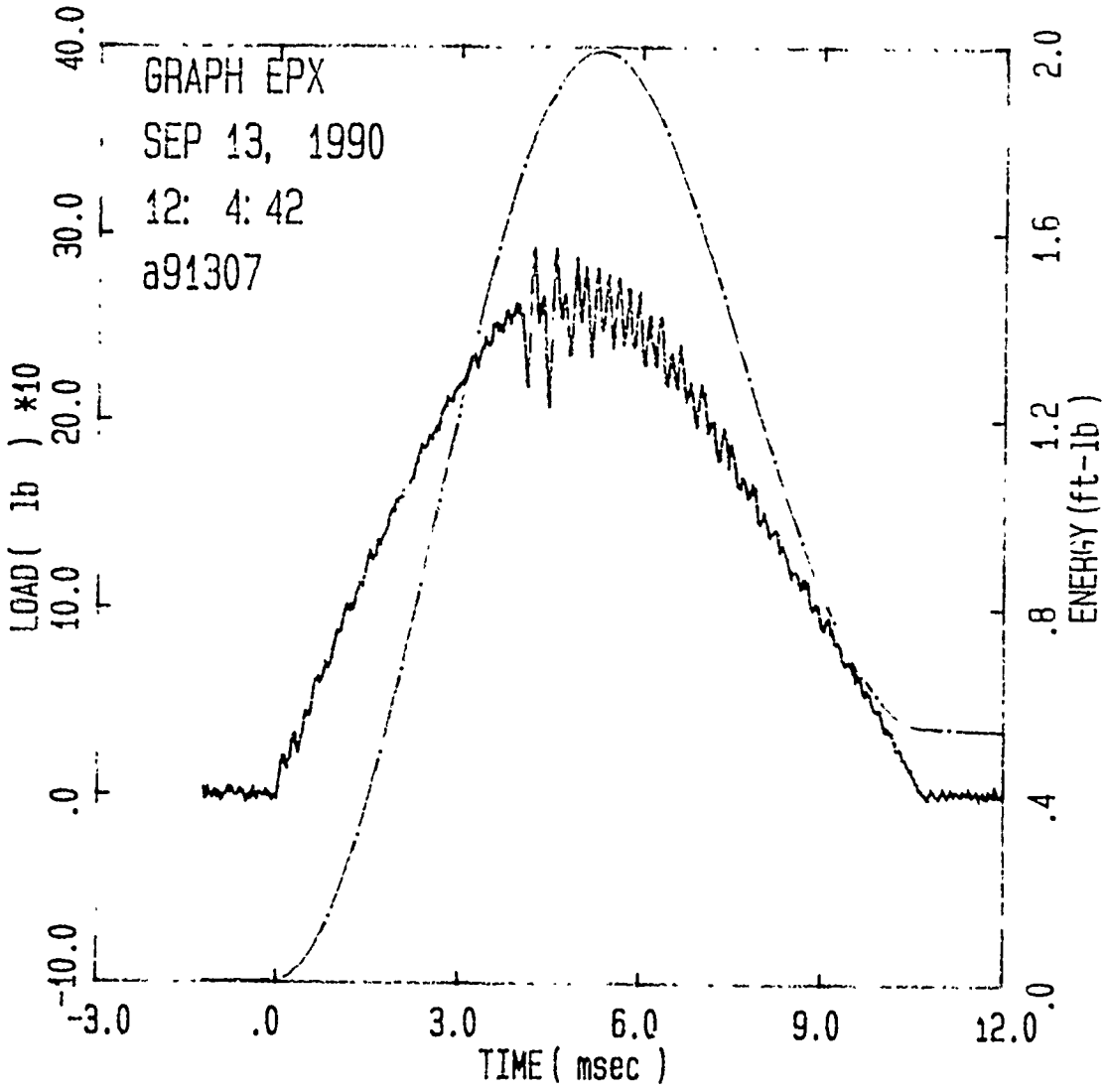


| Specimen Id | Temp ( f) | Impact Veloc. (ft/sec) | Energy (ft-lb ) | Time ( msec ) Max Ld | Time ( msec ) Total | Load ( lb ) Max | Energy (ft-lb ) MaxId | Energy (ft-lb ) Total |
|---|---|---|---|---|---|---|---|---|
| a91307 | 70. | 4.22 | 1.89 | 4.22 | 10.75 | 292.5 | 1.813 | .546 |

Figure B.16. Load and Energy from Dynatup for $[0/90]_{3S}$ Panel, Impact Energy = 1.89 ft-lb

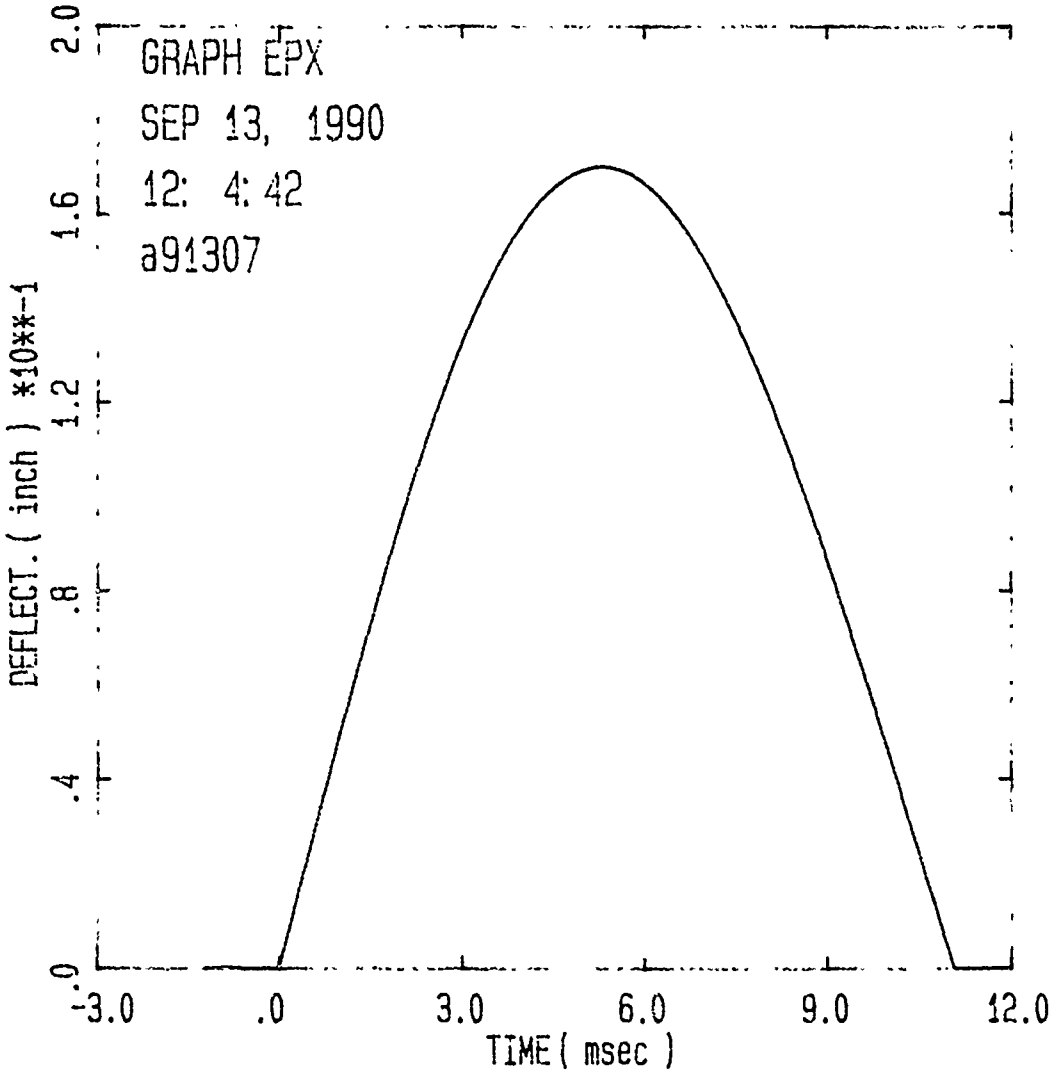


| Specimen Id | Temp ( f) | Impact Veloc. (ft/sec) | Energy (ft-lb ) | Time ( msec ) Max Ld | Time ( msec ) Total | Load ( lb ) Max | Energy (ft-lb ) Maxld | Energy (ft-lb ) Total |
|---|---|---|---|---|---|---|---|---|
| a91307 | 70. | 4.22 | 1.89 | 4.22 | 10.75 | 292.5 | 1.813 | .546 |

Figure B.17. Deflection from Dynatup for $[0/90]_{3S}$ Panel, Impact Energy = 1.89 ft-lb

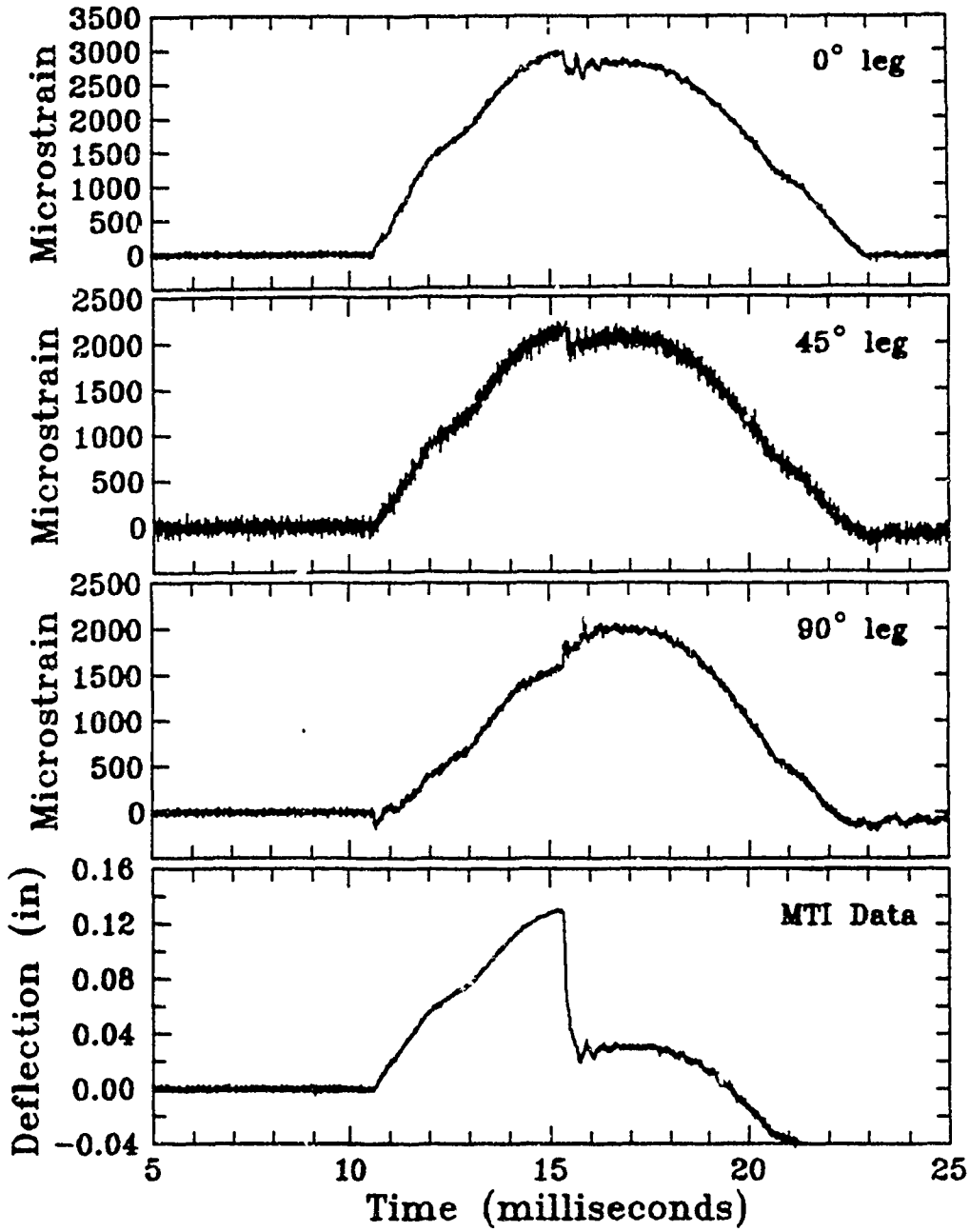


Figure B.18. Strain and Deflection for $[0/90]_{3S}$ Panel, Impact Energy = 1.89 ft-lb

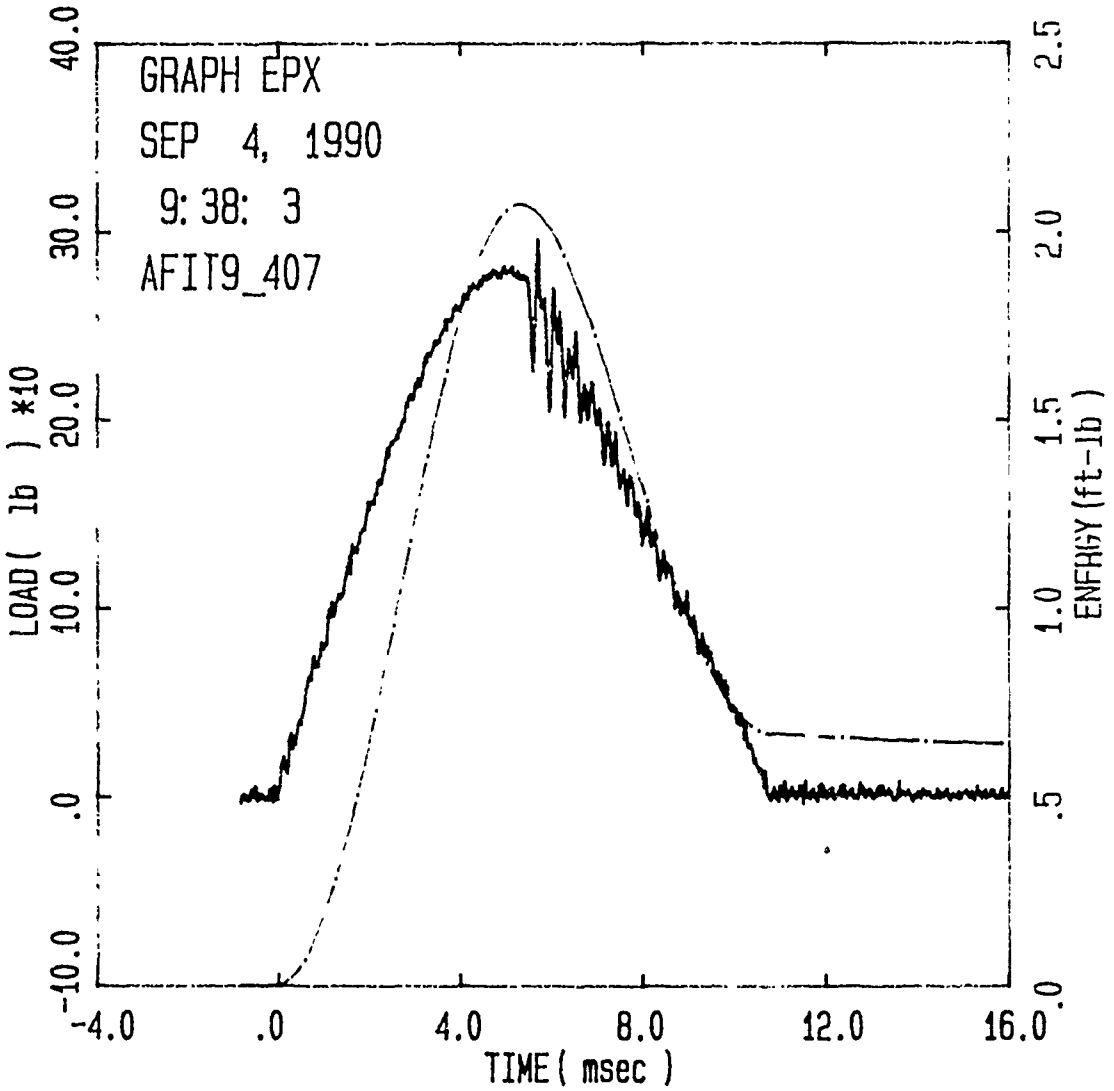


| Specimen Id | Temp (f) | Impact Veloc. (ft/sec) | Impact Energy (ft-lb) | Time (msec) Max Ld | Time (msec) Total | Load (lb) Max | Energy (ft-lb) Maxld | Energy (ft-lb) Total |
|---|---|---|---|---|---|---|---|---|
| AFIT9_407 | 70. | 4.31 | 1.97 | 5.70 | 10.77 | 295.9 | 2.049 | .669 |

Figure B.19. Load and Energy from Dynatup for $[0/90]_{3S}$ Panel, Impact Energy = 1.97 ft-lb

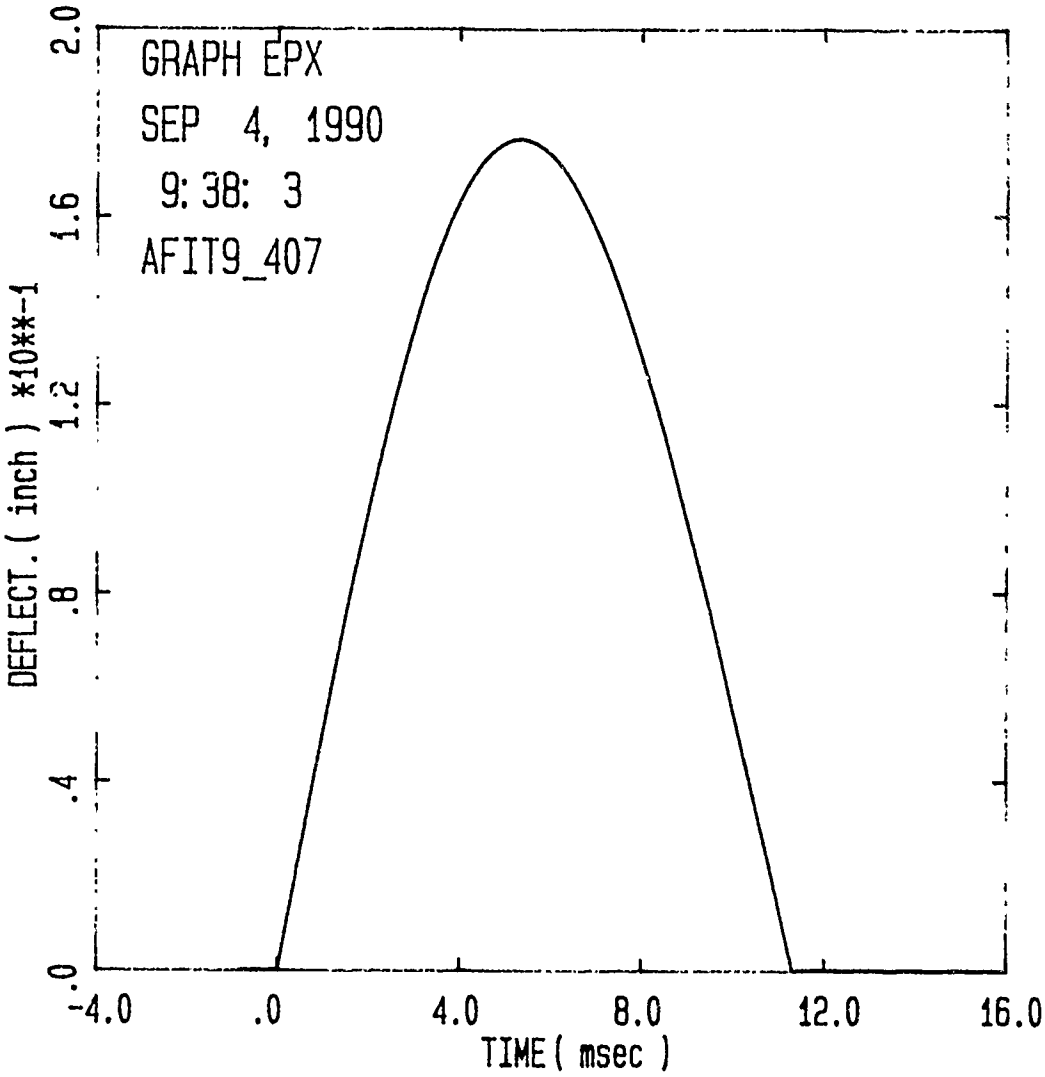


| Specimen Id | Temp ( f) | Impact Veloc. (ft/sec) | Energy (ft-lb ) | Time ( msec ) Max Ld | Time ( msec ) Total | Load ( lb ) Max | Energy (ft-lb ) Maxld | Energy (ft-lb ) Total |
|---|---|---|---|---|---|---|---|---|
| AFIT9_407 | 70. | 4.31 | 1.97 | 5.70 | 10.77 | 295.9 | 2.049 | .669 |

Figure B.20. Deflection from Dynatup for $[0/90]_{3S}$ Panel, Impact Energy = 1.97 ft-lb

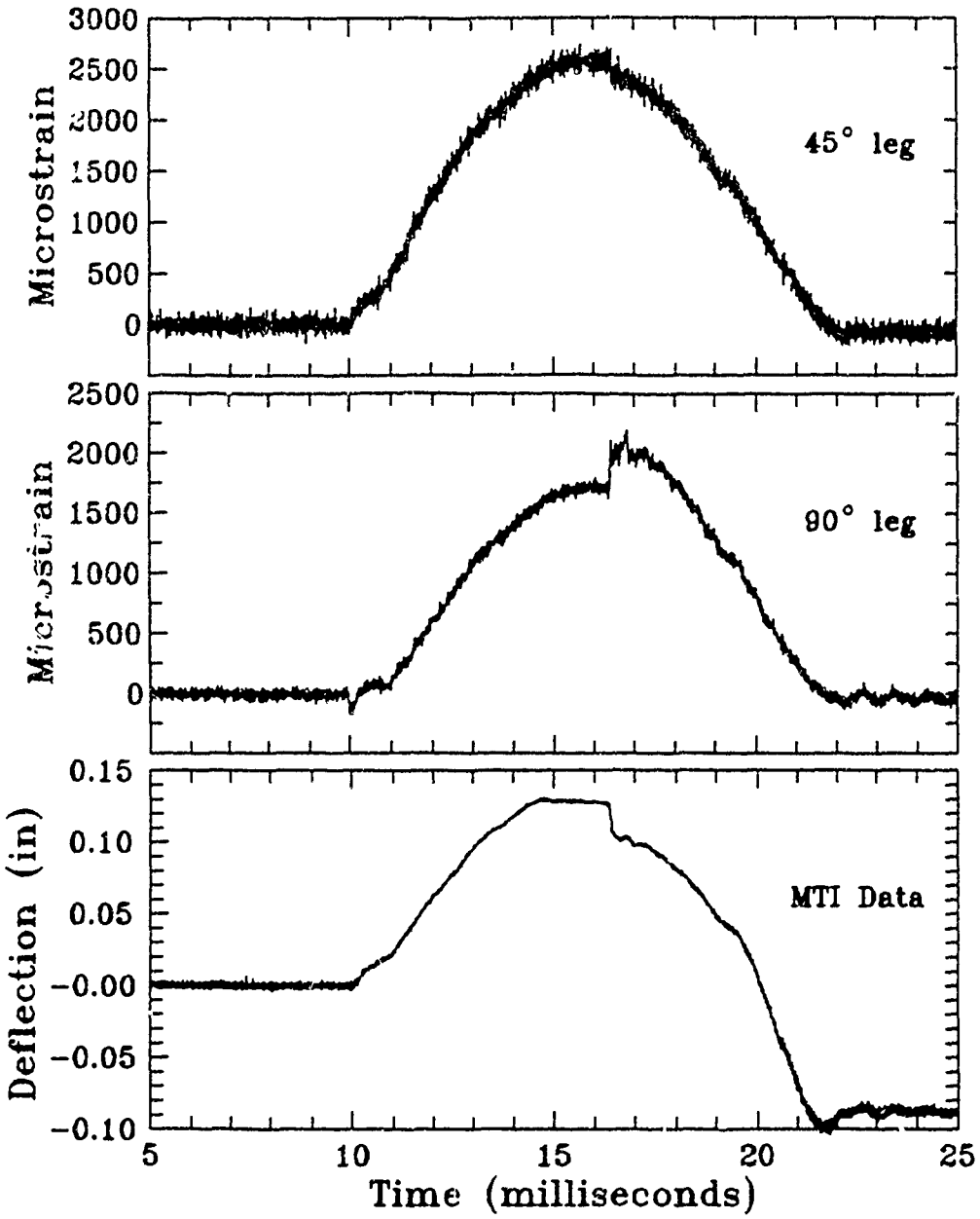


Figure B.21. Strain and Deflection for $[0/90]_{3S}$ Panel, Impact Energy = 1.97 ft-lb

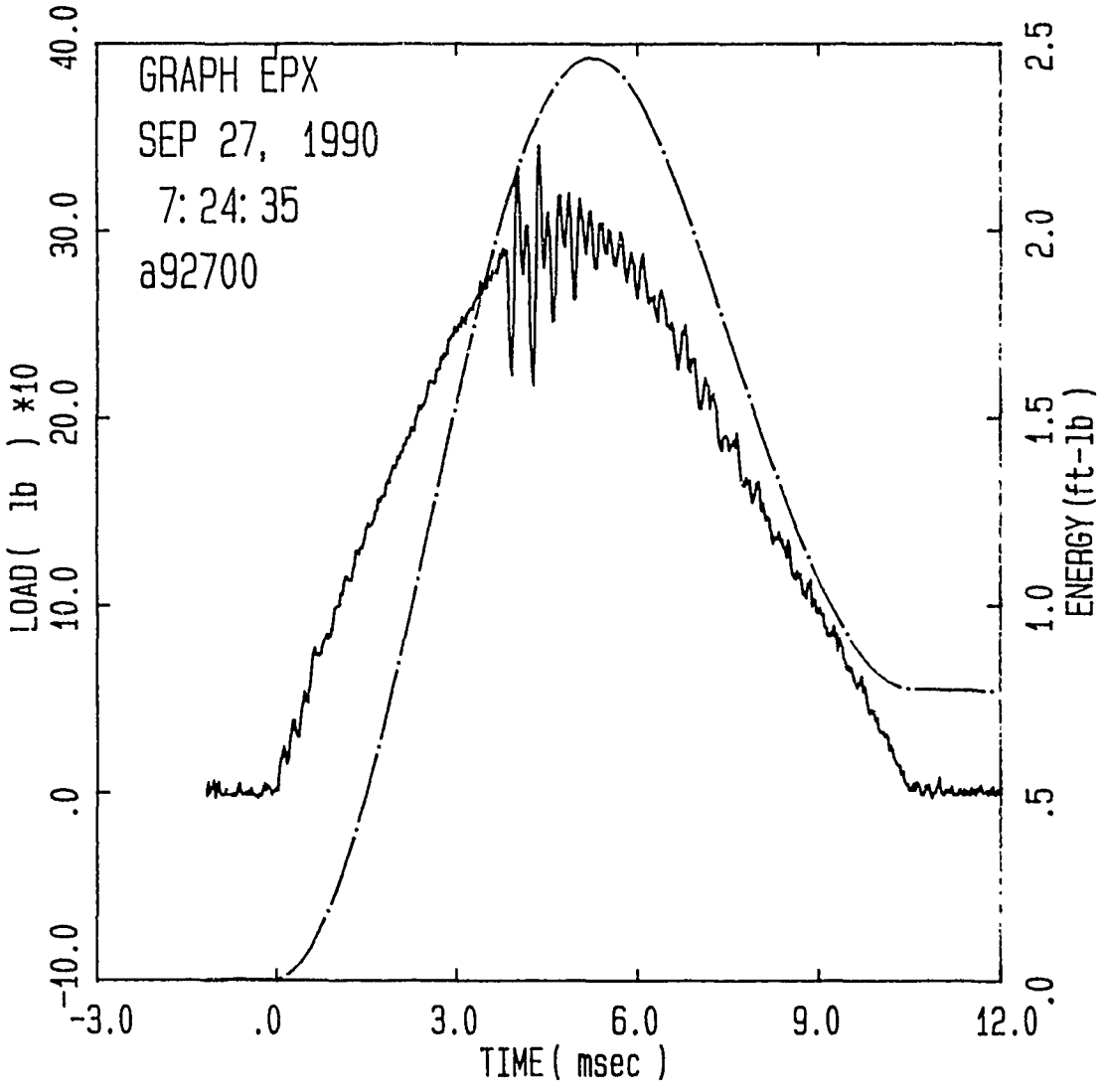


| Specimen Id | Temp ( f) | Impact Veloc. (ft/sec) | Energy (ft-lb ) | Time ( msec ) Max Ld | Time ( msec ) Total | Load ( lb ) Max | Energy (ft-lb ) Maxld | Energy (ft-lb ) Total |
|---|---|---|---|---|---|---|---|---|
| a92700 | 70. | 4.71 | 2.35 | 4.38 | 10.70 | 345.3 | 2.306 | .777 |

Figure B.22. Load and Energy from Dynatup for $[0/90]_{3S}$ Panel, Impact Energy = 2.35 ft-lb

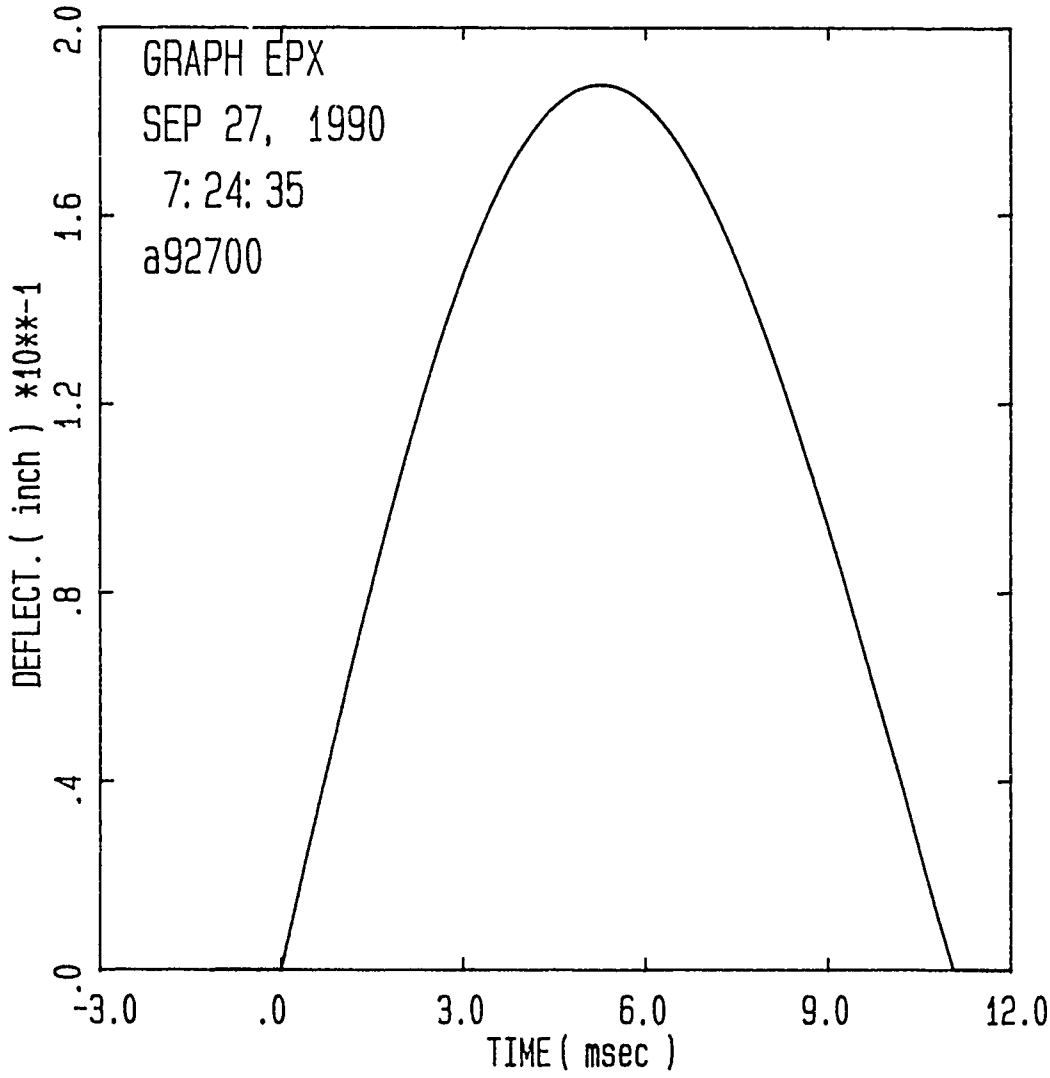


| Specimen Id | Temp ( f) | Impact Veloc. (ft/sec) | Impact Energy (ft-lb ) | Time ( msec ) Max Ld | Time ( msec ) Total | Load ( lb ) Max | Energy (ft-lb ) Maxld | Energy (ft-lb ) Total |
|---|---|---|---|---|---|---|---|---|
| a92700 | 70. | 4.71 | 2.35 | 4.38 | 10.70 | 345.3 | 2.306 | .777 |

Figure B.23. Deflection from Dynatup for $[0/90]_{3S}$ Panel, Impact Energy = 2.35 ft-lb

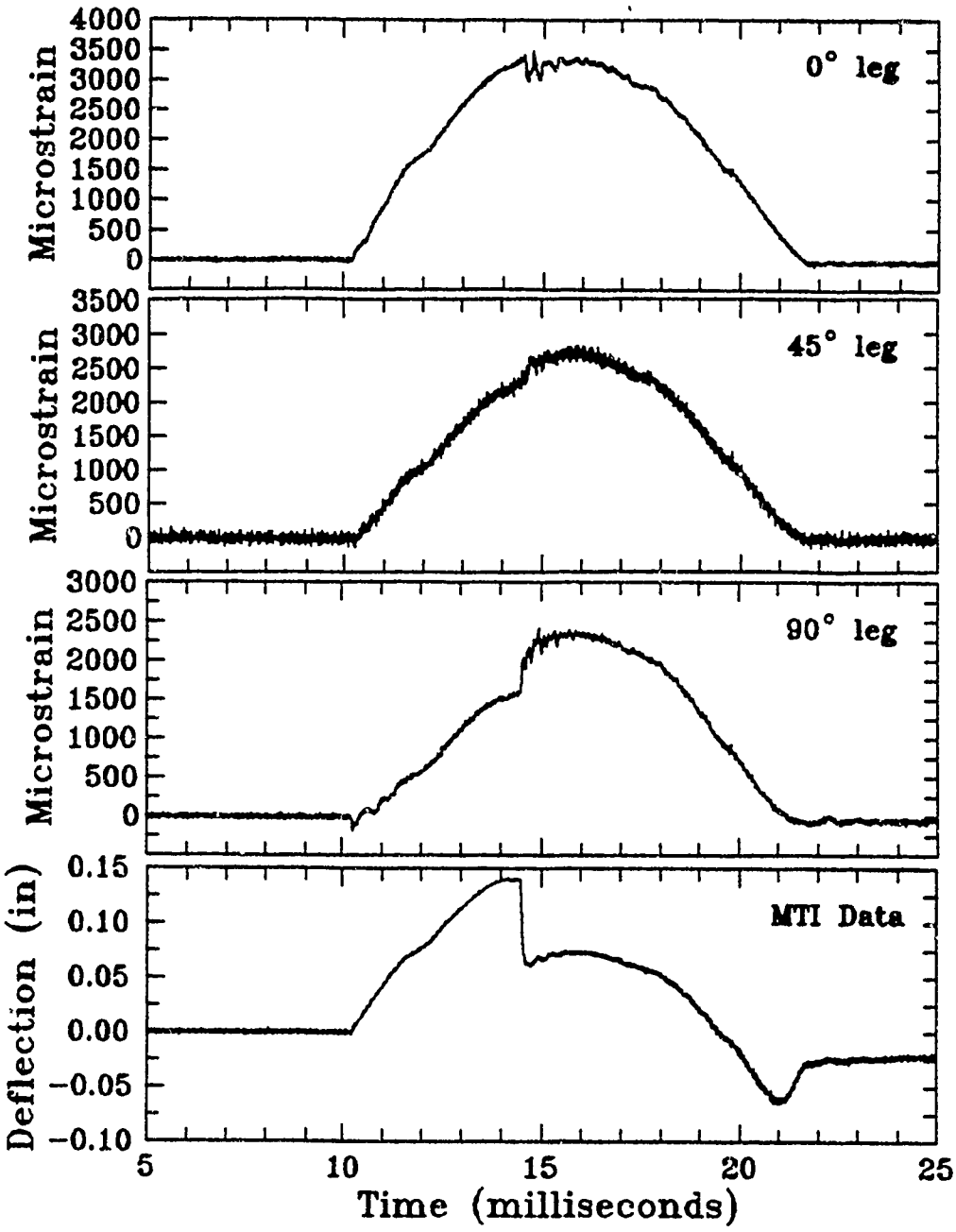


Figure B.24. Strain and Deflection for $[0/90]_{3S}$ Panel, Impact Energy = 2.35 ft-lb

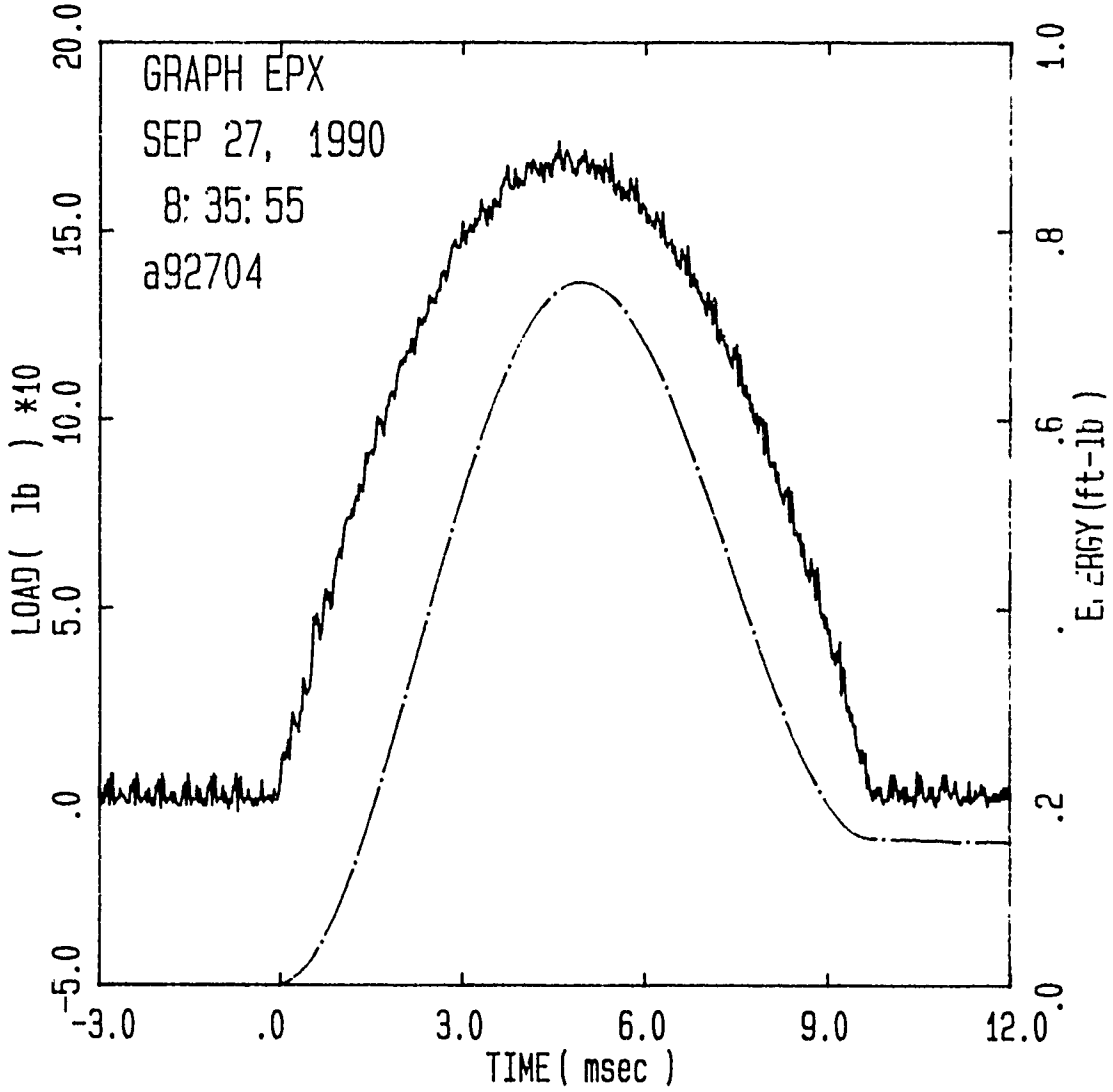


| Specimen Id | Temp ( f) | Impact Veloc. (ft/sec) | Impact Energy (ft-lb ) | Time ( msec ) Max Ld | Time ( msec ) Total | Load ( lb ) Max | Energy (ft-lb ) Maxld | Energy (ft-lb ) Total |
|---|---|---|---|---|---|---|---|---|
| a92704 | 70. | 2.55 | .69 | 4.57 | 9.75 | 173.6 | .736 | .157 |

Figure B.25. Load and Energy from Dynatup for $[90/0]_{3S}$ Panel, Impact Energy = 0.69 ft-lb

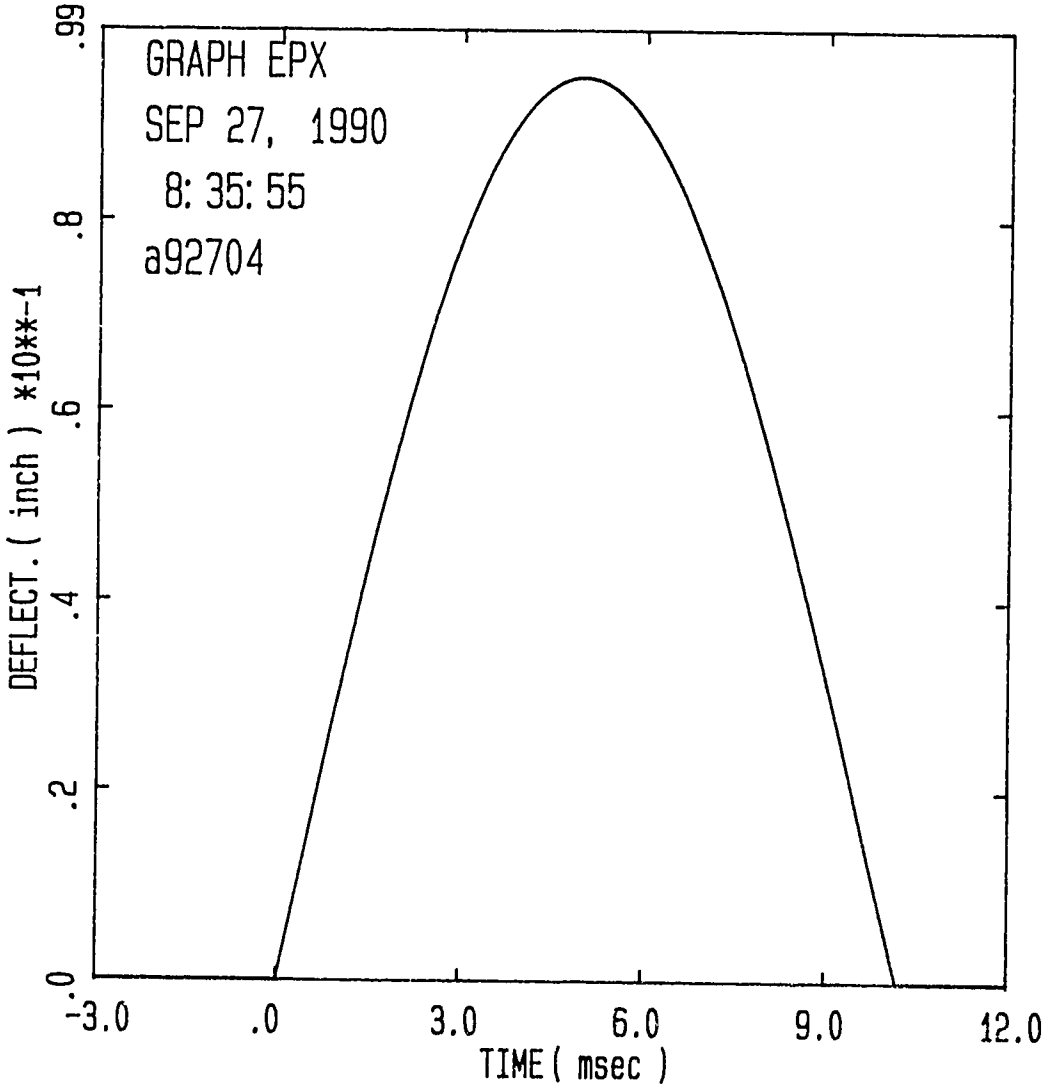


| Specimen Id | Temp ( f) | Impact Veloc. (ft/sec) | Impact Energy (ft-lb ) | Time ( msec ) Max Ld | Time ( msec ) Total | Load ( lb ) Max | Energy (ft-lb ) Maxld | Energy (ft-lb ) Total |
|---|---|---|---|---|---|---|---|---|
| a92704 | 70. | 2.55 | .69 | 4.57 | 9.75 | 173.6 | .736 | .157 |

Figure B.26. Deflection from Dynatup for $[90/0]_{3S}$ Panel, Impact Energy = 0.69 ft-lb

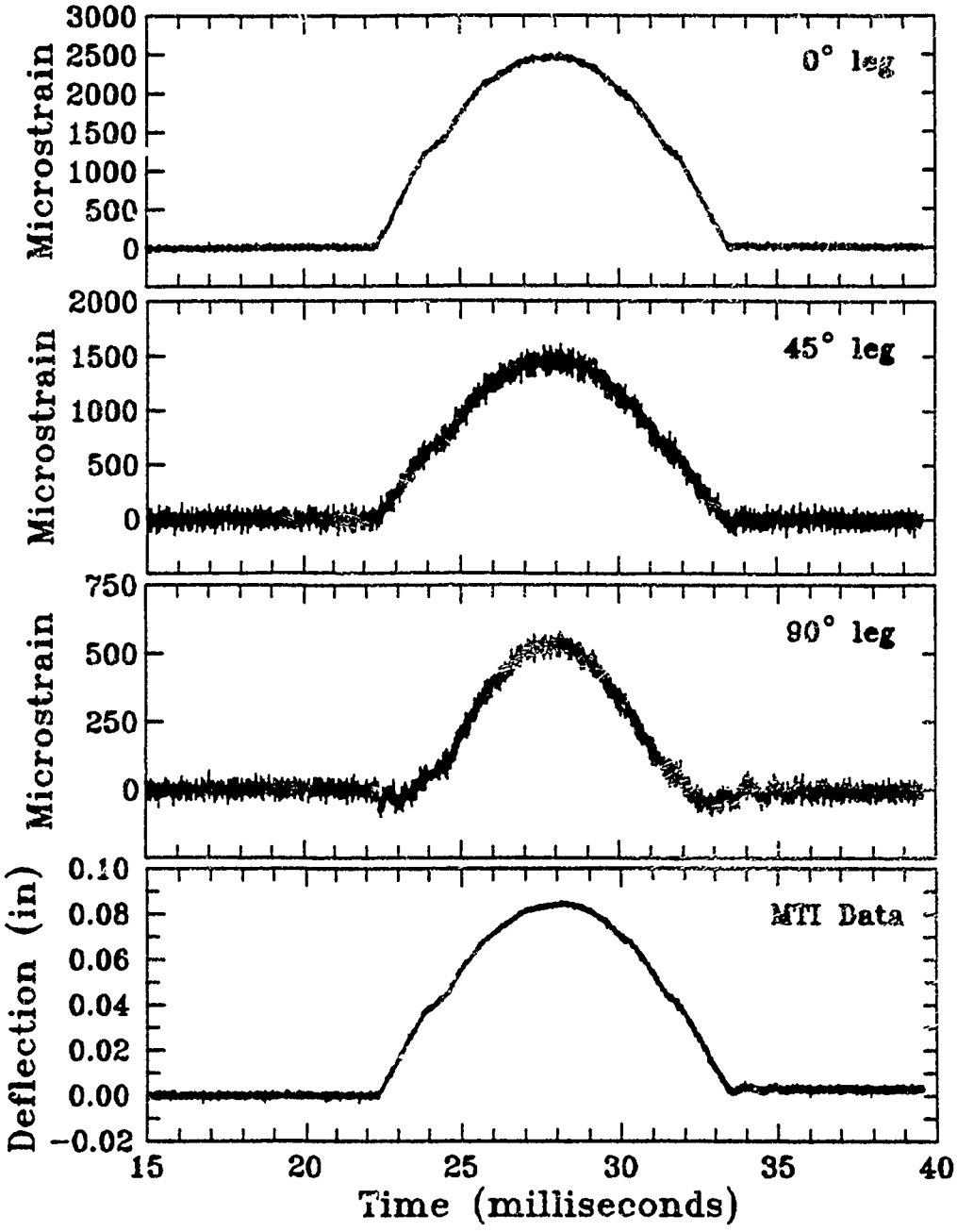


Figure B.27. Strain and Deflection for $[90/0]_{3S}$ Panel, Impact Energy = 0.69 ft-lb

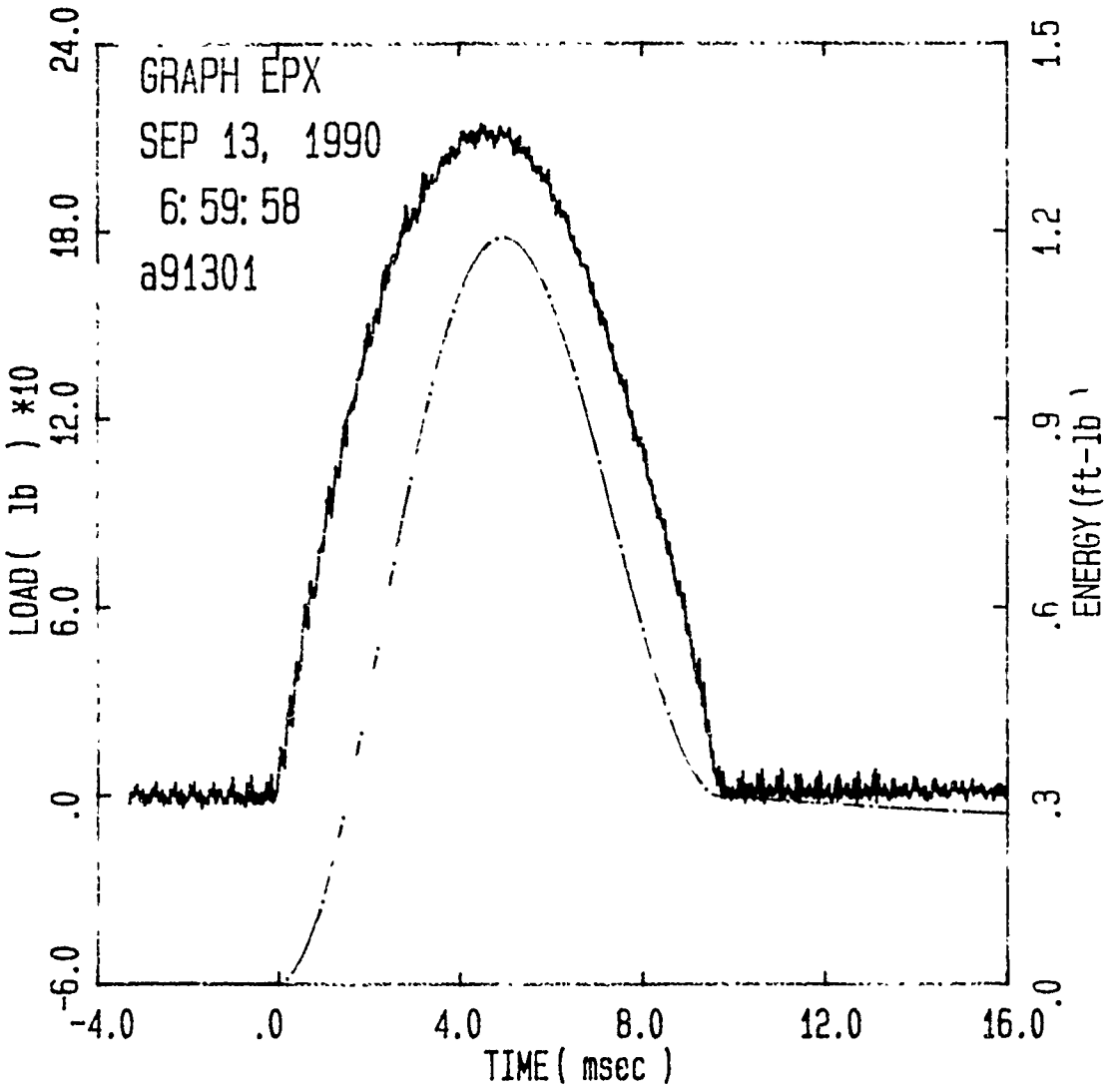


| Specimen Id | Temp ( f) | Impact Veloc. (ft/sec) | Energy (ft-lb ) | Time ( msec ) Max Ld | Time ( msec ) Total | Load ( lb ) Max | Energy (ft-lb ) Maxld | Energy (ft-lb ) Total |
|---|---|---|---|---|---|---|---|---|
| a91301 | 70. | 3.25 | 1.12 | 4.47 | 9.75 | 214.0 | 1.166 | .297 |

Figure B.28. Load and Energy from Dynatup for $[90/0]_{3S}$ Panel, Impact Energy = 1.12 ft-lb

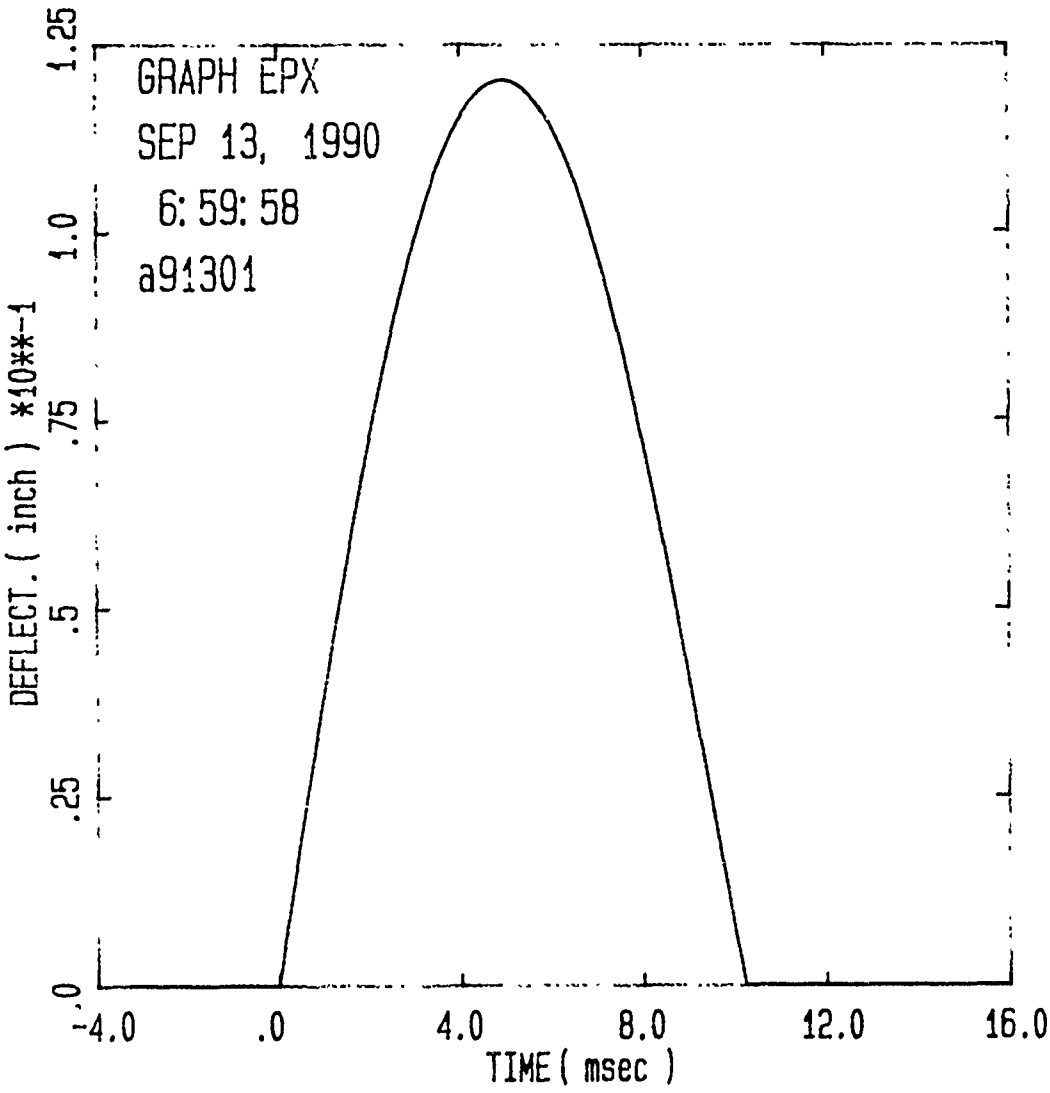


| Specimen Id | Temp ( f) | Impact Veloc. (ft/sec) | Impact Energy (ft-lb ) | Time ( msec ) Max Ld | Time ( msec ) Total | Load ( lb ) Max | Energy (ft-lb ) Maxld | Energy (ft-lb ) Total |
|---|---|---|---|---|---|---|---|---|
| a91301 | 70. | 3.25 | 1.12 | 4.47 | 9.75 | 214.0 | 1.166 | .297 |

Figure B.29. Deflection from Dynatup for $[90/0]_{3S}$ Panel, Impact Energy = 1.12 ft-lb

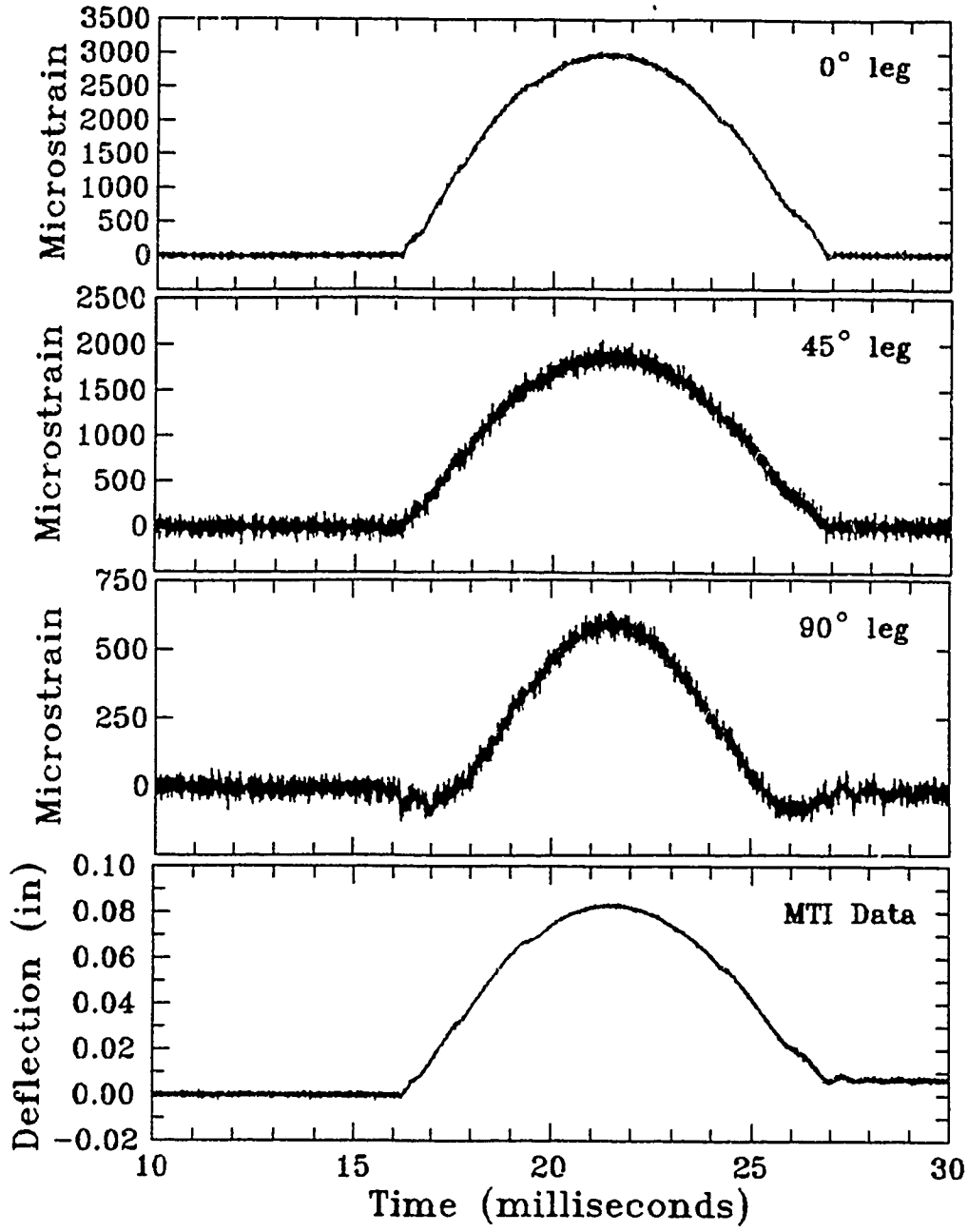


Figure B.30. Strain and Deflection for $[90/0]_{3S}$ Panel, Impact Energy = 1.12 ft-lb

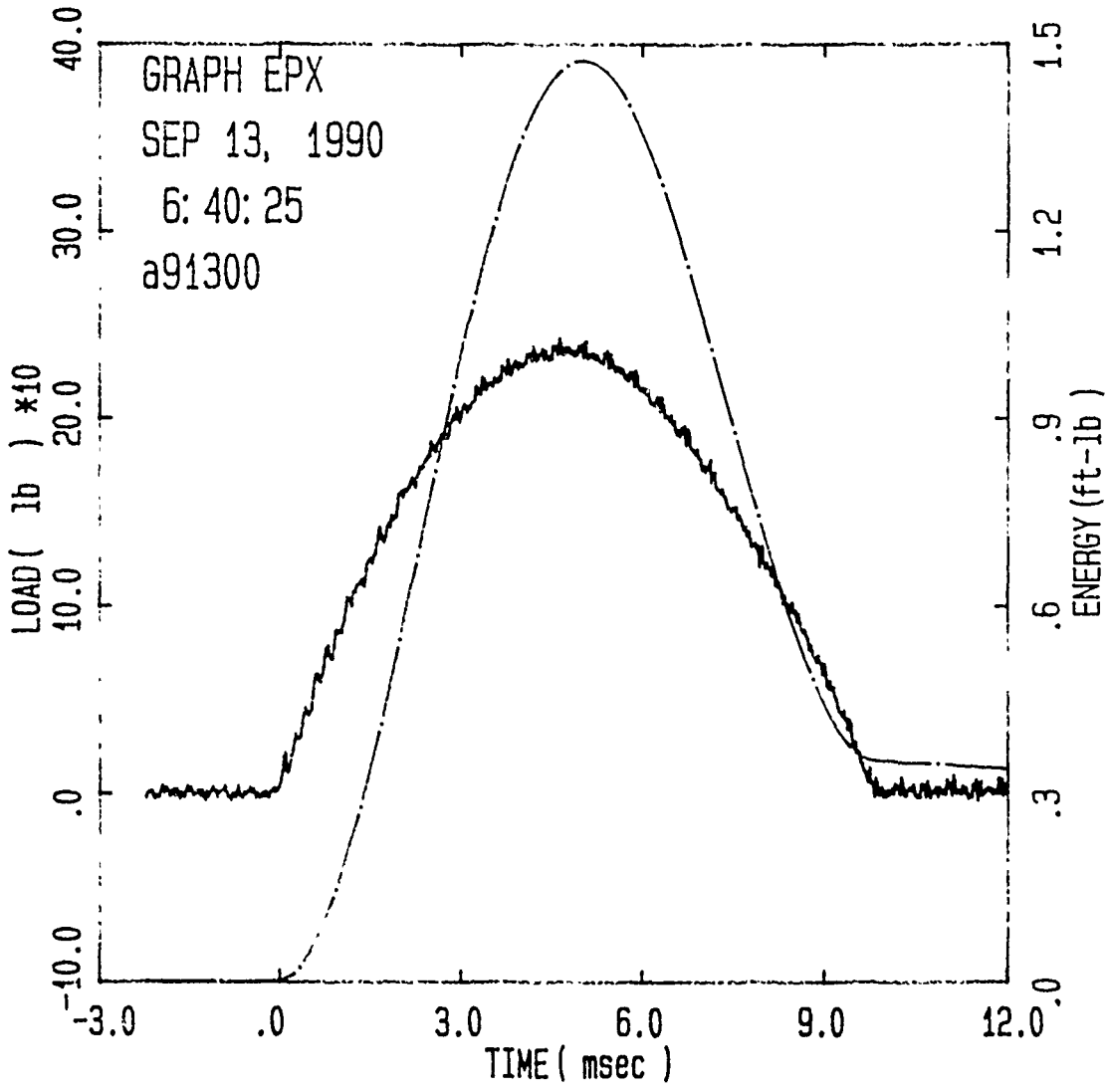


| Specimen Id | Temp ( f) | Impact Veloc. (ft/sec) | Energy (ft-lb ) | Time ( msec ) | | Load ( lb ) | Energy (ft-lb ) | |
|---|---|---|---|---|---|---|---|---|
| | | | | Max Ld | Total | Max | Maxld | Total |
| a91300 | 70. | 3.62 | 1.40 | 4.63 | 9.82 | 242.6 | 1.456 | .353 |

Figure B.31. Load and Energy from Dynatup for $[90/0]_{3S}$ Panel, Impact Energy = 1.40 ft-lb

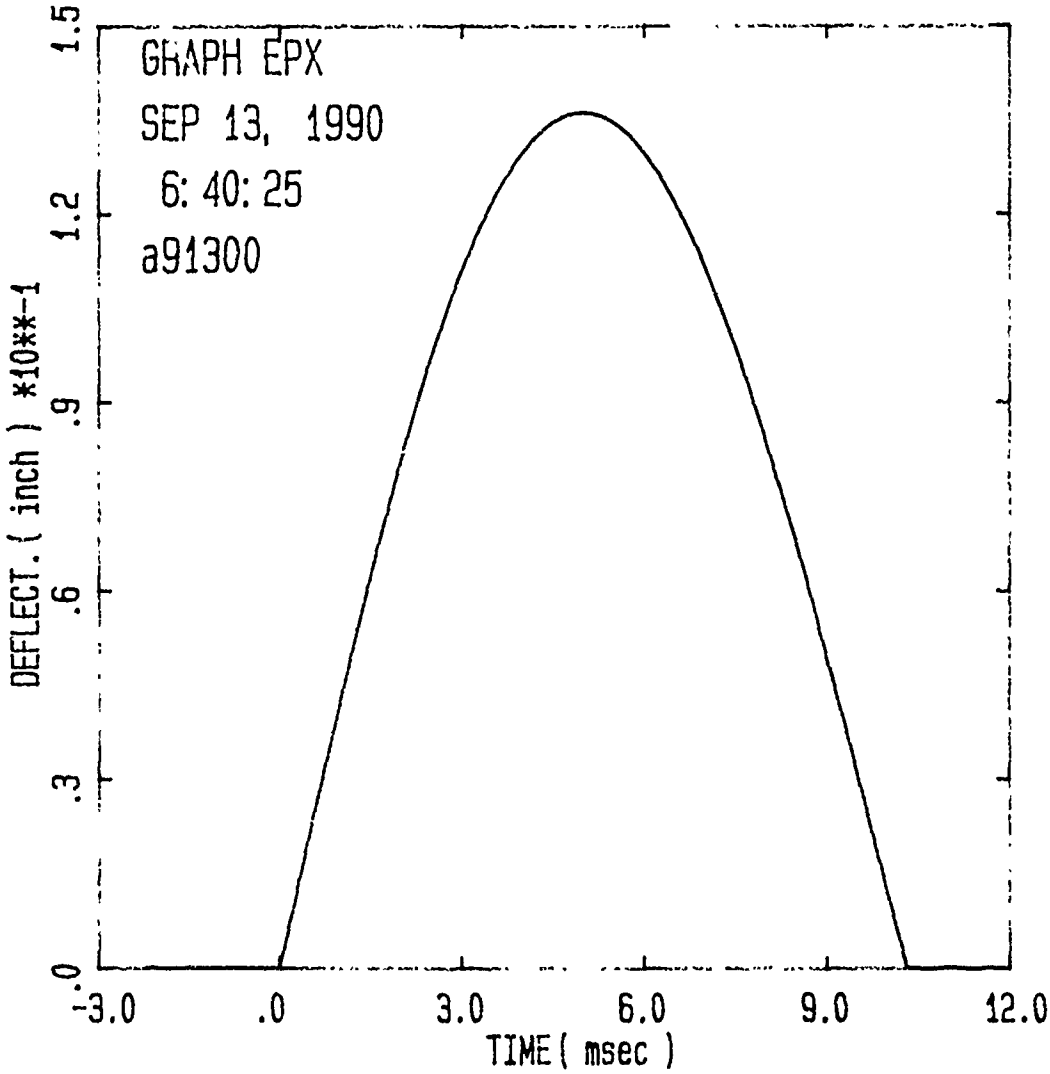


| Specimen Id | Temp (f) | Impact Veloc. (ft/sec) | Impact Energy (ft-lb) | Time (msec) Max Ld | Time (msec) Total | Load (lb) Max | Energy (ft-lb) Maxld | Energy (ft-lb) Total |
|---|---|---|---|---|---|---|---|---|
| a91300 | 70. | 3.62 | 1.40 | 4.63 | 9.82 | 242.6 | 1.456 | .353 |

Figure B.32. Deflection from Dynatup for $[90/0]_{3S}$ Panel, Impact Energy = 1.40 ft-lb

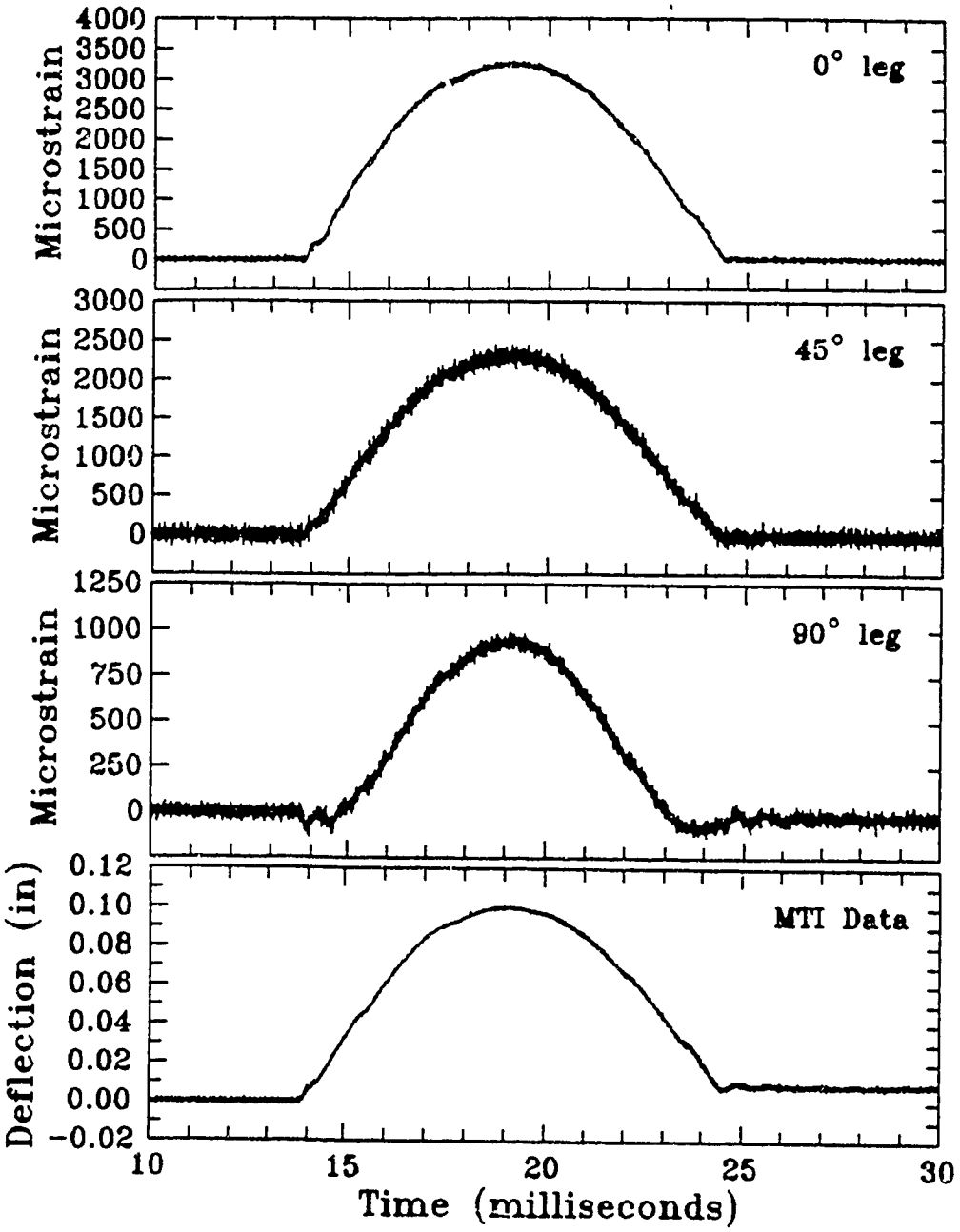


Figure B.33. Strain and Deflection for $[90/0]_{3S}$ Panel, Impact Energy = 1.40 ft-lb

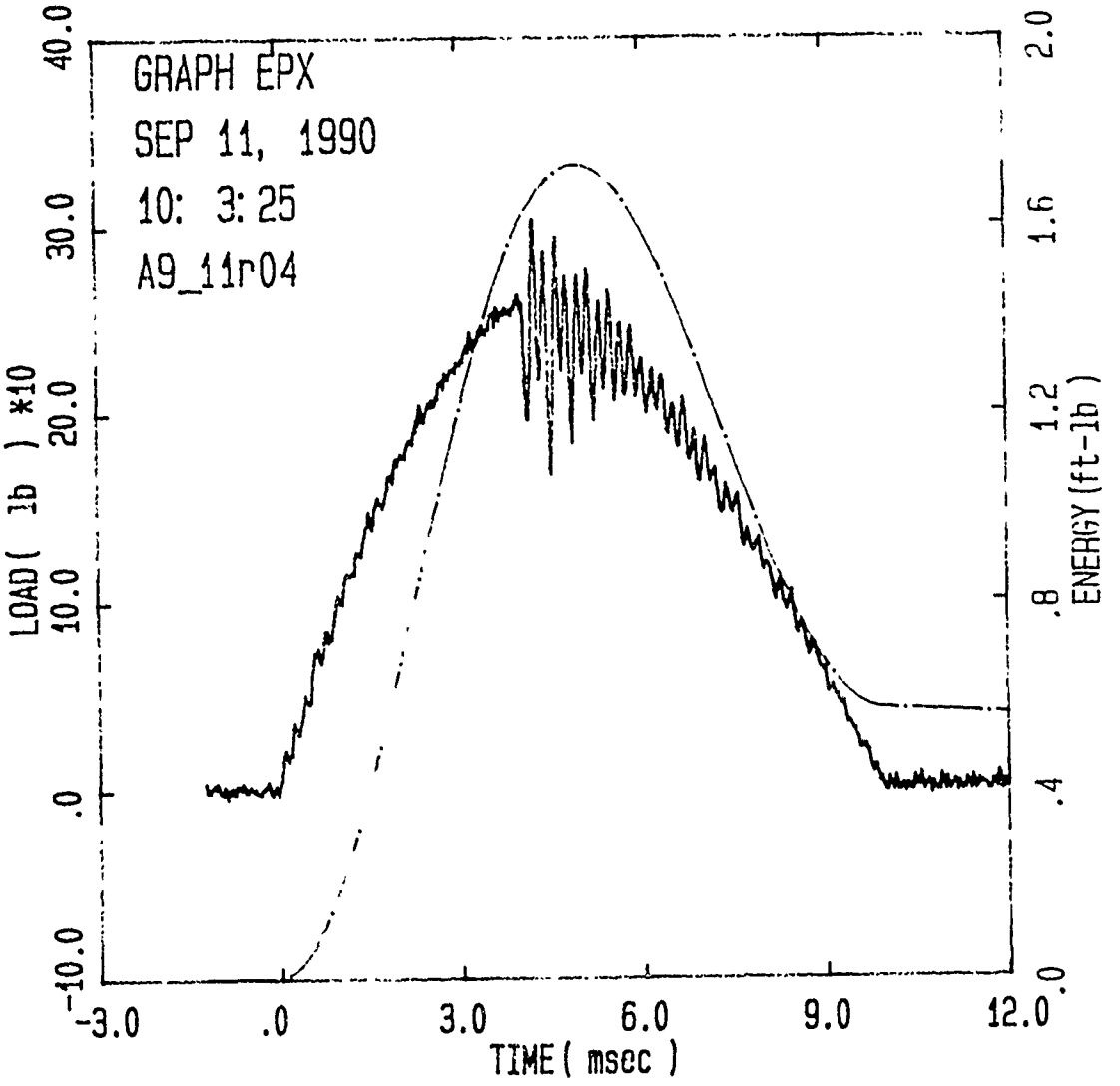


| Specimen Id | Temp (f) | Impact Veloc. (ft/sec) | Energy (ft-lb) | Time (msec) Max Ld | Time (msec) Total | Load (lb) Max | Energy (ft-lb) Maxld | Energy (ft-lb) Total |
|---|---|---|---|---|---|---|---|---|
| A9_11r04 | 70. | 3.93 | 1.64 | 4.25 | 10.00 | 302.9 | 1 660 | .571 |

Figure B.34. Load and Energy from Dynatup for $[90/0]_{3S}$ Panel, Impact Energy = 1.64 ft-lb

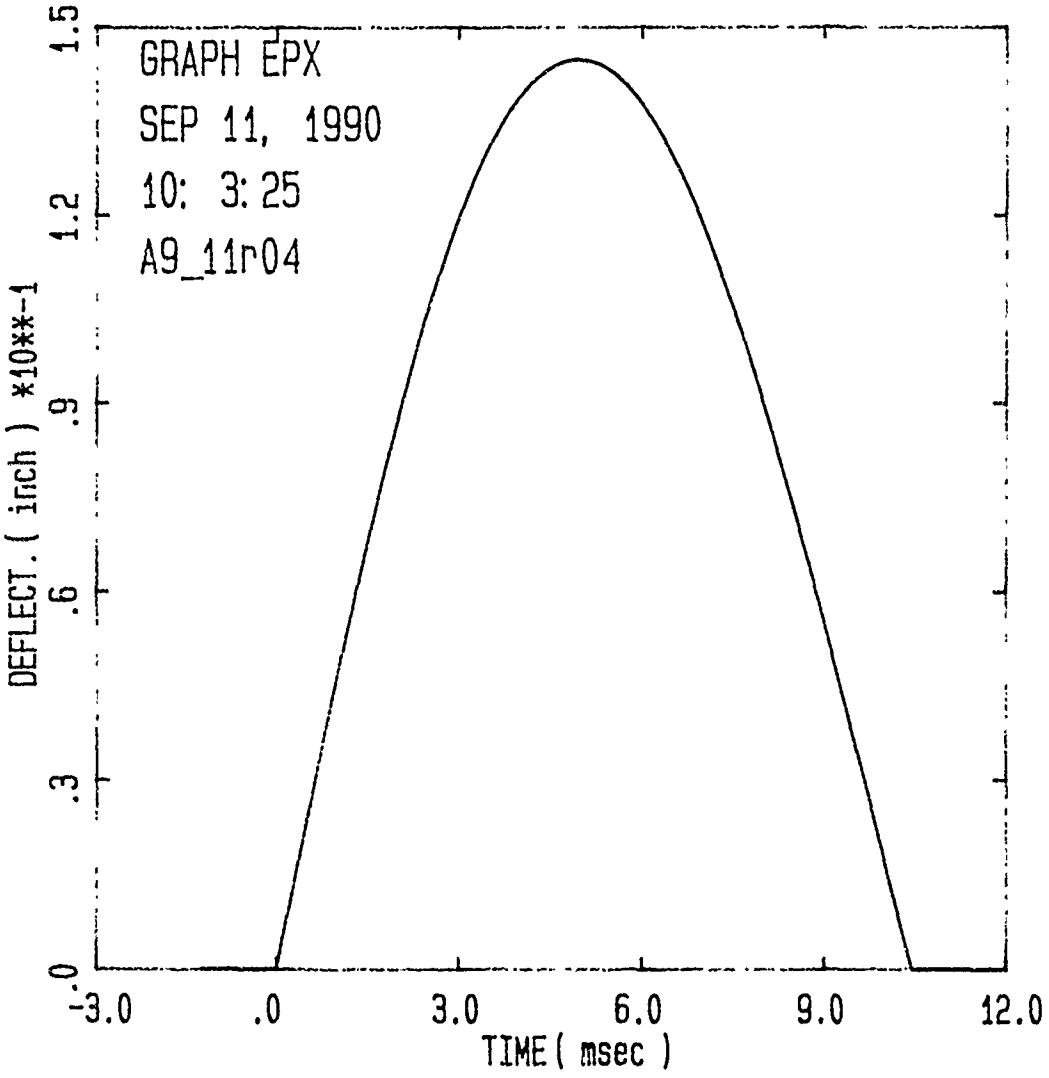


| Specimen Id | Temp (f) | Impact Veloc. (ft/sec) | Impact Energy (ft-lb) | Time (msec) Max Ld | Time (msec) Total | Load (lb) Max | Energy (ft-lb) Maxld | Energy (ft-lb) Total |
|---|---|---|---|---|---|---|---|---|
| A9_11r04 | 70. | 3.93 | 1.64 | 4.25 | 10.00 | 302.9 | 1.660 | .5[illegible] |

Figure B.35. Deflection from Dynatup for $[90/0]_{3S}$ Panel, Impact Energy = 1.64 ft-lb

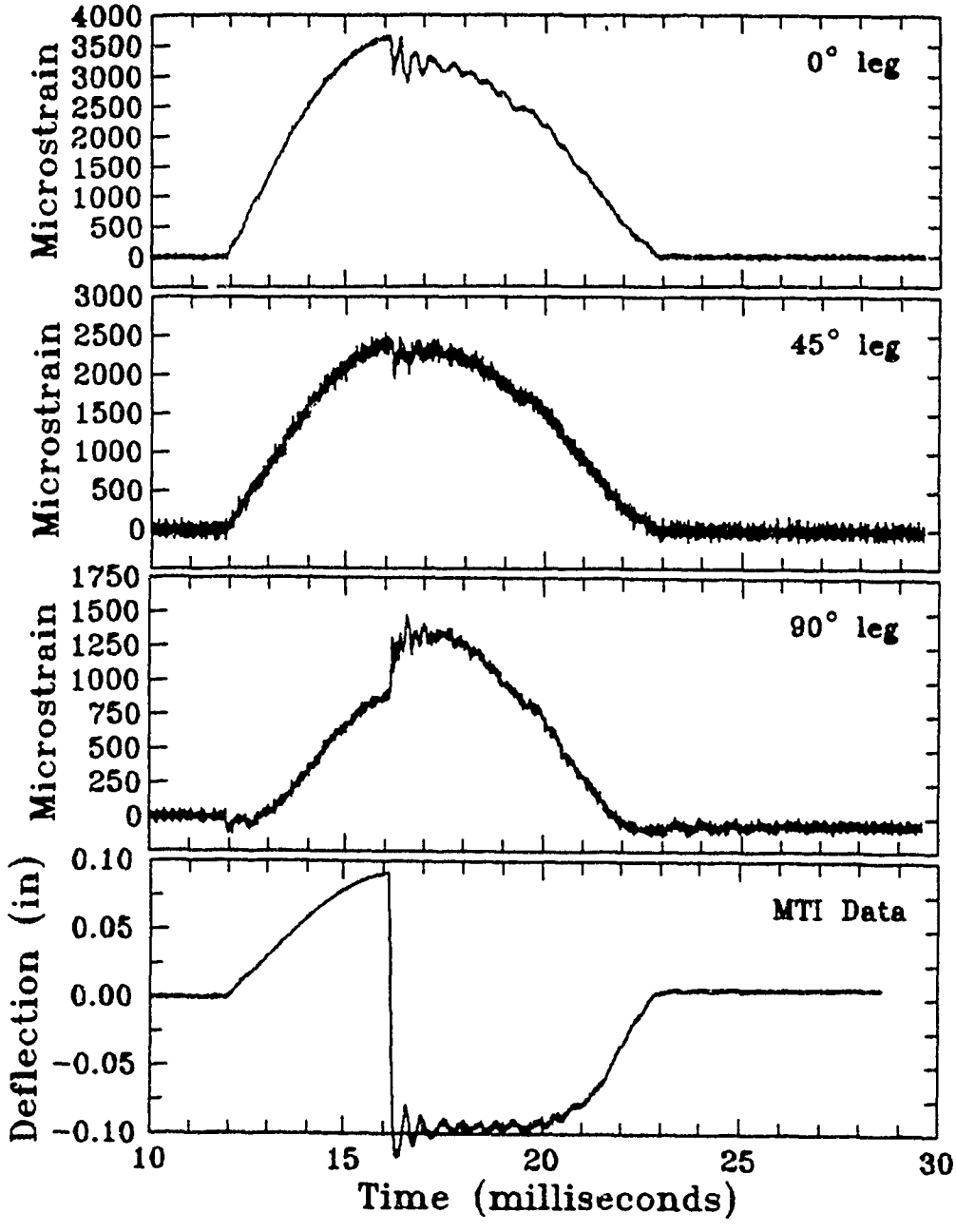


Figure B.36. Strain and Deflection for $[90/0]_{3S}$ Panel, Impact Energy = 1.64 ft-lb

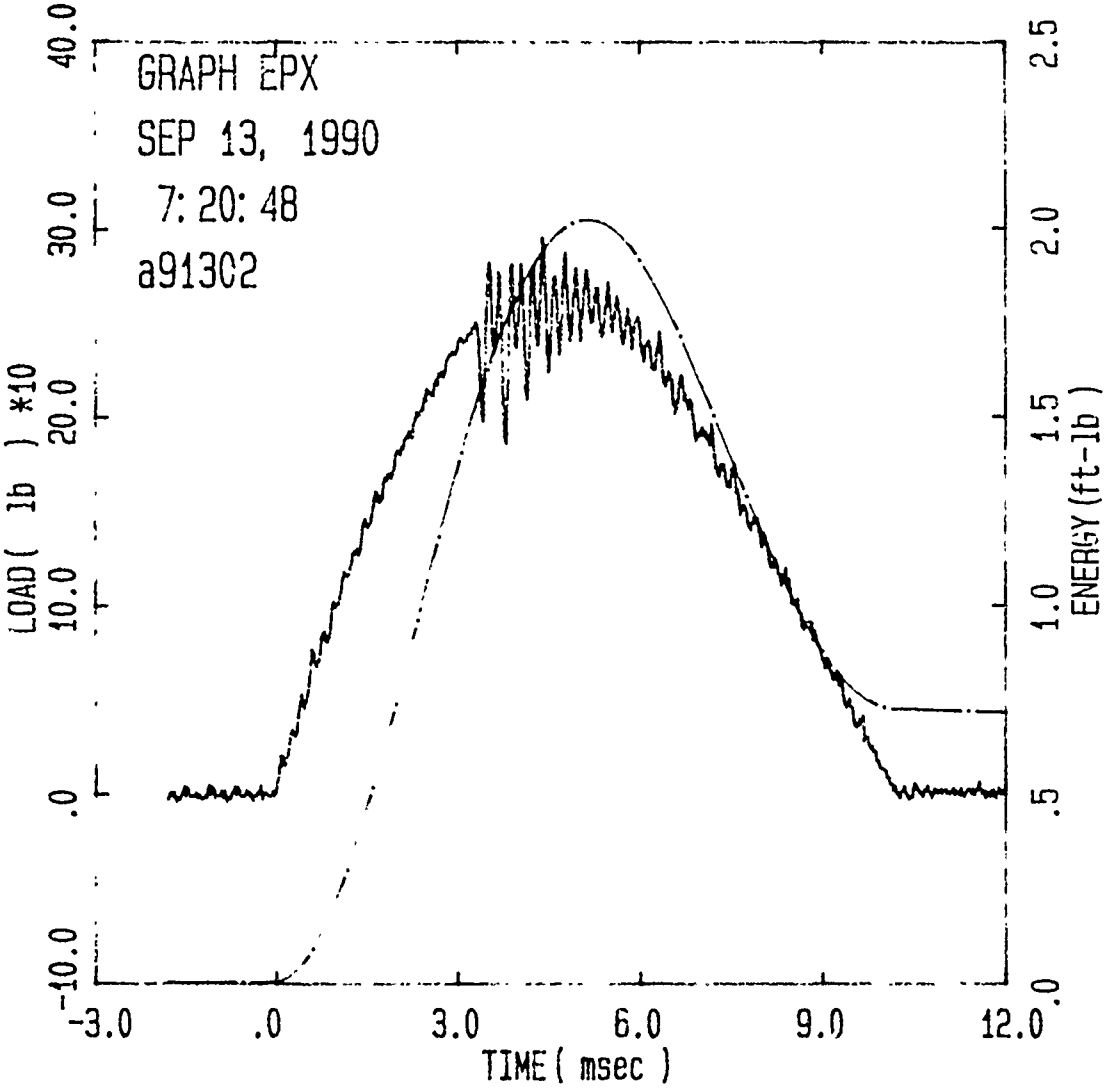


| Specimen Id | Temp (f) | Impact Veloc. (ft/sec) | Impact Energy (ft-lb) | Time (msec) Max Ld | Time (msec) Total | Load (lb) Max | Energy (ft-lb) MaxId | Energy (ft-lb) Total |
|---|---|---|---|---|---|---|---|---|
| a91302 | 70. | 4.26 | 1.93 | 4.40 | 10.25 | 295.4 | 1.938 | .724 |

Figure B.37. Load and Energy from Dynatup for $[90/0]_{3S}$ Panel, Impact Energy = 1.93 ft-lb

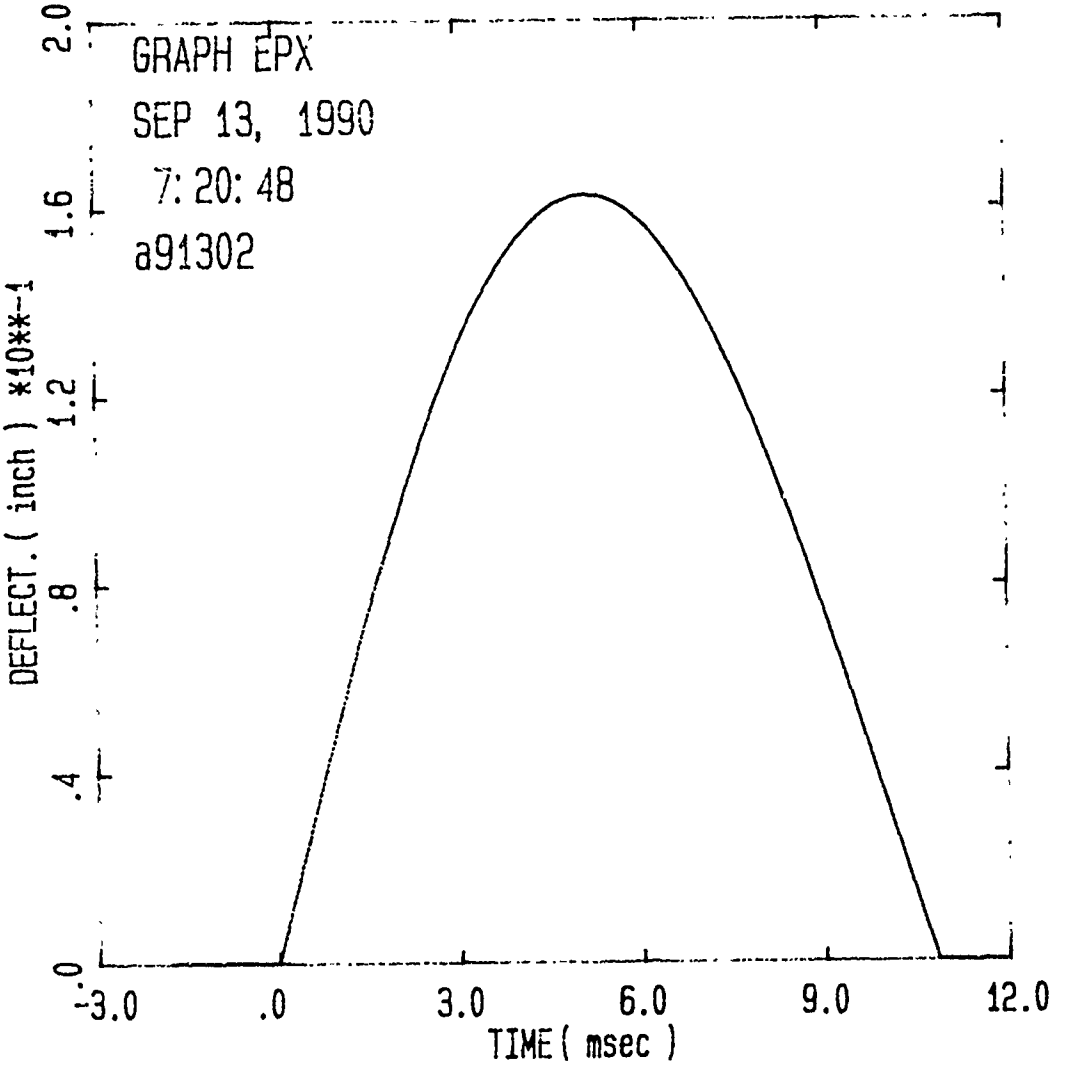


| Specimen Id | Temp ( f) | Impact Veloc. (ft/sec) | Impact Energy (ft-lb ) | Time ( msec ) Max Ld | Time ( msec ) Total | Load ( lb ) Max | Energy (ft-lb ) Maxld | Energy (ft-lb ) Total |
|---|---|---|---|---|---|---|---|---|
| a91302 | 70. | 4.26 | 1.93 | 4.40 | 10.25 | 295.4 | 1.938 | .724 |

Figure B.38. Deflection from Dynatup for $[90/0]_{3S}$ Panel, Impact Energy = 1.93 ft-lb

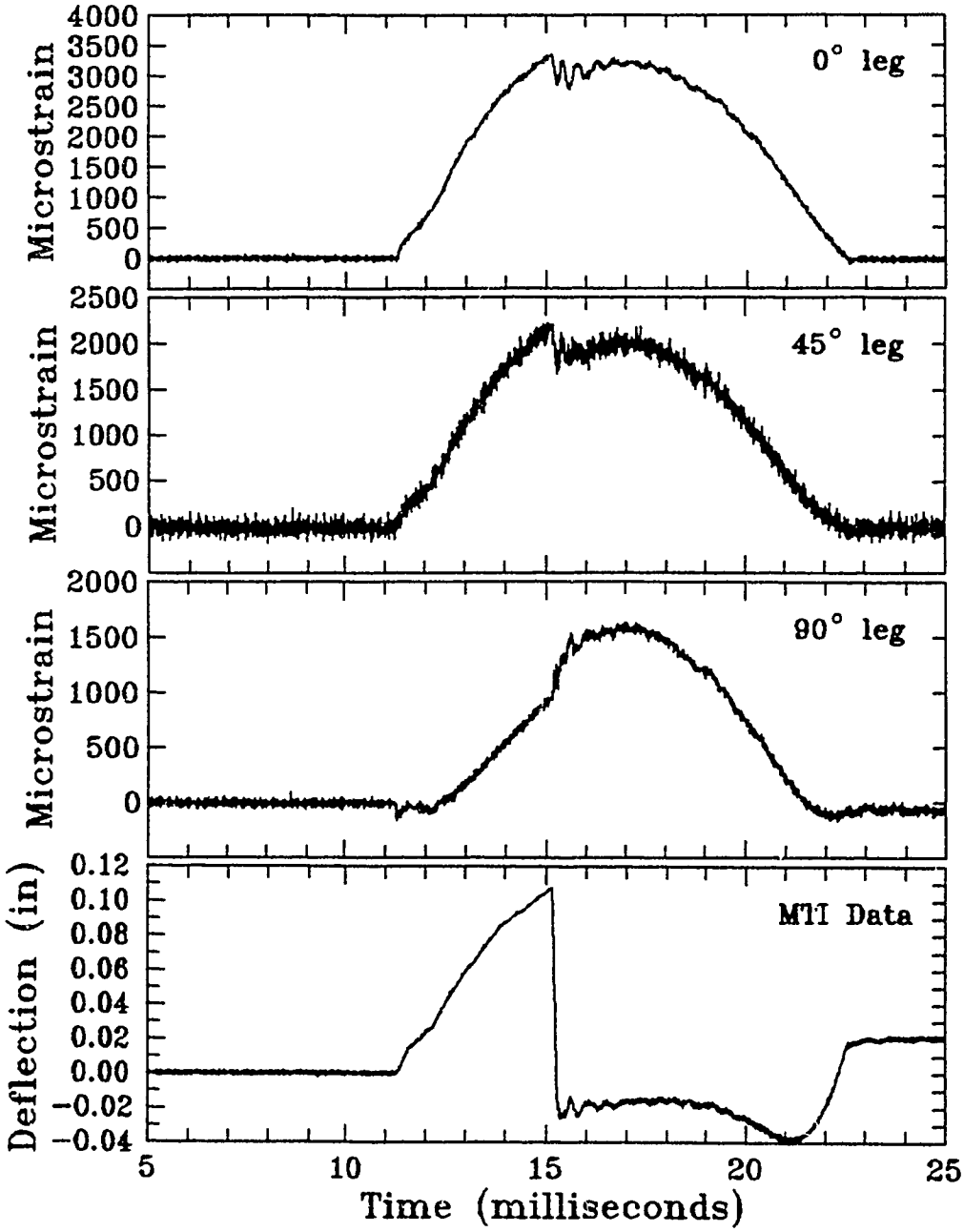


Figure B.39. Strain and Deflection for $[90/0]_{3S}$ Panel, Impact Energy = 1.93 ft-lb

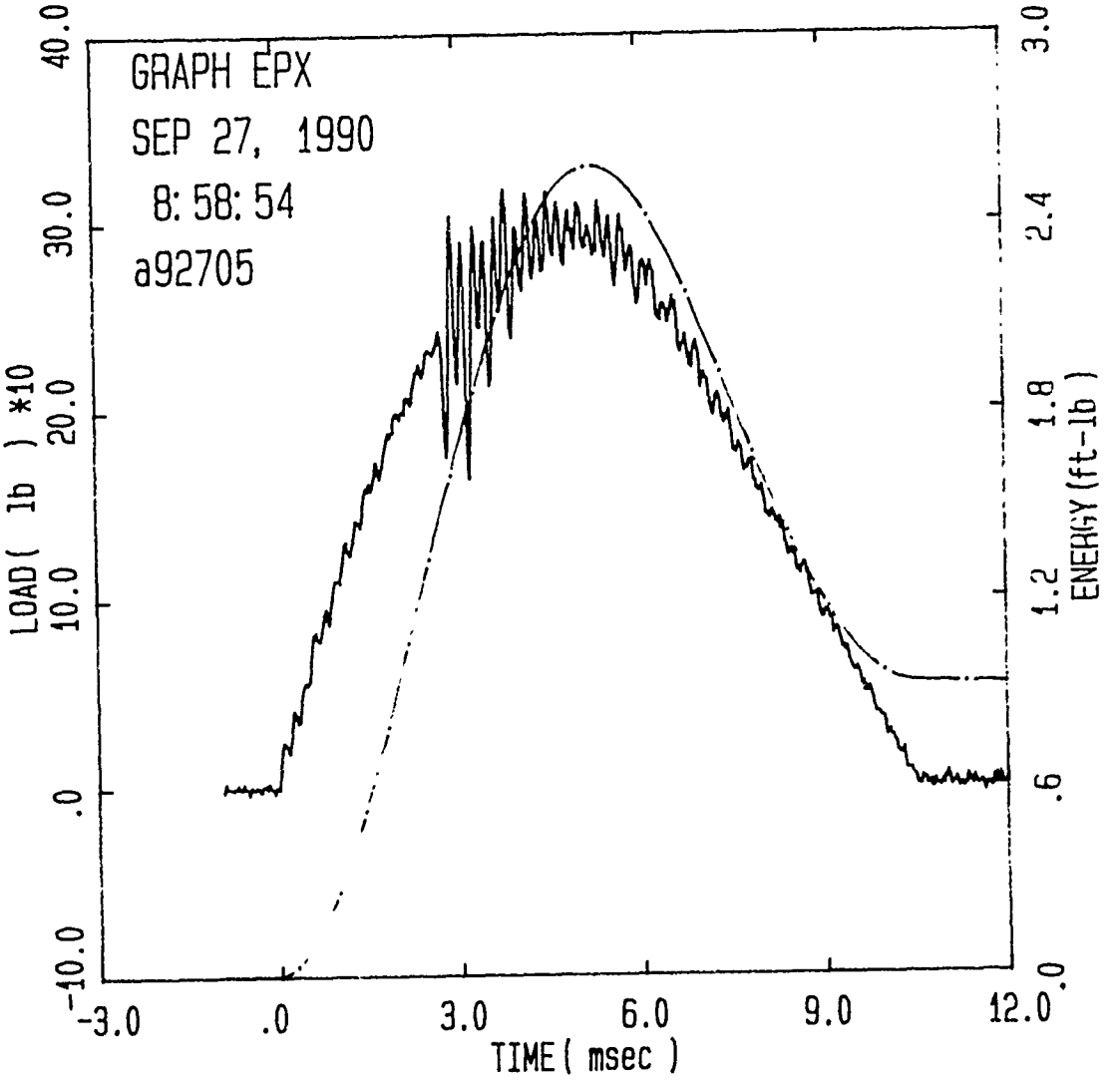


| Specimen Id | Temp ( f) | Impact Veloc. (ft/sec) | Impact Energy (ft-lb ) | Time ( msec ) Max Ld | Time ( msec ) Total | Load ( lb ) Max | Energy (ft-lb ) Max Ld | Energy (ft-lb ) Total |
|---|---|---|---|---|---|---|---|---|
| a92705 | 70. | 4.82 | 2.47 | 3.82 | 10.52 | 317.4 | 2.187 | .927 |

Figure B.40. Load and Energy from Dynatup for $[90/0]_{3S}$ Panel, Impact Energy = 2.47 ft-lb

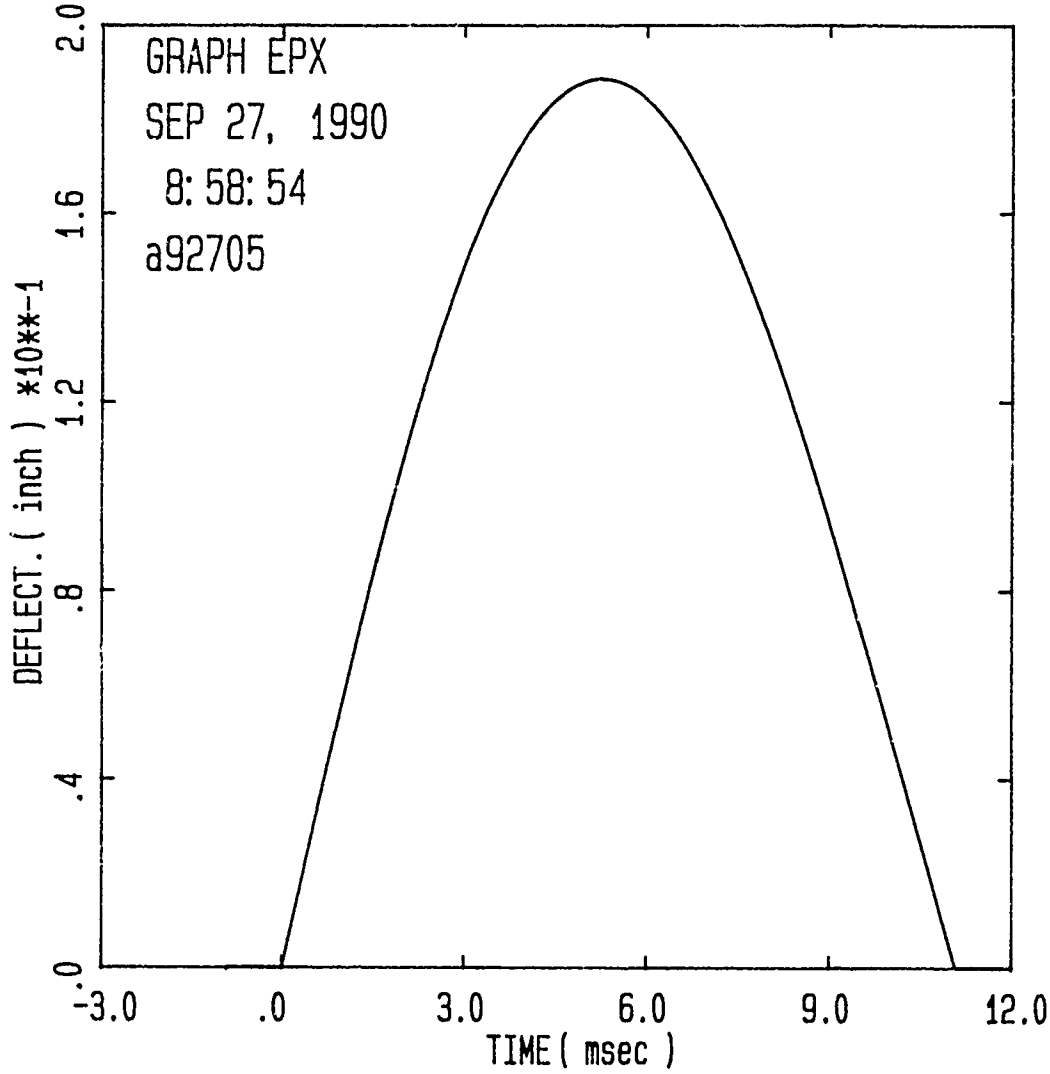


| Specimen Id | Temp ( f) | Impact Veloc. (ft/sec) | Energy (ft-lb ) | Time ( msec ) Max Ld | Time ( msec ) Total | Load ( lb ) Max | Energy (ft-lb ) Maxld | Energy (ft-lb ) Total |
|---|---|---|---|---|---|---|---|---|
| a92705 | 70. | 4.82 | 2.47 | 3.82 | 10.52 | 317.4 | 2.187 | .927 |

Figure B.41. Deflection from Dynatup for $[90/0]_{3S}$ Panel, Impact Energy = 2.47 ft-lb

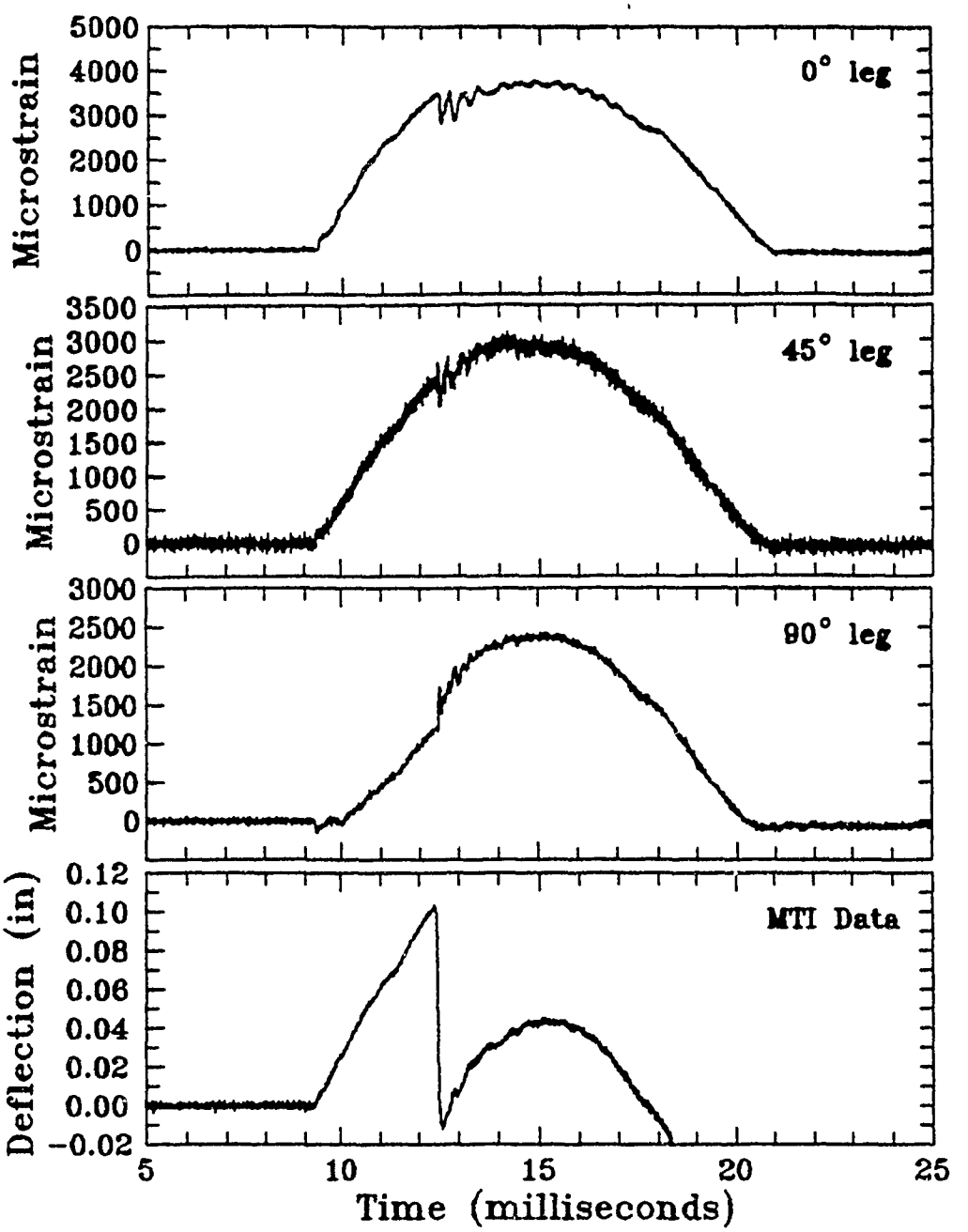


Figure B.42. Strain and Deflection for $[90/0]_{3S}$ Panel, Impact Energy = 2.47 ft-lb

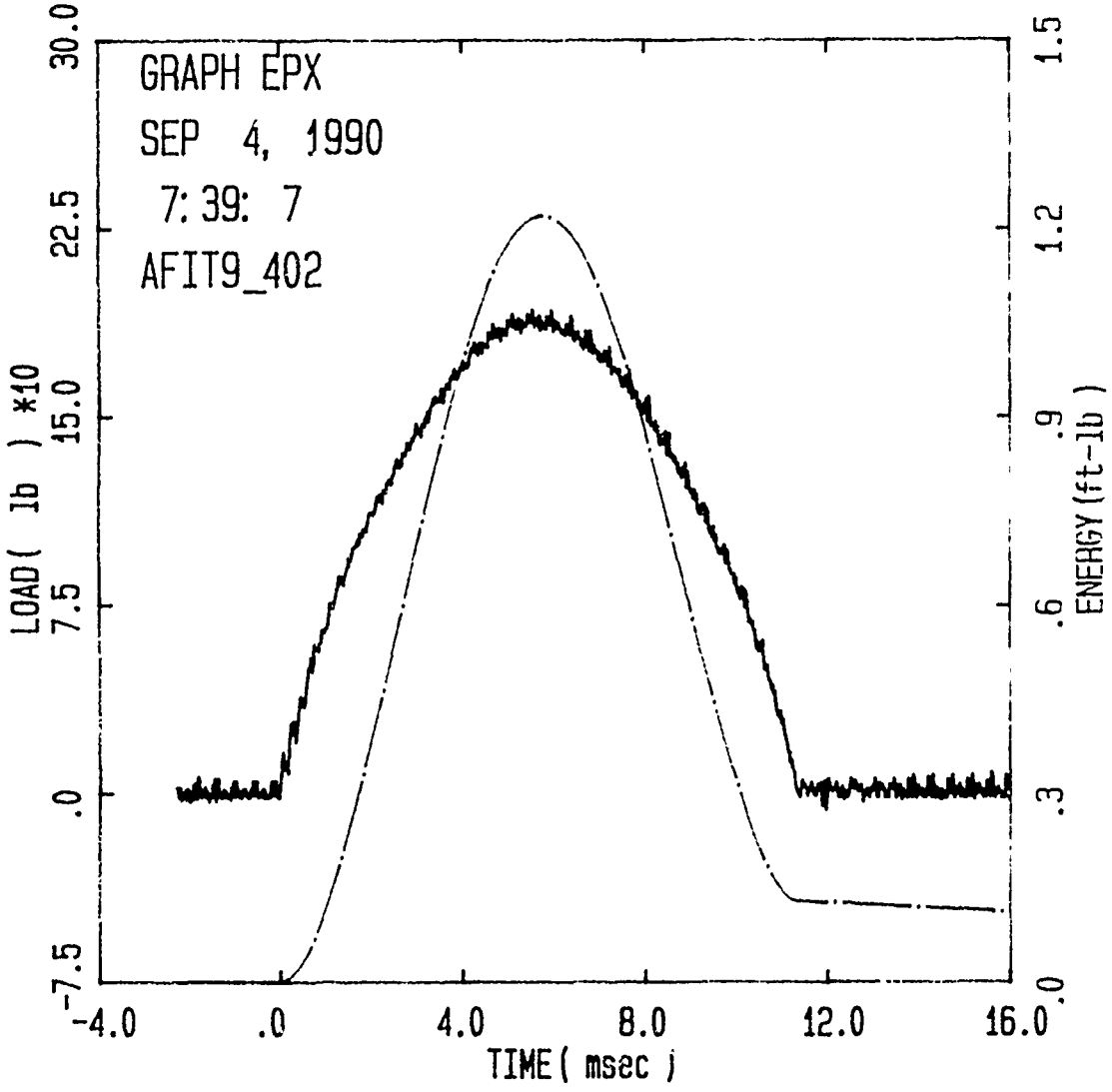


Figure B.43. Load and Energy from Dynatup for $[\pm 45]_{3S}$ Panel, Impact Energy = 1.14 ft-lb

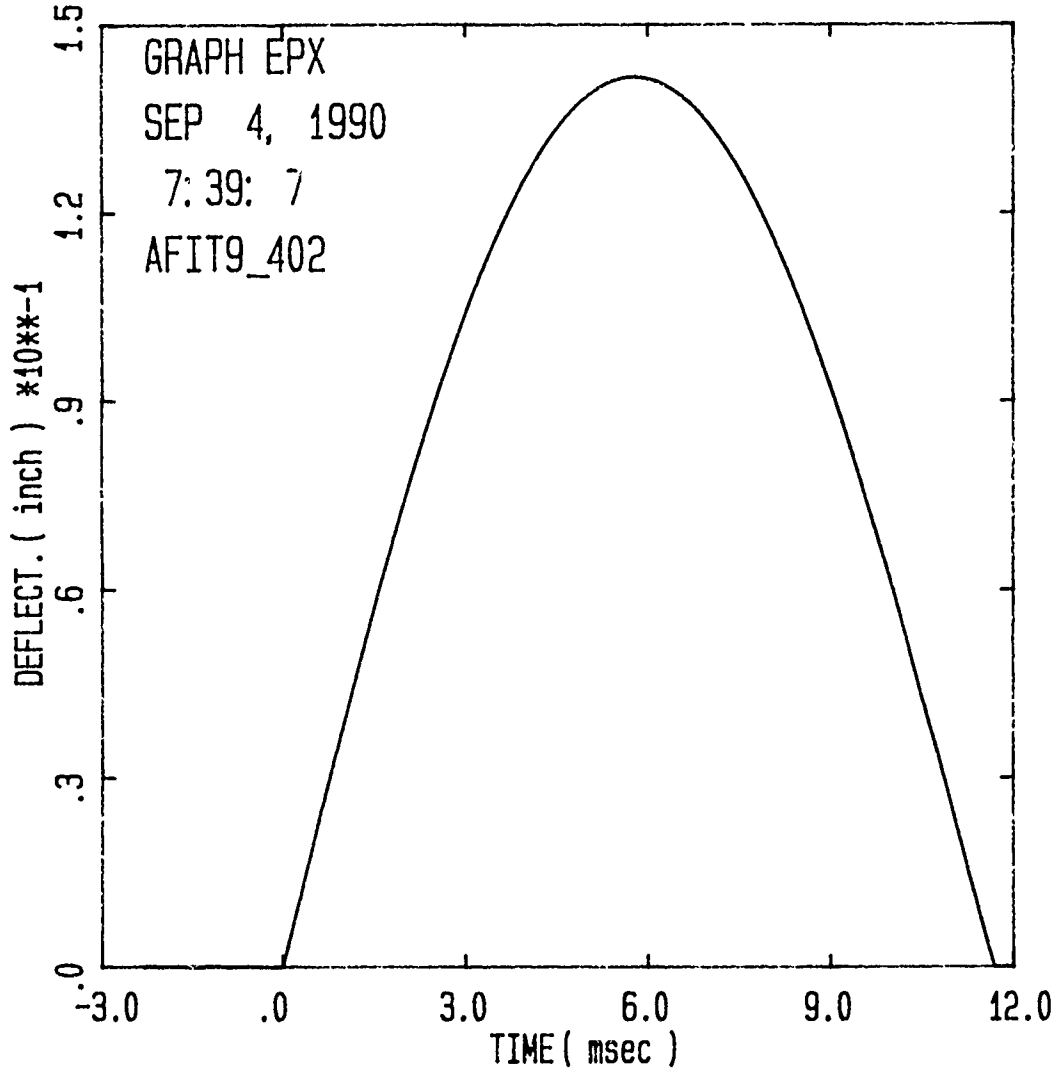


Figure B.44. Deflection from Dynatup for $[\pm 45]_{3S}$ Panel, Impact Energy = 1.14 ft-lb

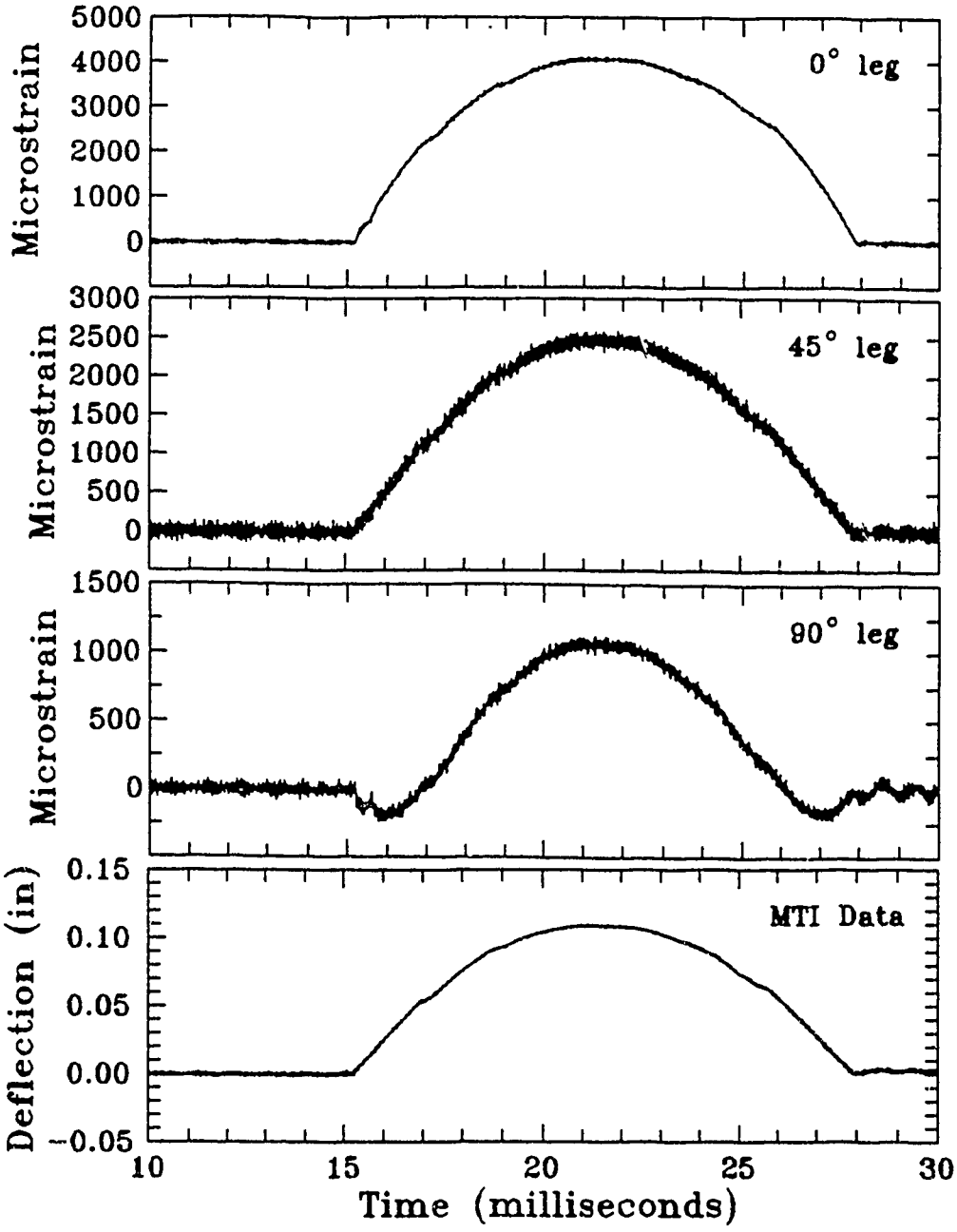


Figure B.45. Strain and Deflection for $[\pm 45]_{3S}$ Panel, Impact Energy = 1.14 ft-lb

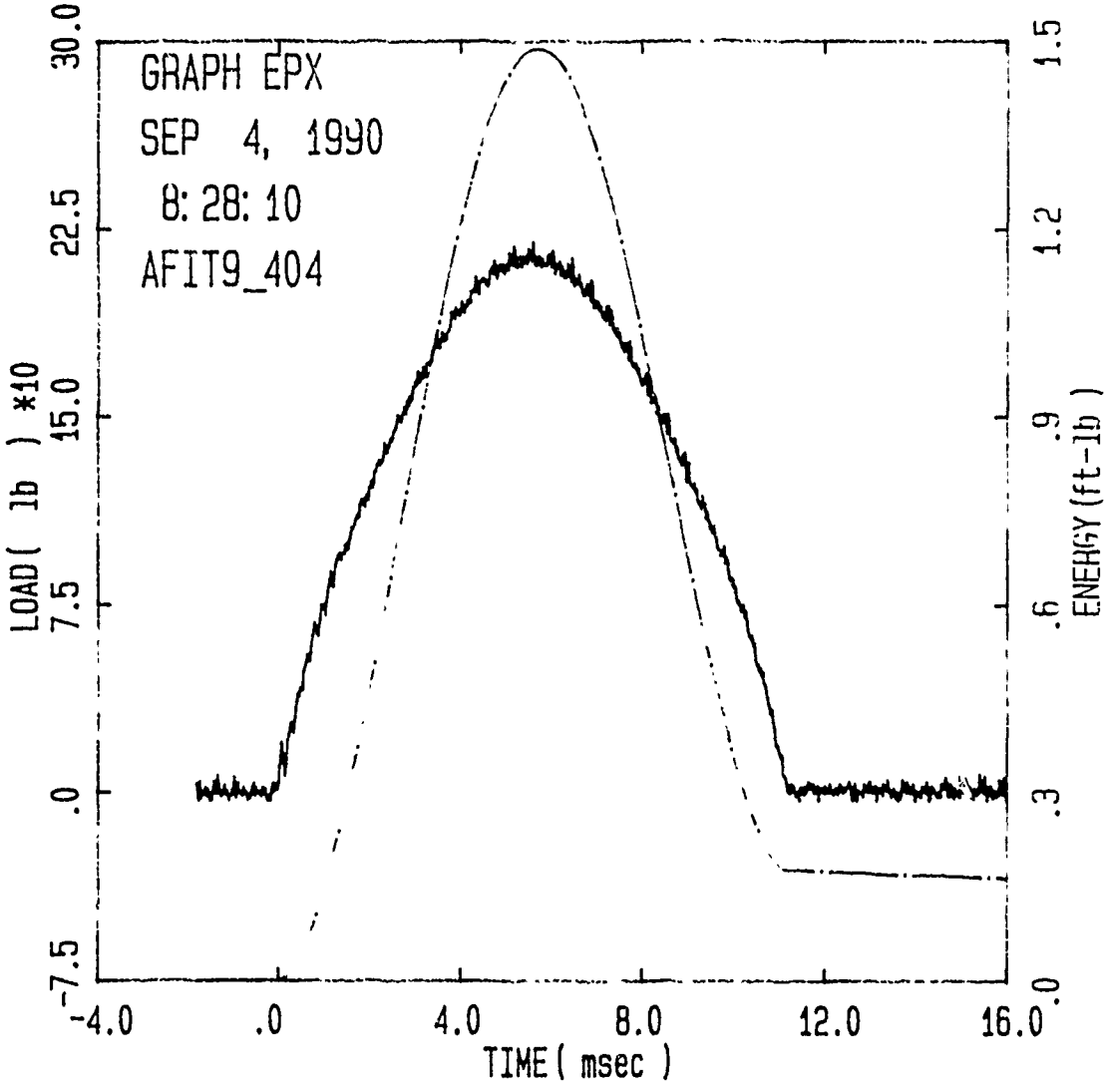


| Specimen Id | Temp (f) | Impact Veloc. (ft/sec) | Impact Energy (ft-lb) | Time (msec) Max Ld | Time (msec) Total | Load (lb) Max | Energy (ft-lb) Maxld | Energy (ft-lb) Total |
|---|---|---|---|---|---|---|---|---|
| AFIT9_404 | 70. | 3.63 | 1.40 | 5.60 | 11.23 | 219.3 | 1 488 | .178 |

Figure B.46. Load and Energy from Dynatup for $[\pm 45]_{3S}$ Panel, Impact Energy = 1.40 ft-lb

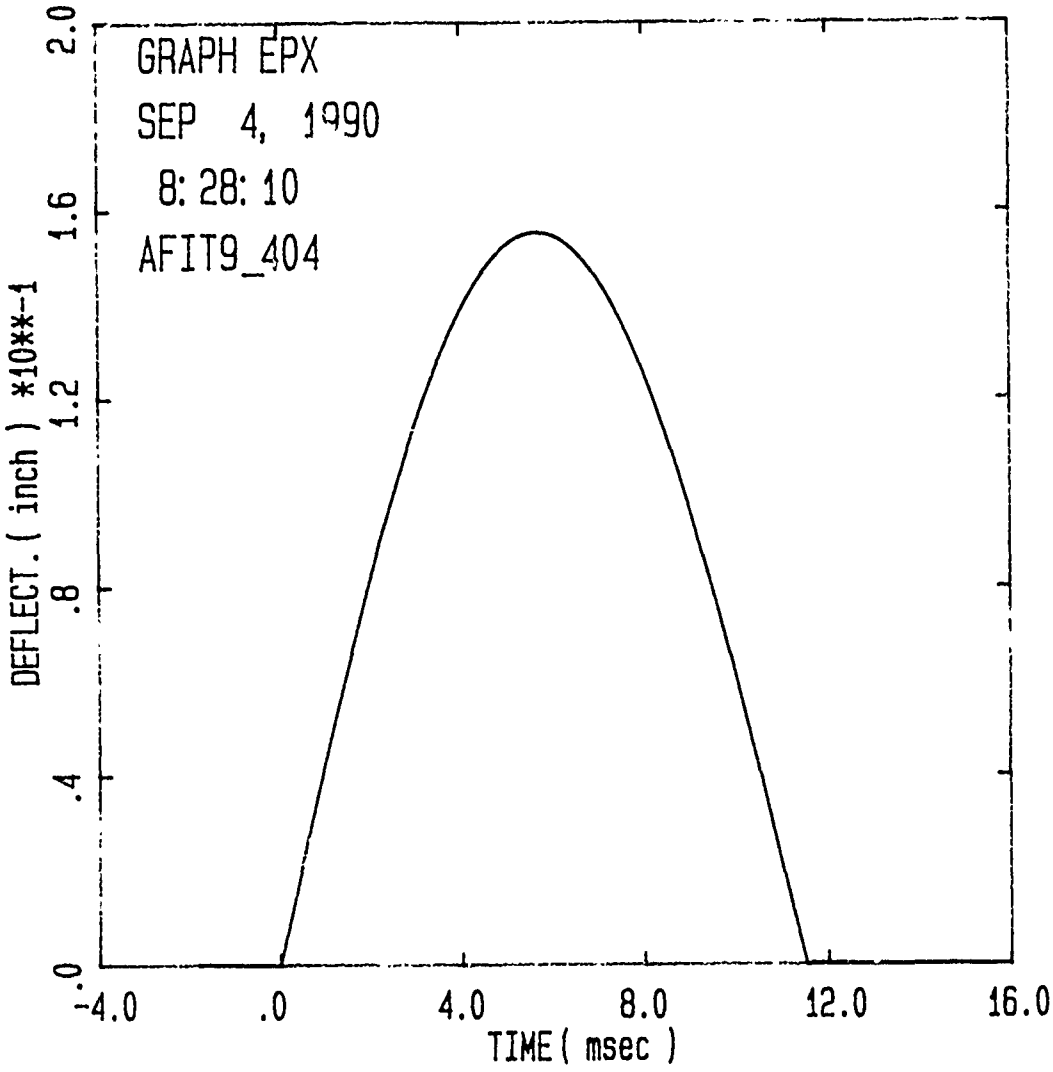


| Specimen Id | Temp ( f) | Impact Veloc. (ft/sec) | Energy (ft-lb ) | Time ( msec ) Max Ld | Time ( msec ) Total | Load ( lb ) Max | Energy (ft-lb ) Maxld | Energy (ft-lb ) Total |
|---|---|---|---|---|---|---|---|---|
| AFIT9_404 | 70. | 3.63 | 1.40 | 5.60 | 11.23 | 219.3 | 1.488 | .178 |

Figure B.47. Deflection from Dynatup for $[\pm 45]_{3S}$ Panel, Impact Energy = 1.40 ft-lb

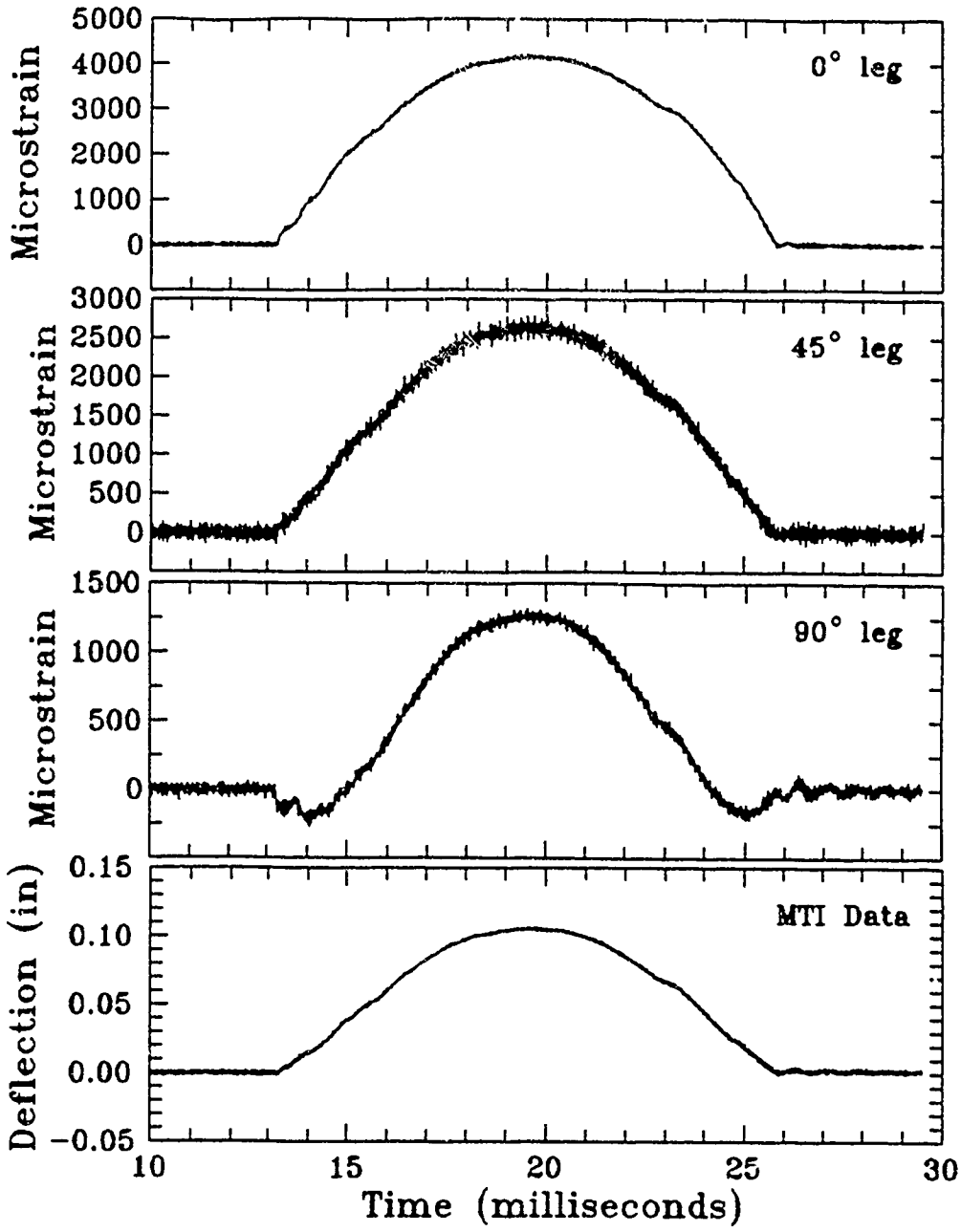


Figure B.48. Strain and Deflection for $[\pm 45]_{3S}$ Panel, Impact Energy = 1.40 ft-ib

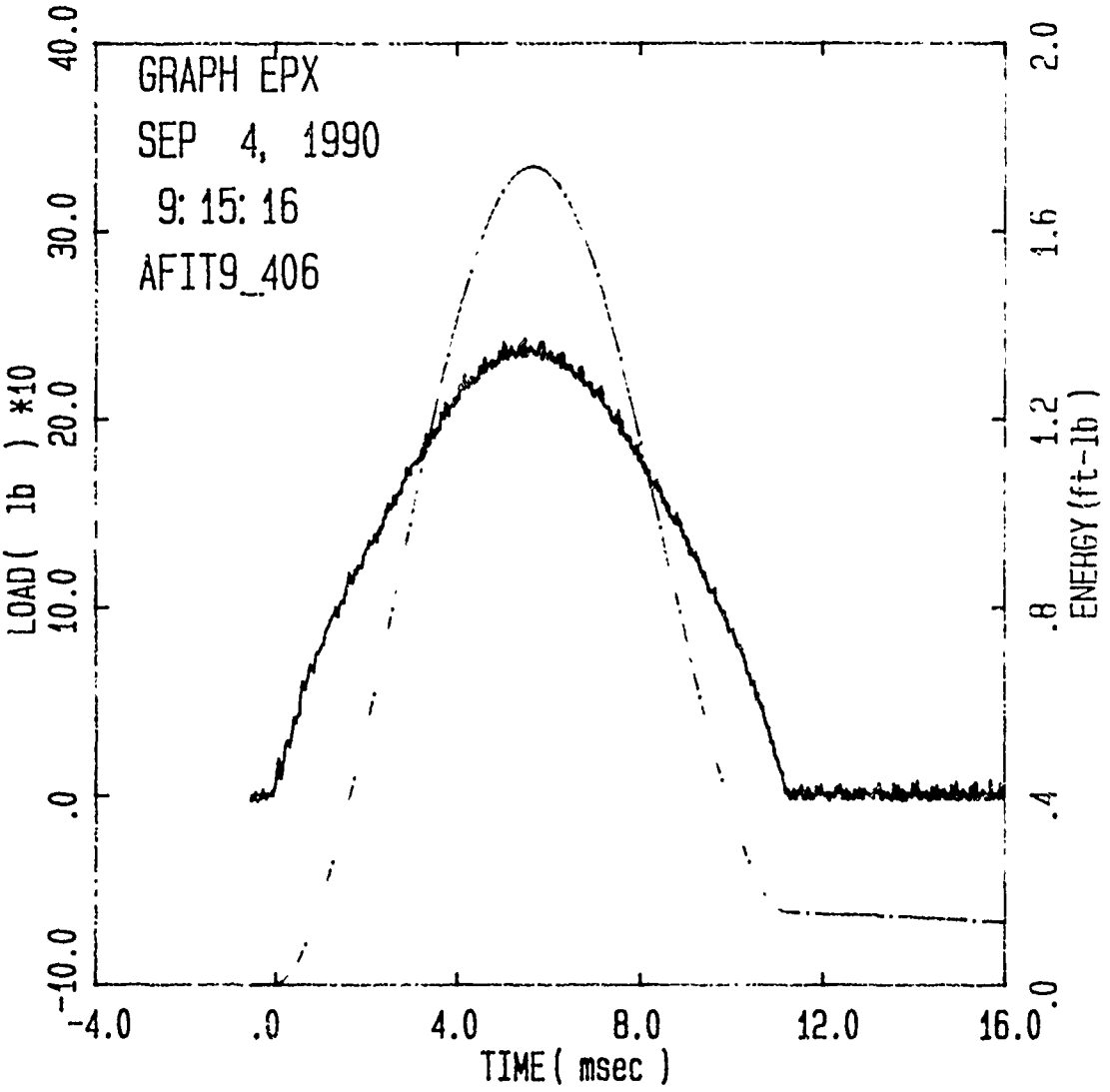


| Specimen Id | Temp | Impact Veloc. | Energy | Time | | Load | Energy | |
|---|---|---|---|---|---|---|---|---|
| | ( f) | (ft/sec) | (ft-lb ) | ( msec ) | | ( lb ) | (ft-lb ) | |
| | | | | Max Ld | Total | Max | Maxld | Total |
| AFIT9_406 | 70. | 3.93 | 1.64 | 5.47 | 11.27 | 242.1 | 1.732 | .153 |

Figure B.49. Load and Energy from Dynatup for $[\pm 45]_{3S}$ Panel, Impact Energy = 1.64 ft-lb

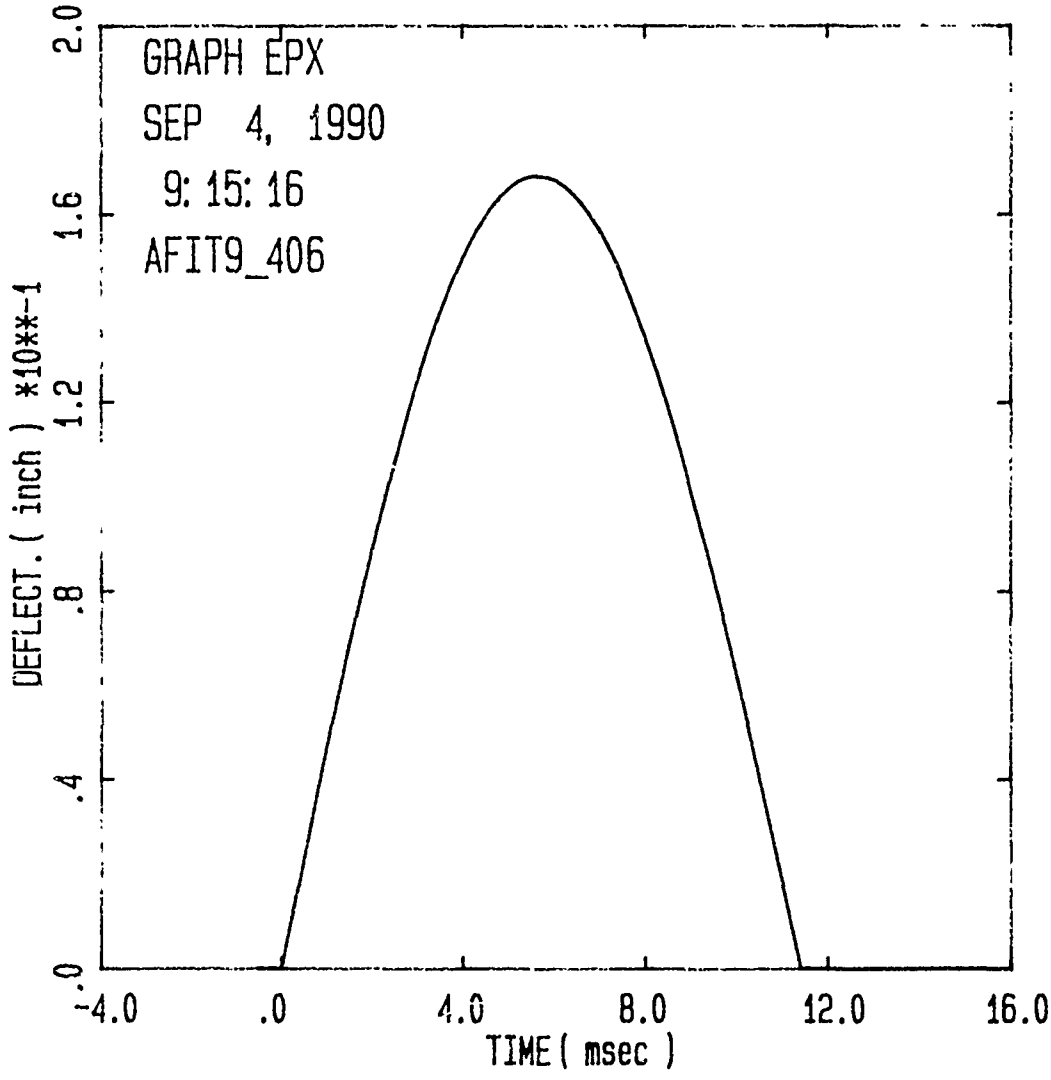


| Specimen Id | Temp ( f) | Impact Veloc. (ft/sec) | Impact Energy (ft-lb ) | Time ( msec ) Max Ld | Time ( msec ) Total | Load ( lb ) Max | Energy (ft-lb ) Maxld | Energy (ft-lb ) Total |
|---|---|---|---|---|---|---|---|---|
| AFIT9_406 | 70. | 3.93 | 1.64 | 5.47 | 11.27 | 242.1 | 1.732 | .153 |

Figure B.50. Deflection from Dynatup for $[\pm 45]_{3S}$ Panel, Impact Energy = 1.64 ft-lb

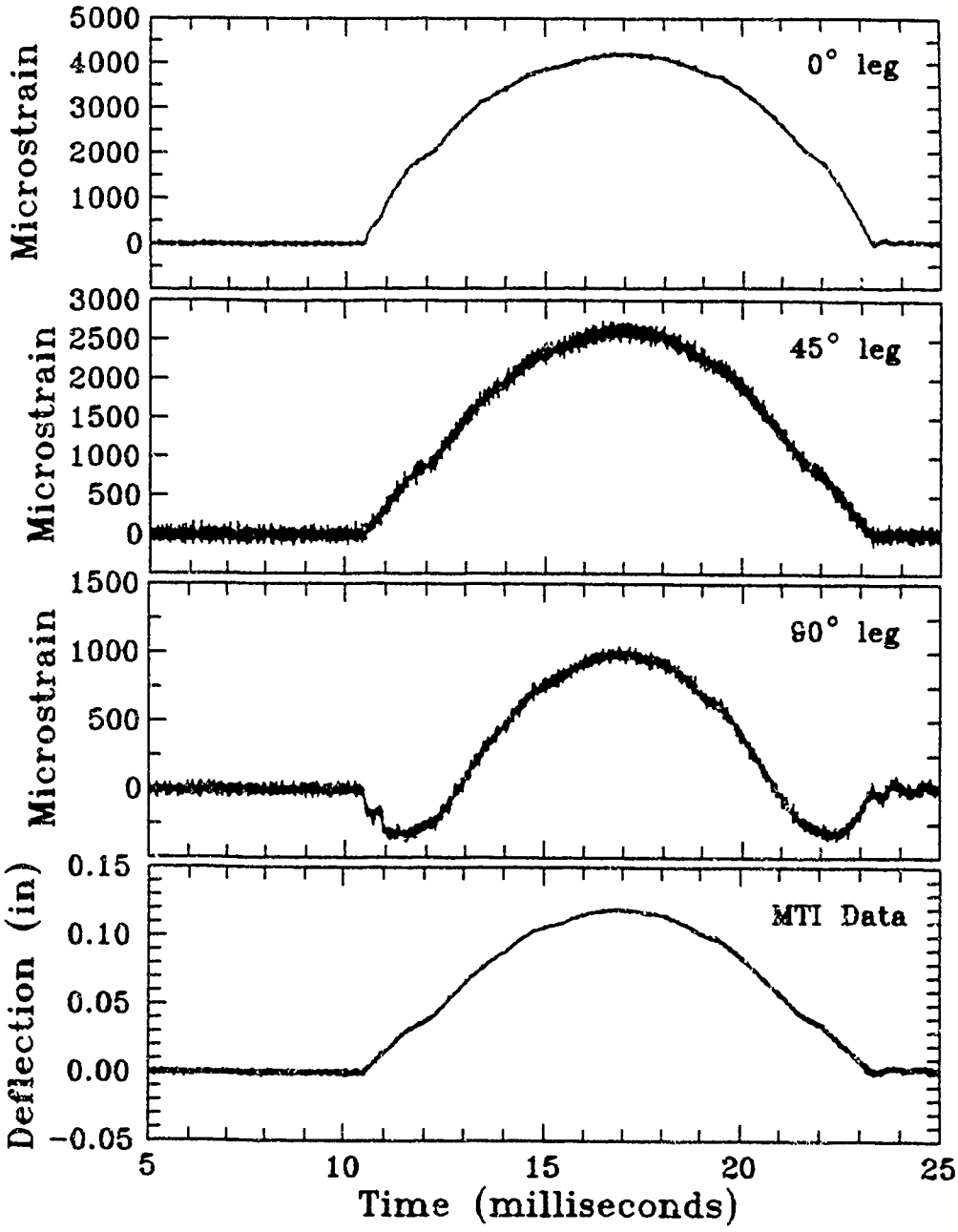


Figure B.51. Strain and Deflection for $[\pm 45]_{3S}$ Panel, Impact Energy = 1.64 ft-lb

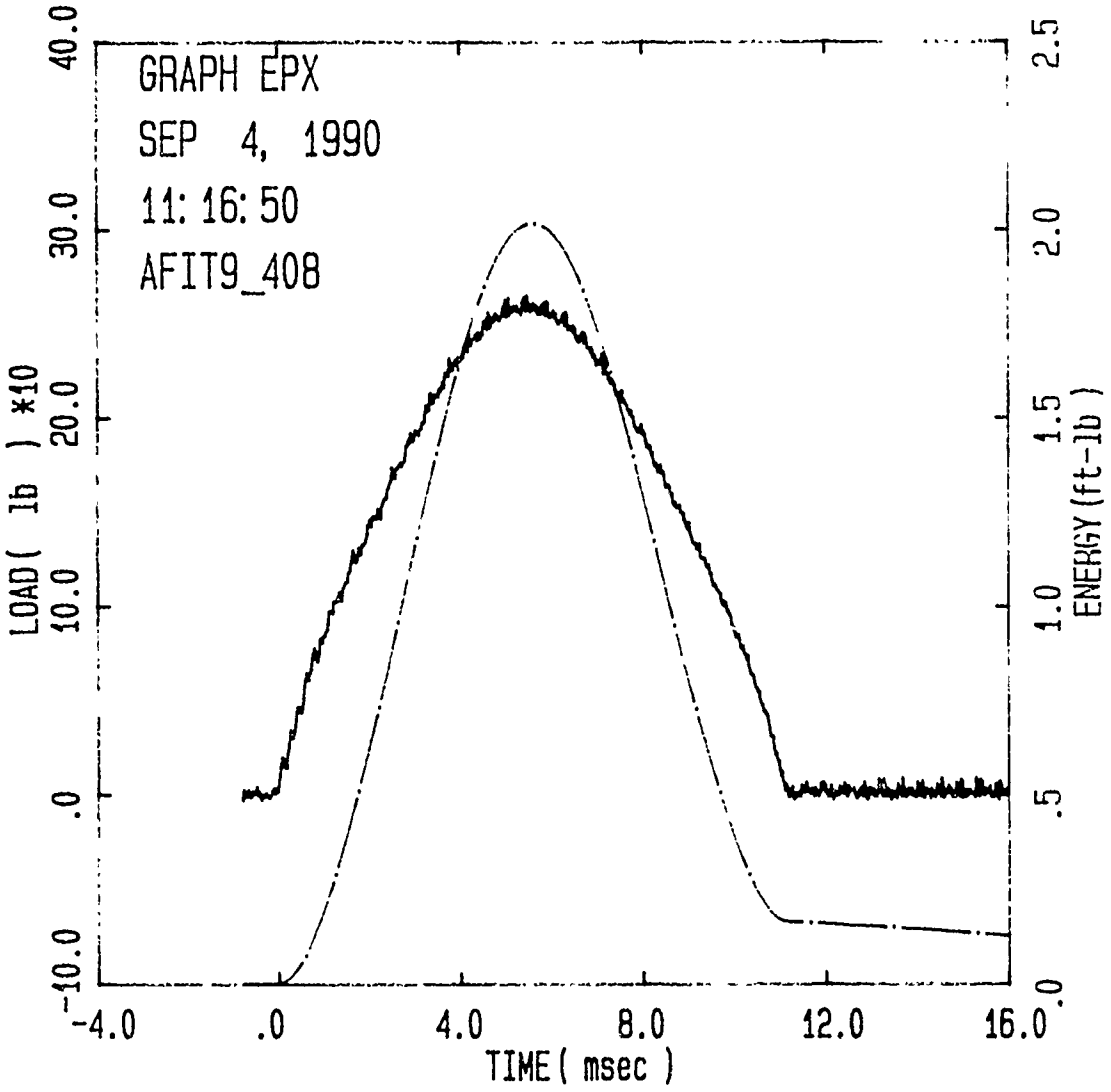


| Specimen Id | Temp | Impact Veloc. | Impact Energy | Time | | Load | Energy | |
|---|---|---|---|---|---|---|---|---|
| | ( f) | (ft/sec) | (ft-lb ) | ( msec ) | | ( lb ) | (ft-lb ) | |
| | | | | Max Ld | Total | Max | Maxld | Total |
| AFIT9_408 | 70. | 4.24 | 1.91 | 5.47 | 11.20 | 264.8 | 2.014 | .165 |

Figure B.52. Load and Energy from Dynatup for $[\pm 45]_{3S}$ Panel, Impact Energy = 1.91 ft-lb

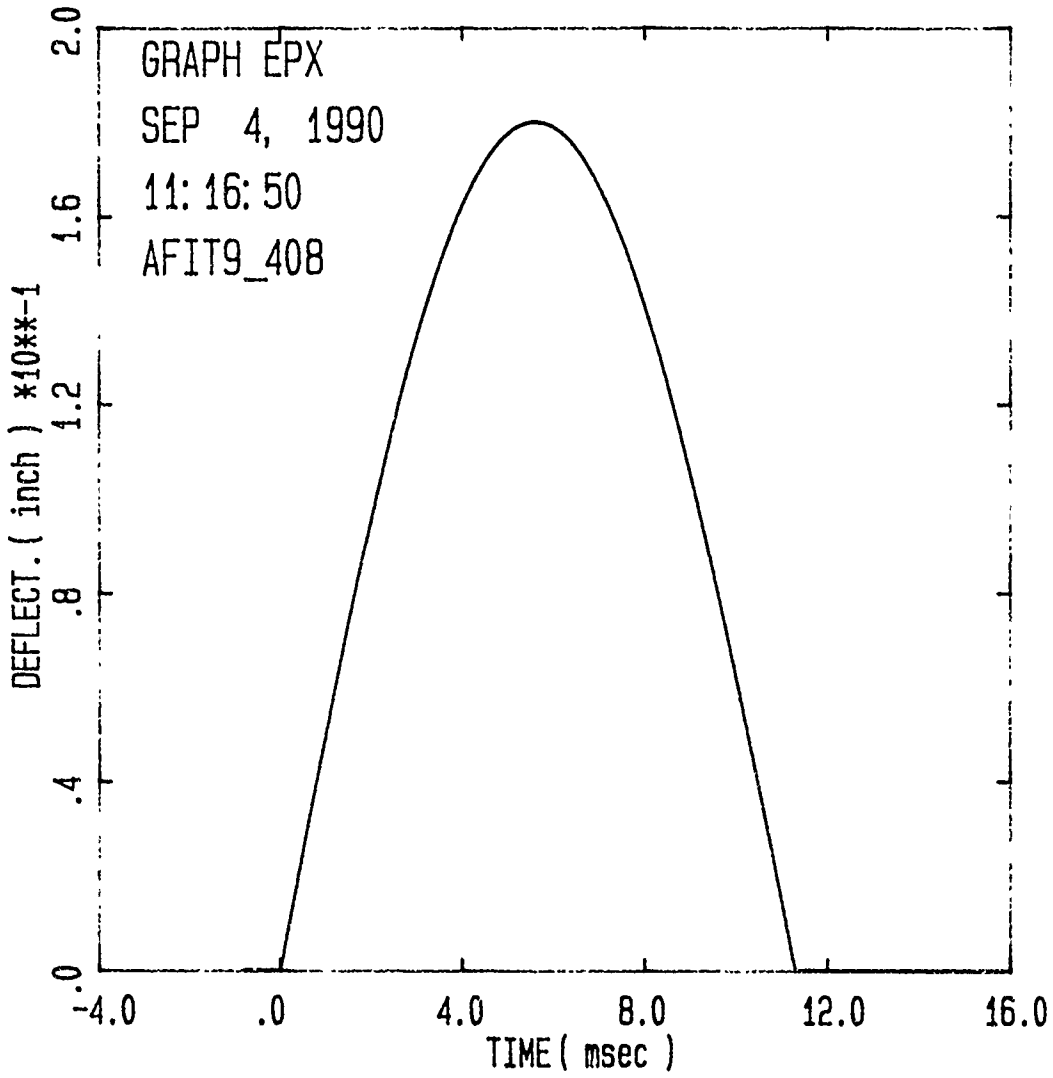


| Specimen Id | Temp ( f) | Impact Veloc. (ft/sec) | Impact Energy (ft-lb ) | Time ( msec ) Max Ld | Time ( msec ) Total | Load ( lb ) Max | Energy (ft-lb ) Maxld | Energy (ft-lb ) Total |
|---|---|---|---|---|---|---|---|---|
| AFIT9_408 | 70. | 4.24 | 1.91 | 5.47 | 11.20 | 264.8 | 2.014 | .165 |

Figure B.53. Deflection from Dynatup for $[\pm 45]_{3S}$ Panel, Impact Energy = 1.91 ft-lb

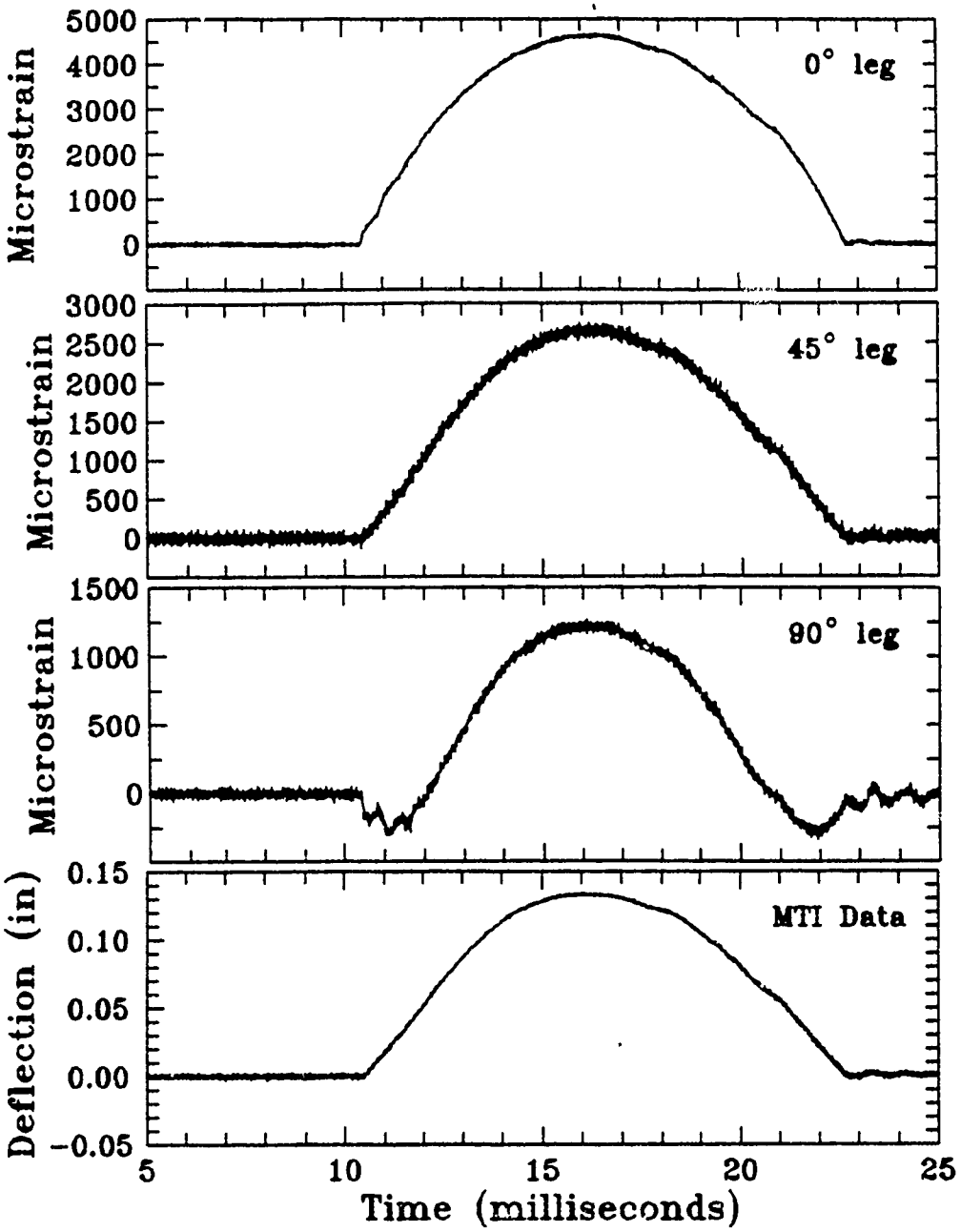


Figure B.54. Strain and Deflection for $[\pm 45]_{3S}$ Panel, Impact Energy = 1.91 ft-lb

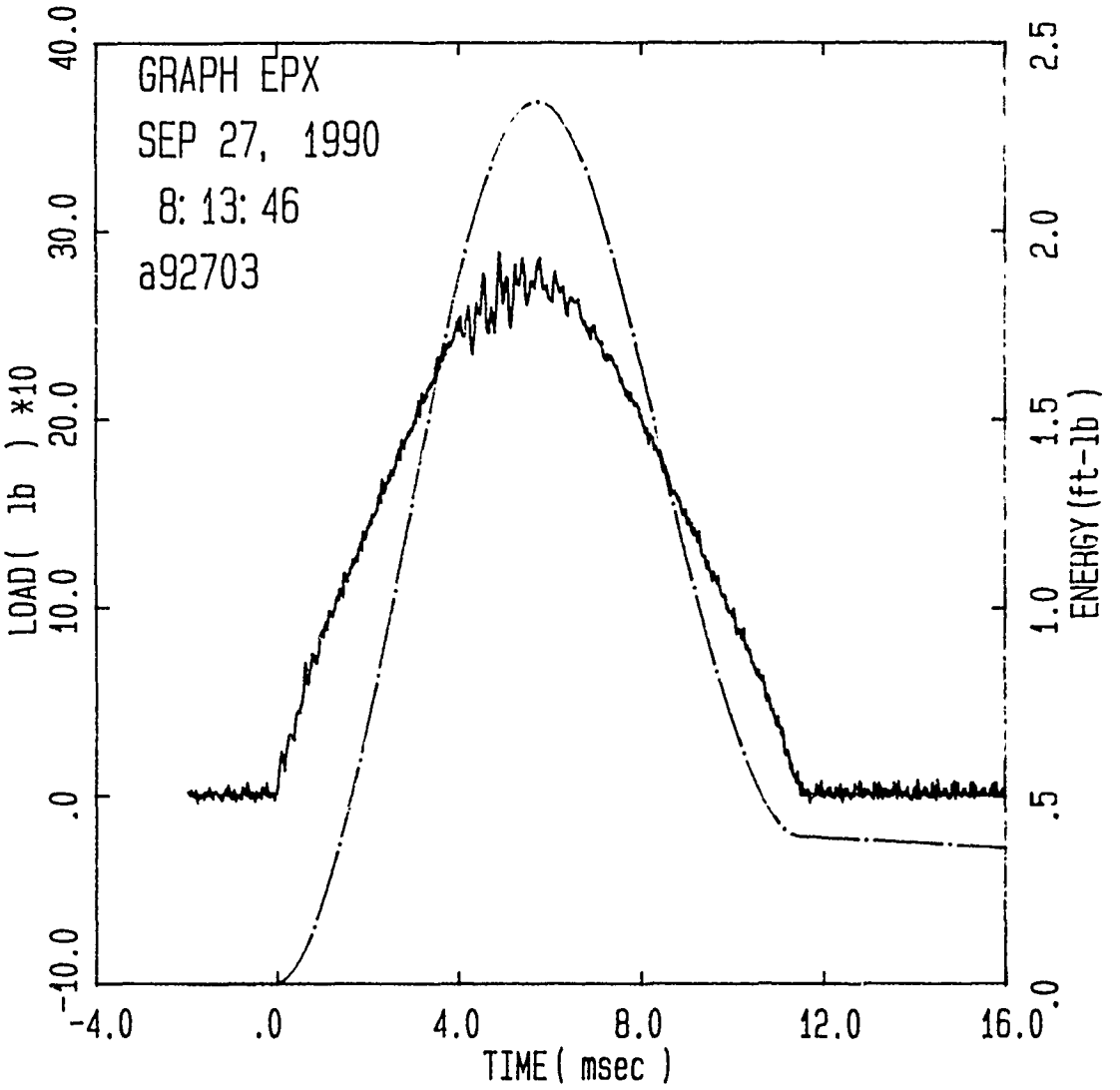


| Specimen Id | Temp | Impact Veloc. | Energy | Time | | Load | Energy | |
|---|---|---|---|---|---|---|---|---|
| | ( f) | (ft/sec) | (ft-lb ) | ( msec ) | | ( lb ) | (ft-lb ) | |
| | | | | Max Ld | Total | Max | Maxld | Total |
| a92703 | 70. | 4.58 | 2.23 | 4.90 | 11.50 | 288.2 | 2.224 | .393 |

Figure B.55. Load and Energy from Dynatup for $[\pm 45]_{3S}$ Panel, Impact Energy = 2.23 ft-lb

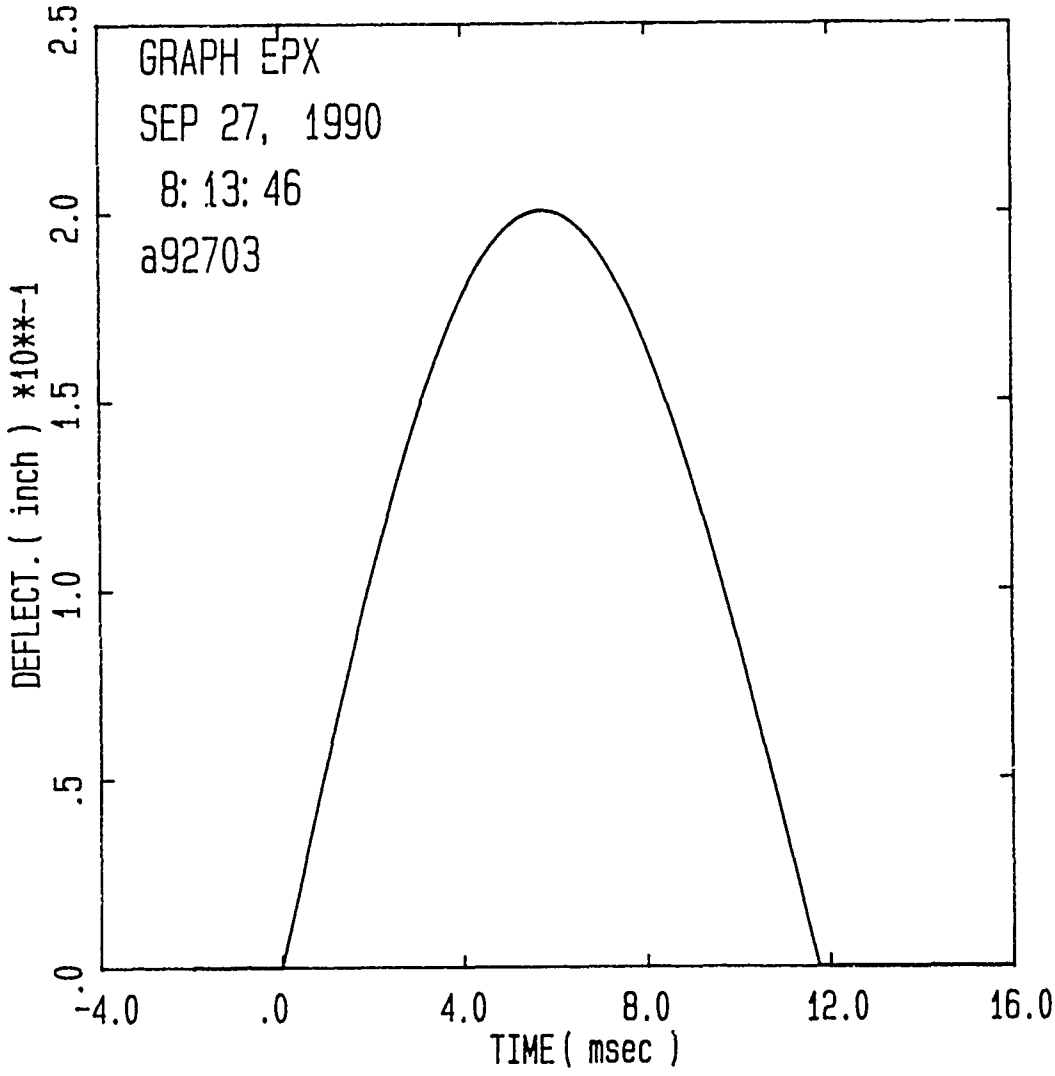


| Specimen Id | Temp ( f) | Impact Veloc. (ft/sec) | Impact Energy (ft-lb ) | Time ( msec ) Max Ld | Time ( msec ) Total | Load ( lb ) Max | Energy (ft-lb ) Maxld | Energy (ft-lb ) Total |
|---|---|---|---|---|---|---|---|---|
| a92703 | 70. | 4.58 | 2.23 | 4.90 | 11.50 | 288.2 | 2.224 | .393 |

Figure B.56. Deflection from Dynatup for $[\pm 45]_{3S}$ Panel, Impact Energy = 2.23 ft-lb

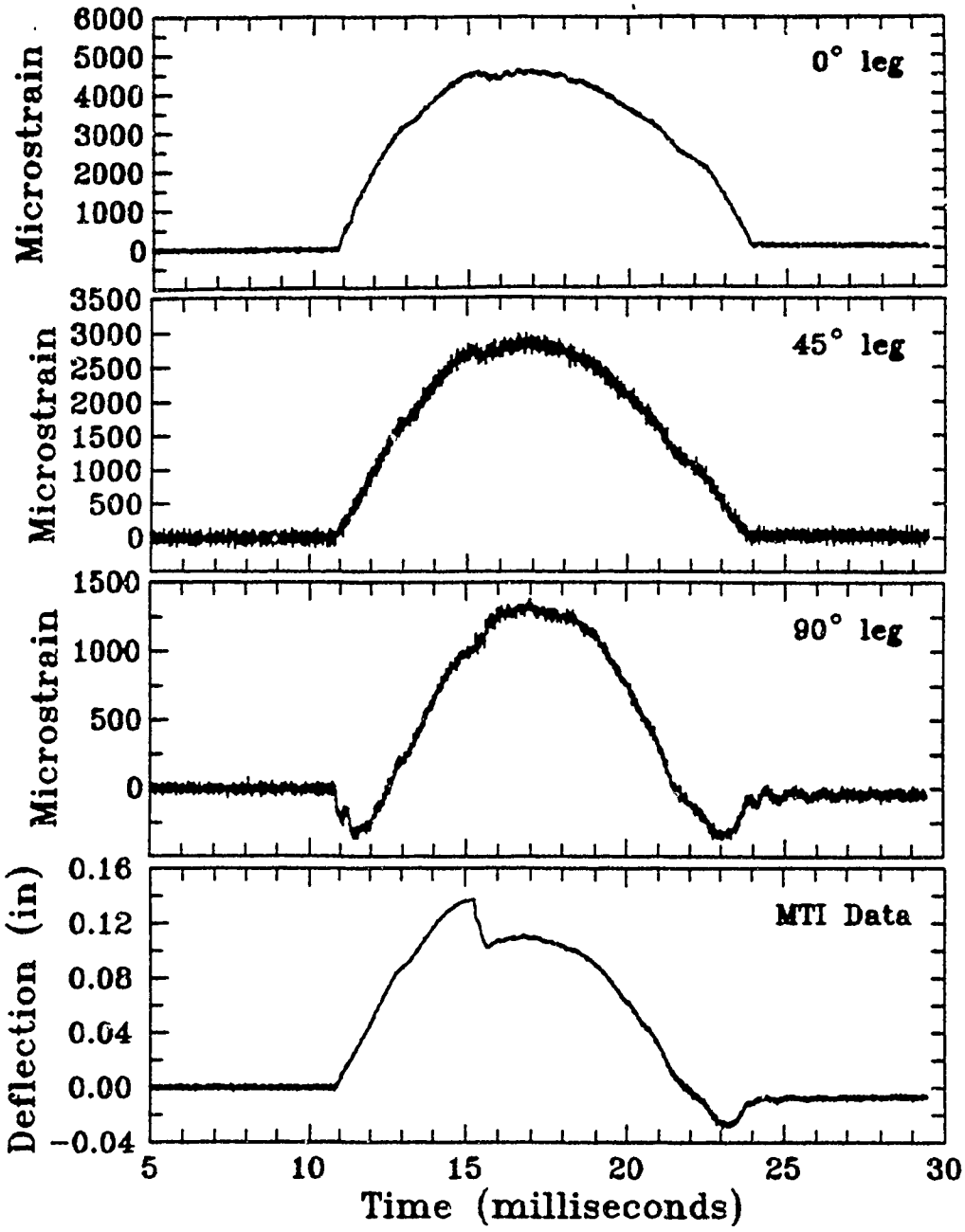


Figure B.57. Strain and Deflection for $[\pm 45]_{3S}$ Panel, Impact Energy = 2.23 ft-lb

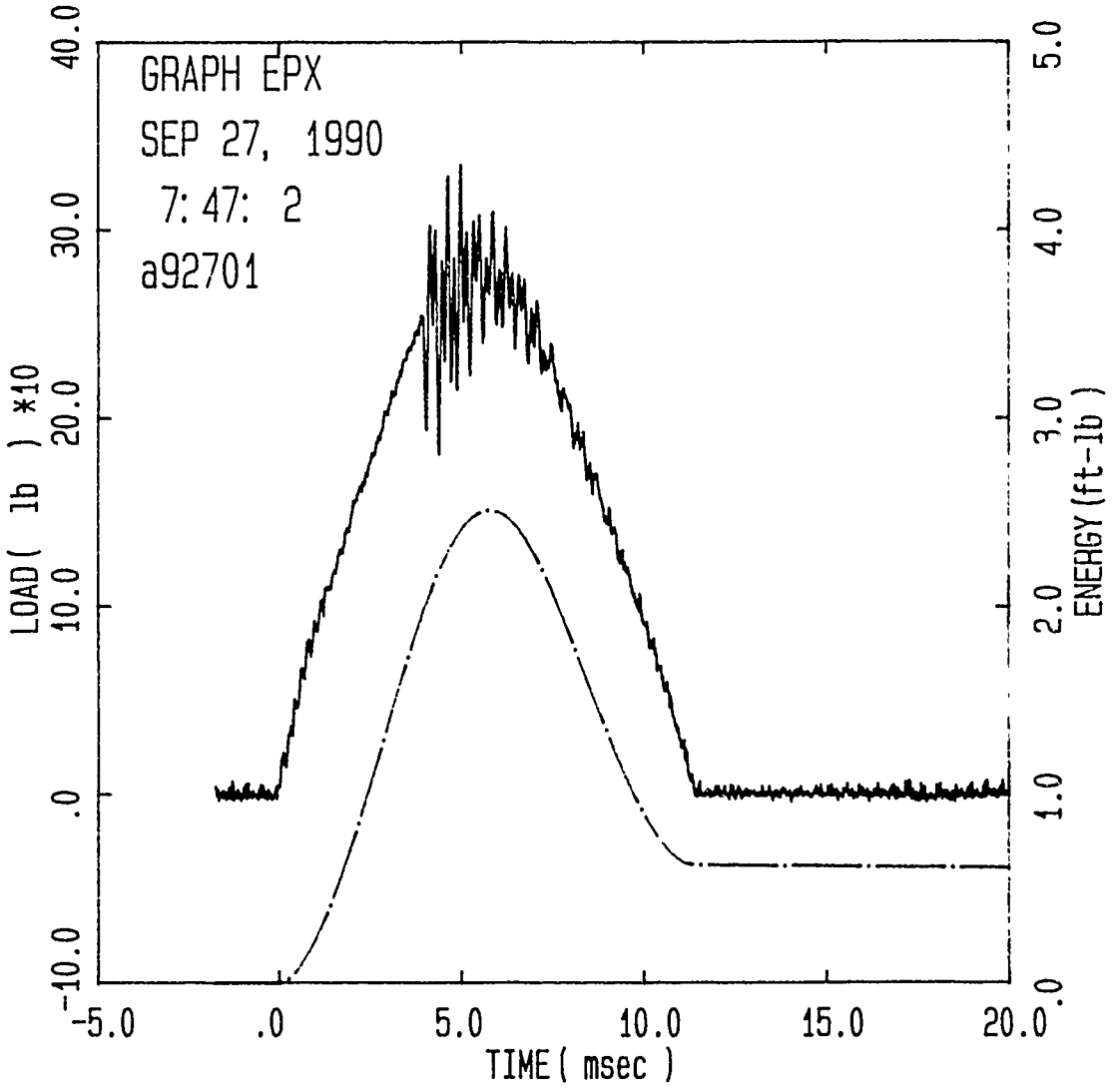


Figure B.58. Load and Energy from Dynatup for $[\pm 45]_{3S}$ Panel, Impact Energy = 2.39 ft-lb

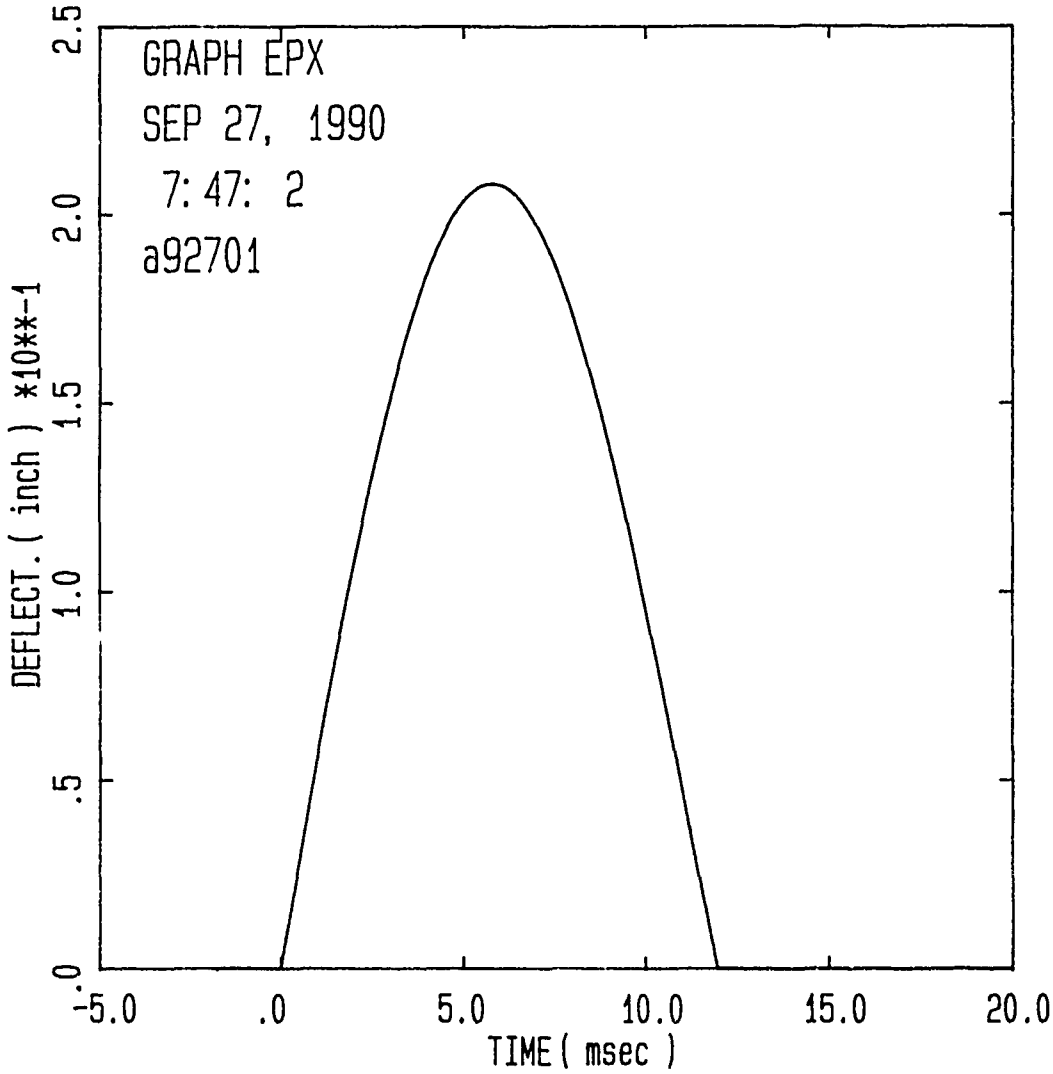


Figure B.59. Deflection from Dynatup for $[\pm 45]_{3S}$ Panel, Impact Energy = 2.39 ft-lb

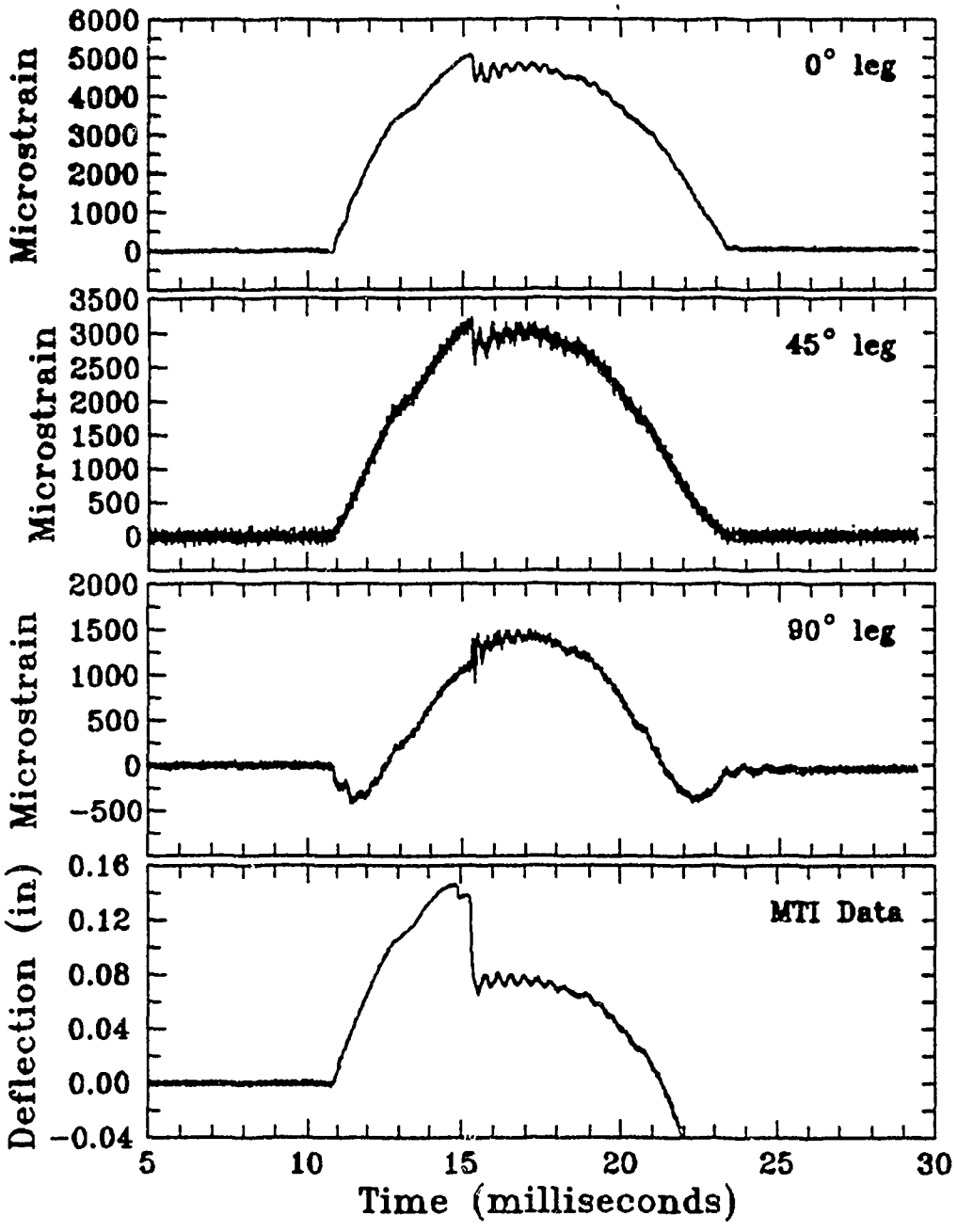


Figure B.60. Strain and Deflection for $[\pm 45]_{3S}$ Panel, Impact Energy = 2.39 ft-lb

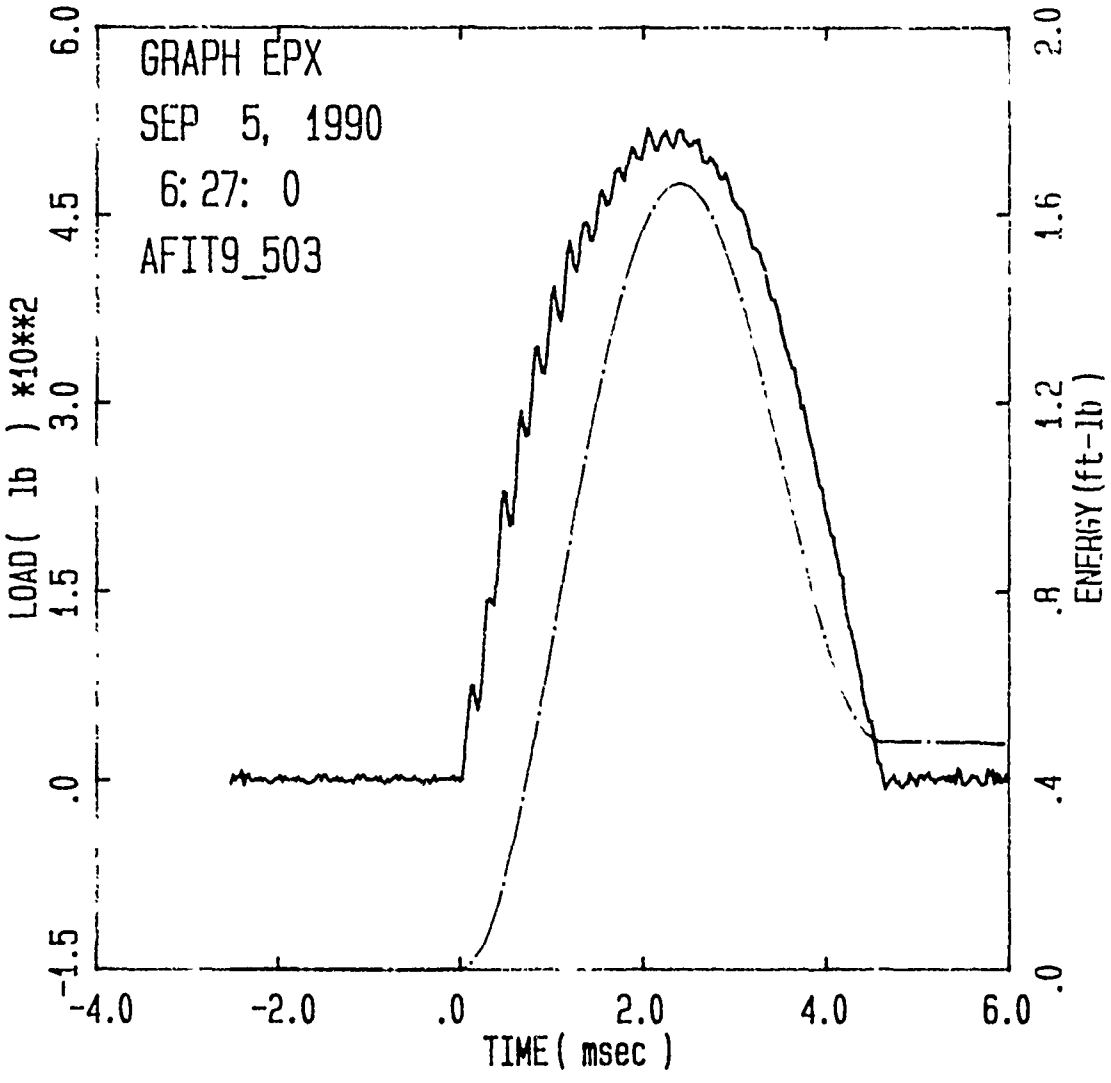


| Specimen Id | Temp ( f) | Impact Veloc. (ft/sec) | Impact Energy (ft-lb ) | Time ( msec ) Max Ld | Time ( msec ) Total | Load ( lb ) Max | Energy (ft-lb ) Maxld | Energy (ft-lb ) Total |
|---|---|---|---|---|---|---|---|---|
| AFIT9_503 | 70. | 3.91 | 1.63 | 2.05 | 4.65 | 518.4 | 1.592 | .482 |

Figure B.61. Load and Energy from Dynatup for $[0/90]_{6S}$ Panel, Impact Energy = 1.63 ft-lb

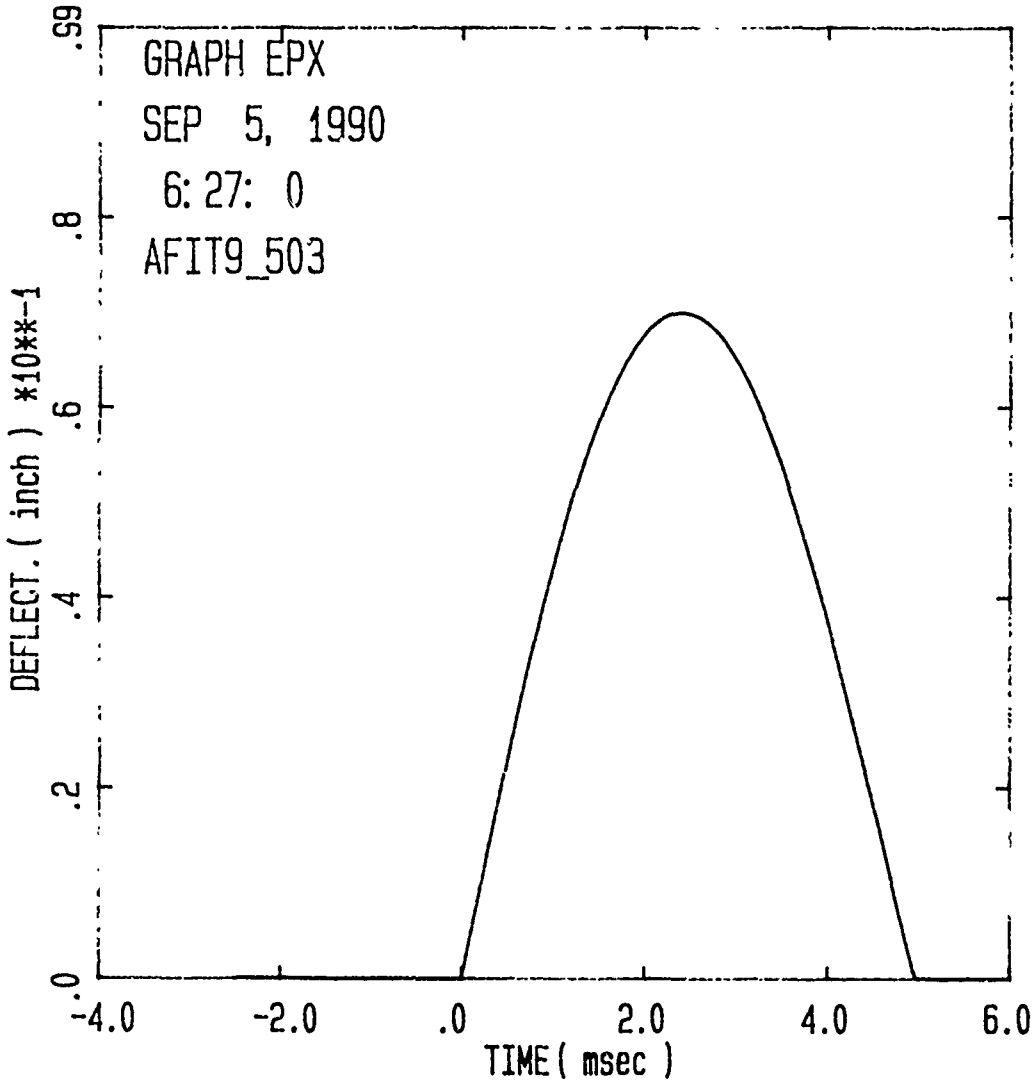


| Specimen Id | Temp ( f) | Veloc. (ft/sec) | Impact Energy (ft-lb ) | Time ( msec ) Max Ld | Time ( msec ) Total | Load ( lb ) Max | Energy (ft-lb ) Maxld | Energy (ft-lb ) Total |
|---|---|---|---|---|---|---|---|---|
| AFIT9_503 | 70. | 3.91 | 1.63 | 2.05 | 4.65 | 518.4 | 1.592 | .482 |

Figure B.62. Deflection from Dynatup for $[0/90]_{6S}$ Panel, Impact Energy = 1.63 ft-lb

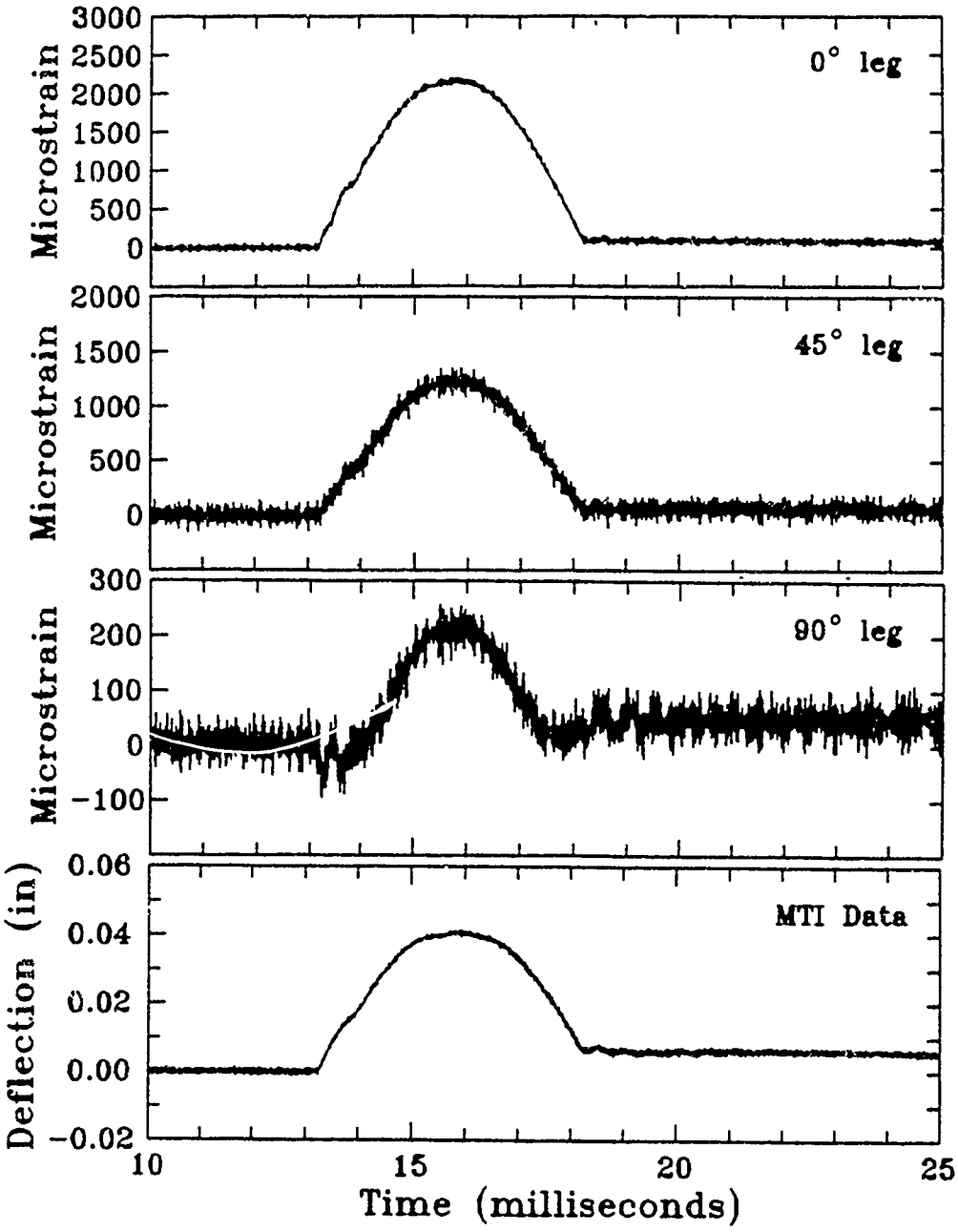


Figure B.63. Strain and Deflection for $[0/90]_{6S}$ Panel, Impact Energy = 1.63 ft-lb

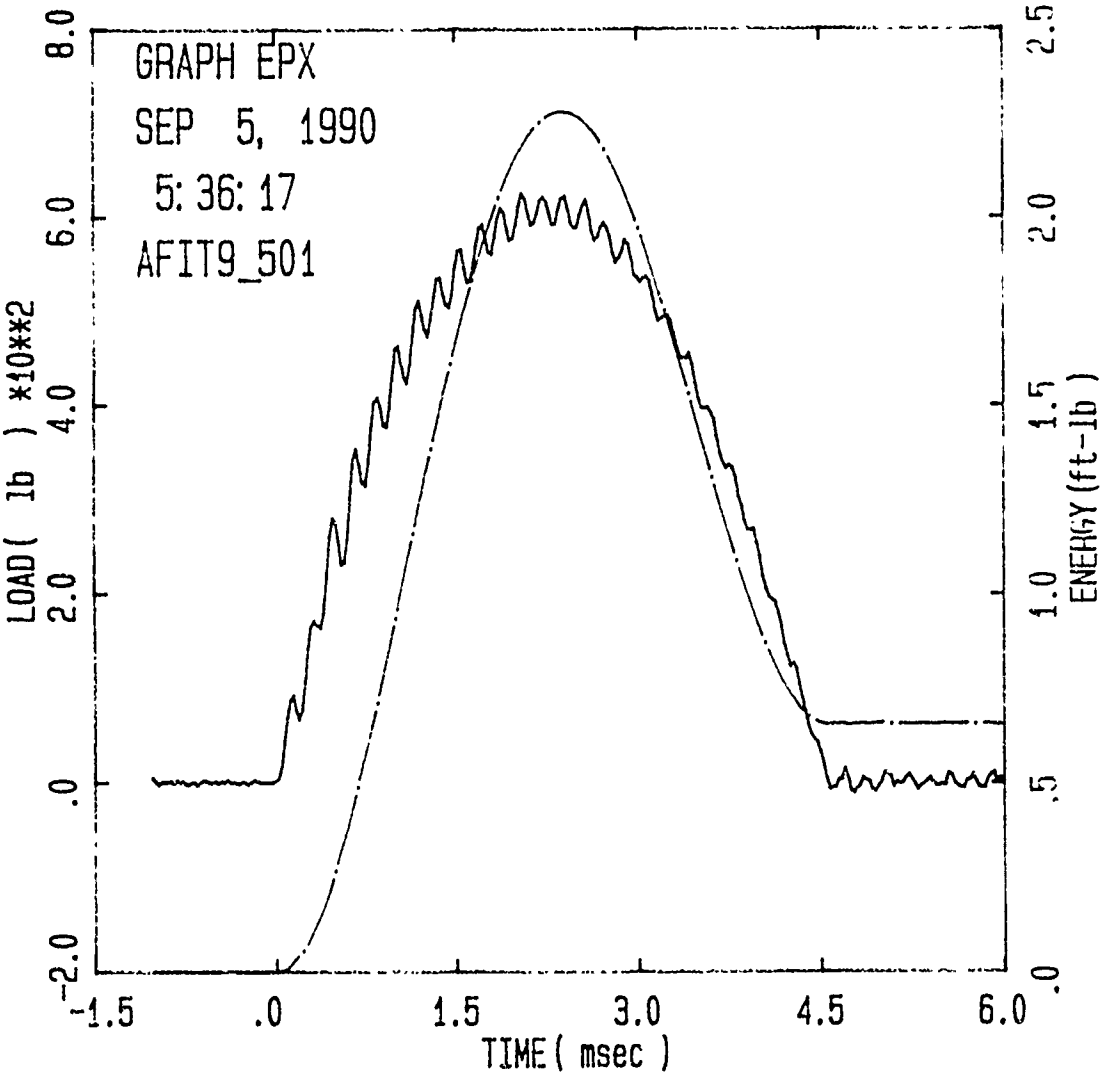


| Specimen Id | Temp ( f) | Impact Veloc. (ft/sec) | Impact Energy (ft-lb ) | Time ( msec ) Max Ld | Time ( msec ) Total | Load ( lb ) Max | Energy (ft-lb ) MaxId | Energy (ft-lb ) Total |
|---|---|---|---|---|---|---|---|---|
| AFIT9_501 | 70. | 4.58 | 2.23 | 2.05 | 4.57 | 624.1 | 2.189 | .655 |

Figure B.64. Load and Energy from Dynatup for $[0/90]_{6S}$ Panel, Impact Energy = 2.23 ft-lb

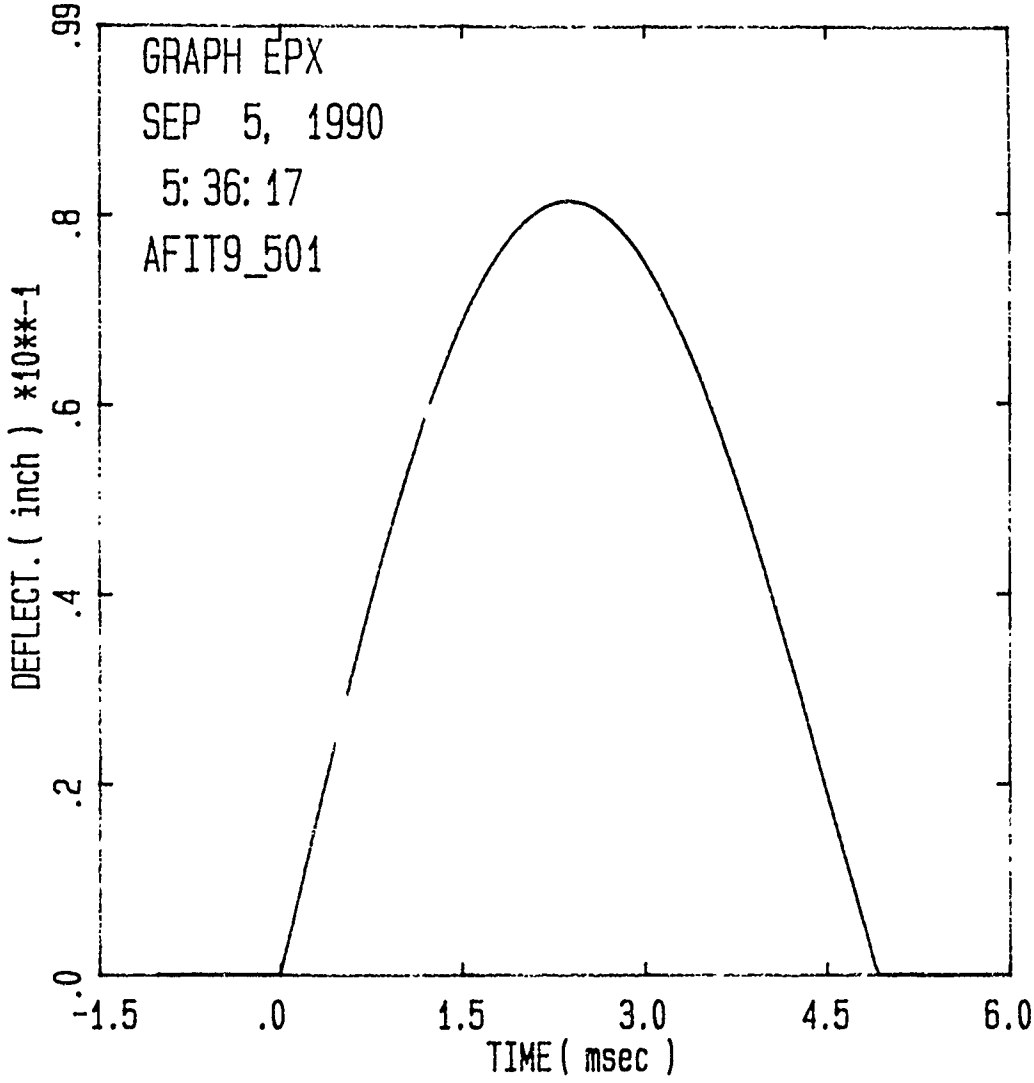


| Specimen Id | Temp ( f) | Impact Veloc. (ft/sec) | Impact Energy (ft-lb ) | Time ( msec ) Max Ld | Time ( msec ) Total | Load ( lb ) Max | Energy (ft-lb ) Maxld | Energy (ft-lb ) Total |
|---|---|---|---|---|---|---|---|---|
| AFIT9_501 | 70. | 4.58 | 2.23 | 2.05 | 4.57 | 624.1 | 2.189 | .655 |

Figure B.65. Deflection from Dynatup for $[0/90]_{6S}$ Panel, Impact Energy = 2.23 ft-lb

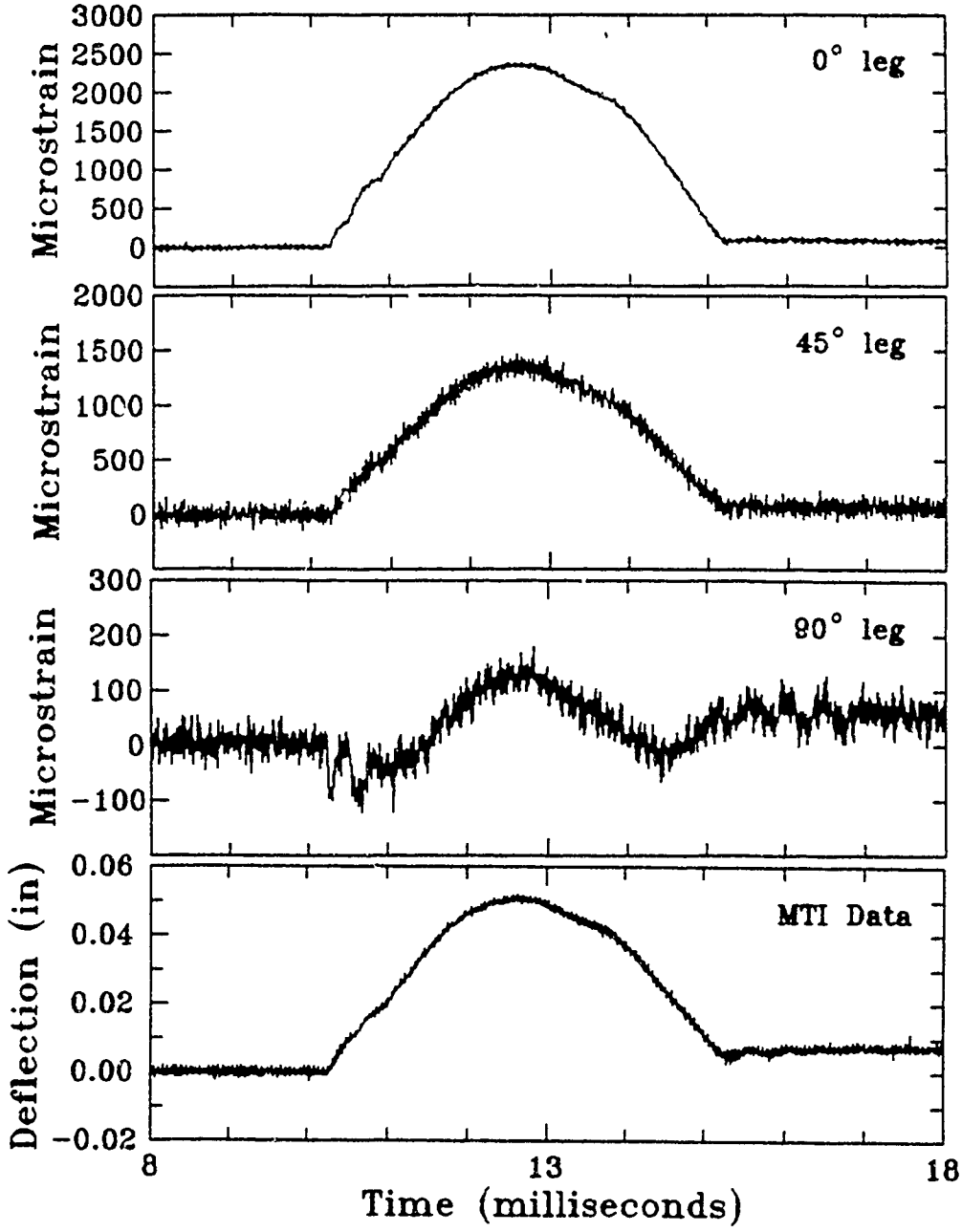


Figure B.66. Strain and Deflection for $[0/90]_{6S}$ Panel, Impact Energy = 2.23 ft-lb

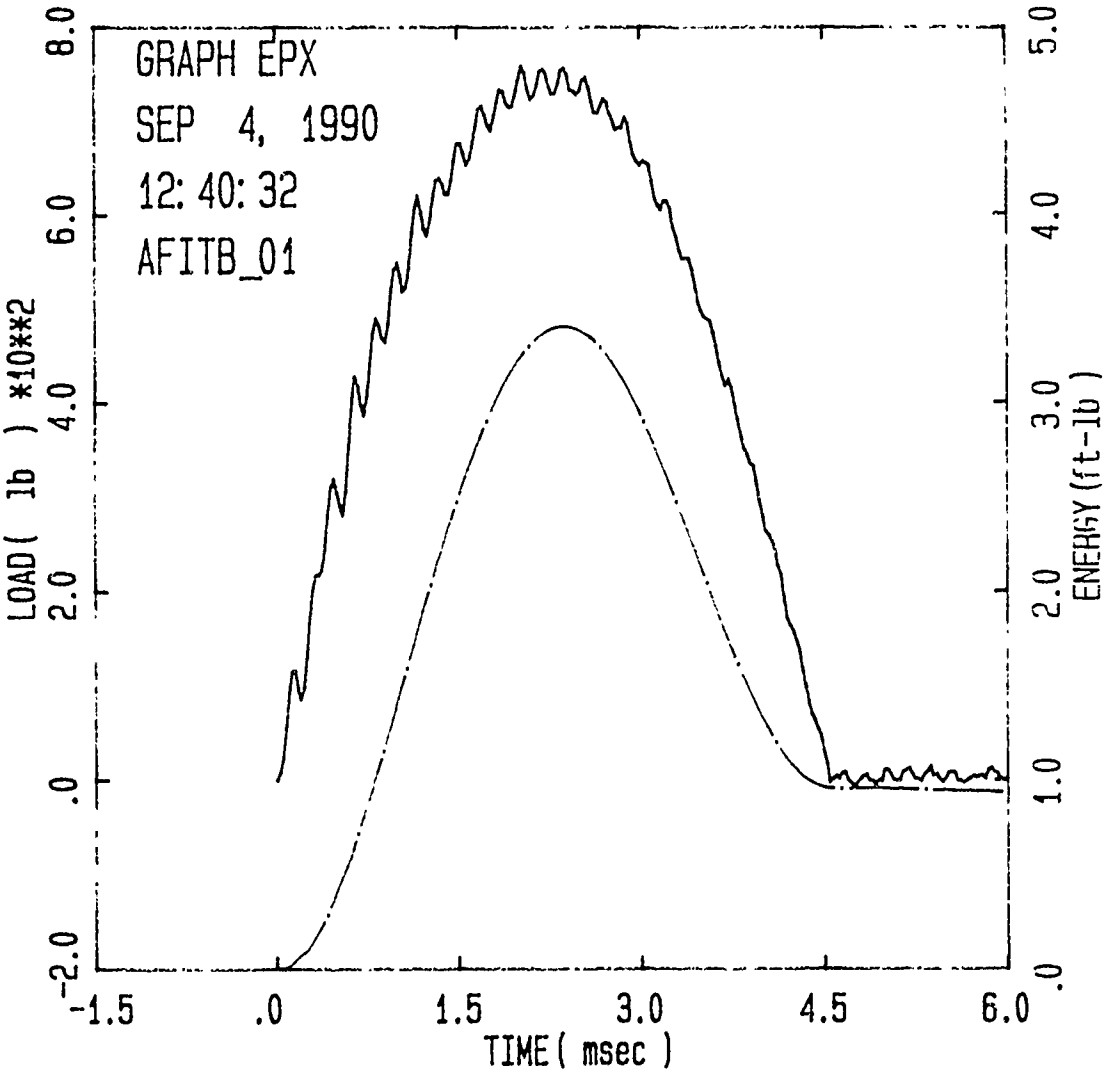


| Specimen Id | Temp ( f) | Impact Veloc. (ft/sec) | Energy (ft-lb ) | Time ( msec ) Max Ld | Time ( msec ) Total | Load ( lb ) Max | Energy (ft-lb ) MaxId | Energy (ft-lb ) Total |
|---|---|---|---|---|---|---|---|---|
| AFITB_01 | 70. | 5.61 | 3.35 | 2.03 | 4.55 | 758.1 | 3.255 | .956 |

Figure B.67. Load and Energy from Dynatup for $[0/90]_{6S}$ Panel, Impact Energy = 3.35 ft-lb

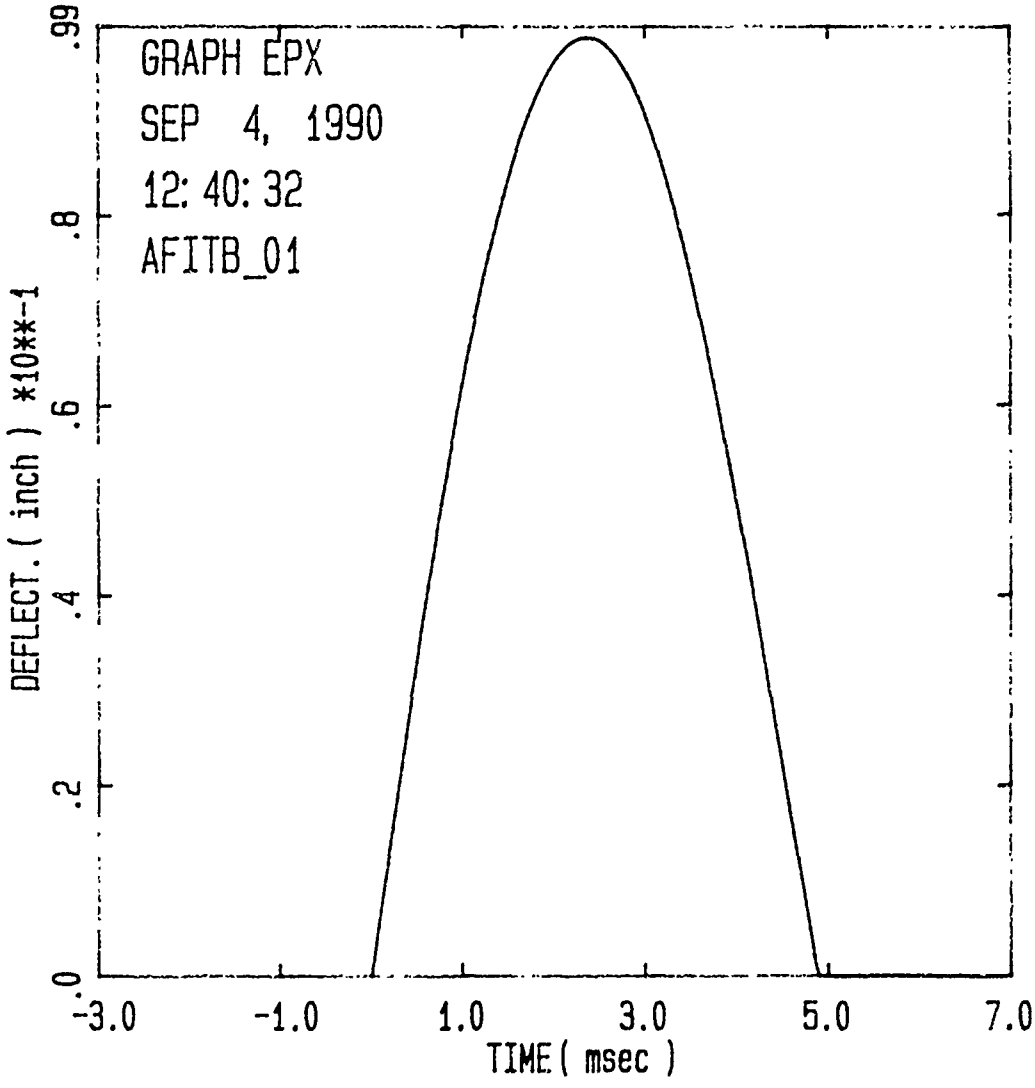


| Specimen Id | Temp ( f) | Impact Veloc. (ft/sec) | Impact Energy (ft-lb ) | Time ( msec ) Max Ld | Time ( msec ) Total | Load ( lb ) Max | Energy (ft-lb ) MaxId | Energy (ft-lb ) Total |
|---|---|---|---|---|---|---|---|---|
| AFITB_01 | 70. | 5.61 | 3.35 | 2.03 | 4.55 | 758.1 | 3.255 | .956 |

Figure B.68. Deflection from Dynatup for $[0/90]_{6S}$ Panel, Impact Energy = 3.35 ft-lb

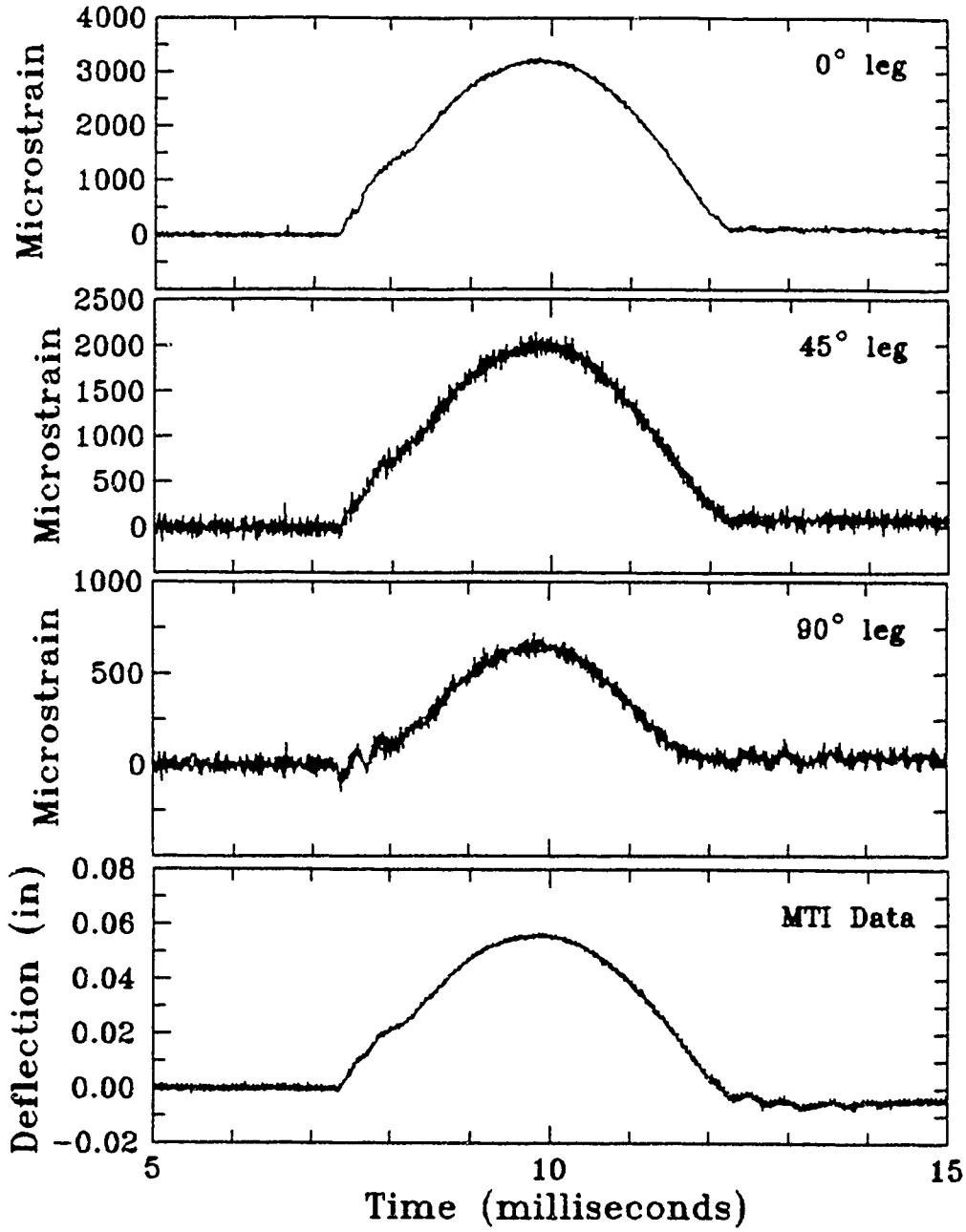


Figure B.69. Strain and Deflection for $[0/90]_{6S}$ Panel, Impact Energy = 3.35 ft-lb

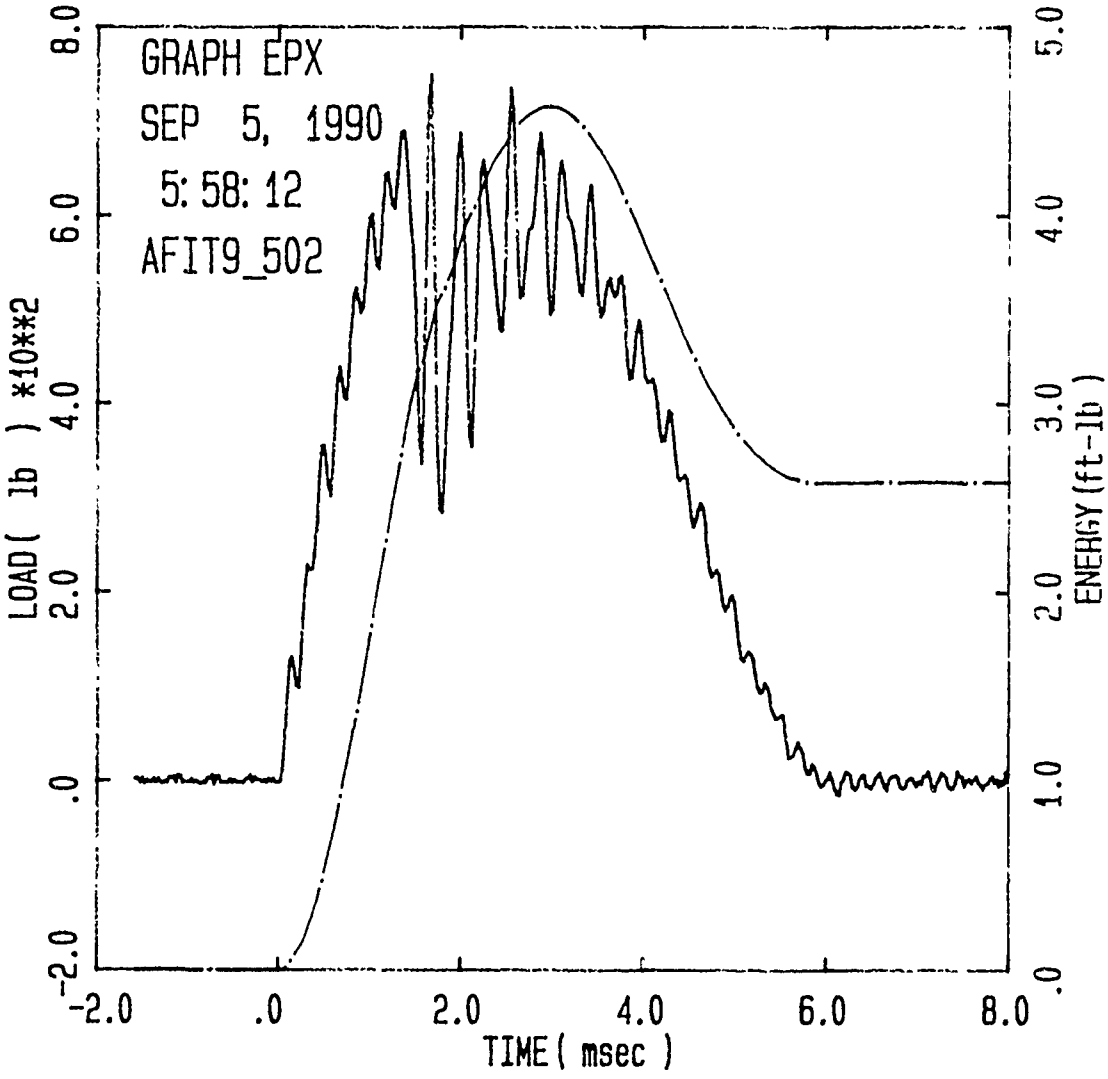


| Specimen Id | Temp ( f) | Impact Veloc. (ft/sec) | Impact Energy (ft-lb ) | Time ( msec ) Max Ld | Time ( msec ) Total | Load ( lb ) Max | Energy (ft-lb ) Maxld | Energy (ft-lb ) Total |
|---|---|---|---|---|---|---|---|---|
| AFIT9_502 | 70. | 6.51 | 4.50 | 1.67 | 5.92 | 749.6 | 3.412 | 2.582 |

Figure B.70. Load and Energy from Dynatup for $[0/90]_{6S}$ Panel, Impact Energy = 4.50 ft-lb

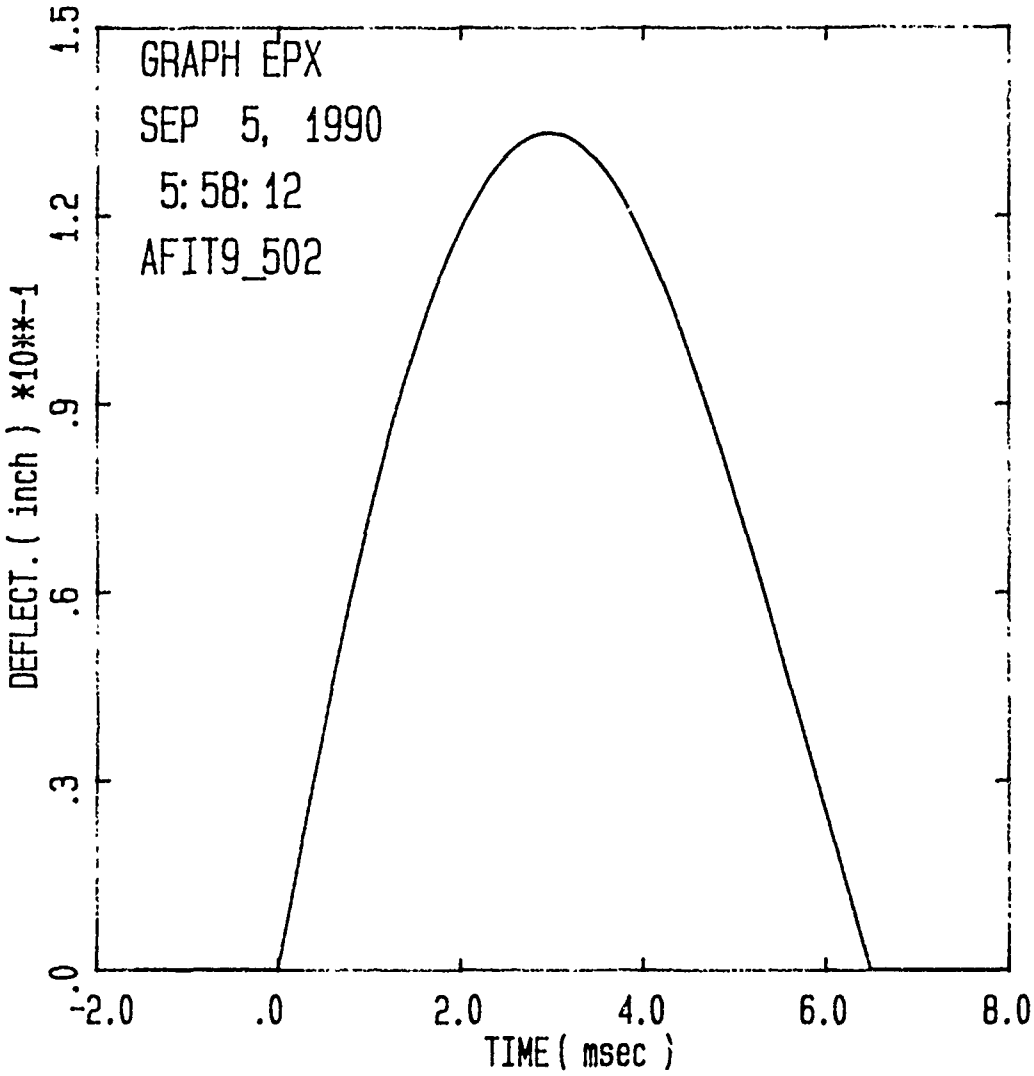


| Specimen Id | Temp (f) | Impact Veloc. (ft/sec) | Impact Energy (ft-lb) | Time (msec) Max Ld | Time (msec) Total | Load (lb) Max | Energy (ft-lb) Maxld | Energy (ft-lb) Total |
|---|---|---|---|---|---|---|---|---|
| AFIT9_502 | 70. | 6.51 | 4.50 | 1.67 | 5.92 | 749.6 | 3.412 | 2.582 |

Figure B.71. Deflection from Dynatup for $[0/90]_{6S}$ Panel, Impact Energy = 4.50 ft-lb

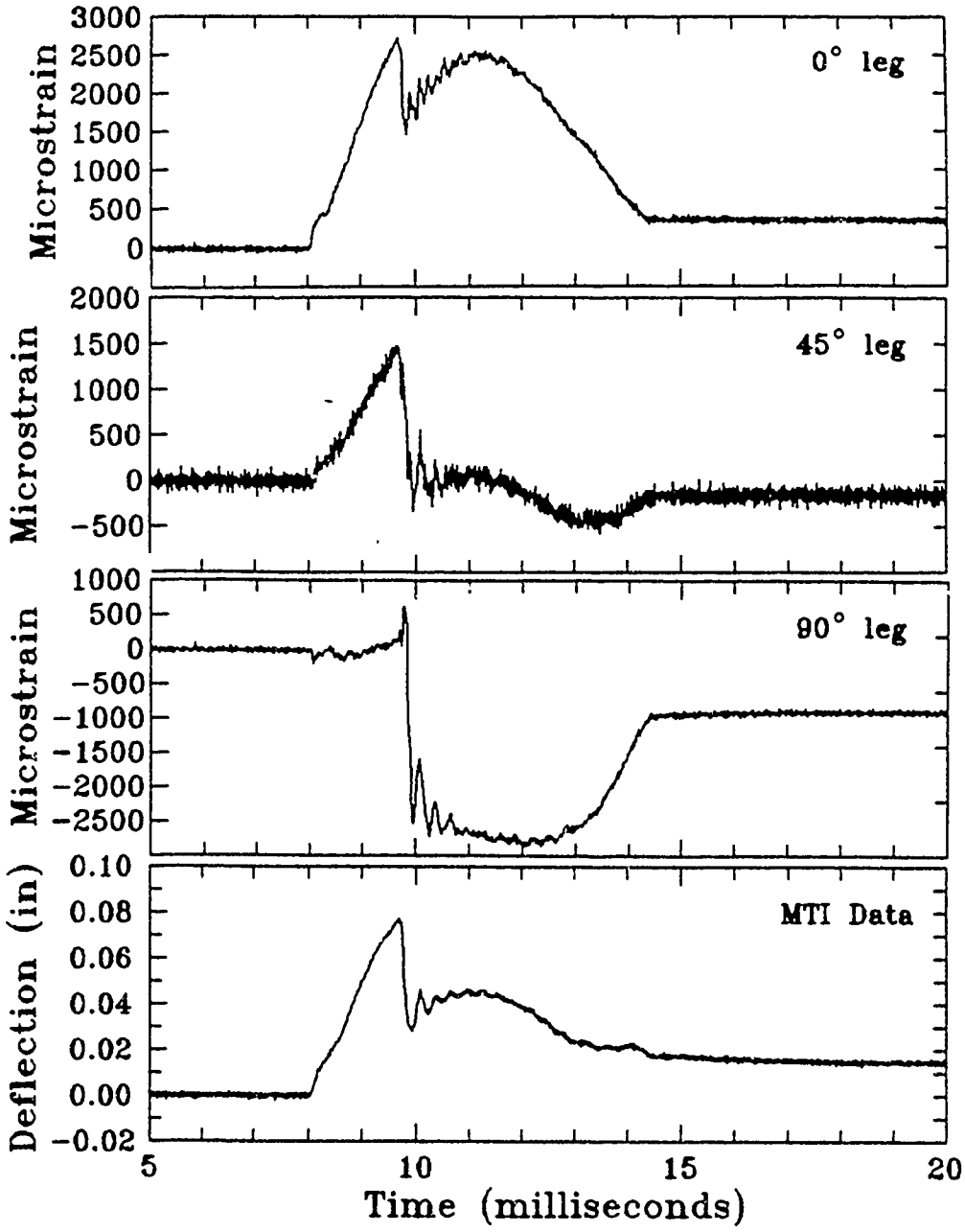


Figure B.72. Strain and Deflection for $[0/90]_{6S}$ Panel, Impact Energy = 4.50 ft-lb

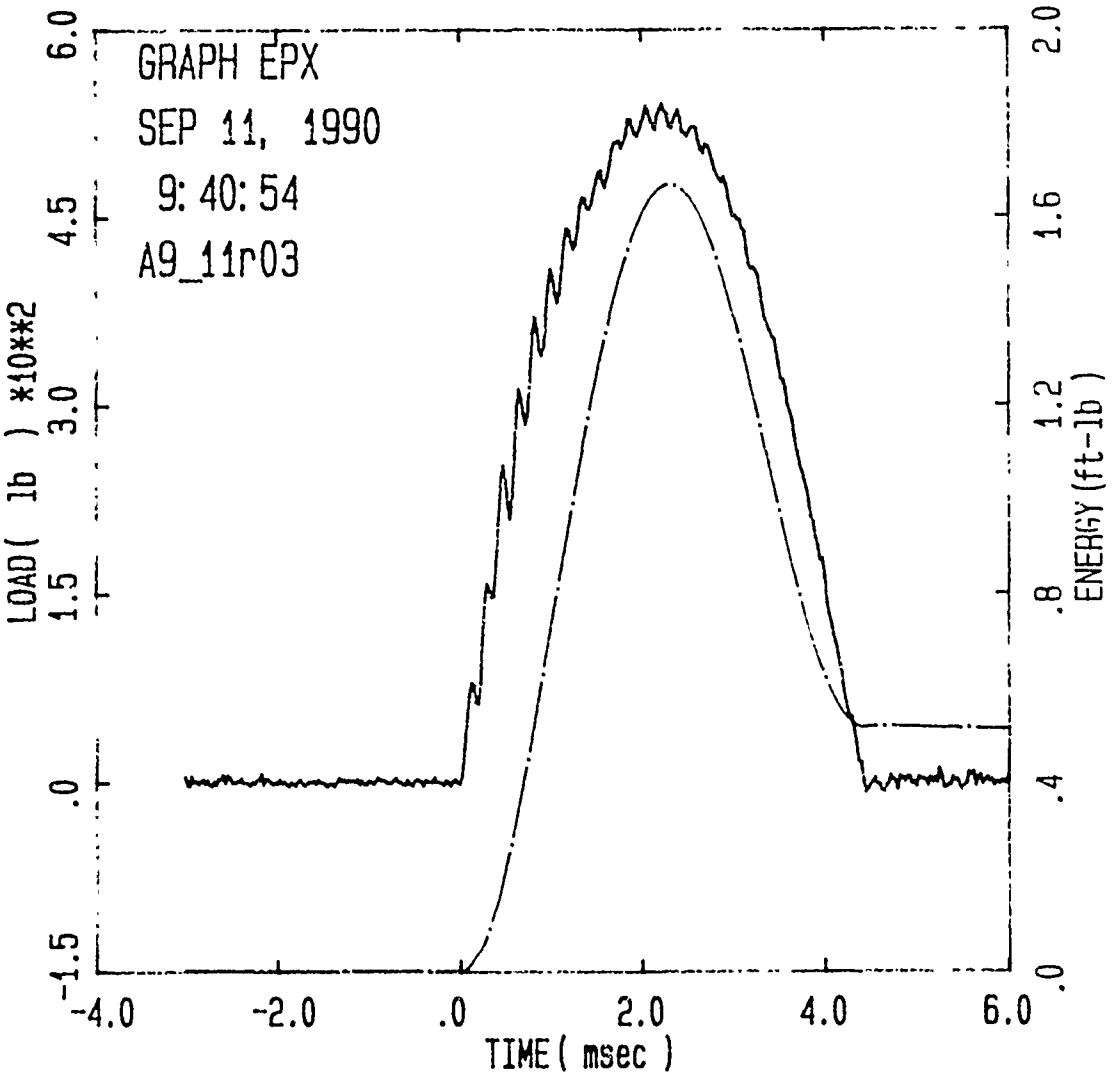


| Specimen Id | Temp ( f) | Impact Veloc. (ft/sec) | Impact Energy (ft-lb ) | Time ( msec ) Max Ld | Time ( msec ) Total | Load ( lb ) Max | Energy (ft-lb ) Maxld | Energy (ft-lb ) Total |
|---|---|---|---|---|---|---|---|---|
| A9_11r03 | 70. | 3.92 | 1.63 | 2.22 | 4.45 | 539.9 | 1.663 | .516 |

Figure B.73. Load and Energy from Dynatup for $[90/0]_{6S}$ Panel, Impact Energy = 1.63 ft-lb

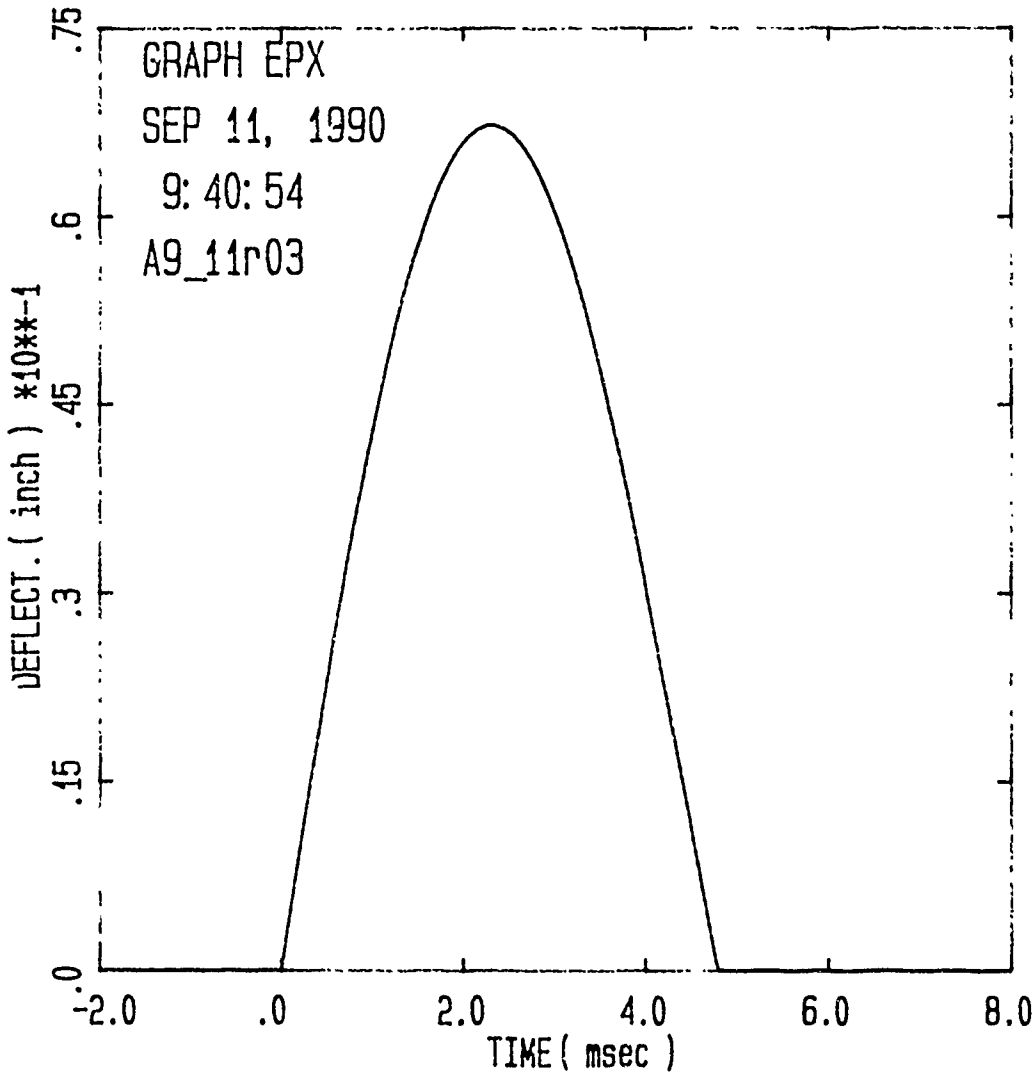


| Specimen Id | Temp ( f) | Impact Veloc. (ft/sec) | Impact Energy (ft-lb ) | Time ( msec ) Max Ld | Time ( msec ) Total | Load ( lb ) Max | Energy (ft-lb ) Maxld | Energy (ft-lb ) Total |
|---|---|---|---|---|---|---|---|---|
| A9_11r03 | 70. | 3.92 | 1.63 | 2.22 | 4.45 | 539.9 | 1.663 | .516 |

Figure B.74. Deflection from Dynatup for $[90/0]_{6S}$ Panel, Impact Energy = 1.63 ft-lb

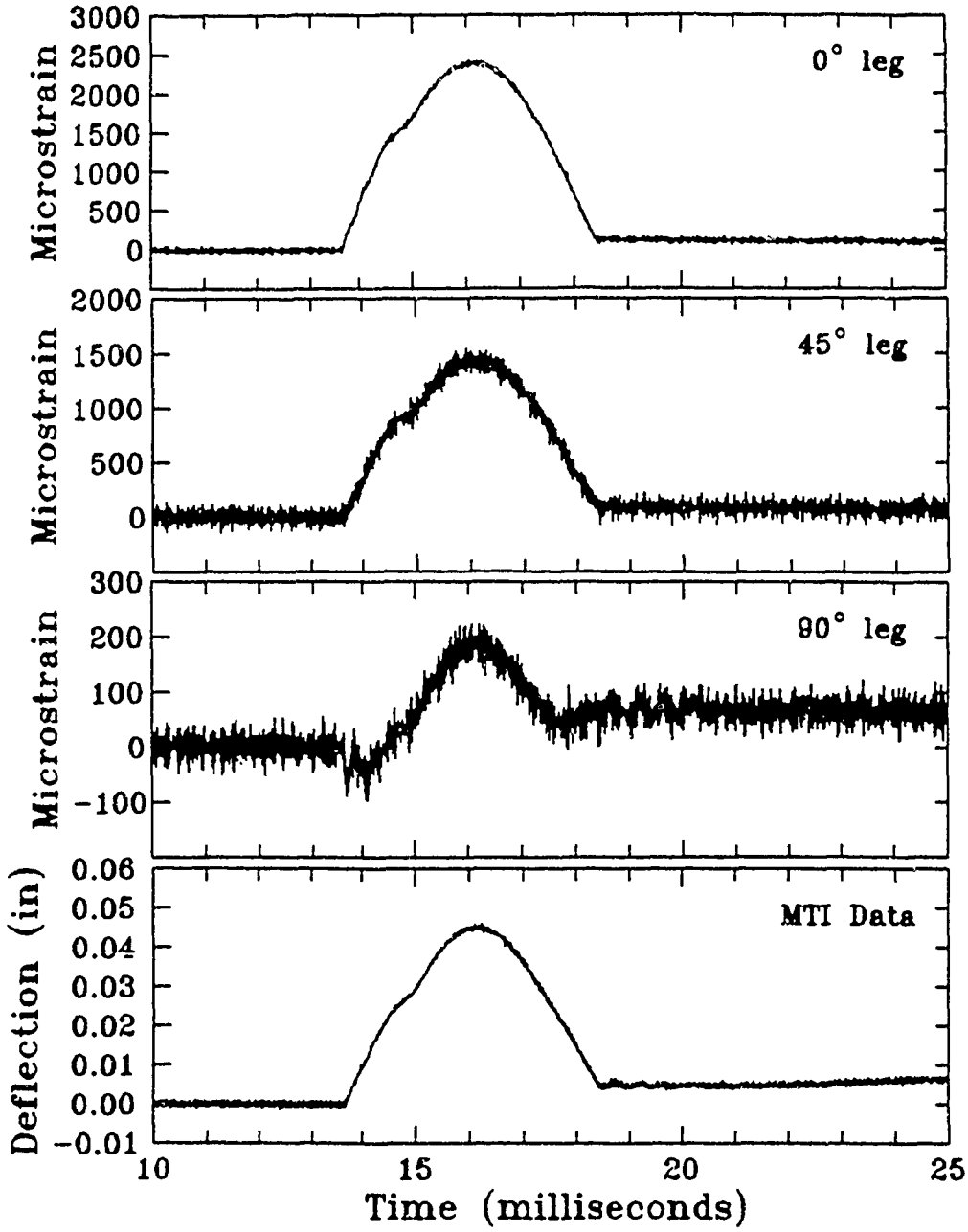


Figure B.75. Strain and Deflection for $[90/0]_{6S}$ Panel, Impact Energy = 1.63 ft-lb

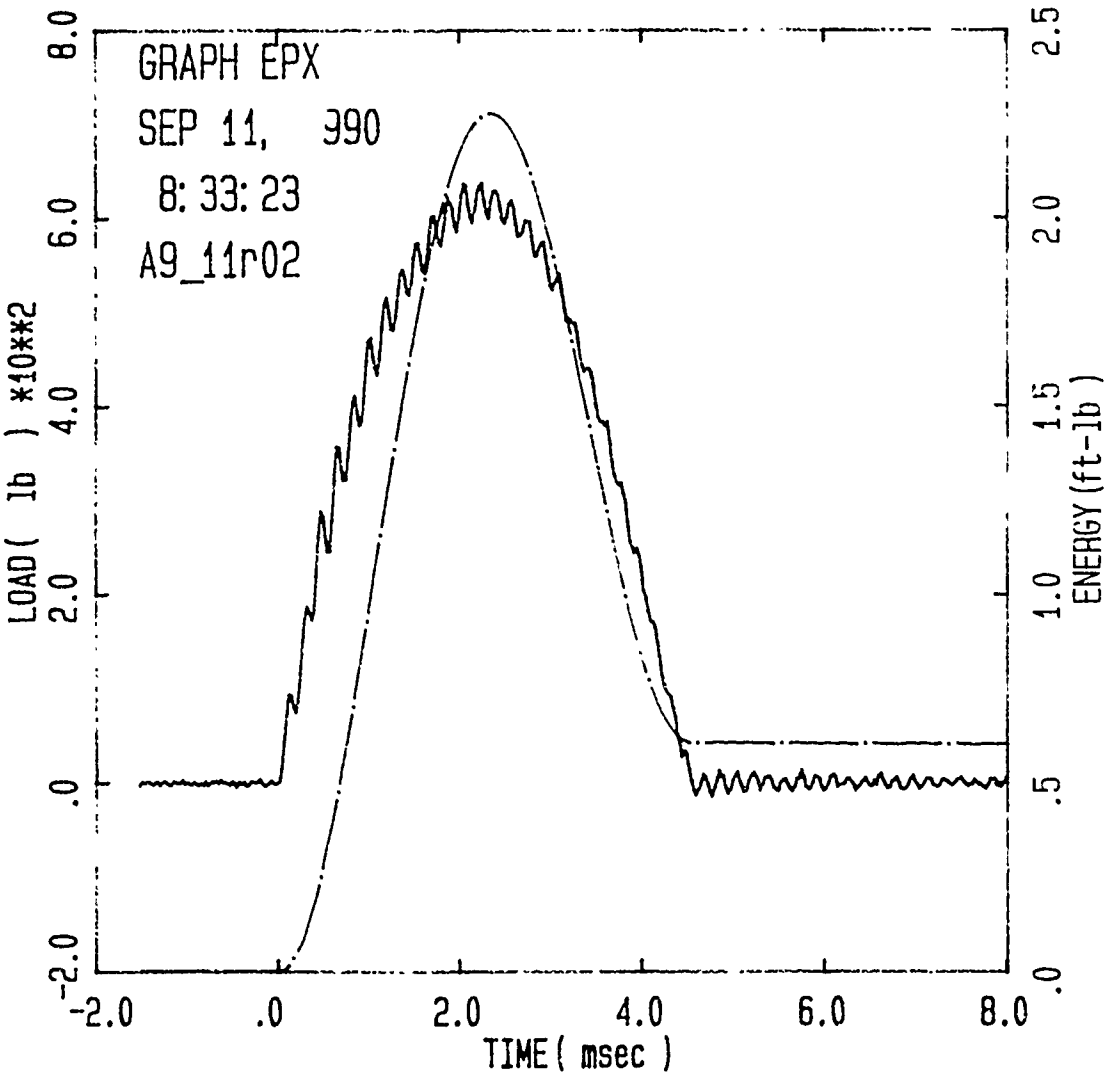


| Specimen Id | Temp ( f) | Impact Veloc. (ft/sec) | Impact Energy (ft-lb ) | Time ( msec ) Max Ld | Time ( msec ) Total | Load ( lb ) Max | Energy (ft-lb ) Maxld | Energy (ft-lb ) Total |
|---|---|---|---|---|---|---|---|---|
| A9_11r02 | 70. | 4.58 | 2.23 | 2.05 | 4.57 | 636.3 | 2.202 | .603 |

Figure B.76. Load and Energy from Dynatup for $[90/0]_{6S}$ Panel, Impact Energy = 2.23 ft-lb

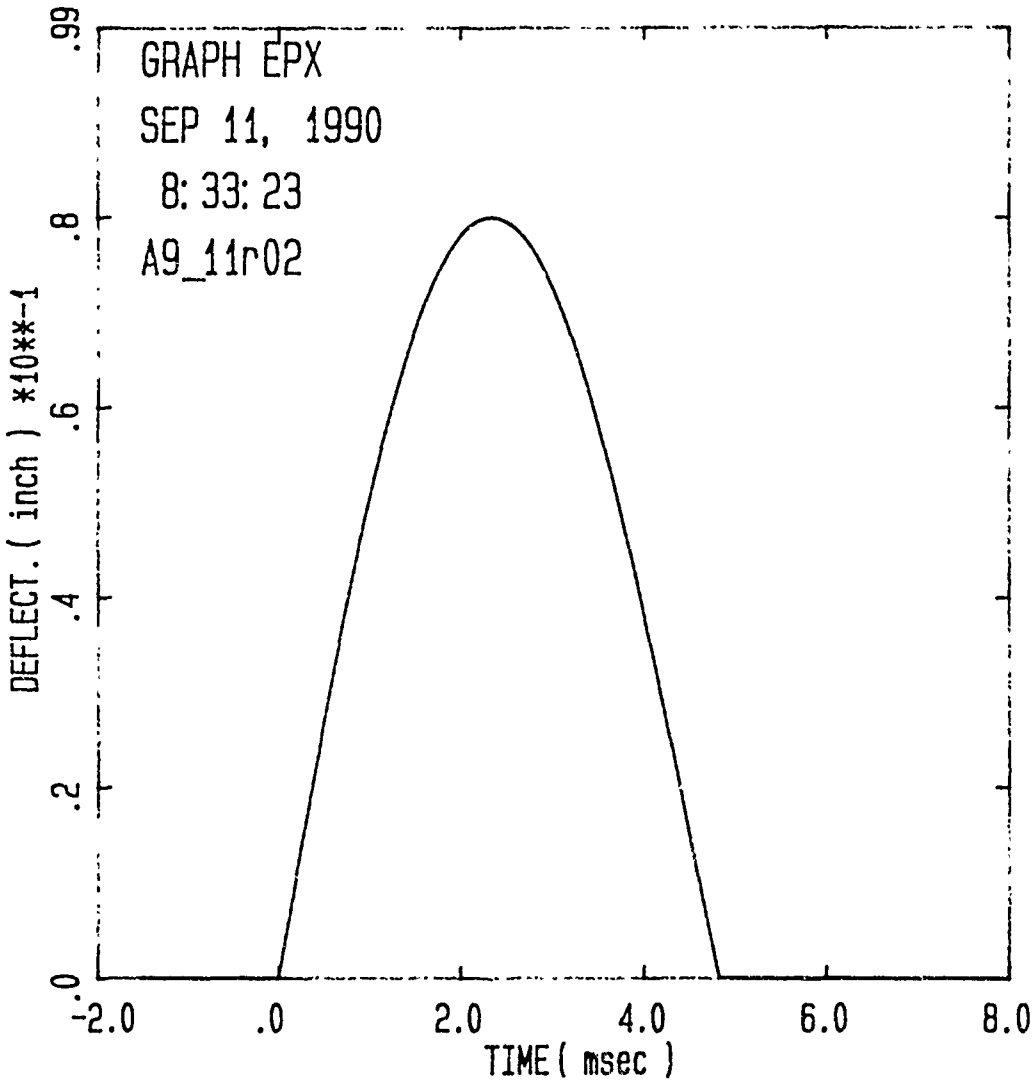


| Specimen Id | Temp ( f) | Impact Veloc. (ft/sec) | Impact Energy (ft-lb ) | Time ( msec ) Max Ld | Time ( msec ) Total | Load ( lb ) Max | Energy (ft-lb ) MaxId | Energy (ft-lb ) Total |
|---|---|---|---|---|---|---|---|---|
| A9_11r02 | 70. | 4.58 | 2.23 | 2.05 | 4.57 | 636.3 | 2.202 | .603 |

Figure B.77. Deflection from Dynatup for $[90/0]_{6S}$ Panel, Impact Energy = 2.23 ft-lb

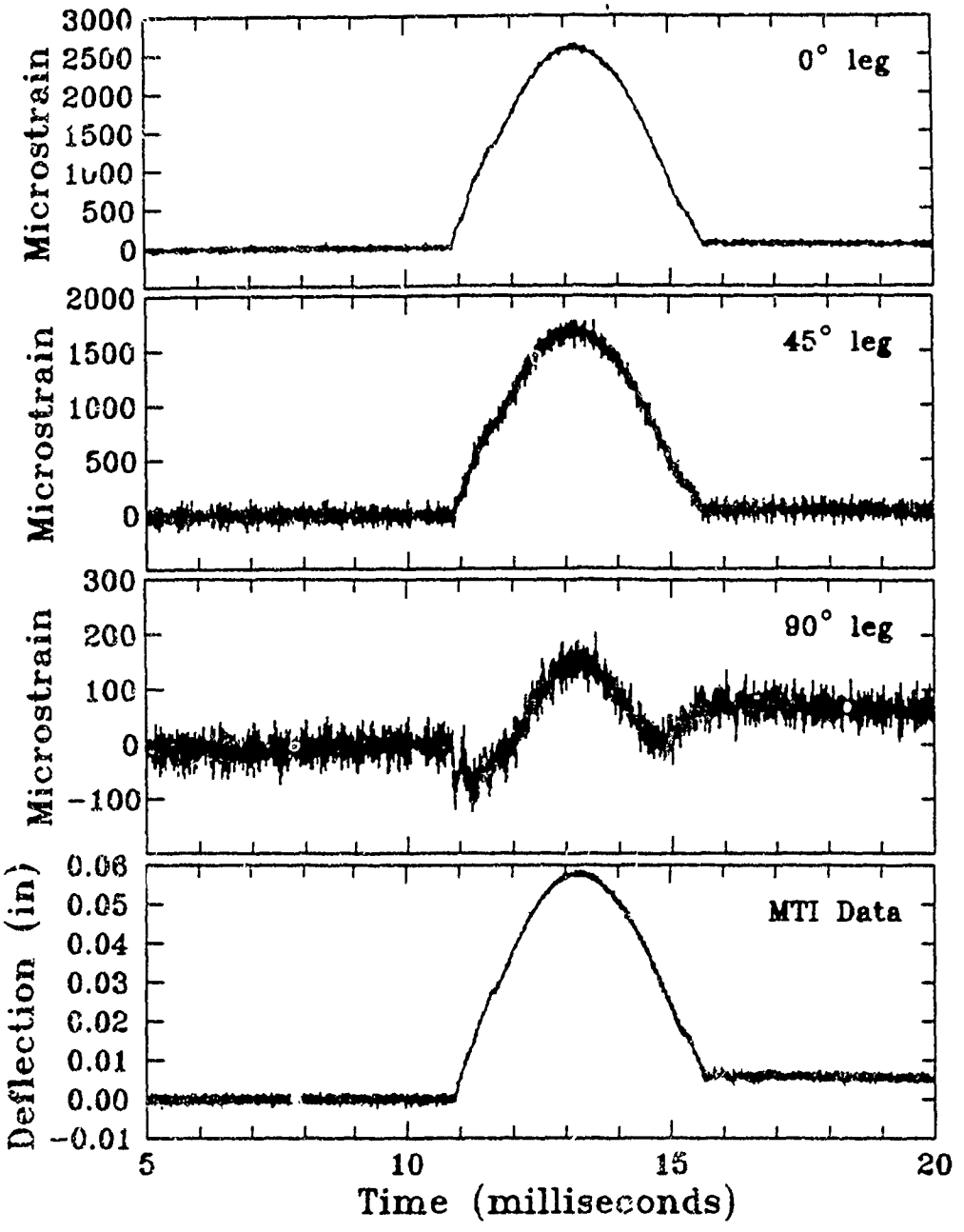


Figure B.78. Strain and Deflection for $[90/0]_{6S}$ Panel, Impact Energy = 2.23 ft-lb

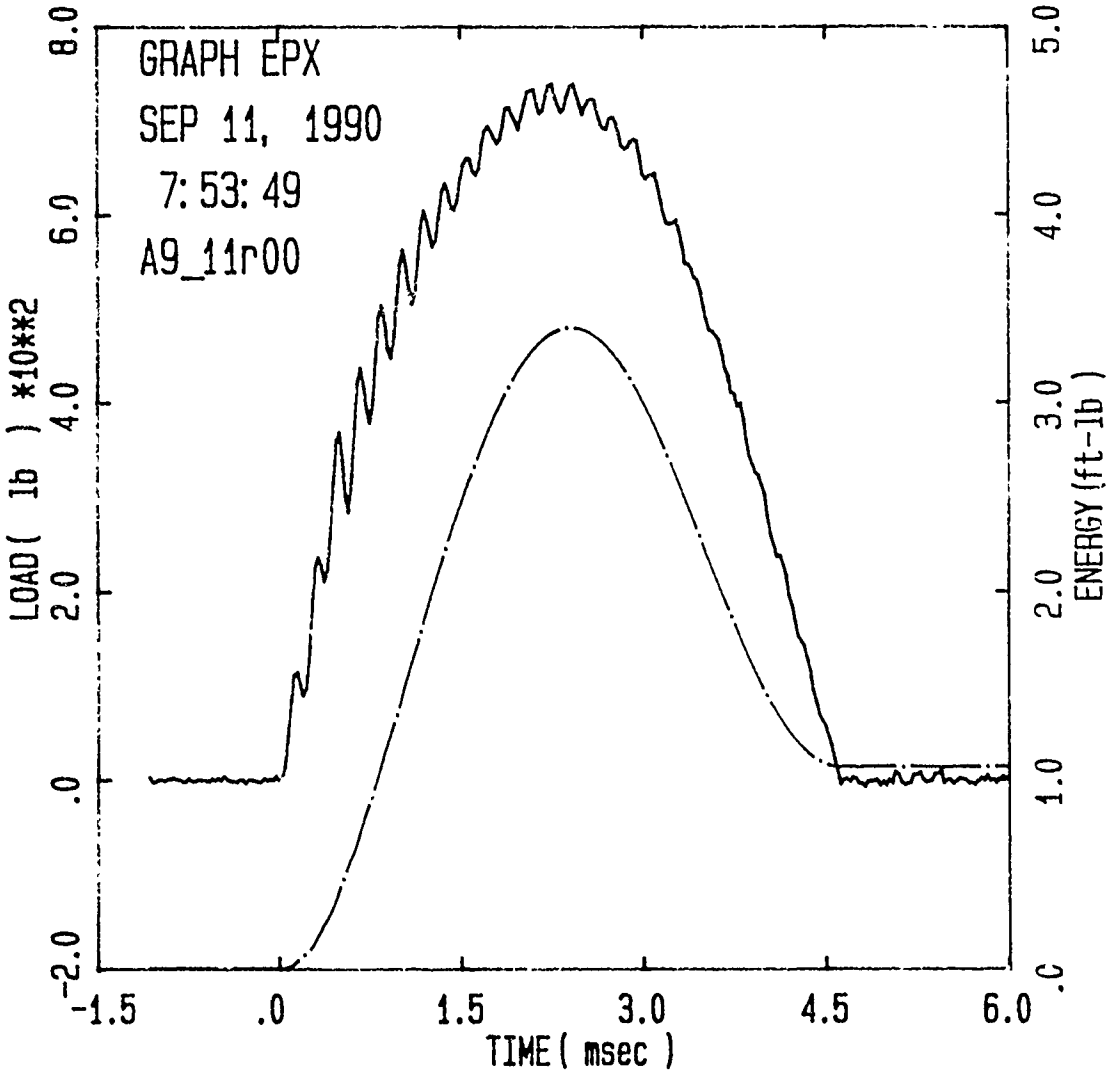


| Specimen Id | Temp ( f) | Impact Veloc. (ft/sec) | Impact Energy (ft-lb ) | Time ( msec ) Max Ld | Time ( msec ) Total | Load ( lb ) Max | Energy (ft-lb ) Maxld | Energy (ft-lb ) Total |
|---|---|---|---|---|---|---|---|---|
| A9_11r00 | 70. | 5.60 | 3.34 | 2.25 | 4.63 | 738.0 | 3.367 | 1.066 |

Figure B.79. Load and Energy from Dynatup for $[90/0]_{6S}$ Panel, Impact Energy = 3.34 ft-lb

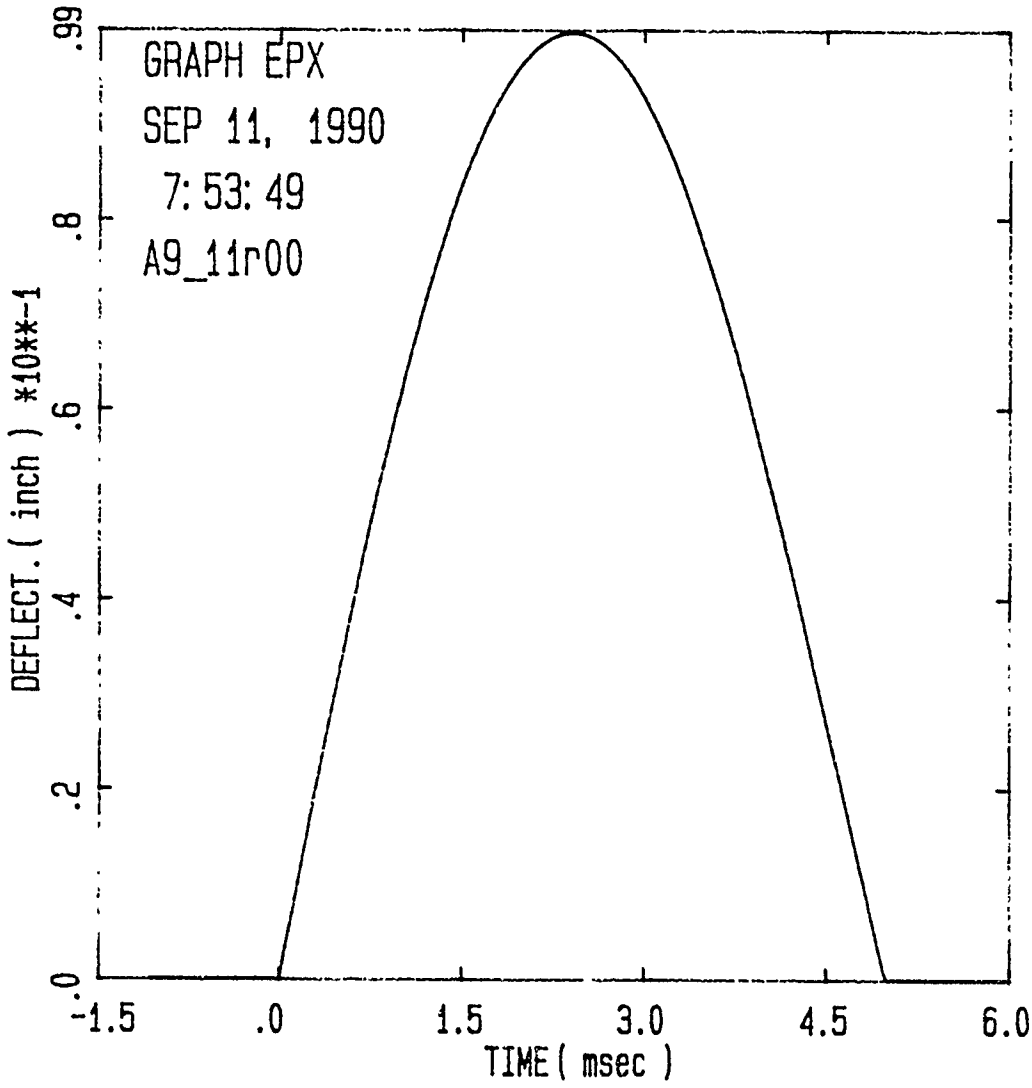


| Specimen Id | Temp ( f) | Impact Veloc. (ft/sec) | Impact Energy (ft-lb ) | Time ( msec ) Max Ld | Time ( msec ) Total | Load ( lb ) Max | Energy (ft-lb ) Maxld | Energy (ft-lb ) Total |
|---|---|---|---|---|---|---|---|---|
| A9_11r00 | 70. | 5.60 | 3.34 | 2.25 | 4.63 | 738.0 | 3.367 | 1.066 |

Figure B.80. Deflection from Dynatup for $[90/0]_{6S}$ Panel, Impact Energy = 3.34 ft-lb

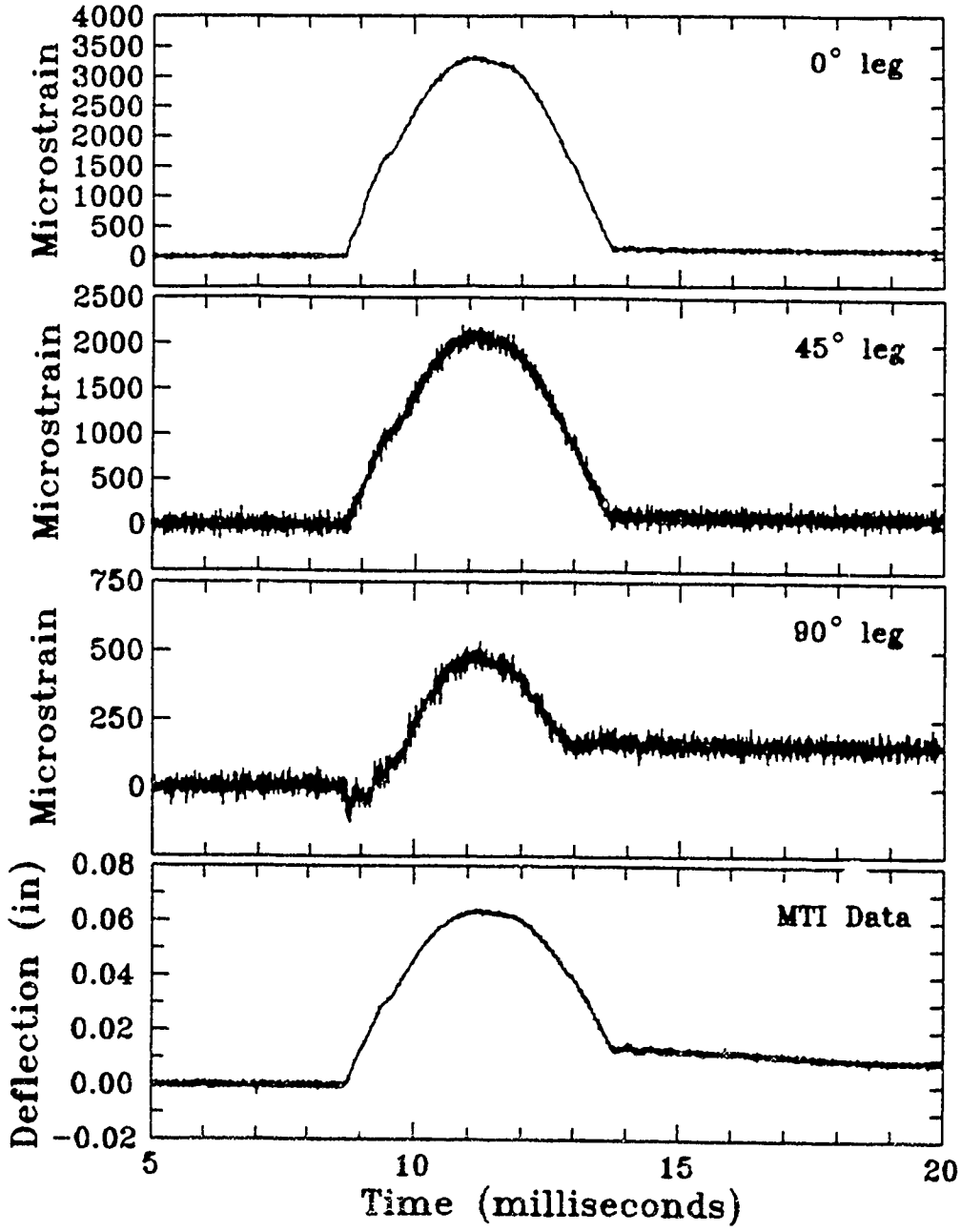


Figure B.81. Strain and Deflection for $[90/0]_{6S}$ Panel, Impact Energy = 3.34 ft-lb

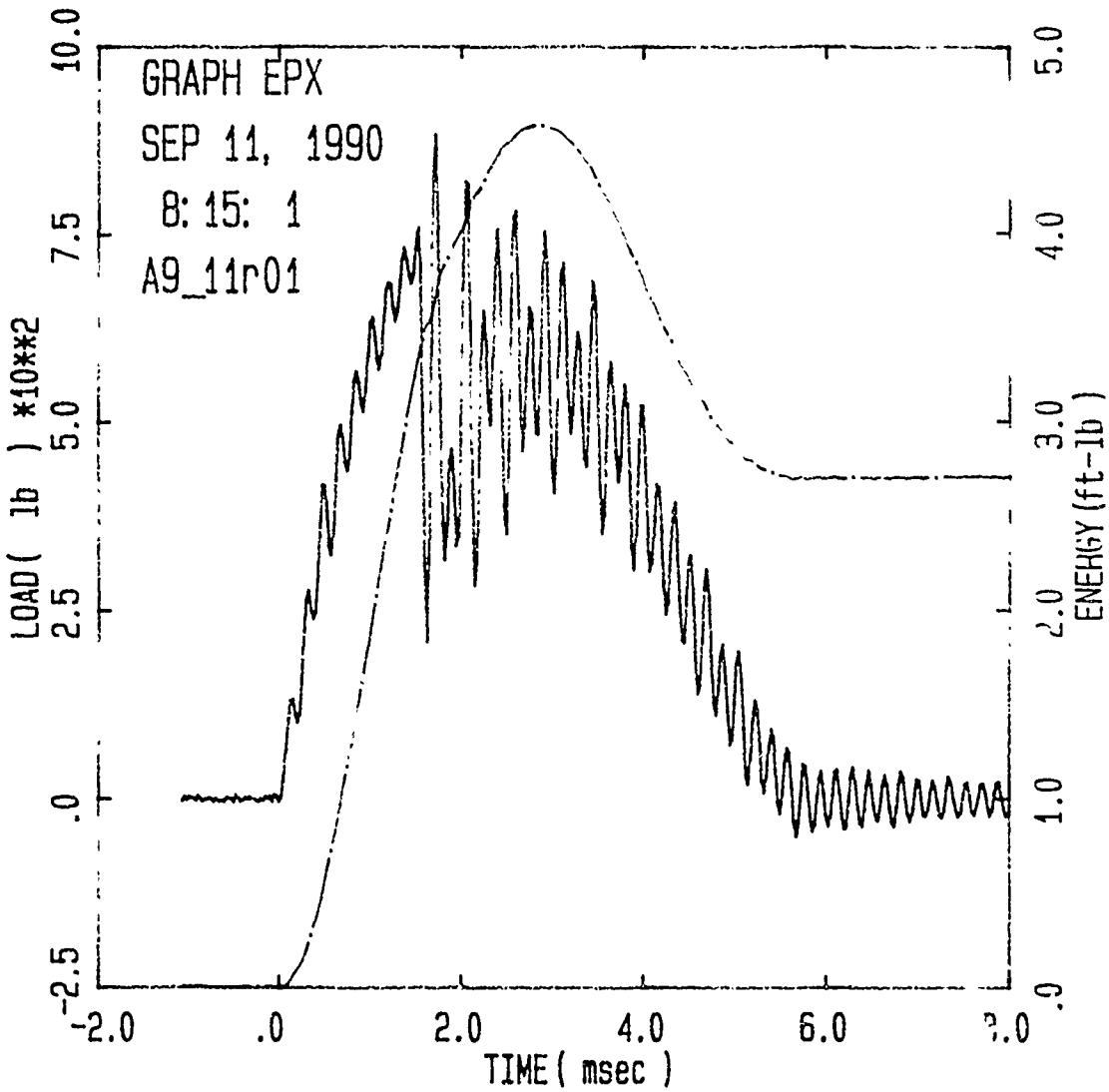


| Specimen Id | Temp ( f) | Impact Veloc. (ft/sec) | Energy (ft-lb ) | Time ( msec ) Max Ld | Time ( msec ) Total | Load ( lb ) Max | Energy (ft-lb ) MaxId | Energy (ft-lb ) Total |
|---|---|---|---|---|---|---|---|---|
| A9_11r01 | 70. | 6.51 | 4.51 | 1.73 | 5.47 | 682.3 | 3.694 | 2.711 |

Figure B.82. Load and Energy from Dynatup for $[90/0]_{6S}$ Panel, Impact Energy = 4.51 ft-lb

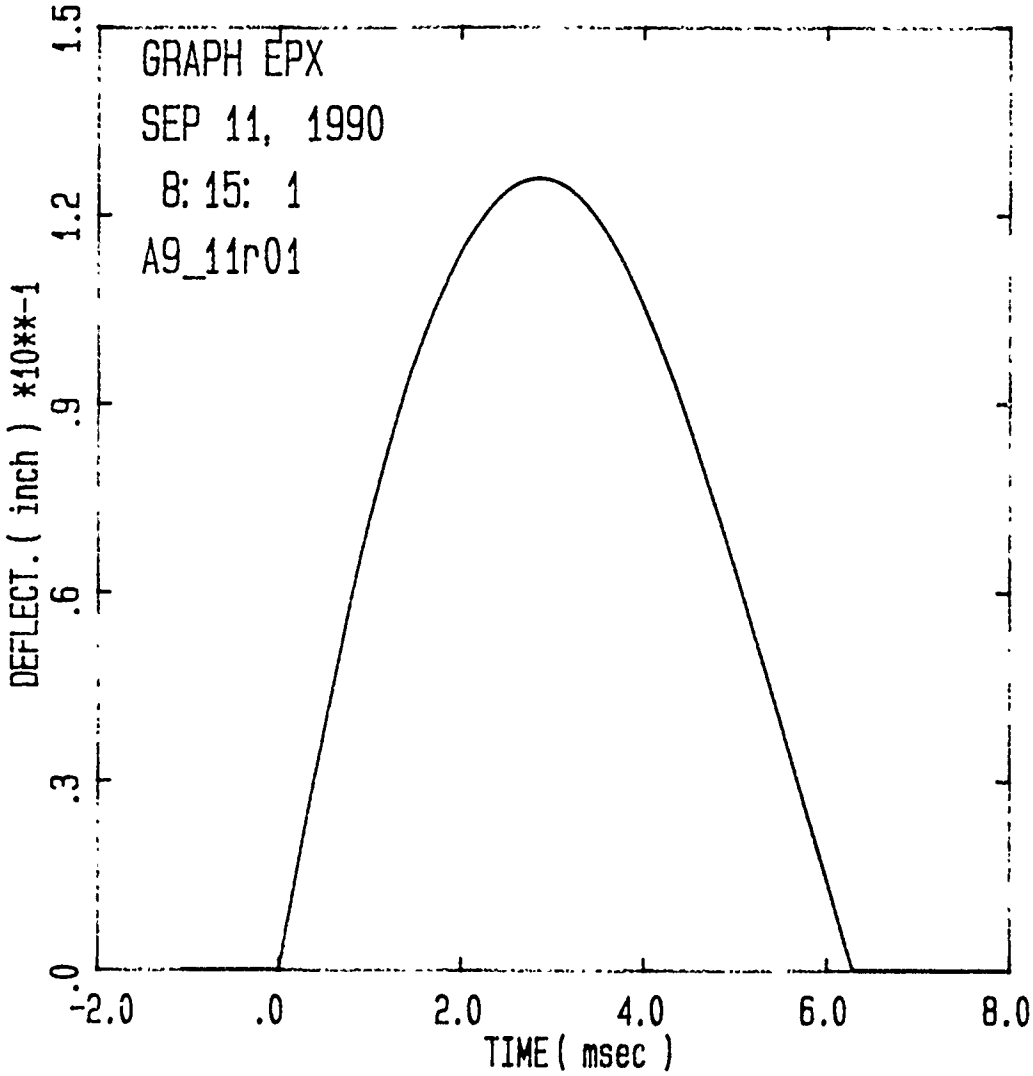


| Specimen Id | Temp ( f) | Impact Veloc. (ft/sec) | Impact Energy (ft-lb ) | Time ( msec ) Max Ld | Time ( msec ) Total | Load ( lb ) Max | Energy (ft-lb ) Maxld | Energy (ft-lb ) Total |
|---|---|---|---|---|---|---|---|---|
| A9_11r01 | 70. | 6.51 | 4.51 | 1.73 | 5.47 | 882.3 | 3.694 | 2.711 |

Figure B.83. Deflection from Dynatup for $[90/0]_{6S}$ Panel, Impact Energy = 4.51 ft-lb

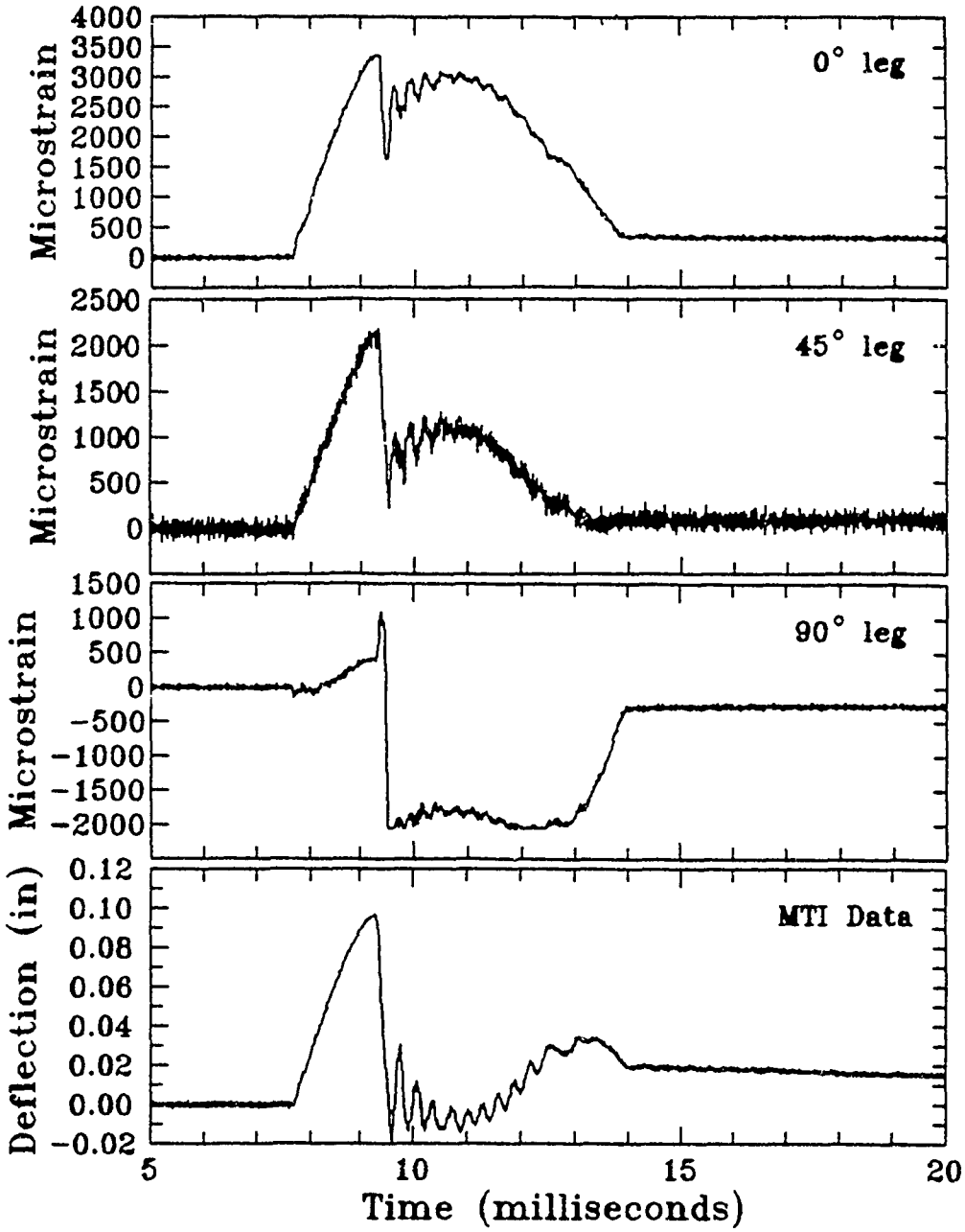


Figure B.84. Strain and Deflection for $[90/0]_{6S}$ Panel, Impact Energy = 4.51 ft-lb

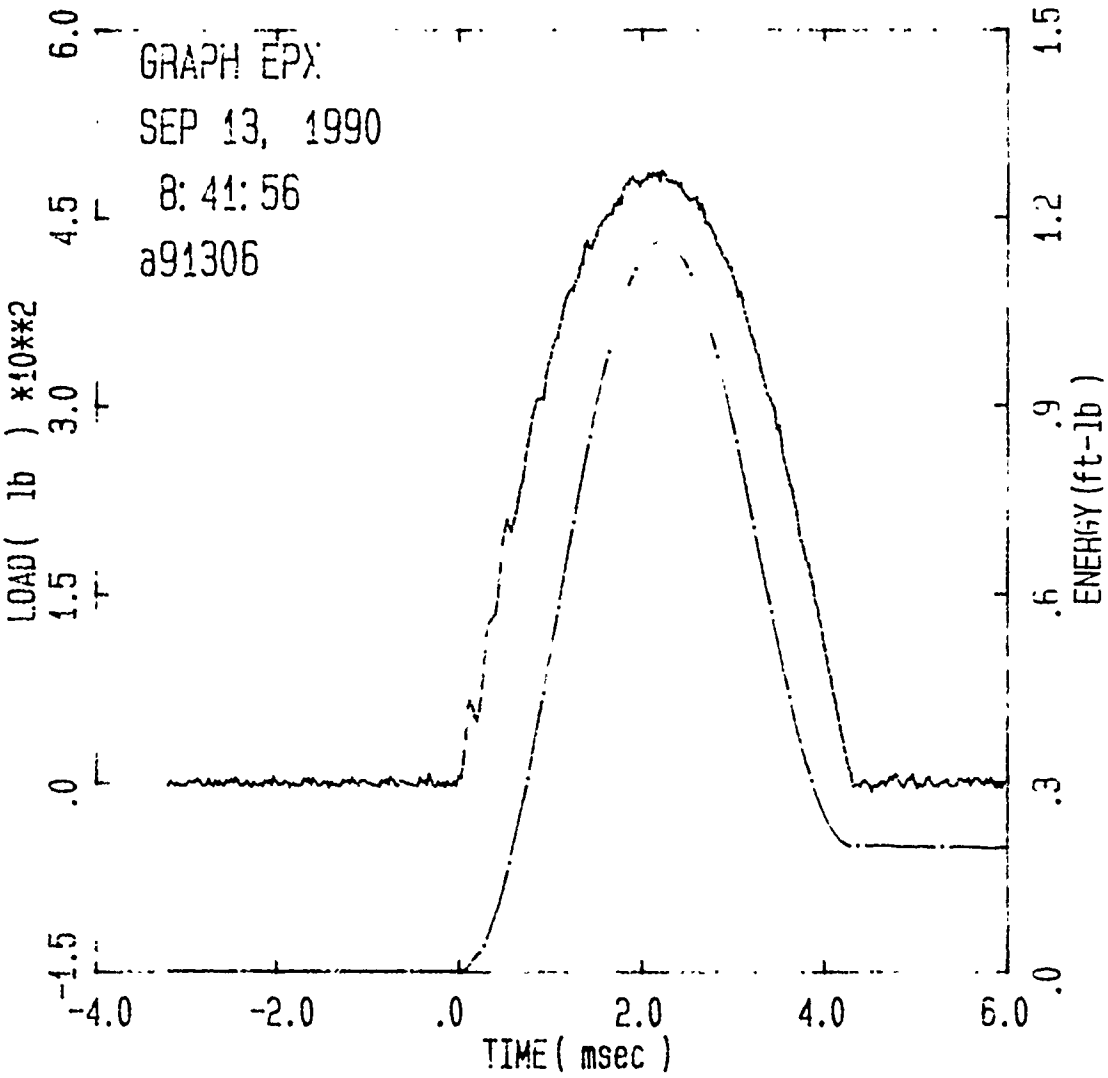


| Specimen Id | Temp ( f) | Impact Veloc. (ft/sec) | Energy (ft-lb ) | Time ( msec ) Max Ld | Time ( msec ) Total | Load ( lb ) Max | Energy (ft-lb ) Max Ld | Energy (ft-lb ) Total |
|---|---|---|---|---|---|---|---|---|
| a91306 | 70. | 3.26 | 1.13 | 2.22 | 4.33 | 486.8 | 1.160 | .198 |

Figure B.85. Load and Energy from Dynatup for $[\pm 45]_{6S}$ Panel, Impact Energy = 1.13 ft-lb

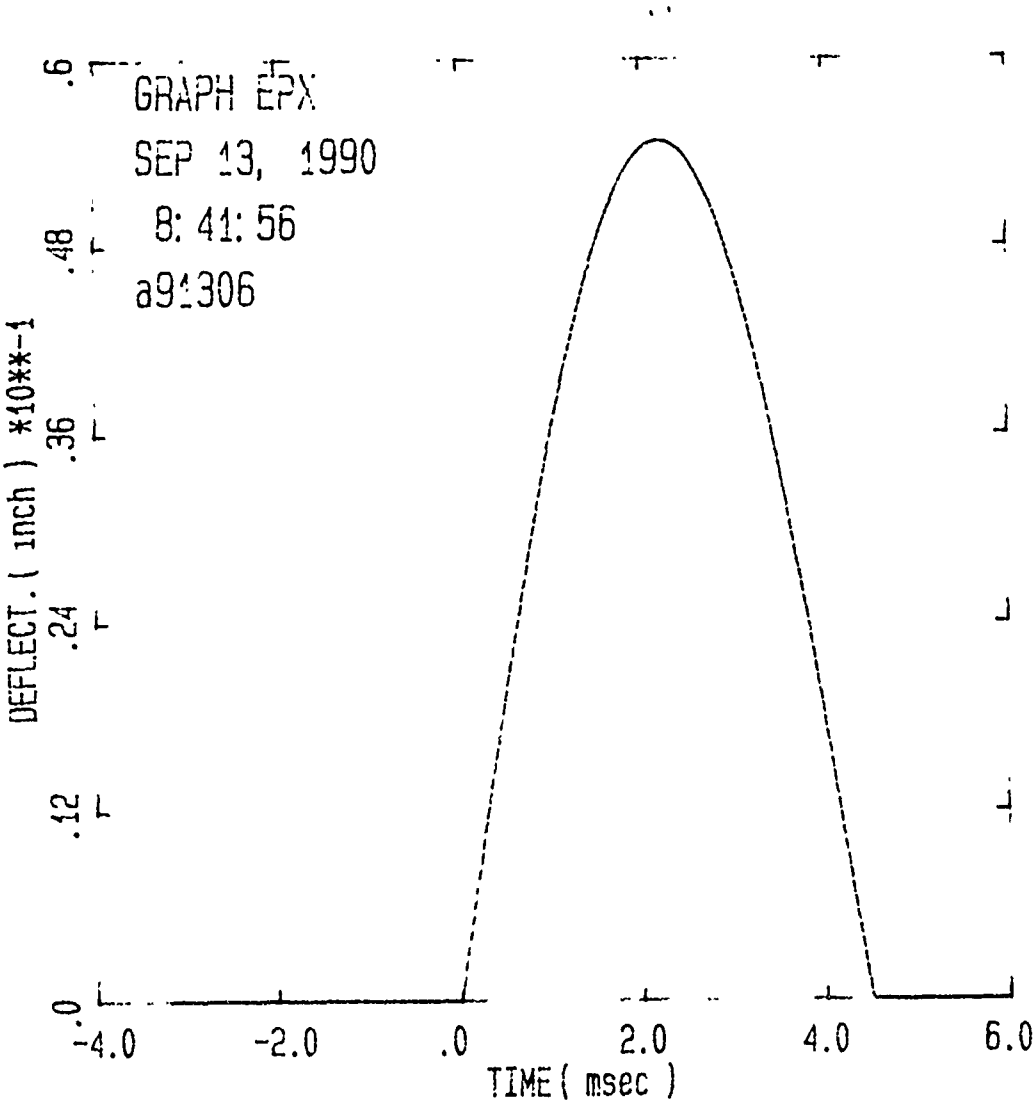


| Specimen Id | Temp ( f) | Impact Veloc. (ft/sec) | Impact Energy (ft-lb ) | Time ( msec ) Max Ld | Time ( msec ) Total | Load ( lb ) Max | Energy (ft-lb ) Max ld | Energy (ft-lb ) Total |
|---|---|---|---|---|---|---|---|---|
| a91306 | 70. | 3.26 | 1.13 | 2.22 | 4.33 | 486.8 | 1.160 | .198 |

Figure B.86. Deflection from Dynatup for $[\pm 45]_{6S}$ Panel, Impact Energy = 1.13 ft-lb

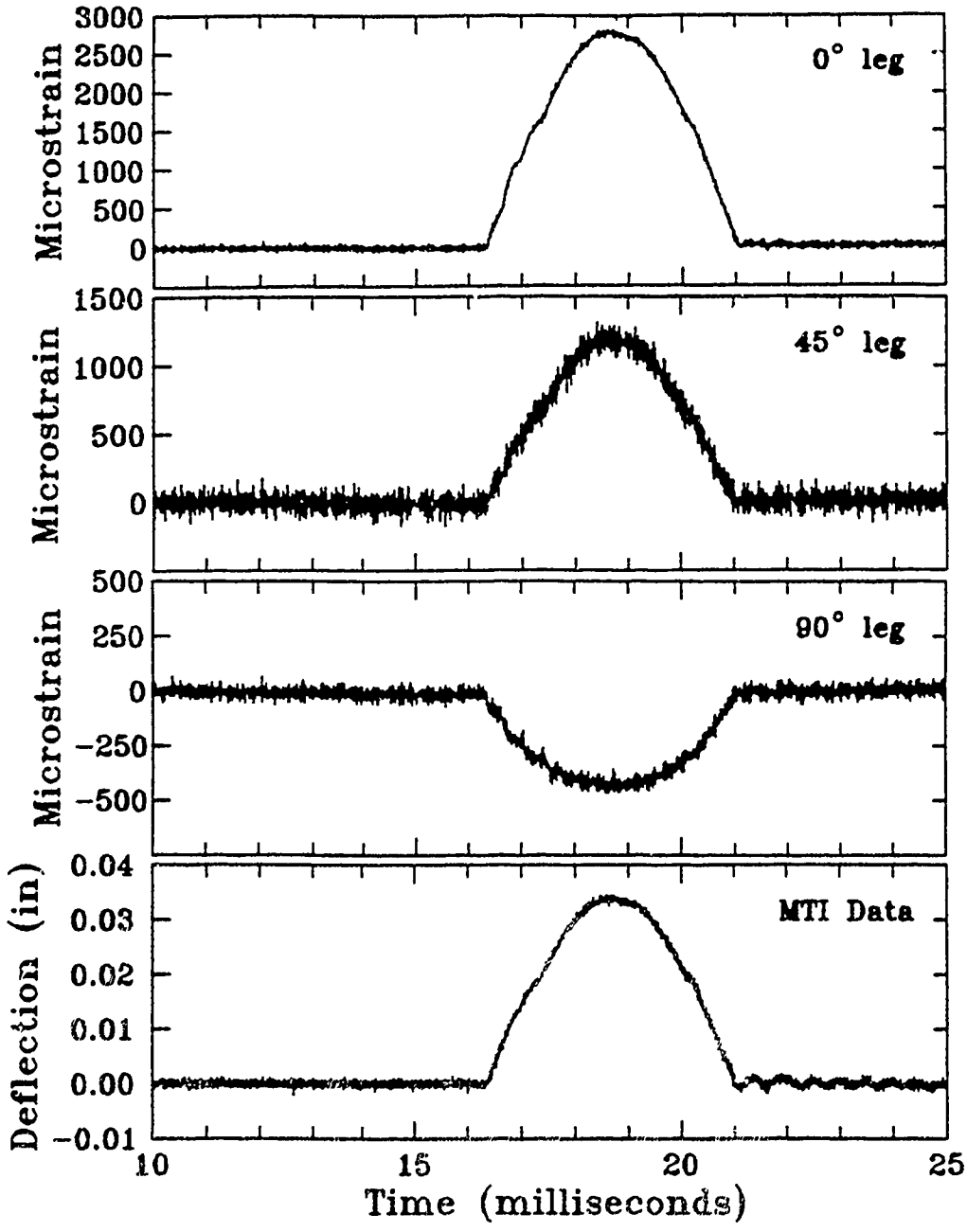


Figure B.87. Strain and Deflection for $[\pm 45]_{6S}$ Panel, Impact Energy = 1.13 ft-lb

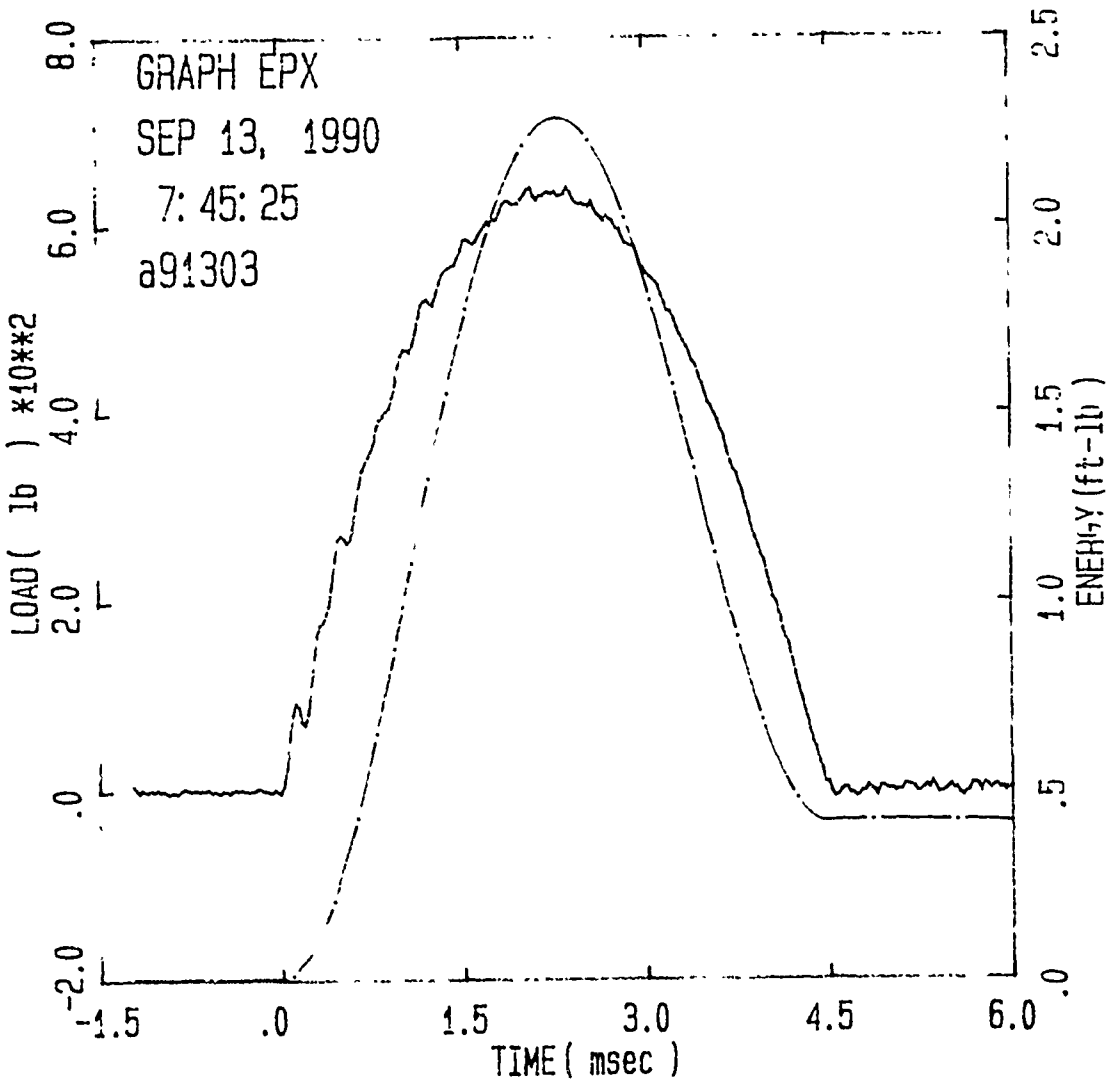


| Specimen Id | Temp ( f) | Impact Veloc. (ft/sec) | Impact Energy (ft-lb ) | Time ( msec ) Max Ld | Time ( msec ) Total | Load ( lb ) Max | Energy (ft-lb ) Max Ld | Energy (ft-lb ) Total |
|---|---|---|---|---|---|---|---|---|
| a91303 | 70. | 4.59 | 2.23 | 2.08 | 4.52 | 639.2 | 2.234 | .411 |

Figure B.88. Load and Energy from Dynatup for $[\pm 45]_{6S}$ Panel, Impact Energy = 2.23 ft-lb

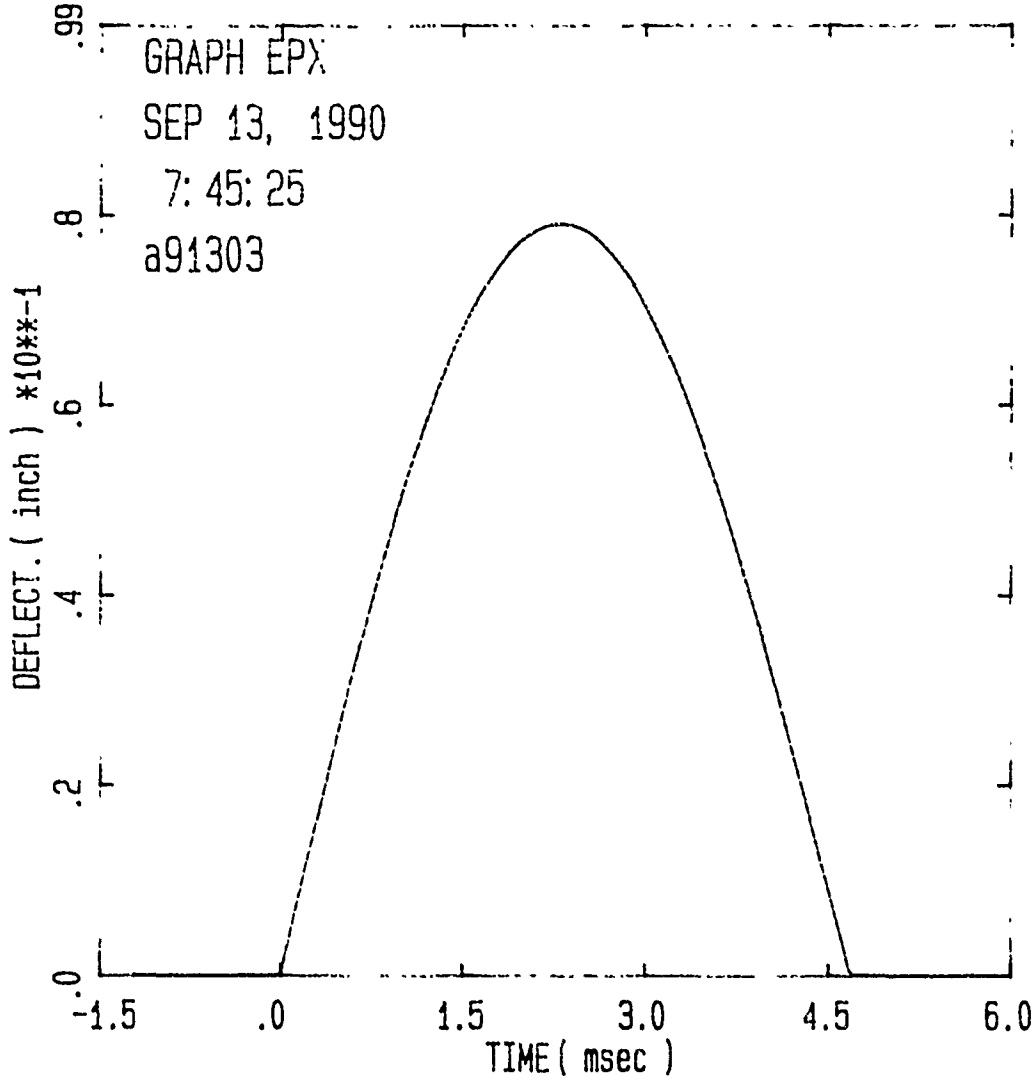


| Specimen Id | Temp ( f) | Impact Veloc. (ft/sec) | Energy (ft-lb ) | Time ( msec ) Max Ld | Time ( msec ) Total | Load ( lb ) Max | Energy (ft-lb ) Maxld | Energy (ft-lb ) Total |
|---|---|---|---|---|---|---|---|---|
| a91303 | 70. | 4.59 | 2.23 | 2.08 | 4.52 | 639.2 | 2.234 | .411 |

Figure B.89. Deflection from Dynatup for $[\pm 45]_{6S}$ Panel, Impact Energy = 2.23 ft-lb

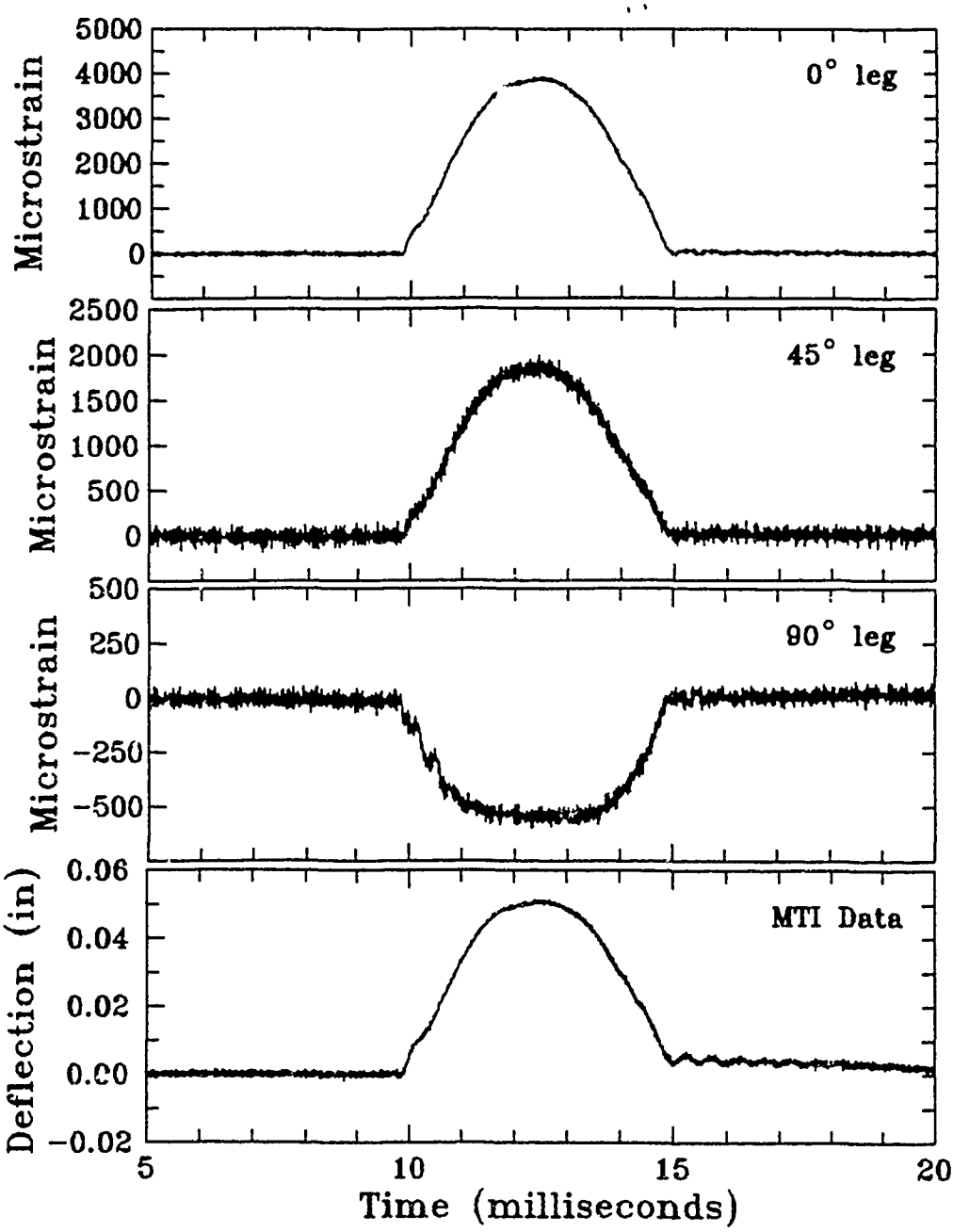


Figure B.90. Strain and Deflection for $[\pm 45]_{6S}$ Panel, Impact Energy = 2.23 ft-lb

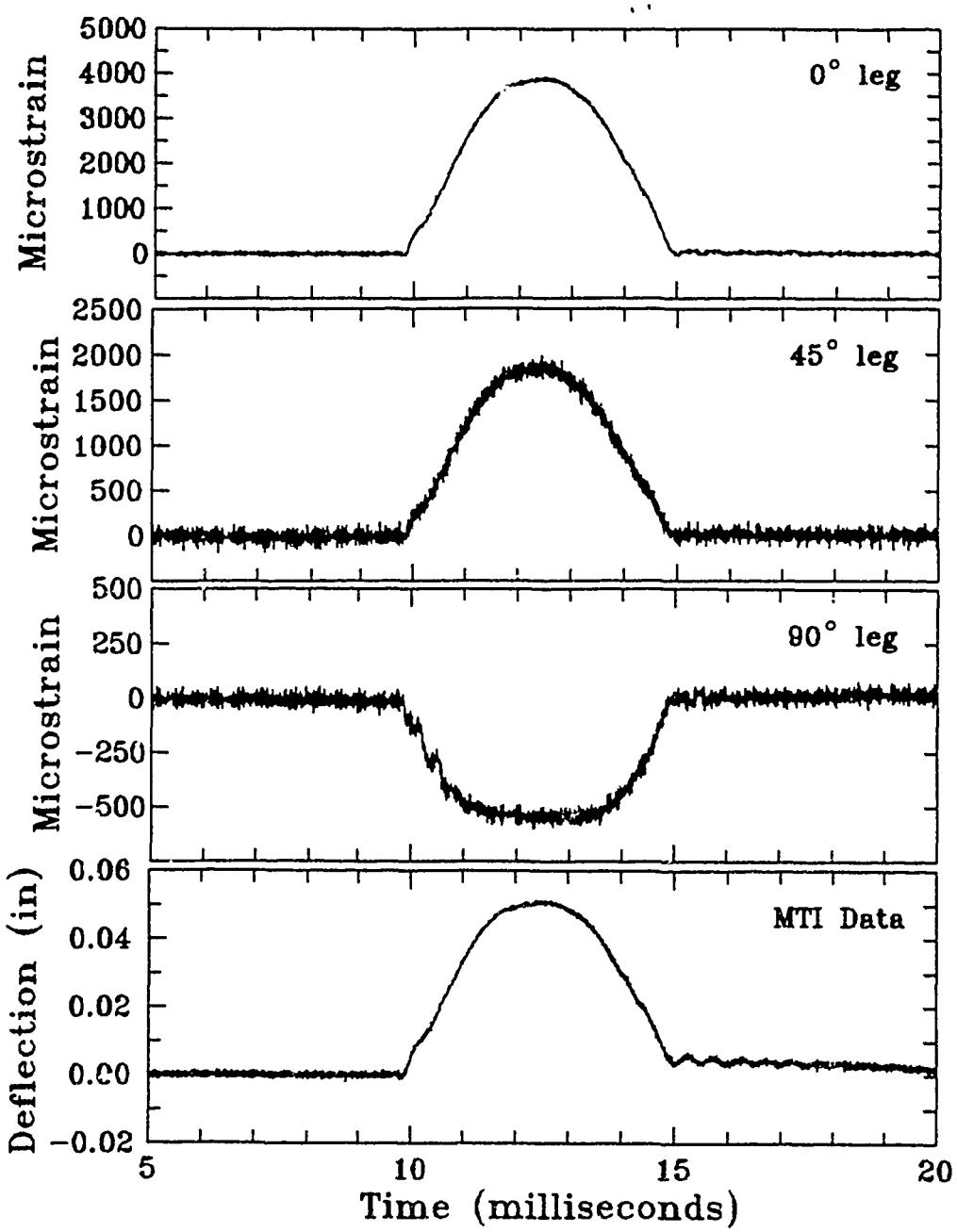


Figure B.90. Strain and Deflection for $[\pm 45]_{6S}$ Panel, Impact Energy = 2.23 ft-lb

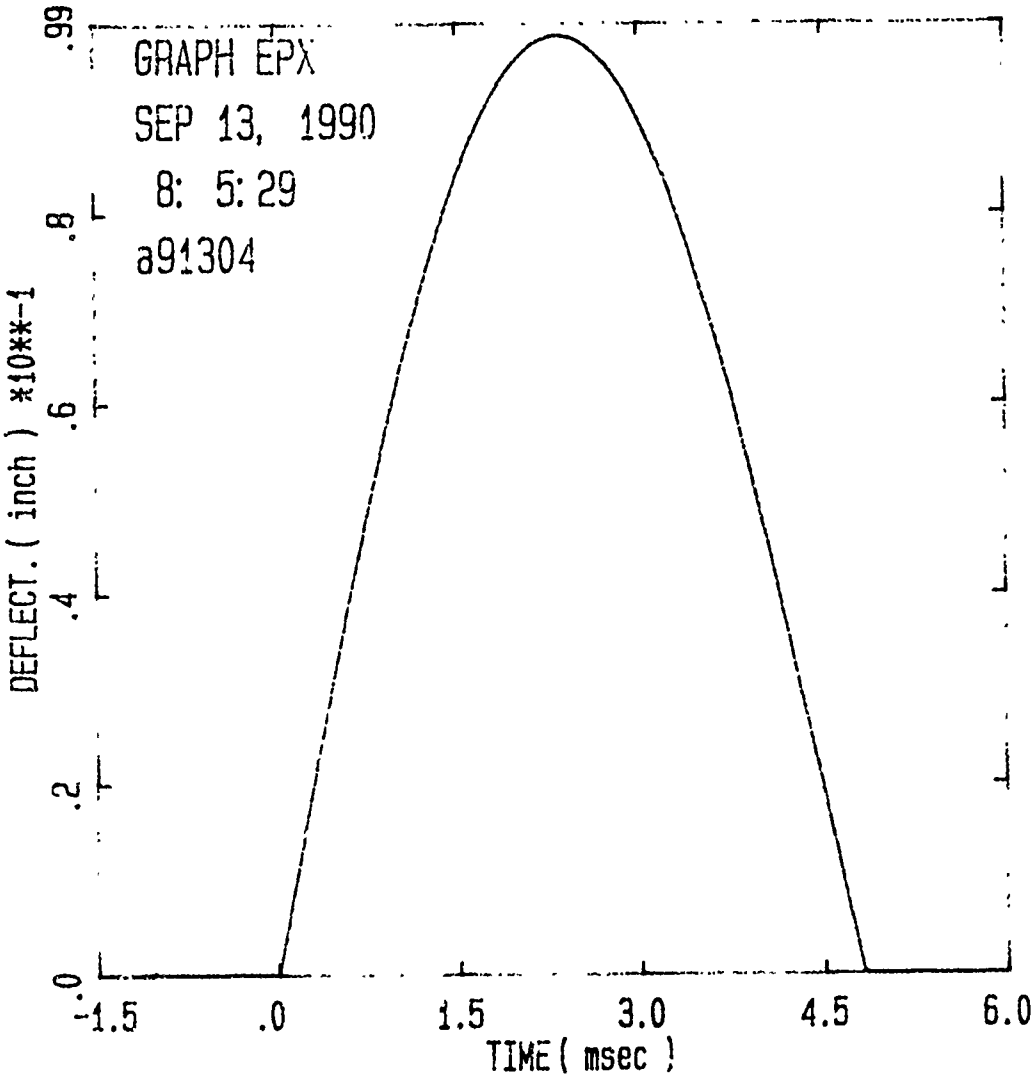


| Specimen Id | Temp (f) | Impact Veloc. (ft/sec) | Impact Energy (ft-lb) | Time (msec) Max Ld | Time (msec) Total | Load (lb) Max | Energy (ft-lb) MaxId | Energy (ft-lb) Total |
|---|---|---|---|---|---|---|---|---|
| a91304 | 70. | 5.60 | 3.33 | 2.08 | 4.55 | 762.4 | 3.291 | .793 |

Figure B.92. Deflection from Dynatup for $[\pm 45]_{6S}$ Panel, Impact Energy = 3.33 ft-lb

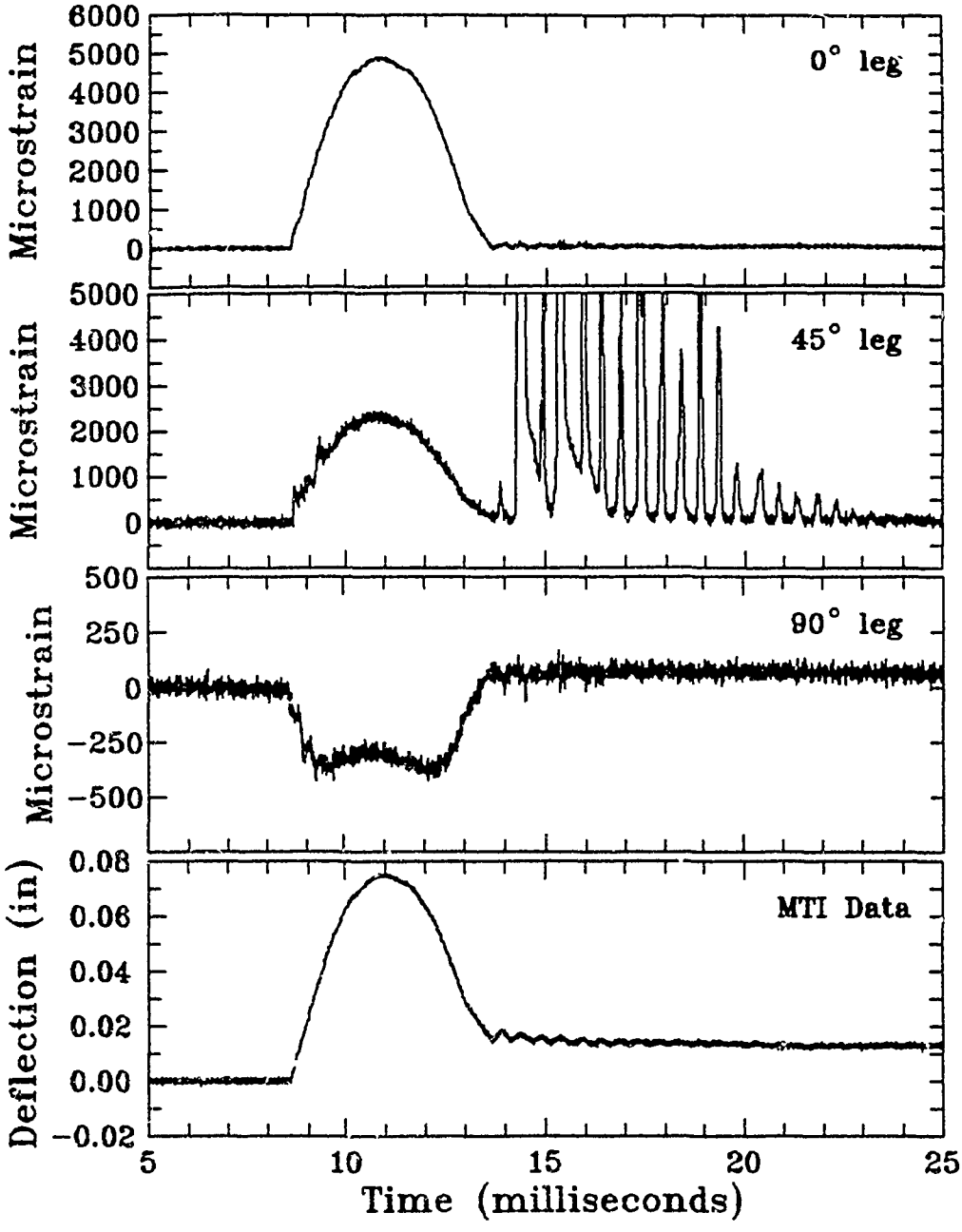


Figure B.93. Strain and Deflection for $[\pm 45]_{6S}$ Panel, Impact Energy = 3.33 ft-lb

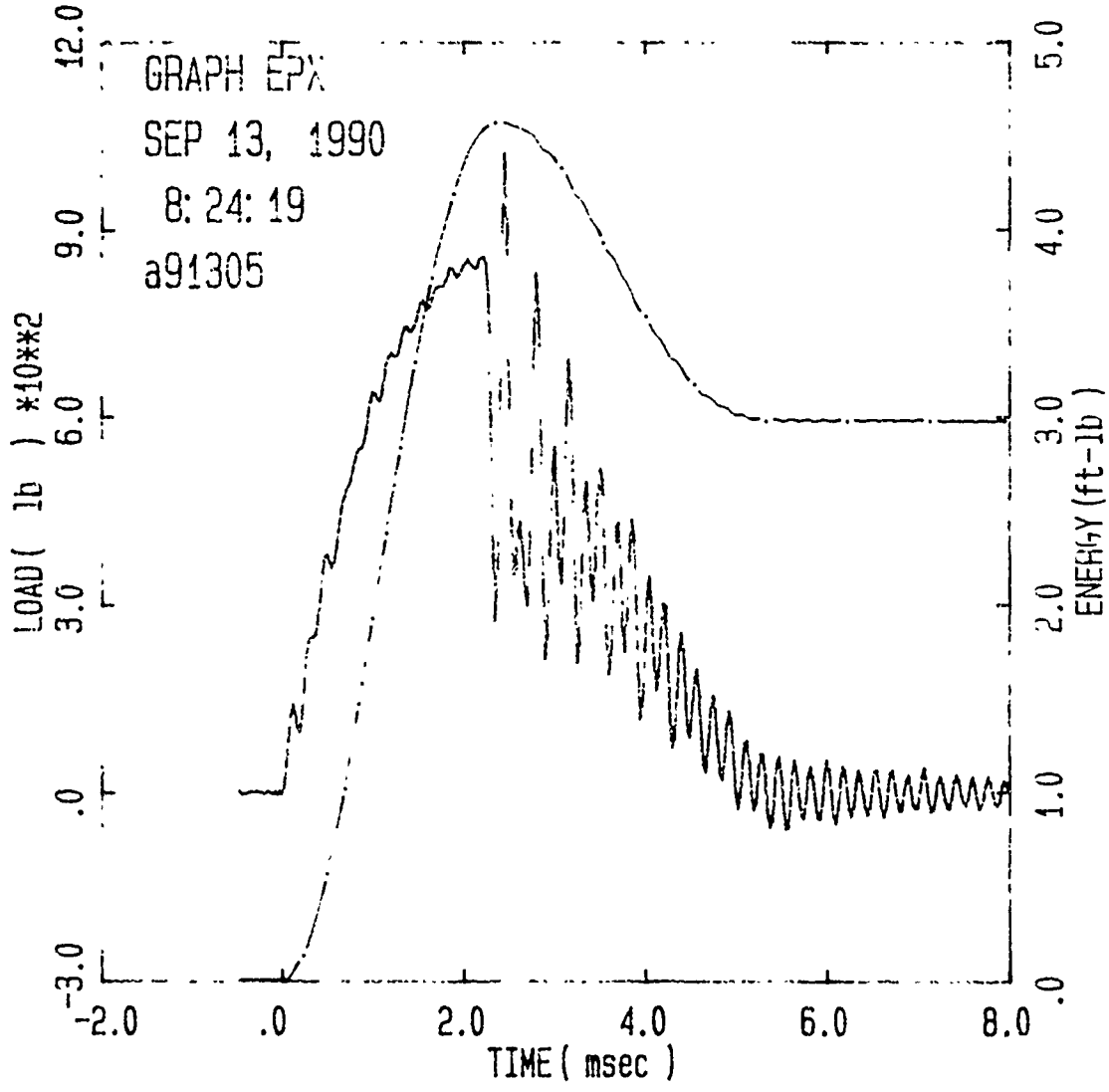


| Specimen Id | Temp ( f) | Impact Veloc. (ft/sec) | Impact Energy (ft-lb ) | Time ( msec ) Max Ld | Time ( msec ) Total | Load ( lb ) Max | Energy (ft-lb ) Max Ld | Energy (ft-lb ) Total |
|---|---|---|---|---|---|---|---|---|
| a91305 | 70. | 6.51 | 4.50 | 2.45 | 5.02 | 1023.1 | 4.564 | 3.007 |

Figure B.94. Load and Energy from Dynatup for $[\pm 45]_{6S}$ Panel, Impact Energy = 4.50 ft-lb

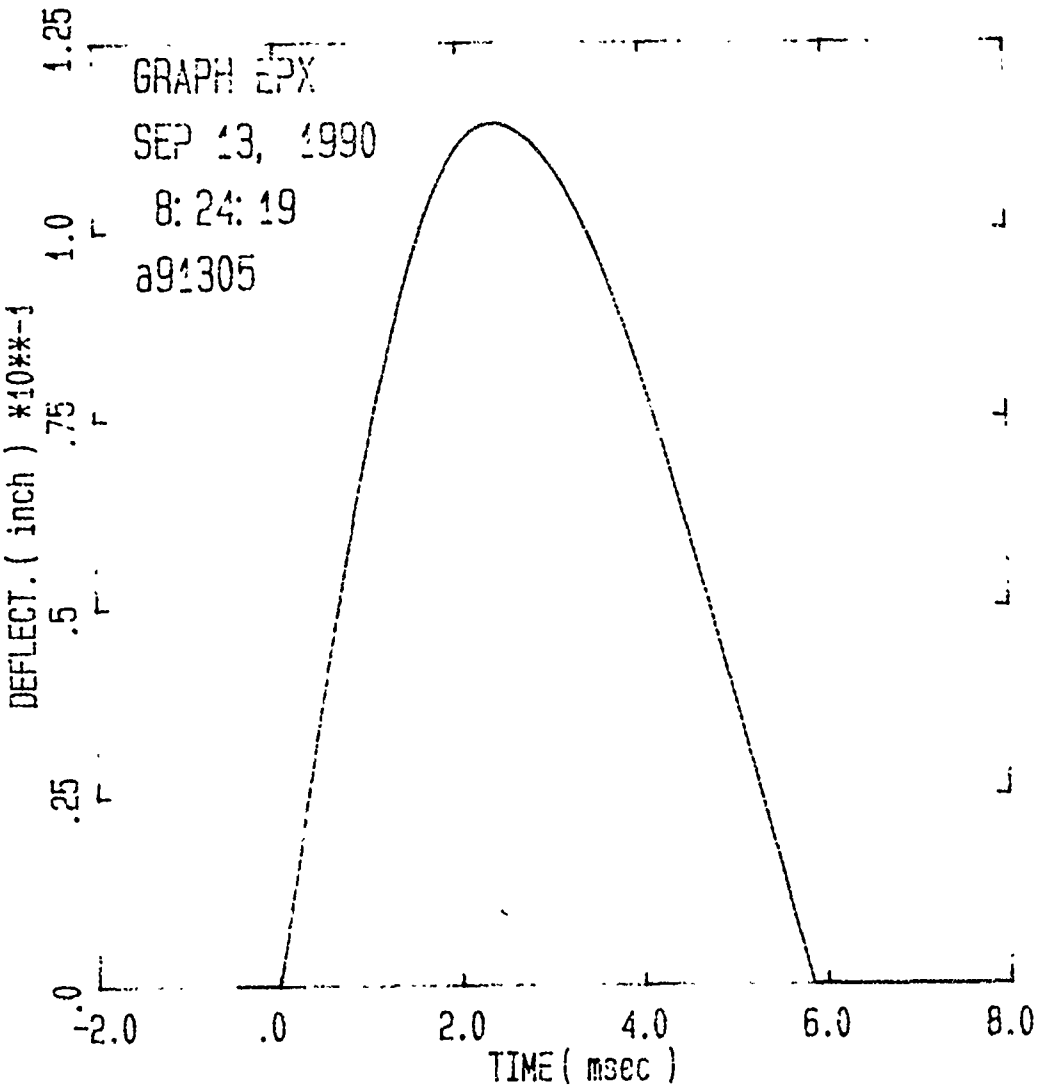


| Specimen Id | Temp ( f) | Impact Veloc. (ft/sec) | Impact Energy (ft-lb ) | Time ( msec ) Max Ld | Time ( msec ) Total | Load ( lb ) Max | Energy (ft-lb ) Maxld | Energy (ft-lb ) Total |
|---|---|---|---|---|---|---|---|---|
| a91305 | 70. | 6.51 | 4.50 | 2.45 | 5.02 | 1023.1 | 4.564 | 3.007 |

Figure B.95. Deflection from Dynatup for $[\pm 45]_{6S}$ Panel, Impact Energy = 4.50 ft-lb

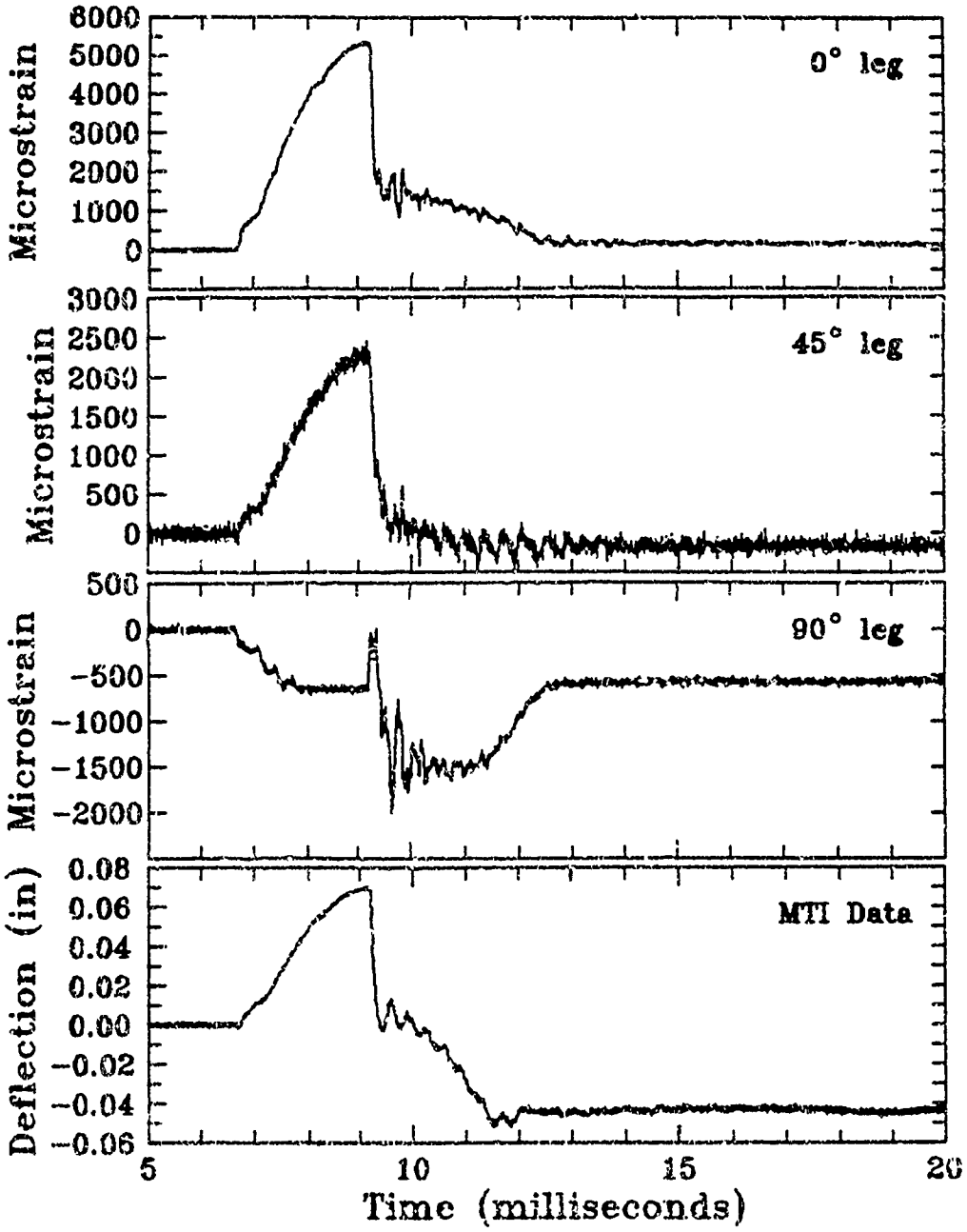


Figure B.96. Strain and Deflection for $[\pm 45]_{6S}$ Panel, Impact Energy = 4.50 ft-lb

## Bibliography


1. Cantwell, W.J. and J. Morton. "Impact Perforation of Carbon Fibre Reinforced Plastic," Composites Science and Technology, Vol 38, pp 119-141, 1990.

2. Cheresh, Matthew C. and Steven McMichael. "Instrumented Impact Test Data Interpretation," Instrumented Impact Testing of Plastics and Composite Materials, ASTM STP 936, S.L. Kessler, G.C. Adams, S.B. Driscoll, and D.R. Ireland, Eds., pp 9-23, 1987.

3. Christoforou, A.P. and S.R. Swanson. "Analysis of Impact Response in Composite Plates," International Journal of Solids and Structures, Vol 27, pp 161-170, 1991.

4. DC/Bridge/Transducer Programmable Signal Conditioner User's Manual, Gould Electronics, Cleveland OH, December 1987.

5. Dennis, Capt Scott T. Large Displacement and Rotational Formulation for Laminated Cylindrical Shells including Parabolic Transverse Shear. PhD Dissertation. School of Engineering, Air Force Institute of Technology (AU), Wright-Patterson AFB OH, May 1988.

6. Dobyns, A.L. "Analysis of Simply-Supported Orthotropic Plates Subject to Static and Dynamic Loads," AIAA Journal, Vol 19, pp 642-650.

7. Donnell, L.H. Stability of Thin Walled Tubes Under Torsion, NACA 479, 1933.

8. Foos, Bryan C. Damage Progression in Composite Plates due to Low Velocity Impact. MS Thesis. Department of Civil Engineering, The Ohio State University, Columbus OH, 1990.

9. GRC 730-I Instrumented Impact Test Data System Instruction Manual, General Research Corporation, Santa Barbara CA, 1987.

10. Ishai, O. and A. Shragai, "Effect of Impact Loading on Damage and Residual Compressive Strength of CFRP Laminated Beams," Composite Structures, 1990.

11. Jones, Robert M. Mechanics of Composite Materials, Scripta Book Company, Washington D.C., 1975.

12. Kissinger, Curtis "Displacement Measurement by Fiber Optics," Measurements and Control, April 1988.

13. Lin, H.J. and Y.J. Lee. "On the Inelastic Impact of Composite Laminated Plate and Shell Structures," Composite Structures, Vol 14, pp 89-111, 1990.

14. MTI 1000 Fotonic Sensor Instruction Manual, Mechanical Technologies, Inc., Latham NY.

15. Oi, Koshiro. "Transient Response of Bonded Strain Gages," Experimental Mechanics, pp 463-469, September 1966.

16. O'Kane, B.A.A. and P.P. Benham. "Damage Thresholds for Low Velocity Impact on Aircraft Structural Composites," Aeronautical Journal, pp 368-372, November 1986.

17. Qian, Yibo and Stephen R. Swanson. "A Comparison of Solution Techniques for Impact Response of Composite Plates," Composite Structures, Vol 14, pp 177-192, 1990.

18. Ramkumar, R.L. and Y.R. Thakar. "Dynamic Response of Curved Laminated Plates Subjected to Low Velocity Impact," Journal of Engineering Materials and Technology, Vol 109, pp 67-71, January 1987.

19. Reddy, J.N. Energy and Variational Methods in Applied Mechanics, John Wiley and Sons, 1984.

20. Senn, Eugene A. Impact Damage Tolerance of Composite Cylindrical Panels. MS Thesis, AFIT/GAE/ENY/89D-34. School of Engineering, Air Force Institute of Technology (AU), Wright-Patterson AFB OH, December 1989.

21. Sun, C.T. and S. Chattopadhyay. "Dynamic Response of Anisotropic Laminate Plates under Initial Stress to Impact of a Mass," Journal of Applied Mechanics, Vol 42, pp 693-698, September 1975.

22. Tsai, C.T. and A.N. Palazotto. "On the Finite Element Analysis of Nonlinear Vibration for Cylindrical Shells with High-Order Shear Deformation Theory," Department of Aeronautics and Astronautics, Air Force Institute of Technology (AU), Wright-Patterson AFB OH, to be published in International Journal of Nonlinear Mechanics.

23. Whitney, J.M. and Pagano, N.J. "Shear Deformation in Heterogeneous Anisotropic Plates," Journal of Applied Mechanics, Vol 37, pp 1031-1036, 1970.

24. Wu, Hsi-Yung T. and George S. Springer. "Impact Induced Stresses, Strains, and Delaminations in Composite Plates," Journal of Composite Materials, Vol 22, pp 533-560, June 1980.

25. Yang, P.C., Norris, C.H., and Stavsky, Y. "Elastic Wave Propagation in Heterogeneous Plates," International Journal of Solids and Structures, Vol 2, pp 665-684, 1966.

# REPORT DOCUMENTATION PAGE

Form Approved
OMB No. 0704-0188



| 1. AGENCY USE ONLY (Leave blank) | 2. REPORT DATE | 3. REPORT TYPE AND DATES COVERED |
|---|---|---|
| | December 1990 | Master's Thesis |

**4. TITLE AND SUBTITLE**
IMPACT DAMAGE IN CURVED GRAPHITE/EPOXY PANELS WITH CLAMPED EDGES

**5. FUNDING NUMBERS**

**6. AUTHOR(S)**
Ronald B. Perry, Captain, USAF

**7. PERFORMING ORGANIZATION NAME(S) AND ADDRESS(ES)**
Air Force Institute of Technology, WPAFB OH 45433-6583

**8. PERFORMING ORGANIZATION REPORT NUMBER**
AFIT/GAE/ENY/90D-19

**9. SPONSORING/MONITORING AGENCY NAME(S) AND ADDRESS(ES)**
Dr Spencer T. Wu
AFOSR/NA
Bolling AFB
Washington DC 20332-6448

**10. SPONSORING/MONITORING AGENCY REPORT NUMBER**

**11. SUPPLEMENTARY NOTES**

**12a. DISTRIBUTION/AVAILABILITY STATEMENT**
Approved for public release; distribution unlimited

**12b. DISTRIBUTION CODE**

**13. ABSTRACT** (Maximum 200 words)

Graphite/epoxy curved cylindrical panels were impacted in the center by an impact machine capable of measuring load during the test. Load, deflection and strain as functions of time were measured for six symmetric layup configurations for impact energies of 0.5 to 4.5 ft-lb. Damage was produced in all panels for certain impact energies. The extent and location of damage was determined from C-scans and optical microscopy of panel cross-sections. The cross-sections indicated that both delamination and transverse cracking contribute to internal damage. An in-house nonlinear finite element code was used to predict the panel deflections and stresses. The analysis produced good results in predicting the $[0/90]_{3s}$ panel deflection and indicated transverse failure stresses were present in the panel center region. The deflections indicated that the panel was in between simply supported and clamped boundary conditions, with good agreement obtained for hinged support at each edge.

* Epoxy resins, * Graphite materials, Curved profiles, * Panels,

**14. SUBJECT TERMS**
* Impact, ~~Materials,~~ Composite Materials, Material Testing, * Damage, Delamination, Graphite/Epoxy, Theses.

**15. NUMBER OF PAGES**
184

**16. PRICE CODE**

| 17. SECURITY CLASSIFICATION OF REPORT | 18. SECURITY CLASSIFICATION OF THIS PAGE | 19. SECURITY CLASSIFICATION OF ABSTRACT | 20. LIMITATION OF ABSTRACT |
|---|---|---|---|
| Unclassified | Unclassified | Unclassified | UL |